NAS4-17900

[redacted]

p. 206

Investigation of Hypervelocity Impact Damage to Space Station Truss Tubes

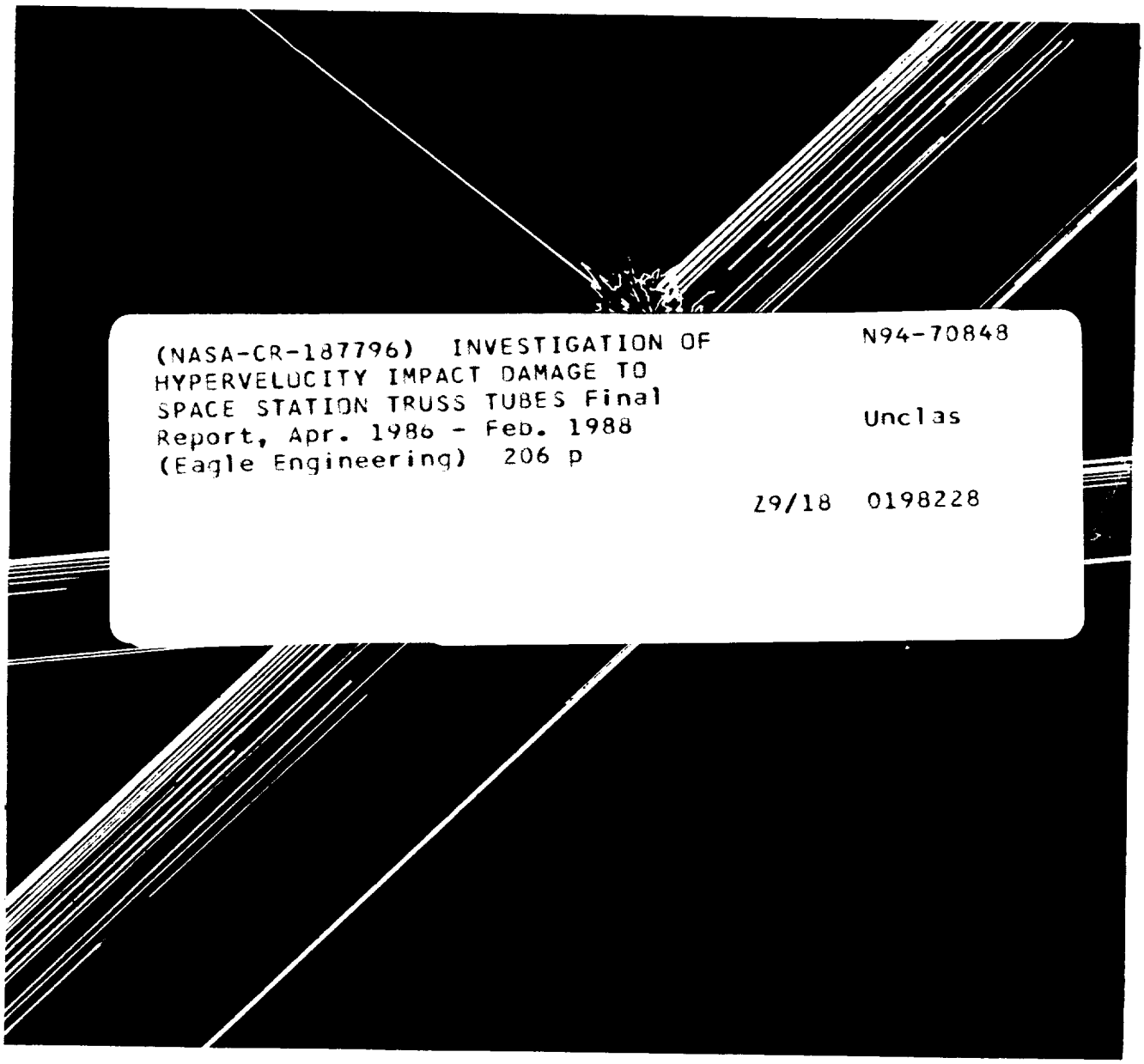

(NASA-CR-187796) INVESTIGATION OF HYPERVELOCITY IMPACT DAMAGE TO SPACE STATION TRUSS TUBES Final Report, Apr. 1986 - Feb. 1988 (Eagle Engineering) 206 p

N94-70848

Unclas

Z9/18 0198228

EAGLE

Final Report

Eagle Report Number 88-176

February 15, 1988

Investigation of Hypervelocity Impact Damage to Space Station Truss Tubes

Prepared under Subcontract to

Lockheed Engineering and Management Services Co., Inc.

for the

Space Sciences Branch

NASA Johnson Space Center

by

Eagle Engineering, Inc.

Houston, Texas

NASA Contract NAS9-17900

Lockheed P.O. 02-001-12133, 02-001-16769

Eagle Contract TO-86-68, TO-87-61

Final Report

Eagle Report No. 88-176

February 15, 1988

Foreword

The purpose of this study was to assess the susceptiblity of graphite-epoxy tube specimens, representative of Space Station truss elements, to damage and failure by hypervelocity impact. A second purpose was to determine the effect that tube properties, such as ply orientation, fiber elastic modulus, wall thickness, and surface coatings, have on the extent of impact damage. The study was conducted between April 1986 and February 1988 through a Lockheed Engineering and Management Services Company subcontract for the Space Sciences Branch of the Solar System Exploration Division at the NASA Johnson Space Center.

Mr. Burton G. Cour-Palais was the NASA technical monitor for this study. Mr. Glen Jolly was the Lockheed contract administrator. Excellent hypervelocity impact test support was provided by Ms. Jeanne L. Crews (NASA JSC) and Lockheed personnel assigned to the JSC Hypervelocity Impact Laboratory: Mr. Thomas Thompson, Mr. Kenneth Oser, and Mr. Earl Brownfield. Additional impact testing was carried out by the NDE Technology, Inc. hypervelocity test facility in Torrance, California. John R. Mastandrea and Christopher A. Lorenze were NDE supervisors of this activity.

Structural testing of the graphite-epoxy tube specimens was coordinated by Dr. Lubert J. Leger (NASA JSC), Mr. Calvin Schomburg (NASA JSC), and Mr. Ike Spiker (Lockheed). Technical advice was provided by Mr. Orvis E. Pigg (NASA JSC). Ms. Beatrice Santos-Mason (NASA JSC) coordinated the application of aluminum coatings on selected tube specimens.

Ultrasonic C-scans of the targets prior to and after impact were graciously provided by Dr. Ching H. Yew and graduated student Mr. Chung Y. Wang from the University of Texas.

Graphite-epoxy tubes and flat plates were produced by Amoco. Additional tube specimens were donated by Morton Thiokol, McDonnell Douglas, and Sikorsky Division of United Technologies. Hercules, Inc. performed an analytical failure analysis of a damaged tube with finite element models.

Mr. Eric L. Christiansen was the Eagle Project Manager. Technical contributions were made by Mr. William R. Stump and Mr. Christopher C. Varner. Mr. David A. Carson provided editorial assistance.

Table of Contents

	Page
Foreword	ii
Table of Contents	iii
List of Figures	v
List of Tables	vii
1.0 Executive Summary	1
2.0 Introduction	4
3.0 Hypervelocity Impact Test Conditions	6
3.1 Space Station Truss Structure	6
3.2 Truss Failure Sources	8
3.2.1 Truss and Node Impact Summary	9
3.2.2 Meteoroid Environment	10
3.2.3 Orbital Debris Environment	11
3.2.4 Atomic Oxygen Attack	12
3.2.5 Predicted Perforations in Truss Protective Coatings	13
3.2.6 Matrix Microcracking	15
3.3 Impact Test Plan	15
3.4 Target Specimens	16
3.5 Pre- and Post-Impact Target Examination	19
3.5.1 Mass and Dimensions	19
3.5.2 Acoustic Velocity and Modulus	19
3.5.3 Structural Tests	20
3.5.4 C-Scans	23
3.5.5 Impact Damage Measurements	23
3.6 Projectiles	24
3.7 Meteoroid and Orbital Debris Flux with Equivalent Size to Test Projectiles	25
4.0 Test Results	55
4.1 Effect of Projectile Size/Mass	66
4.2 Effect of Ply Orientation	80
4.3 Effect of Fiber Elastic Modulus	88
4.4 Effect of Surface Coatings	97
4.5 Effect of Target Thickness	107
4.6 Flat Plates	117
4.7 Effect of Projectile Obliquity	127
4.8 Effect of Tube Manufacturing Technique	132
4.9 Summary of Derived Equations	142
5.0 Impact Damage Estimates for Space Station Truss Tubes	146
5.1 Groundrules for Space Station Truss Failure Study	146
5.2 Truss Failure Criteria Study	147
5.3 Lifetime Impact Damage Projections	148
5.4 Atomic Oxygen Protective Coating Considerations	152

6.0 Conclusions 157
7.0 Recommendations 164
8.0 References 166
Appendix A - Shot Data 169
Appendix B - Hercules Failure Criteria Study 214
Appendix C - C-Scan Records 239
Appendix D - Compression Test Records 287

List of Figures

Page

Figure 3-1. Space Station First Element Launch (FEL) 26
Figure 3-2. Man-Tended Capability (MTC) Space Station 27
Figure 3-3. Permanently Manned Capability (PMC) Space Station 28
Figure 3-4. Phase I Space Station 29
Figure 3-5. Phase II Space Station 30
Figure 3-6. Baseline 5m Erectable Truss Structure 31
Figure 3-7. Meteoroid and Debris Impacts on Phase I Truss Tubes 32
Figure 3-8. Meteoroid and Debris Impacts on Phase II Truss Tubes 33
Figure 3-9. Meteoroid and Orbital Debris Flux 34
Figure 4-1. Definition of Encounter Parameters 57
Figure 4-2. Projectile Size Effects: Photographic Documentation of Shot NDE-11 69
Figure 4-3. Projectile Size Effects: Photographic Documentation of Shot JSC-A204 . . . 70
Figure 4-4. Projectile Size Effects: Photographic Documentation of Shot JSC-A292 . . . 71
Figure 4-5. Projectile Size Effects: Photographic Documentation of Shot JSC-A249 . . . 72
Figure 4-6. Projectile Size Effects: Photographic Documentation of Shot JSC-A308 . . . 73
Figure 4-7. Projectile Size Effects: Photographic Documentation of Shot JSC-A334 . . . 74
Figure 4-8. First Wall Hole Size for 6T Series Tubes 75
Figure 4-9. First Wall C-Scan Size for 6T Series Tubes 76
Figure 4-10. C-Scan Size Correlation for Data from Previous Study 77
Figure 4-11. Combined First and Second Wall Hole Size for 6T Series Tubes. 78
Figure 4-12. Combined First and Second Wall C-Scan Size for 6T Series Tubes 79
Figure 4-13. Ply Orientation Effects: Photographic Documentation of Shot JSC-A293 . . . 82
Figure 4-14. Ply Orientation Effects: Photographic Documentation of Shot JSC-A294 . . . 83
Figure 4-15. 9T and 10T Tube First Wall Hole Diameter Versus 6T Correlation 84
Figure 4-16. First Wall Hole Diameter for all Amoco, Uncoated, Low-Modulus Tubes. . . 85
Figure 4-17. 9T and 10T Tube Data for Combined Wall Hole Diameter 86
Figure 4-18. Combined Wall C-Scan Diameter for Low Modulus, Amoco Tubes 87
Figure 4-19. Target Fiber Modulus Effects: Photographic Documentation of Shot JSC-A291 90
Figure 4-20. Target Fiber Modulus Effects: Photographic Documentation of Shot JSC-A302 91
Figure 4-21. First Wall Hole Diameter for Low and High Modulus Amoco Tubes 92
Figure 4-22. First Wall C-Scan Diameter for Low and High Modulus Amoco Tubes. . . . 93
Figure 4-23. Combined Wall Hole Diameter for High Modulus Amoco Tubes 94
Figure 4-24. High Modulus Combined Wall C-Scan Diameter Vs. Low Modulus Correlation. 95
Figure 4-25. Combined Wall C-Scan Diameter for Low and High Modulus Amoco Tubes 96
Figure 4-26. Target Surface Coating Effects: Photographic Documentation of Shot JSC-A250 99
Figure 4-27. Target Surface Coating Effects: Photographic Documentation of Shot JSC-A307 100
Figure 4-28. Target Surface Coating Effects: Photographic Documentation of Shot NDE-24 101
Figure 4-29. First Wall Hole Diameter for 2 mil and 6 mil Aluminum Coated Tubes. . . . 102
Figure 4-30. First Wall C-Scan Diameter for Aluminum Coated Tubes 103
Figure 4-31. Combined Wall Equivalent Circular Hole Diameter for Aluminum Coated Tubes 104
Figure 4-32. Combined Wall C-Scan Diameter for Aluminum Coated Tubes 105
Figure 4-33. Exposed Area for 2 mil Aluminum Coated Tubes 106

Figure 4-34. Tube Wall Thickness Effects: Photographic Documentation of Shot NDE-22 . . . 109
Figure 4-35. Tube Wall Thickness Effects: Photographic Documentation of Shot NDE-28 . . . 110
Figure 4-36. Tube Wall Thickness Effects: Photographic Documentation of Shot NDE-29 . . . 111
Figure 4-37. First Wall Hole Diameter Data for Thick Wall Tubes . . . 112
Figure 4-38. First Wall C-Scan Diameter Data for Thick Wall Tubes vs. Thin Wall Curve . . . 113
Figure 4-39. First Wall C-Scan Diameter Data for Thick and Thin Wall Tubes . . . 114
Figure 4-40. Combined Wall Hole Diameter for Thick Wall Tubes . . . 115
Figure 4-41. Combined C-Scan Diameter for Thick Wall Tubes . . . 116
Figure 4-42. Flat Plate Effects: Photographic Documentation of Shot JSC-A333 . . . 118
Figure 4-43. Flat Plate Effects: Photographic Documentation of Shot JSC-A411 . . . 119
Figure 4-44. Flat Plate Effects: Photographic Documentation of Shot JSC-A410 . . . 120
Figure 4-45. Flat Plate Effects: Photographic Documentation of Shot JSC-A352 . . . 121
Figure 4-46. Flat Plate Effects: Photographic Documentation of Shot JSC-A407 . . . 122
Figure 4-47. Flat Plate Effects: Photographic Documentation of Shot JSC-A413 . . . 123
Figure 4-48. Hole Diameter Data for Low Modulus Flat Plates . . . 124
Figure 4-49. Hole Diameter Data for High Modulus Flat Plates . . . 125
Figure 4-50. C-Scan Diameter Data for Low and High Modulus Flat Plates . . . 126
Figure 4-51. Impact Obliquity Effects: Photographic Documentation of Shot JSC-A313 . . . 129
Figure 4-52. Impact Obliquity Effects: Photographic Documentation of Shot JSC-A329 . . . 130
Figure 4-53. First Wall Hole Size for Oblique Impacts on Tubes . . . 131
Figure 4-54. Tube Manufacturing Effects: Photographic Documentation of Shot JSC-A261 . . . 134
Figure 4-55. Tube Manufacturing Effects: Photographic Documentation of Shot JSC-A246 . . . 135
Figure 4-56. Tube Manufacturing Effects: Photographic Documentation of Shot JSC-A245 . . . 136
Figure 4-57. First Wall Hole Diameter for McDonnell Douglas and Morton Thiokol Tubes . . . 137
Figure 4-58. First Wall Hole Diameter Correlation for McDonnell Douglas Tubes . . . 138
Figure 4-59. First Wall C-Scan Diameter for McDonnell Douglas and Morton Thiokol Tubes . . . 139
Figure 4-60. Combined Wall Hole Diameter for McDonnell Douglas and Morton Thiokol Tubes . . . 140
Figure 4-61. Combined Wall C-Scan Diameter for McDonnell and Thiokol Tubes . . . 141

List of Tables

		Page
Table 3-1.	Orbital Debris and Meteoroid Impacts on Phase I Space Station Tubes	35
Table 3-2.	Orbital Debris & Meteoroid Impacts on Phase II Space Station Tubes	36
Table 3-3.	Orbital Debris & Meteoroid Impacts on Phase II Space Station Nodes	37
Table 3-4.	Truss Node Failure Analysis	38
Table 3-5.	Predicted Perforations in Tube Coating (0.002" Al 2024-T3)	39
Table 3-6.	Predicted Perforations in Tube Coating (0.006" Al 2024-T3)	40
Table 3-7.	Predicted Perforations in Tube Coating (0.002" Al 1100-0)	41
Table 3-8.	Predicted Perforations in Tube Coating (0.006" Al 1100-0)	42
Table 3-9.	Graphite-Epoxy Tube and Plate Characteristics	43
Table 3-10.	Target Dimensions and Mass	44
Table 3-11.	Target Sonic Velocity and Elastic Modulus	46
Table 3-12.	Predicted Tube Specimen Ultimate Compressive Loads	48
Table 3-13.	Results of Compression Tests on Undamaged Tubes	49
Table 4-1.	Shot Data Summary (Ordered by Target Serial Number)	58
Table 5-1.	Failure Frequency for Phase I Space Station Truss Tubes	154
Table 5-2.	Failure Frequency for Phase II Space Station Truss Tubes	155
Table 5-3.	Exposure of 2 mil Aluminum Coating Compensated for Peeling	156

1.0 Executive Summary

On the average, every square meter of the space station truss will be subjected to 335 impacts per year from 0.01 mm and larger meteoroid and orbital debris particles. The objectives of this study were to 1) determine how susceptible the truss tubes were to failure from hypervelocity impact, 2) assess how tube properties (such as ply orientation, fiber elastic modulus, wall thickness, and surface coatings) affect the extent of impact damage, and 3) assess how projectile parameters (size, density, velocity, and impact obliquity angle) affect target damage.

The study involved hypervelocity impact testing using light gas guns at the NASA Johnson Space Center (JSC) and at NDE Technology, Inc. in Torrance, California. Aluminum, glass, and nylon projectiles from 0.55 mm to 4.4 mm diameter were launched at velocities ranging from 4 to 7.5 km/sec. Data from 58 shots was used in the correlation analyses. Most of the shots were made at an impact angle normal to the target surface (0° obliquity). Unavoidable aiming dispersions resulted in impact obliquity angles of up to 40° for some of the tube shots. Intentional oblique impact shots were performed on selected tube specimens at a 45° angle to the longitudinal axis and 45° to the axis defined by a radius connecting the tube center and impact point.

The materials and construction of the graphite-epoxy tube and flat plate targets were chosen to be representative of potential Space Station truss structures. They were manufactured from unidirectional plies and were constructed with three different layups, two fiber elastic moduli (34M psi and 75M psi), and three thicknesses (nominally 0.07", 0.11", and 0.14"). Candidate coatings for atomic oxygen protection, 2 mil and 6 mil aluminum foil, were bonded to selected tubes for impact testing. Additional tubes, including some made by filament winding, were donated by other companies for comparison purposes.

The results of the impact testing revealed that fiber modulus influenced the magnitude of hypervelocity impact damage to a greater extent than ply orientation. Targets with low modulus (34M psi) fibers exhibited peeling of the surface plies near the impact point while high modulus (75M psi) targets did not peel. Although surface peeling is not expected to significantly affect tube mechanical properties, the 2 mil aluminum coating on low modulus tubes peeled in a similar manner to uncoated tubes. The 6 mil aluminum coating resisted peeling to a greater extent. Larger holes in both walls were created in

the high modulus tubes compared to similar impacts into low modulus targets. Both low and high modulus targets experience approximately the same size of internal delaminations and damage around the impact point and on the second side of tube specimens as revealed by ultrasonic scans. The ultrasonic scans, or C-scans, are non-destructive tests that record the location of internal faults and ply damage greater than 1 mm^2 area. Differences in ply orientation made no notable difference in the overall area of impact induced holes, craters, and C-scan damage.

Many specific correlations were developed from the impact test data to relate hole size, delamination C-scan size, projectile energy, and other variables. A few of the key derivations follow. For tubes with low modulus fibers (34M psi) and 0.07" thick walls, an equation relating projectile energy, E (J), when E is less than 155 J, to combined first and second wall equivalent circular hole diameter, D_{hb} (mm), is:

$$D_{hb} = 1.14\ E^{0.33} - 1.29$$

For E greater than 155 J:

$$D_{hb} = 4.54\ E^{0.33} - 19.5$$

The transition at projectile energies above 155 J to a steeper sloped curve results from the greater damage to the second wall of the tube due to expansion of projectile and target debris behind the first wall. Similar equations for high modulus (75M psi) fiber tubes with 0.07" thick walls were developed. At projectile energies of less than 158 J:

$$D_{hb} = 1.424\ E^{0.33} + 0.034$$

And for E greater than 158 J:

$$D_{hb} = 6.281\ E^{0.33} - 26.22$$

The diameter of the combined ultrasonic C-scan region for both walls, D_{cb} (mm), was correlated for high and low modulus tubes with projectile energy, E (J), projectile diameter, d (mm), and tube wall thickness, t (mm). For (E * t/d) less than 230 J:

$$D_{cb} = 6.31\ (E * t/d)^{0.33} - 5.72$$

And for (E * t/d) greater than 230 J:

$$D_{cb} = 15.5\ (E * t/d)^{0.33} - 61.8$$

These equations imply that a 1 mm orbital debris particle (2.8 g/cc, 9 km/sec) will create a 3.2 mm hole mainly in the first wall of a 0.07" thick, low modulus tube and a 5.6 mm hole in a high modulus tube. The same projectile would create a delamination zone in both walls with a combined diameter of 24 mm.

The truss tubes will experience primarily axial loads on-orbit. An analysis of the critical damage required to cause a space station tube to fail under the ultimate compressive load was completed using a finite element model. It was concluded that a 5.4 in^2 damage area (hole and delamination zone) is required to cause failure of a baseline 0.07" thick, 5m long, low-modulus tube under a 2,100 lb_f axial load. Using the above equations and the meteoroid and debris environment models, it was estimated that a maximum of 5 tubes on the Phase II space station would require replacement over a 30 year lifetime.

Based on this result, it is concluded that regardless of tube layup or fiber modulus, graphite-epoxy tubes for the Space Station will be resilient to failure from hypervelocity impacts. It is suggested that additional finite element modelling and scaled or full-scale buckling tests of damaged graphite-epoxy tubes are warranted to confirm the predicted damage size that will result in tube failure under ultimate load. It is also recommended that damaged tubes be thermally and mechanically cycled to understand if the delamination zone grows under cyclical loading. Crew procedures and non-destructive inspection equipment will need to be developed to identify on-orbit those critically damaged tubes requiring replacement from the many tubes with lesser non-threatening damage.

2.0 Introduction

The primary purposes of this study were to 1) understand what graphite-epoxy tube properties effect the extent of damage from hypervelocity impacts, 2) determine how damage is related to projectile conditions, and 3) provide a preliminary assessment of the failure rate of Space Station struts from hypervelocity impact.

The expected number of impacts on the truss structure from meteoroid and debris particles directly depends on the exposed surface area of the truss. Thus, the total number of impacts will change as the Space Station grows. Section 3.1 describes the proposed evolution of the Space Station through Phase I and Phase II. As explained in Section 3.2, impact induced failure of the truss or degradation of mechanical properties can occur from a number of sources: 1) a single impact, 2) atomic oxygen attack on unprotected surfaces, 3) multiple smaller impacts and delamination of protective surface coating, 4) microcraking following impact, 5) delamination growth, 6) low speed impact, and 7) single impact on a truss tube node. The expected number of impacts also depends on exposure time, orbital altitude, and the attitude of the station. An impact summary on truss elements; a description of the meteoroid, orbital debris, and atomic oxygen environments; and the predicted number of perforations in atomic oxygen protective coatings are also given in Section 3.2.

A brief description of the JSC and NDE ballistic ranges along with the impact test plan is given in Section 3.3. The target parameters studied include fiber modulus, layup ply orientation, wall thickness, surface coatings, and roll-wrap versus filament wound manufacturing technique. Target specimen property data is presented in Section 3.4. Section 3.5 describes the examination and testing procedures applied to the targets prior to and after impacting, including determination of mass/dimensions, measurement of acoustic velocity and modulus, structural compression tests, ultrasonic C-scans, and optical (microscopic) examination and measurement of through-hole and crater dimensions. Properties of the projectiles used in the tests are given in Section 3.6. The flux and number of impacts expected on the truss from equivalent sized meteoroid and debris particles are determined in Section 3.7.

The results of the impact testing are presented in Section 4. Included are sections describing the effects of projectile size and velocity, ply orientation, fiber modulus, surface

coating, target thickness, target shape (tube versus flat plate), projectile obliquity, and tube manufacturing technique on the extent of target damage. A summary of all derived correlations is given in Section 4.9.

Section 5 describes the groundrules and results of the truss failure criteria study. In Section 5.3, the experimentally derived correlations and failure criteria results are applied to predict the lifetime replacement rate of impact damaged truss tubes. Impact induced peeling of the atomic oxygen protective coating is addressed in Section 5.4.

Study conclusions and recommendations are given in Sections 6 and 7, respectively. Appendix A contains a detailed table of all shot data, ordered by shot number (chronological order). The Hercules report on the truss failure criteria study is given in Appendix B. All C-scan and structural test records are contained in Appendices C and D.

3.0 Hypervelocity Impact Test Conditions

This section describes tests conducted during this study including tests made prior to impact, the impact tests themselves, and post-impact testing. The subjects of the testing were graphite-epoxy (G/E) plates and tubes. Tube specimen ply layups and physical properties were selected as representative of typical tubes for the Space Station truss structure. The objective of the testing was to determine if differences in G/E ply layup, fiber elastic modulus, target thickness, and surface coatings affected the amount of damage sustained from high velocity particles. Damage as a function of projectile parameters (size, velocity, impact obliquity angle) was also studied. This data was used to assess the effects of orbital debris and meteoroid impacts on space station truss tubes.

3.1 Space Station Truss Structure

The space station consists of both pressurized and unpressurized elements held together directly or indirectly as a station by the truss assembly element (6). First element launch (FEL) is currently scheduled for January 1994 (5). As depicted in Figure 3-1, FEL involves construction of 8 truss bays inboard of the alpha gimbal joint for the photovoltaic (PV) array and another 3 bays containing the solar power module (SPM). The next flight delivers the remaining truss needed for the second major assembly milestone, man-tended capability (MTC). Figure 3-2 illustrates the MTC station configuration which is achieved after the sixth assembly flight (January 1995). Additional primary support truss structure is not added until after permanently manned capability (PMC) is attained after the tenth assembly flight in October 1995. The PMC station is shown in Figure 3-3. Truss bays are added with supplementary SPMs flown prior to completing the Phase I station after the twentieth assembly flight in November 1996. The phase I station contains 29 truss bays in a single transverse boom as depicted in Figure 3-4.

Growth to the phase II dual-keel station will triple the number of truss elements. As illustrated in Figure 3-5, 18 truss bays are added to form the upper starboard and port keels, 18 are needed for the lower starboard and port keels, and 18 for the upper and lower booms. The solar dynamic power modules require another 10 bays. At completion of the phase II station in May 1998 (7, p.J6-14), a total of 93 truss bays will have been assembled.

The baseline truss structure consists of an erectable series of 5 m cubic assemblies or "bays" which contain longeron, batten, and diagonal elements as given in Figure 3-6 (8). The longerons and battens are 5 m (16.4') long, and diagonals 7 m (23.2'). The truss tubes are approximately 2.1" outside diameter to facilitate handling by EVA crew (corresponding to the nominal grasp of a pressurized suit glove). Each additional bay requires 4 longerons, 4 battens, and 5 diagonals. Graphite-epoxy (G/E) is the baselined material for the tubes due to its low coefficient of thermal expansion (decreasing payload pointing difficulties) and high specific strength and stiffness (reducing mass) relative to aluminum alternatives (9, 10). The tubes are connected by truss nodes, the design of which has not been selected. One particular joint design is a 3.7" diameter spherical aluminum ball with screwed sockets for quick connect posts that interface with end fittings on the tubes (10). The geometry of this design allows 18 mounting points per node for struts and 8 for payloads. This node concept could be either spherical or a 26-sided polyhedron (rhombi-cuboctahedron). Typical phase I space station nodes would join either 5 or 8 struts while phase II nodes would connect 5, 7, 8, or 10 struts (or more with payload mounts, etc.).

The space station orbit is near circular at an inclination of 28.5°. Nominal operating altitude can range from as low as 333 km (180 nm) at solar minimum to as high as 463 km (250 nm) at solar maximum (11). Assembly altitudes as low as 278 km (150 nm) with reboost to assure minimum 90-day orbital lifetime have been allowed in previous program requirements (11), however, this is apparently now under review (12). Maximum altitude is 500 km (270 nm). Station flight mode before the first four assembly flights (September 1994) is in the "arrow mode," where the longitudinal axis of the transverse boom is parallel to the station velocity vector (13, Attachment 3). After attitude control is functional, the normal station flight mode will be in a local vertical-local horizontal orientation with the transverse boom perpendicular to the orbit plane (parallel to the Earth and perpendicular to the velocity vector). The dual keels of the phase II station will be oriented in the local vertical direction.

Station altitude and orientation are important in assessing the vulnerability of the truss structure to possible hazards. Atomic oxygen degradation is more severe at lower altitudes and on forward or ram-facing surfaces (13-17). For instance, at solar minimum the atomic oxygen fluence is two orders of magnitude greater at 300 km altitude than at 500 km. On the other hand, the orbital debris threat lessens at lower altitudes. The

flux of orbital debris larger than 1 mm at 400 km is about 20 percent of the flux at 500 km (18). Truss orientation also affects the number of impacts due to the highly direction nature of orbital debris. The next section describes potential truss threats in more detail.

3.2 Truss Failure Sources

In preparation for hypervelocity impact testing, possible sources leading to failure of the Space Station truss structure were considered (1) including:

1) Hypervelocity Impact. A single impact from a high speed meteoroid or orbital debris particle that is large enough to remove sufficient material to cause the truss element to fail immediately or when it is exposed to a mechanical load.

2) Atomic Oxygen. Degradation from atomic oxygen which causes truss element failure or reduces mechanical property margins below acceptable limits.

3) Multiple Impacts. A number of small impacts from high speed particles that erode, delaminate, or removes a protective coating leading to subsequent failure.

4) Microcracking. Matrix microcracking of the graphite-epoxy which adversely affects thermal expansion characteristics or other mechanical properties of the composite.

5) Delamination Growth. Growth of delamination areas produced by previous damage incidents to unacceptable levels by thermal or mechanical cycling during the lifetime of the truss element.

6) Low Speed Impact. Truss damage or failure from low speed impact during external crew or remote machine activities.

7) Node Impact. Failure of a truss node from hypervelocity impact would result in the effective simultaneous loss of several tubes.

This study will only address truss failure modes induced by meteoroid and orbital debris impacts, including failure due to single hypervelocity impact on a tube (#1) or node

(#2), and the effect of hypervelocity impacts on typical coatings for atomic oxygen protection (#1-3).

3.2.1 Truss and Node Impact Summary

The 5 m long longerons and battens have a surface area of 0.84 m^2 each while the 7 m diagonals have a surface area of 1.2 m^2 each. Phase I space station has approximately 236 5m-struts and 146 7m-struts for a total truss surface area of 225 m^2. Figure 3-7 shows the number and size distribution of impacts from orbital debris and meteoroids. For the 30 year lifetime of the space station truss structure (11, p.3-4), approximately 13 meteoroids and 8 orbital debris particles greater than 1 mm diameter would strike the phase I truss. A 2.7 mm particle is the largest that is likely to hit the truss over 30 years (having a 0.37 probability of no impact, or 2 out 3 chance of striking a strut). Orbital debris and meteoroid no impact probabilities as a function of particle size are given in Table 3-1.

The phase II station truss has approximately 744 longerons and battens, and 465 diagonals with a surface area of 710 m^2. As given in Figure 3-8 and Table 3-2, the phase II truss would be impacted over 30 years by approximately 41 meteoroid and 25 debris particles greater than 1 mm diameter. The largest particle likely to impact a strut on the dual keel station would be 4 mm in diameter (having a 2 out of 3 probability of impact).

Phase I space station has approximately 120 nodes with a surface area of 3.3 m^2 assuming a 9.4 cm diameter spherical joint. Phase II has approximately 372 nodes with a total surface area of 10.3 m^2. Based on the phase II node surface area and assuming as a worse case zero shielding from the truss struts, Table 3-3 lists the number of meteoroid and debris impacts on the phase II truss nodes. Over 30 years, a 1 mm diameter or larger particle is likely to impact a node (2 out of 3 chance of impact). The probability of impact drops to 3 percent for a 3 mm or greater particle. Using an empirical penetration model developed by JSC for aluminum on aluminum impacts (24), an impact by a 3 mm diameter orbital debris particle would create a crater 7 mm deep into an aluminum node, or less than 10 percent of the node diameter (see Table 3-4). The node diameter is estimated to be 5 times greater than the minimum diameter to prevent spall damage from the rear of the node. Although the test plan did not include a study of node

failure, this analysis indicates the damage expected from the worst case impacting particle will not cause complete failure of a truss node (releasing all tubes). Experimental impact tests in a later test phase should be included to confirm this.

3.2.2 Meteoroid Environment

The meteoroid environment in the impact analyses of the previous section used the NASA recommended meteoroid model (19, 25) with an assumed orbital altitude of 500 km. The average near-Earth flux, F_{met} (impacts/year/m^2 surface area), of meteoroids with mass M_{met} (g) and larger is given by the following equations:

for $M_{met} >= 10^{-6}$ g,

$$\mathrm{Log}(F_{met}) = -1.22\ \mathrm{Log}(M_{met}) - 6.911$$

and for $M_{met} < 10^{-6}$ g,

$$\mathrm{Log}(F_{met}) = -0.063\ (\mathrm{Log}(M_{met}))^2 - 1.58\ \mathrm{Log}(M_{met}) - 6.841$$

The meteoroid flux is assumed omnidirectional although recent work (26) indicates directional dependence exists for an orbiting object with a majority of meteoroid impacts on the forward surface as viewed from the orbiter. Earth partially shields space station from meteoroids and the equation used to multiplicatively compensate the meteoroid flux for this effect is:

$$SF = (1 + \cos(\arcsin(R/(R+H))))/2$$

where the shielding factor SF (0.69 at 500 km altitude) depends on the Earth's radius + 100 km atmosphere (R=6478 km) and on station height above atmosphere (H=400 km). Because meteoroids are attracted by the Earth's gravity field, the meteoroid flux is also factored by a Earth defocusing factor, DF (0.97 at 500 km), which depends on the distance from station to the center of Earth in units of Earth's radius, r:

$$DF = 0.568 + (0.432/r)$$

Meteoroids are assumed spherical with a typical density of 0.5 g/cc and relative collisional velocity of 20 km/sec. The probability of no impact, P, is related to the impact flux, surface area A (m^2), and time t (yrs) by:

$$P = \exp(-F_{met} * SF * DF * A * t)$$

3.2.3 Orbital Debris Environment

The calculations in Section 3.2.1 used the 1990's predicted orbital debris flux, F_d, given by:

for debris particles less than 1 cm diameter at 500 km altitude and 30° inclination (18),

$$\text{Log } F_d = -2.52 \text{ Log } D - 5.46$$

and for particles greater than 1 cm,

$$\text{Log } F_d = 0.352 (\text{Log } D)^2 - 1.358 \text{ Log } D - 5.46$$

where F_d is the number of impacts from particles with diameter D (cm) and greater per surface area A (m^2) per year on a randomly oriented surface. The flux of debris at 400 km altitude is lower than at 500 km as indicated by the following equation derived from Figure 3-9:

$$\text{Log } F_d = -2.1 \text{ Log } D - 5.9$$

The total number of debris impacts, N_d, and probability of no impact was calculated using the 500 km flux with the following equations:

$$N = F_d * A * t$$
$$P = \exp(-F_d * A * t)$$

Debris particles smaller than 1 cm are assumed spherical with an average mass density defined as 2.8 g/cc (expected to be the same as aluminum). For 30° inclination orbits, average debris velocity is 9 km/sec.

Debris particles are highly directional, appearing to an orbiting spacecraft to come from directions in a 180° arc centered on the spacecraft's velocity direction (forward direction) and impacting almost entirely within the plane parallel to the Earth (at space station altitude, objects with elevation angles greater than ~10° to local horizontal will enter the atmosphere). The directionality of debris and the fixed orientation of the space station truss means that a greater areal impact density (impacts per area) will occur on forward surfaces of the truss struts. Due to the fixed positions of the struts, the total number of impacts calculated by the above approach using total surface area is an approximation of the actual number of impacts from orbital debris. An integrated debris flux that is corrected for the strut orientation to the debris distribution and flight direction would be slightly lower than calculated above except for struts aligned in the local vertical direction. The directional effect was not included because station attitude changes during assembly from the arrow flight mode (one year) to the nominal operational attitude. However, the effect of this correction on predicted total debris impacts on the truss is expected to be less significant than the effect of station altitude variation from the 500 km debris model. The predicted debris impact total is therefore conservative in that the nominally lower station altitude than 500 km will reduce the actual debris flux.

Shelf-shielding of the truss struts from the directional debris flux will reduce to some extent the exposed area of truss to impact. However, this may not be significant. For instance, only a 0.5° station pitch angle is required to place all longerons on different planes (and thus fully exposed to the planar debris flux).

3.2.4 Atomic Oxygen Attack

Atomic oxygen interactions with organic and some metallic materials in low Earth orbit have resulted in material recession, degradation of optical and thermal coatings, and conversion of conductive coatings to nonconductive oxides. In general, materials containing only carbon, hydrogen, oxygen, and nitrogen have high reaction rates. Silicones and fluorinated polymers such as Teflon are basically stable. Metals, except for silver and osmium, resist atomic oxygen erosion. The primary effects are found on the forward or ram-facing surfaces of susceptible materials (13-17). Given an average annual atomic oxygen fluence of 1.09E21 atoms/cm^2 and a 2.6E-24 cm^3/atom graphite-epoxy reaction

efficiency, unprotected ram-facing space station truss surfaces will experience a 0.012" material recession rate over a 11-year solar cycle. Approximately 50 percent of the wall thickness for a 0.066" thick graphite-epoxy tube would be lost over the 30 year lifetime of the station. Thus, space station graphite-epoxy truss tubes will be protected by a suitable coating from atomic oxygen attack and ultraviolet radiation degradation.

Candidate coatings include aluminum, teflon, and conductive ceramic overlays. Teflon is a marginal coating material because studies suggest that teflon suffers from ultraviolet embrittlement (10, p.3-128A) and because it does not prevent large thermal gradients around the tube circumference. Ceramic coating materials may lack ruggedness. Other candidate coatings include thin aluminum foil (0.002"-0.006") bonded to the tube, and vapor or sputter deposited aluminum and ceramic (alumina/silica) films. An aluminum foil surface would be treated (anodized) for thermal control and to reduce sun glare. A 0.006" aluminum coating contributes over 10 percent to the overall areal density (mass/unit area) of a 0.066" graphite-epoxy/coating combination.

Because the truss will be subjected to numerous meteoroid and debris impacts, the coating must resist impact induced delamination or tearing as well as erosion from the cumulative small particle flux over the 30 year space station lifetime. Coatings must also be resistant to handling damage, low-velocity impacts, and any possible deleterious effects from translation of or operations from the mobile servicing center. Two coatings, 0.002" and 0.006" bonded aluminum as described in Section 3.4, were tested in this study to determine their hypervelocity impact characteristics.

3.2.5 Predicted Perforations in Truss Protective Coatings

Tables 3-5 through 3-8 indicate the number of perforations expected from meteoroids and debris for soft and hard aluminum tube coatings of two different thicknesses. Results are summarized below:

Aluminum	Thickness	Perforation Flux (#/m^2/yr) Meteoroids	Debris	Combined	Total Perforations over 30-year Lifetime on ea: 5-m Tube	7-m Tube	Perforation Density (#/cm^2)
Soft Aluminum:							
Al 1100-0	0.002"	39.6	13.5	53.1	1,334	1,868	0.159
	0.006"	5.6	1.1	6.7	168	236	0.020
Hard Aluminum:							
Al 2024-T3	0.002"	19.9	5.1	25.0	629	881	0.075
	0.006"	2.3	0.4	2.7	69	97	0.008

The particle size that creates a crater deep enough in the aluminum coating to expose graphite-epoxy was calculated from an empirical penetration equation for aluminum-on-aluminum hypervelocity impacts developed by Cour-Palais and essentially duplicated by Rockwell in Apollo era testing (24, p.265). The flux of orbital debris and meteoroids having that critical size and greater is determined from appropriate environmental models (18,19). These calculations indicate that a hard alloy can decrease the perforation flux by 50 percent over a soft aluminum coating, while thicker aluminum has an even more pronounced effect on the number of perforations.

Tables 3-5 through 3-8 also show results of a preliminary analysis indicating that there is little likelihood that a large enough portion of a typical aluminum coating would be removed by hypervelocity impacts to result in tube failure from atomic oxygen attack. (The only exception is the thin, soft aluminum coating.) As described in Section 5, a 2.6 cm diameter area must be removed from a 5m long strut to produce buckling failure under design loads. The time required for meteoroids and debris to expose a cumulative area equivalent to the failure criterion (5.4 cm^2 damage area) was calculated (assuming no peeling or delamination of the coating). 32 years was the minimum time calculated for the 2 mil Al 1100-0 coating, after which <u>all</u> tubes are predicted to have cumulative exposed areas equal to the failure criterion. Given the inherent uncertainity in these calculated predictions, it appears that a 2 mil <u>soft</u> aluminum coating would provide inadequate atomic oxygen protection unless impact damage was repaired sometime during the 30 year lifetime.

3.2.6 Matrix Microcracking

Matrix microcracking of the composite G/E truss tubes is a concern because of its potential adverse effect on the thermal stability of the tubes (28). The large difference in thermal expansion between the graphite fibers and the epoxy matrix is a major contributor to matrix microcracking in composite structures (29,30). The truss tubes will go through approximately 175,000 thermal cycles during the space station lifetime due to its motion around the Earth. Depending on the coating selected for the tubes, the thermal cycle will be on the order of -100°F to 70°F for tubes periodically exposed to the sun. Microcracking within graphite/epoxy composites can shift the coefficient of thermal expansion because the matrix operates independently of the fibers. Reportedly, microcracking does not significantly change axial mechanical properties of composite tubes (28). Over the long term, microcracking could effect the pointing accuracy of the space station. However, because hypervelocity impact effects are localized, impact induced microcracking is considered a secondary contributor in comparison to thermal cycling induced microcracking, and was therefore not included in this study phase.

3.3 Impact Test Plan

The test program objective was to study certain aspects of hypervelocity impact failure mechanisms in target specimens representative of space station truss tubes. In particular, the tests were designed to develop a better understanding of hypervelocity impact damage as a function of graphite-epoxy ply orientation, fiber moduli, tube thickness, surface coatings, and projectile parameters (size, velocity, impact obliquity angle). Target and projectile properties are presented in Section 3.4 and 3.6, respectively.

Impact tests were carried out in ballistic test laboratories at NDE Technology, Inc. in Torrance California and at the NASA Johnson Space Center hypervelocity impact research laboratory (HIRL). Most of the impact tests at NDE were conducted with a two-stage light gas gun capable of launching 4.3 mm diameter sabot/particles to 7 km/sec.

JSC's HIRL contains two light gas launchers. The small light gas gun has a 1.7 mm launch tube bore and is capable of launching 5 mg nylon slugs (L/D = 1) at 8.5 km/sec. The medium light gas gun has a 4.3 mm bore and is capable of launching saboted 1/8" aluminum spheres (45 mg) at over 7 km/sec and 73 mg nylon slugs (L/D = 1) at 7.4 km/sec.

Additional details of the capabilities for these two launchers are described in another report (20). Only the medium light gas gun was used in this study. A valuable diagnostic tool at JSC's HIRL is a Model 330 IR, high-speed framing camera manufactured by the Cordin Company. This rotating-mirror camera operates at one million frames per second with a 5 nanosecond exposure time (21). In past studies it has been used to determine ejecta (particles released from front surface of target) and spall (particles produced from target back surface) velocities and dispersion angles, and to cross-check projectile velocity (22, 23). In this study, it was used to verify that a shot was "clean", i.e., that just the projectile and no secondary particles (such as fragments of sabot, shear plate, or gun powder debris) hit the target, or to provide clues to the problem if the shot is not clean.

The mass, dimensions, and sonic velocity of all test samples were measured and ultrasonic C-scans recorded prior to impact. The longitudinal elastic modulus in compression for selected tube specimens was determined in structural tests. Hypervelocity impact testing was coordinated with NDE and JSC to determine: (1) the response of low modulus (6T) and high modulus (11T) tubes to a range of particle sizes, (2) the response of all tube layups to the same particle impact conditions, (3) the response of different surface coatings to the same impact conditions, (4) the effect of tube thickness, (5) the response of flat plates to the same particle impact conditions used on the tube with the corresponding layup and moduli, (6) the response as a function of projectile obliquity. The extent of target damage was determined optically and ultrasonically. Pre-impact and post-impact testing is described in more detail in Section 3.5.

3.4 Target Specimens

Graphite-epoxy (G/E) tubes and plates for this study were procured from Amoco in three different ply layups, two fiber elastic moduli, and three tube wall thicknesses as given in Table 3-9. Specifications for the Amoco G/E specimens called for the resin system to be selected from the MY720/DDS family (Amoco elected to use a specially formulated ERLX-1916 resin system) which would have a final cure temperature of 300°F for a minimum of 1 hour. Both flat and tubular specimens were cured using the same cure schedule (time, temperature, and pressure). The Amoco tubes and flat plates were constructed from unidirectional prepreg tape containing approximately 60 percent by volume graphite carbon fibers. The tubes were manufactured by wrapping unidirectional prepregs on a

2" diameter mandrel at specified angles to the longitudinal axis. There was a 1" overlap for every 2 layers to ensure a constant wall thickness around the tube circumference (2). Therefore, due to the ply overlap, the tubes were effectively 2 plies thicker than the corresponding flat plate targets. Tube wall thickness tolerance was reportedly maintained at +/-5% (2).

Each target was assigned a serial number. The 6T series of tubes contain low elastic modulus fibers (34M psi) in a (+10°,-10°,+30°,-30°,+10°,-10°,+10°,-10°,+30°,-30°,+10°,-10°) ply orientation. This arrangement of plies will be abbreviated as (+/-10,+/-30,+/-10)r, where the "r" stands for repetition of the layup, or simply as a (10,30,10) laminate. For the tube specimens, the ply angle is referenced to the tube's longitudinal axis. (Fibers of 0° plies are aligned down the longitudinal axis, fibers in 90° plies would be aligned around the tube's circumference.) Two tubes, 6s-T-1 and 6s-T-2, were constructed in a (+/-10, +/-30,+/-10) symmetric layup pattern, or in long form: (+10°,-10°,+30°,-30°,+10°,+10°,-10°, +10°,-30°,+30°,-10°,+10°). As will be discussed in Section 4, no significant difference was found in the impact response characteristics between symmetric and repeating layups. The same (10,30,10) symmetric layup with low modulus fibers was used in the 6F series of flat plates.

To test potential atomic oxygen protection coatings, thin aluminum foil (fully strain-hardened alloy 1145-H19) was bonded to several of the 6T series tubes. 2 mil thick Al 1145 was bonded to three tubes (6-T-4, 6-T-5, 6-T-6) while 6 mil thick Al 1145 was successfully bonded to two tubes (6-T-6 and 6-T-9) in a vacuum bag process held at 250-350°F for one hour (3). 2 mil coatings were applied by hand while a machine was used to apply the 6 mil aluminum. One tube, 6-T-8, was inadvertently crushed during the machine application process. Cracks, 180° apart, formed down the tube's entire length (6"), a quarter turn from the initial aluminum application point. For all tubes, the aluminum coating was chromic acid anodized on both sides before application to the tubes. Adhesive film, 3-5 mil thick uncured, was used to bond the aluminum to the G/E tube. A modified epoxy adhesive similar to American Cyanamid adhesive FM-73 was used (0.015 g/cm^2 @ 0.13 mm thick). JSC structures coordinated the coating application effort with Boeing (Seattle, Washington) actually applying the coatings (3). Three other tubes (6-T-10, 6-T-11, and 6-T-12) were turned over to JSC structures for testing applications of other atomic oxygen and thermal protection coatings such as aluminum by an ion assisted vacuum

deposition process. Only the aluminum bonded tubes (6-T-4 through 6-T-9) were included in the hypervelocity impact testing of coated tubes.

High modulus fibers (75M psi) were used in the 11T and 11F series of tubes and plates. Both symmetric and repeating (10,30,10) tube layups were constructed, differentiated by 11sT and 11T serial number designations, respectively.

Low modulus fibers in a (+/-80,+/-30,+/-10) layup were used in the 9F and 9T target series, while high modulus fibers with the same layup were used in the 12F and 12T series. Amoco replaced two faulty 9F plates with four 9sF replacements. Tubes with both symmetric and repeating (80,30,10) layups were constructed, designated 9sT and 9T, respectively. Only one 12T tube (12-T-2) remained after pre-impact structural tests because 12-T-1 failed under a 13,600 lb_f compressive load.

Plates and tubes with low modulus fibers in a (+/-45,+/-10,+/-45) layup were included in the test plan (10F and 10T series). Only flat plate specimens with this layup and high modulus fibers were available (13-F-1 and 13-F-2) since the tube specimens were rejected due to manufacturing problems.

Thick-wall tube targets were produced in the (10,30,10) layup with low modulus fiber laminae. The 7T series tubes were nominally 18 plies thick (excluding a 2 ply overlap) and the 8T series tubes were nominally 24 plies thick (excluding a 2 ply overlap).

Other manufacturers donated tubes including Morton Thiokol, McDonnell Douglas, and United Technologies (Sikorsky Division). The Morton Thiokol tubes represented two different layups with high modulus fibers (75M psi). They were constructed in a roll-wrap process using a high pressure cure cycle. A filament wound technique, using approximately 1/8" wide rovings, was used to produce the McDonnell Douglas tubes. These tubes had the same layup (10,30,10) and fiber modulus as the 6T series Amoco tubes. Both the Morton Thiokol and McDonnell Douglas tubes were included in the test program. Because the Sikorsky tubes were longer (48"), they were reserved for a later phase of the hypervelocity impact program.

3.5 Pre- and Post-Impact Target Examination

Before impact testing, targets were weighed, sonic velocity measured, and ultrasonically inspected to reveal defects (>1 mm^2). Compressive load tests were applied to a selected number of tube specimens prior to impact testing to produce a baseline deflection/load curve. Following the impact tests, the targets were reweighed, optically inspected to determine the extent of damage (hole and crater sizes, area of surface ply delamination), and ultrasonically scanned to reveal the extent of internal delamination and laminae damage. The following sections describe the pre- and post-impact testing procedures in more detail.

3.5.1 Mass and Dimensions

Prior to impact and structural testing, the targets were weighed several times on a Sartorius balance (0.00001 g precision) and dimensions measured using micrometer and caliper. Average values are given in Table 3-10. Some targets were occasionally trimmed to better fit the impact chamber. Therefore, for all JSC shots, targets were reweighed immediately prior to impact and directly after impact using a Ohaus Galaxy 1200 balance (accurate to 0.01 g). These masses are documented in the detailed shot data given in Appendix A.

3.5.2 Acoustic Velocity and Modulus

Prior to impacting, the sonic velocity in the principal axes for all targets was determined on an ultrasonic tester by Mr. Ike Spiker (Lockheed) as given in Table 3-11. Flat plate sonic velocities were determined in all three orthogonal axes. For plates, the longitudinal speed is referenced to the 0° ply orientation, radial speed is in the 90° direction, and TTT for through-the-thickness speed. Tube sonic velocities were determined in the longitudinal direction but not in the radial (circumferential) direction due to probe limitations. Sonic elastic modulus was calculated from the product of density and square of sonic velocity (with appropriate conversion factors). Calculated elastic moduli are listed in Table 3-11. An average density of 1.55 g/cc was used for low modulus fiber composites and 1.63 g/cc for high modulus fiber composites (4).

3.5.3 Structural Tests

Structural tests were conducted prior to impact testing to:

1) Measure the longitudinal modulus of elasticity in compression on representative tubes with 3 different ply layups and 2 fiber moduli.

2) Determine the difference in measured compressive modulus between tubes with the same layup and fiber modulus.

3) Determine the variability in measured compressive modulus by repeated tests on the same tube.

The elastic modulus for selected 6" long tube specimens was determined in compressive load tests conducted by JSC structures. Loads up to 80 percent of the tubes predicted ultimate compressive strength were applied (Table 3-12). An Instron strain gage extensometer was used to measure resulting tube deflection. Elastic modulus was calculated from the standard equation (27): $E = P * L/(A * \delta)$ for axial loaded members which relates modulus of elasticity, E, to load, P, rod or gage length, L, cross-sectional area, $A = \pi * (r_o^2 - r_i^2)$, and deflection, δ. As given in Table 3-12, 11 tests with several repetitions each for verification purposes were conducted on 10 tubes. Table 3-13 summarizes the results of all structural tests. The actual records of deflection versus load for these tests are contained in Appendix D. For all tests, the extensometer was zeroed at 2.1" gage length and recorded as a positive signal for decreasing length.

The first test involved 10 repetitive loading and unloading cycles on a low modulus 10,30,10 layup tube (6-T-1) to test the repeatability of the procedure. The standard deviation of the elastic modulus calculated from these tests was under 4 percent as given in Table 3-13. The next test involved 8 repetitions on the same tube to determine the effect of strain gage position. The extensometer was placed at the 0° longitudinal reference on the tube and half-load (7500 lbs) was applied up and down. This sequence was repeated after rotating the extensometer position 45° around the tube until the full tube circumference was covered. The standard deviation of the calculated modulus of elasticity was less than 6 percent. The purpose of the third test on 6-T-3 was to determine the difference in modulus for a similar tube (6-T-1). As given in Table 3-13, the difference

was small (2 percent). The test also indicated that locked heads on the load cell reduced end damage to the specimens and other test problems. Later tests used locked heads and tested each specimen at least twice, usually with the extensometer in the 0° and 180° positions.

The moduli of elasticity in compression determined in these structural tests are given in Table 3-11 with the sonic velocity derived moduli and the vendor supplied moduli. These moduli usually compare within a few percent with each other. No significant difference in the elastic modulus of symmetric versus repeating ply orientations was found.

In a special test on a rejected tube (13-T-2), a circular hole was physically drilled into one wall of the tube, and compressively tested. Subsequent test runs were made after widening the hole. As summarized by the following results, a 1/4" hole was not detectable by measured compression deflections or tube modulus. 1/2" and 1" diameter holes were detectable but the compression tests suffered from several problems such as hysteresis in the loading and unloading curves, wider differences (as hole size increased) in the deflection curves when the strain gage was positioned over the hole or 180° across from the hole, and tube bending (especially with a 1" hole) causing some end damage to the tube.

Tube: 13-T-2

Hole Size (in)	Calc. Modulus (M psi)
0	12.2
0.25	12.1
0.5	9.6
1.0	7.8

Of the ten tube specimens structurally tested, two were broken during the tests. 11-T-1 failed prematurely after the tube shifted within the load cell due to non-parallel tube ends and load cell heads. The tube was split its entire length in a spiral 30° angle. Another tube, 12-T-1, failed at 13,600 lbs due to compressive force overload. The tube was crushed completely around its circumference in a W-pattern. During hypervelocity impact testing, the remaining 8 tubes were impacted at least once, and 4 were impacted multiple times due to the limited number of tube specimens. Those impacted only once were held in reserve for possible follow-up compressive testing to ascertain the effect of combined hole/delamination on compressive stiffness.

As described in Section 4, hypervelocity impacts into thin graphite/epoxy targets create a hole 2-4 times the size of the impacting particle, with an area of delamination and ply disruption surrounding the hole that is 10-20 times the projectile size. It was the original intent of the structural tests to determine the effect of the hole and delaminated zone combination on some mechanical properties of the tubes. A compressive test after impact could be used to relate in a crude way the effect of delamination on axial rigidity (EA). For instance, from the standard equation for deflection of an axial loaded member:

$$\delta = P/E\ (L_{ud}/A_{ud} + L_d/A_d)$$

where, δ is the overall deflection of the tube across the strain gage, P is the compressive load, E is the elastic modulus (assumed constant), L_{ud} is the total axial length of the undamaged portion of the tube across the strain gage (which can be measured from the C-scan record), A_{ud} is the cross-sectional area ($\pi * [r_o^2 - r_i^2]$) in the undamaged region, L_d is the axial length of the damaged region (measured from the C-scan record), the strain gage length $L = L_d + L_{ud}$, and A_d is the cross-sectional area of the damaged region. Thus, the damaged zone cross-sectional area is:

$$A_d = (L_d\ P\ A_{ud})/(E\ \delta\ A_{ud} - L_{ud}\ P)$$

The combined hole and delamination damage area is:

$$A_{hd} = A_{ud} - A_d$$

Assuming a circular damage area, the equivalent diameter of the hole and delamination zone that represents true loss of tube cross-sectional area is:

$$D_{hd} = 2\ [(A_{ud} - A_d)/\pi]^{0.5}$$

Substituting for A_d, the above equation becomes:

$$D_{hd} = 2\ \{[A_{ud}^2\ \delta\ E - L\ P\ A_{ud}]/[\pi\ (\delta\ E\ A_{ud} - L_{ud}\ P)]\}^{0.5}$$

Thus, the combined circular hole/delamination zone that represents loss of cross-sectional area can be found from known and measured quantities. This method results in a crude

estimate of the equivalent hole size for a combination of hole and delamination from compression tests. The method does not give any information on bending rigidity (EI) of the damaged tube which is more important in assessing the critical buckling load. The four tube specimens having only one impact hole (6-T-1, 6s-T-1, 9-T-1, and 10-T-1) will however be made available, along with their C-scan records, for additional structural testing as deemed appropriate. Other tests to consider include thermal cycle and axial (compression) loading tests to determine if repeated thermal and mechanical loading will result in flaw growth within the delamination zone, and perhaps compression tests on a full length (5 or 7 m) tube with a 6" tube spliced into its middle. The end pieces and splices would need to have the same EI as the undamaged portion of the 6" tube specimen. Although the difficulties of working with short 6" tube lengths would make a splice test extremely challenging, such a test has the advantage of directly measuring the buckling load and failure mode of damaged tubes.

3.5.4 C-Scans

Ultrasonic scans of the tube and flat plate test specimens were conducted before and after the impact tests by a University of Texas group under the direction of Dr. Ching H. Yew using a Automation Industries M90 Reflectoscope and US 450A Series Laboratory Scanner. This ultrasonic scanner resolves defects of 1 mm^2 or greater, and records them as a blank area on the C-scan record. C-scan records are contained in Appendix C.

Plate scans used through transmission while tube scans used the pulse echo scanning mode. Tube scans were composites of ~0.19" wide longitudinal strips around the tube (36 in all). Delamination areas were measured directly from the C-scan records of post-impact targets. There was a one-to-one relationship between C-scan dimensions and physical dimensions for the plates. While the length of each tube was the same as the C-scan length, the circumference of the tube was not exactly the same as the width of the scan, necessitating a small correction factor for this dimension (varied for each scan, usually 0.95-1.05). Actual C-scan measurements will be given in Section 4.

3.5.5 Impact Damage Measurements

The projectiles used in this study produced a through hole, usually a defined crater, and in some cases peeling and break off of surface plies. Dimensions of the through hole,

crater, and surface peelings were determined by optical microscope on 10x or 25x magnification as appropriate, or by 8x power lupe with integral scale. Actual values will be discussed in Section 4.

3.6 Projectiles

Aluminum 2024-T4 spheres (density 2.796 g/cc) with diameters of 1/16", 3/32", and 1/8" were used for the major part of the impact tests. Aluminum projectiles were individually weighed and launched.

Because of preliminary difficulties in acquiring certain required small-diameter aluminum projectiles for this study, glass was chosen as a practical substitute because its density is nearly the same as aluminum's. The glass spherical projectiles used in the study were procured from Duke Scientific Corporation (Palo Alto, California) in five nominal diameters: 0.55 mm, 0.756 mm, 0.938 mm, 1.067 mm, and 2.144 mm. Standard deviations were advertised as 5.3%, 3.0%, 6.0%, 4.3%, and 4.6%, respectively, for the 1 g sample sizes procured. However, it was found that a fraction of each sample actually resembled the next smaller size category in weight and size, and apparently was introduced as a contaminate into the sample vials. In addition, a fraction of each sample contained projectiles noticeably oblong in shape. As necessary, off-nominal projectiles were screened and discarded. The glass projectiles were made of standard soda-lime glass with a density of 2.45 and softening temperature of 720°C. The 0.938 mm diameter and larger glass projectiles were often observed on high speed camera films of test shots at JSC to break in-half. Although the NDE ballistic test laboratory did not have similar diagnostic capability, evidence of glass projectile break-up was also evident on returned targets. Shot data with known or suspected glass projectile breakup problems was not used in the test correlations discussed in Section 4. The aluminum projectiles used in the study did not fragment before impacting the target.

In an effort to determine a particle size that would completely break a tube, a 4.4 mm diameter x 4.4 long nylon cylinder (73 mg) was projected against a 6T series tube (0.064" thick, 34M psi fiber modulus, [10,30,10]s layup). This particle represented the largest projectile the JSC gun laboratory was capable of launching. As discussed in Section 4, this particle did not succeed in breaking the tube specimen.

3.7 Meteoroid and Orbital Debris Flux with Equivalent Size to Test Projectiles

The projectiles used in the impact test program generally represent a range of the largest particle sizes expected to hit the phase I space station truss. The flux of meteoroids and debris with the same diameter as the test projectiles is given in Table 3-14. The mass of the test projectiles is essentially equal to an equivalent size debris particle although the velocity of the test projectiles (<7.5 km/sec) was generally less than the average debris velocity (9 km/sec). The energies of given diameter debris (average velocity 9 km/sec, density 2.8 g/cc) and meteoroid (average velocity 20 km/sec, density 0.5 g/cc) particles are essentially the same. As given in Table 3-14, over 30 years the phase I truss is likely to sustain approximately 5 impacts from particles with a diameter equal to or greater than the 1/16" (1.59 mm) projectiles and only a single impact from a 3/32" (2.38 mm) diameter or greater particle. There is only a 1 in 5 chance in 30 years that the phase I truss tubes would be impacted by a particle as large as the largest (4.4 mm) used in this study.

Figure 3-1. Space Station First Element Launch (FEL) (Ref.6)

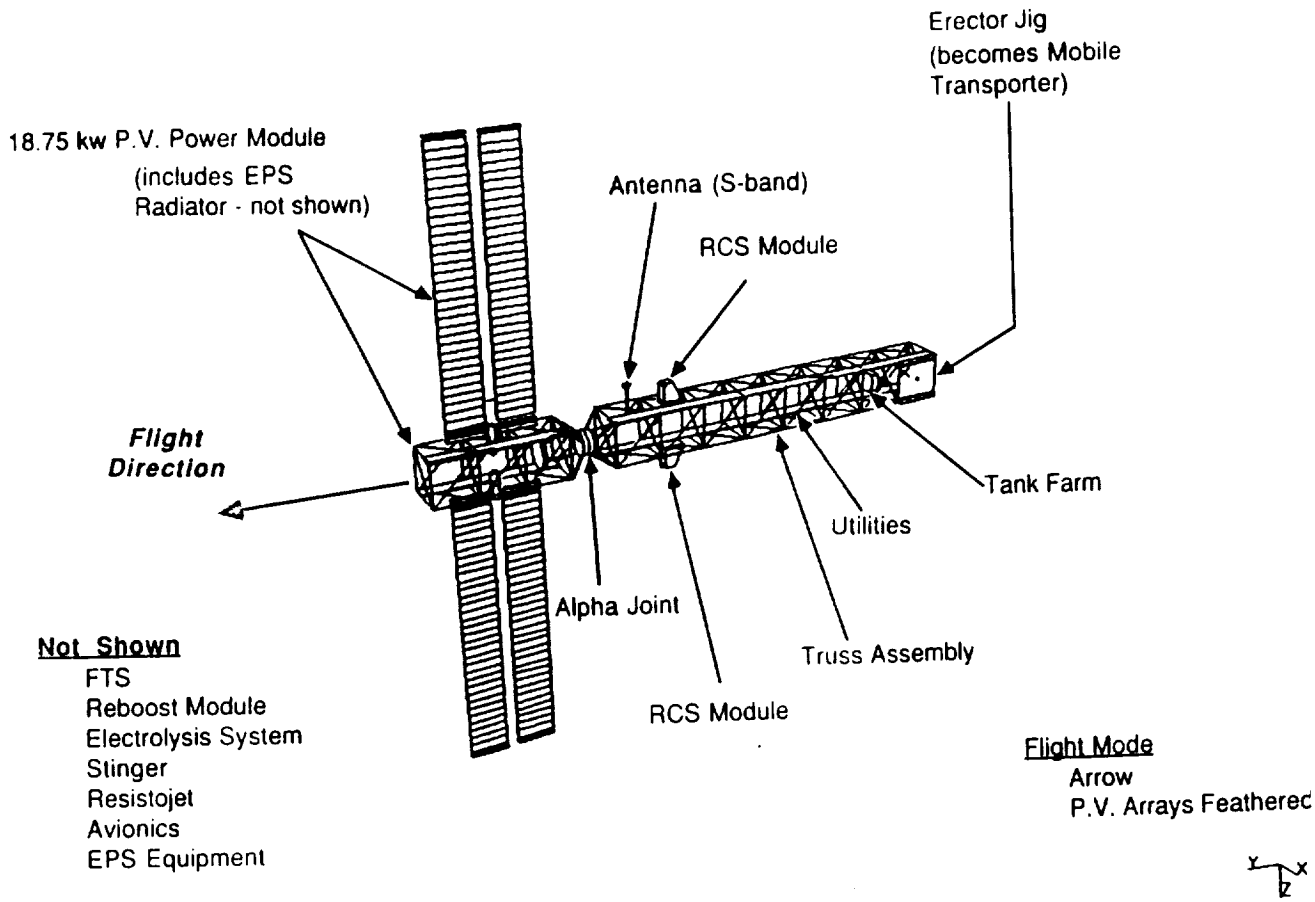

Figure 3-2. Man-Tended Capability (MTC) Space Station (Ref.6)

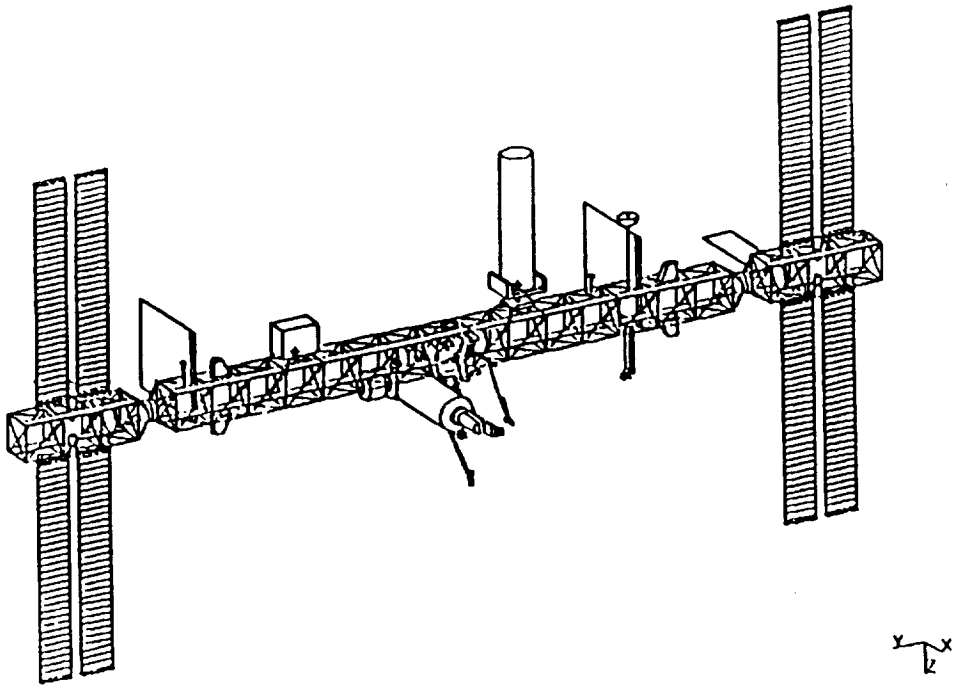

Figure 3-3. Permanently Manned Capability (PMC) Space Station (Ref.6)

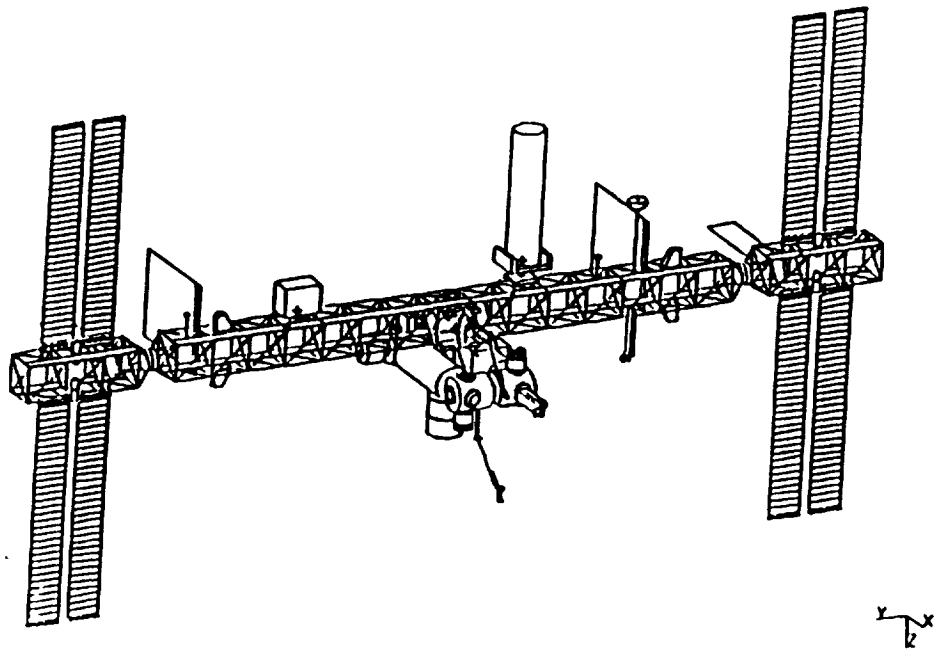

Figure 3-4. Phase I Space Station (Ref.6)

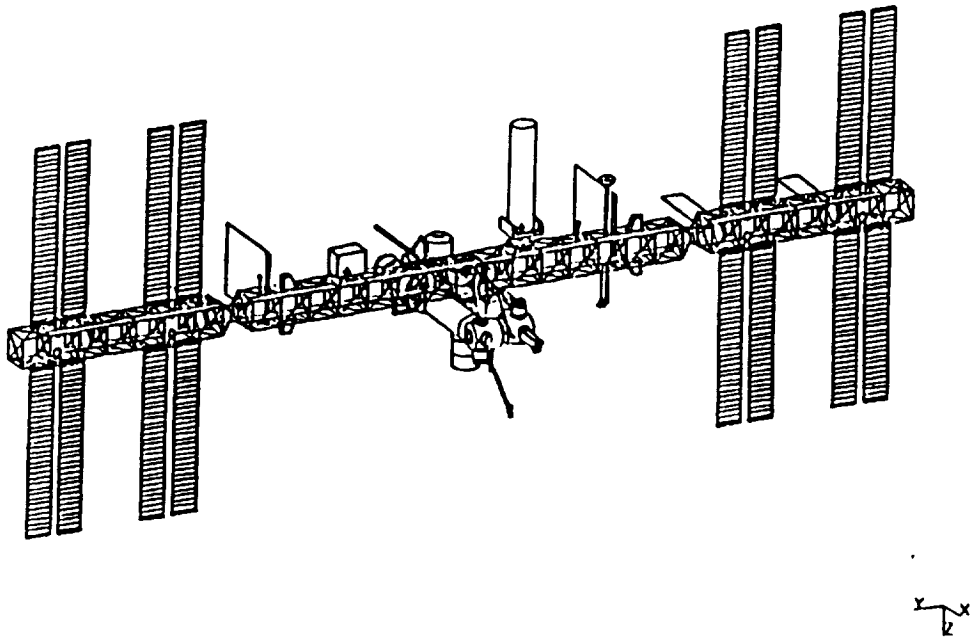

Figure 3-5. Phase II Space Station (Ref.6)

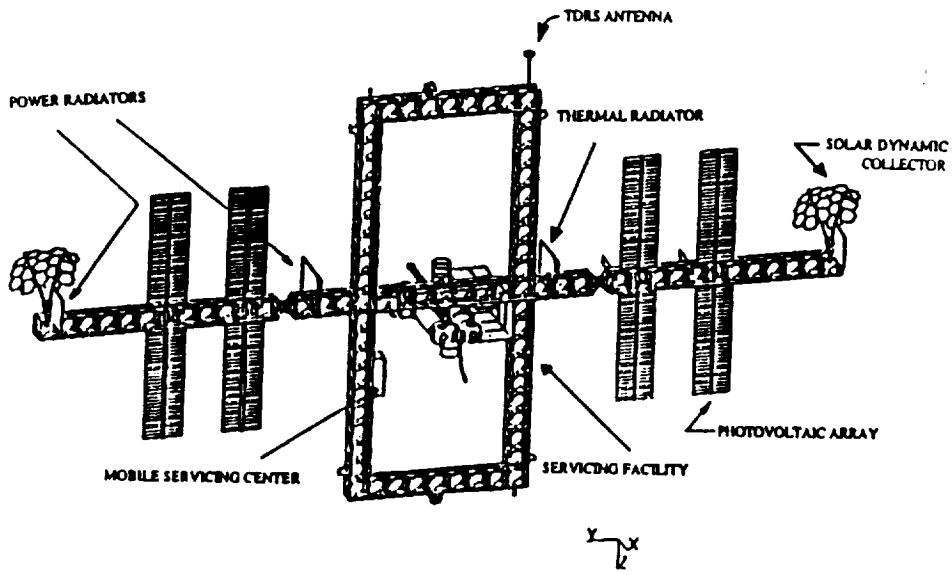

Figure 3-6. Baseline 5m Erectable Truss Structure (Ref. 8)

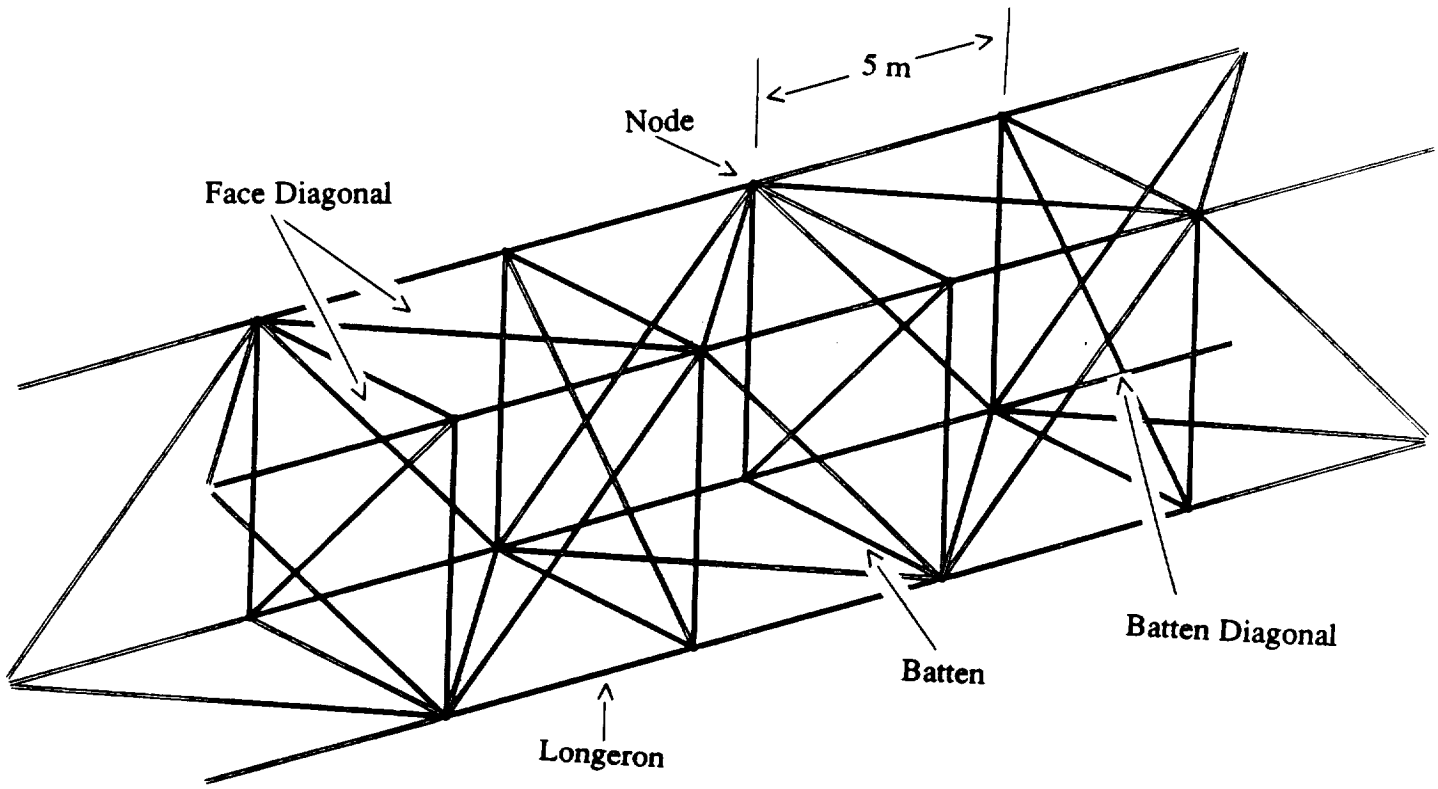

Figure 3-7. Meteoroid and Debris Impacts on Phase I Truss Tubes

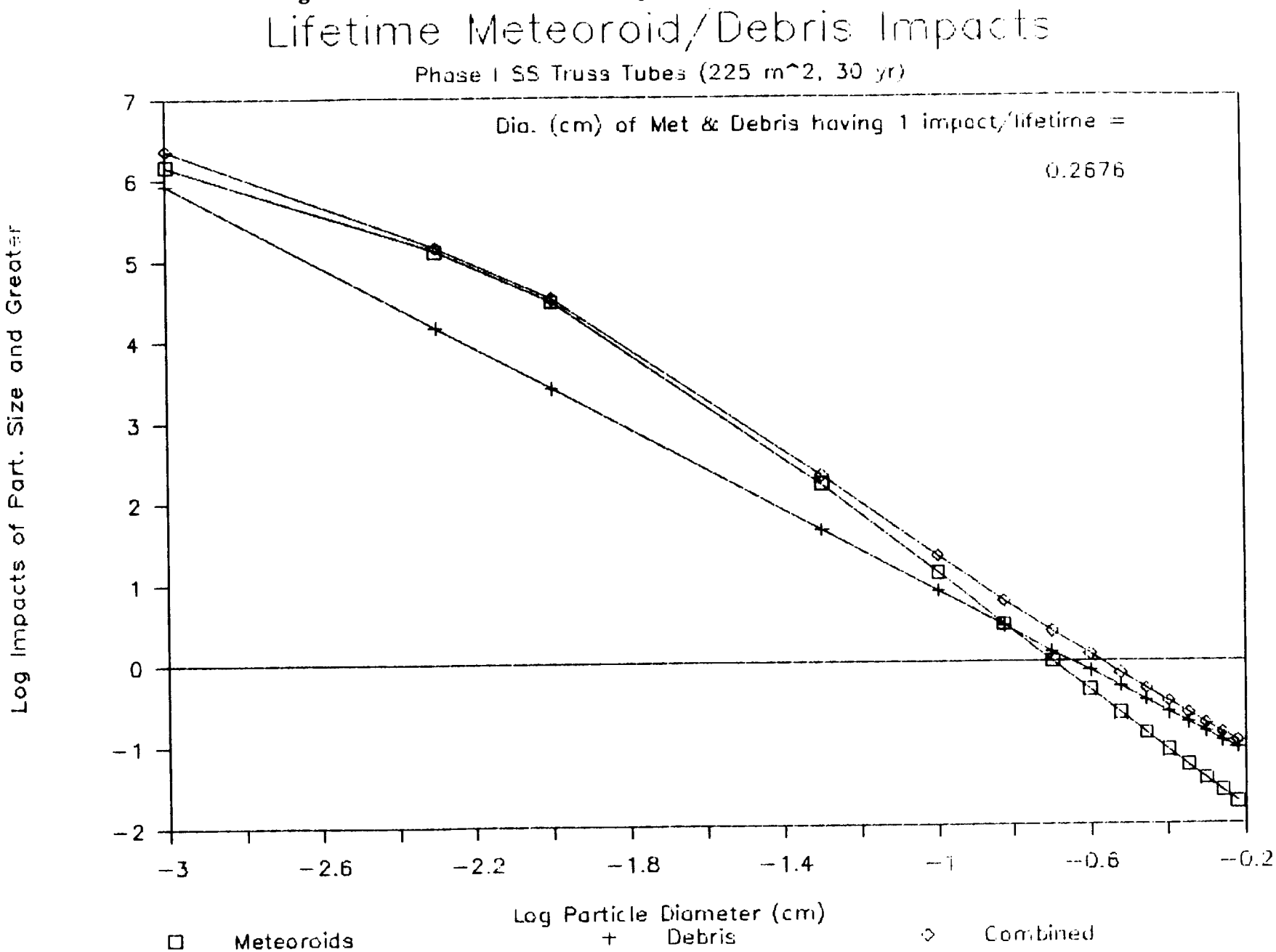

Figure 3-8. Meteoroid and Debris Impacts on Phase II Truss Tubes

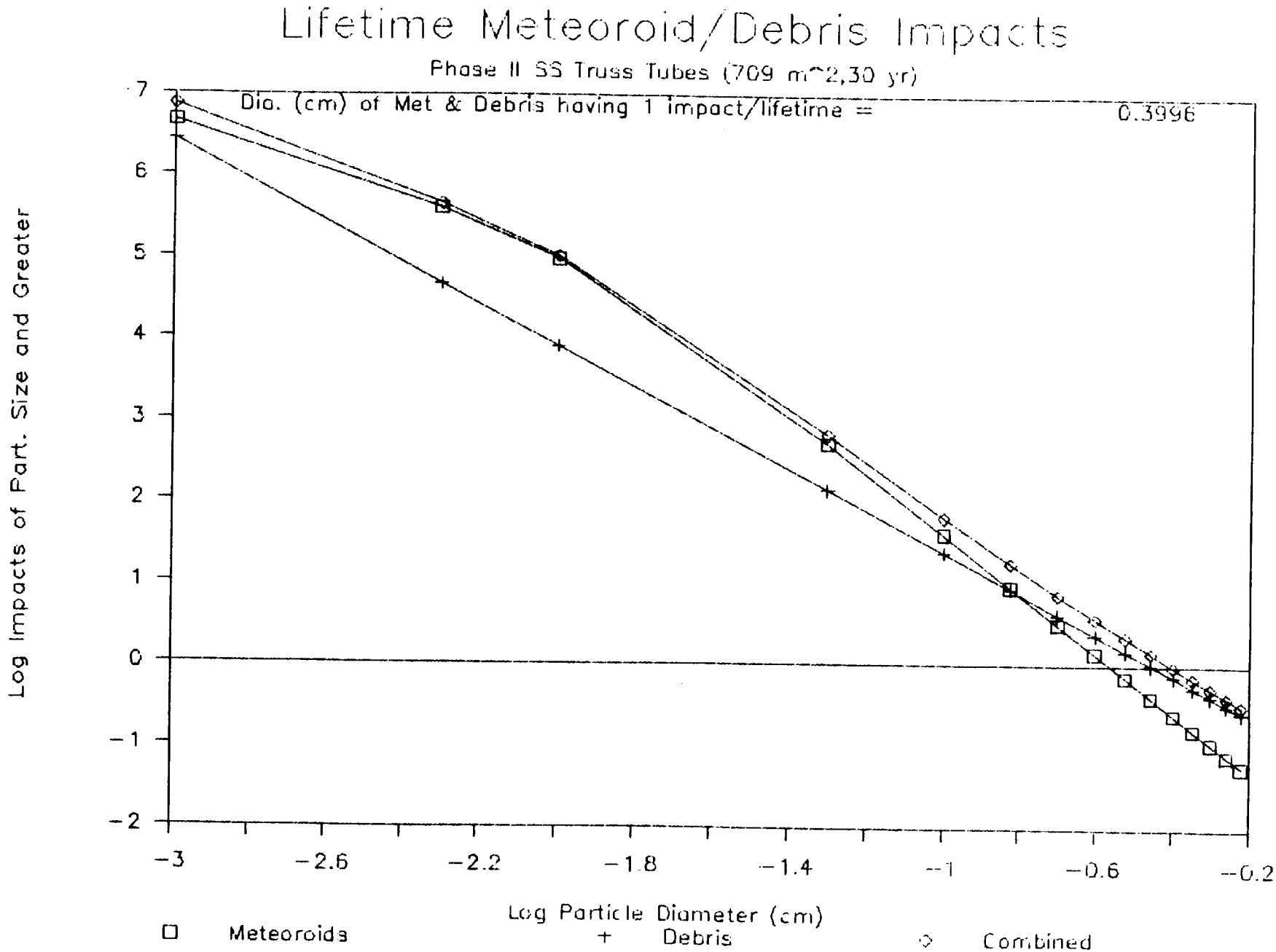

Figure 3-9. Meteoroid and Orbital Debris Flux (Ref.18)

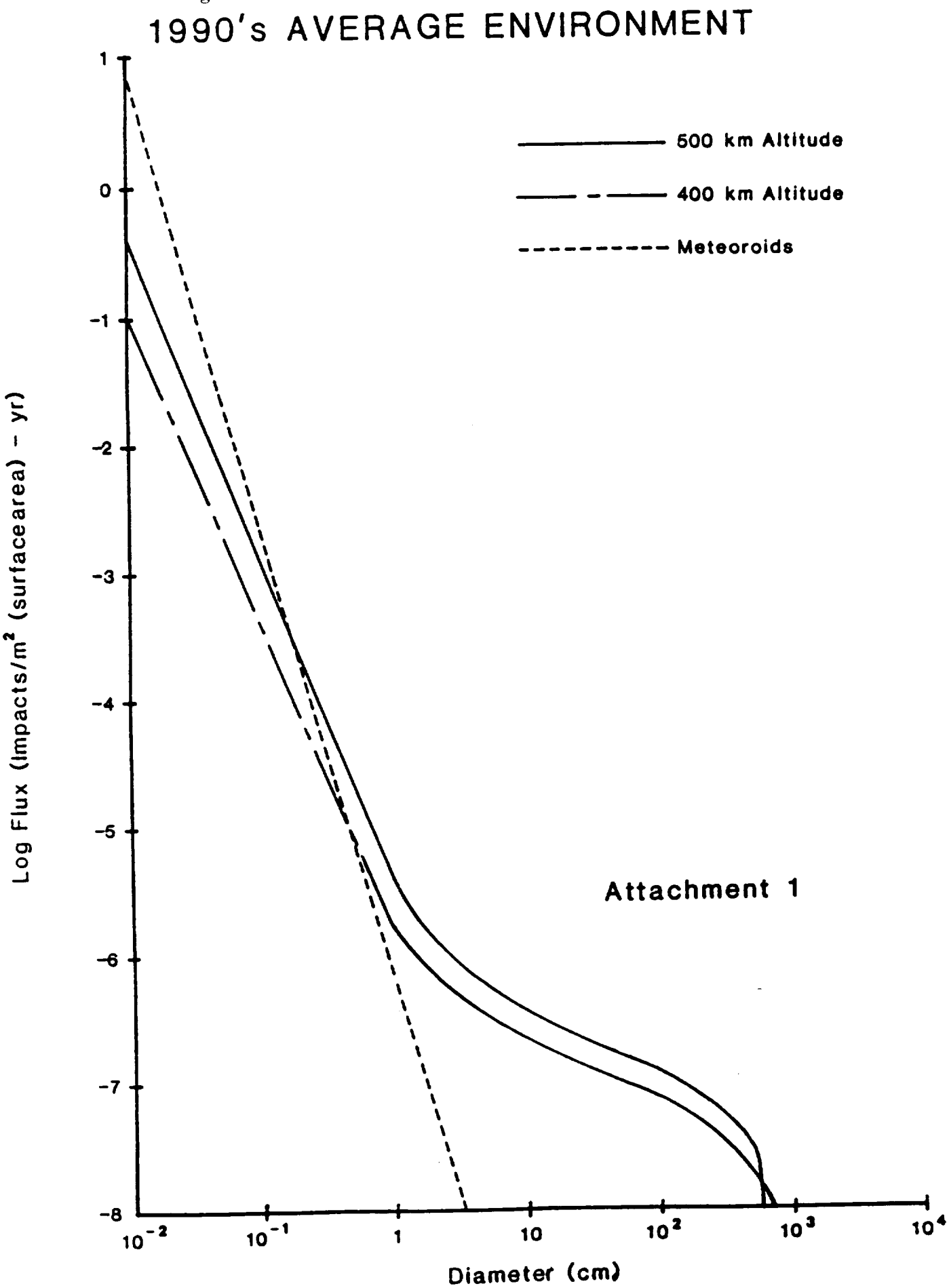

Table 3-1. Orbital Debris and Meteoroid Impacts on Phase I Space Station Tubes

Meteoroid density (g/cc)	0.5		
Debris density (g/cc)	2.8		
Ave. meteoroid velocity (km)	20		
Ave. debris velocity (km/s)	9.3		
Strut Diameter (in)	2.1	(cm)	5.334
Longeron/Batten Length (m)	5	SA (m^2)	0.838
Diagonal Length (m)	7	SA (m^2)	0.184
Number Bays	29		
Number Longerons & Battens	236	SA (m^2)	197.7
Number Diagonals	146	SA (m^2)	26.9
Truss area (m^2)	224.6		
Earth's radius (km)	6378.145		
Station orbital altitude (km)	500		
Earth defocusing factor	0.968596		
Earth shielding factor	0.688024		
Station Lifetime (yrs)	30		

Particle Diameter (mm)	Particle Mass Met. (g)	Particle Mass Debris (g)	Particle Flux Met. (#/m^2-yr)	Particle Flux Debris	Number Impacts of given Diameter and greater Met. (#/30yr life)	Number Impacts Debris	Number Impacts Total	Probability of No Impact Met.	Probability of No Impact Deb.	Probability of No Impact Total
0.01	2.62E-10	1.47E-09	2.11E+02	1.26E+02	1.47E+06	8.48E+05	2.31E+06	0	0	0
0.05	3.27E-08	1.83E-07	1.85E+01	2.18E+00	1.28E+05	1.47E+04	1.43E+05	0	0	0
0.1	2.62E-07	1.47E-06	4.37E+00	3.80E-01	3.03E+04	2.56E+03	3.28E+04	0	0	0
0.5	3.27E-05	1.83E-04	2.35E-02	6.59E-03	1.63E+02	4.44E+01	2.07E+02	0	0	0
1.0	2.62E-04	1.47E-03	1.86E-03	1.15E-03	1.29E+01	7.74E+00	2.06E+01	0	0	0
1.5	8.84E-04	4.95E-03	4.22E-04	4.13E-04	2.93E+00	2.79E+00	5.71E+00	0.05	0.06	0.00
2.0	2.09E-03	1.17E-02	1.47E-04	2.00E-04	1.02E+00	1.35E+00	2.37E+00	0.36	0.26	0.09
2.5	4.09E-03	2.29E-02	6.51E-05	1.14E-04	4.51E-01	7.69E-01	1.22E+00	0.64	0.46	0.30
3.0	7.07E-03	3.96E-02	3.34E-05	7.21E-05	2.31E-01	4.86E-01	7.17E-01	0.79	0.62	0.49
3.5	1.12E-02	6.29E-02	1.90E-05	4.89E-05	1.32E-01	3.29E-01	4.61E-01	0.88	0.72	0.63
4.0	1.68E-02	9.38E-02	1.16E-05	3.49E-05	8.08E-02	2.35E-01	3.16E-01	0.92	0.79	0.73
4.5	2.39E-02	1.34E-01	7.57E-06	2.59E-05	5.25E-02	1.75E-01	2.27E-01	0.95	0.84	0.80
5.0	3.27E-02	1.83E-01	5.15E-06	1.99E-05	3.57E-02	1.34E-01	1.70E-01	0.96	0.87	0.84
5.5	4.36E-02	2.44E-01	3.63E-06	1.56E-05	2.52E-02	1.05E-01	1.31E-01	0.98	0.90	0.88
6.0	5.65E-02	3.17E-01	2.64E-06	1.26E-05	1.83E-02	8.47E-02	1.03E-01	0.98	0.92	0.90
6.5	7.19E-02	4.03E-01	1.97E-06	1.03E-05	1.37E-02	6.92E-02	8.29E-02	0.99	0.93	0.92

Table 3-2. Orbital Debris & Meteoroid Impacts on Phase II Space Station Tubes

Meteoroid density (g/cc)	0.5		
Debris density (g/cc)	2.8		
Ave. meteoroid velocity (km)	20		
Ave. debris velocity (km/s)	9.3		
Strut Diameter (in)	2.1	(cm)	5.334
Longeron/Batten Length (m)	5	SA (m^2)	0.838
Diagonal Length (m)	7	SA (m^2)	0.184
Number Bays	93		
Number Longerons & Battens	744	SA (m^2)	623.4
Number Diagonals	465	SA (m^2)	85.7
Truss area (m^2)	709.0		
Earth's radius (km)	6378.145		
Station orbital altitude (km)	500		
Earth defocusing factor	0.968596		
Earth shielding factor	0.687152		
Station Lifetime (yrs)	30		

Particle Diameter (mm)	Particle Mass Met. (g)	Particle Mass Debris (g)	Particle Flux Met. (#/m^2-yr)	Particle Flux Debris	Number Impacts of given Diameter and greater Met. (#/30yr life)	Number Impacts Debris	Number Impacts Total	Probability of No Impact Met.	Probability of No Impact Deb.	Probability of No Impact Total
0.01	2.62E-10	1.47E-09	2.11E+02	1.26E+02	4.62E+06	2.68E+06	7.30E+06	0	0	0
0.05	3.27E-08	1.83E-07	1.85E+01	2.18E+00	4.04E+05	4.64E+04	4.51E+05	0	0	0
0.1	2.62E-07	1.47E-06	4.37E+00	3.80E-01	9.55E+04	8.09E+03	1.04E+05	0	0	0
0.5	3.27E-05	1.83E-04	2.35E-02	6.59E-03	5.15E+02	1.40E+02	6.55E+02	0	0	0
1.0	2.62E-04	1.47E-03	1.86E-03	1.15E-03	4.07E+01	2.44E+01	6.51E+01	0	0	0
1.5	8.84E-04	4.95E-03	4.22E-04	4.13E-04	9.23E+00	8.79E+00	1.80E+01	0.00	0.00	0.00
2.0	2.09E-03	1.17E-02	1.47E-04	2.00E-04	3.22E+00	4.26E+00	7.48E+00	0.04	0.01	0.00
2.5	4.09E-03	2.29E-02	6.51E-05	1.14E-04	1.42E+00	2.43E+00	3.85E+00	0.24	0.09	0.02
3.0	7.07E-03	3.96E-02	3.34E-05	7.21E-05	7.30E-01	1.53E+00	2.26E+00	0.48	0.22	0.10
3.5	1.12E-02	6.29E-02	1.90E-05	4.89E-05	4.16E-01	1.04E+00	1.45E+00	0.66	0.35	0.23
4.0	1.68E-02	9.38E-02	1.16E-05	3.49E-05	2.55E-01	7.42E-01	9.97E-01	0.78	0.48	0.37
4.5	2.39E-02	1.34E-01	7.57E-06	2.59E-05	1.66E-01	5.52E-01	7.17E-01	0.85	0.58	0.49
5.0	3.27E-02	1.83E-01	5.15E-06	1.99E-05	1.13E-01	4.23E-01	5.36E-01	0.89	0.66	0.59
5.5	4.36E-02	2.44E-01	3.63E-06	1.56E-05	7.95E-02	3.33E-01	4.12E-01	0.92	0.72	0.66
6.0	5.65E-02	3.17E-01	2.64E-06	1.26E-05	5.78E-02	2.67E-01	3.25E-01	0.94	0.77	0.72
6.5	7.19E-02	4.03E-01	1.97E-06	1.03E-05	4.31E-02	2.18E-01	2.62E-01	0.96	0.80	0.77
7.0	8.98E-02	5.03E-01	1.50E-06	8.52E-06	3.29E-02	1.81E-01	2.14E-01	0.97	0.83	0.81
7.5	1.10E-01	6.19E-01	1.17E-06	7.16E-06	2.55E-02	1.52E-01	1.78E-01	0.97	0.86	0.84
8.0	1.34E-01	7.51E-01	9.22E-07	6.08E-06	2.02E-02	1.29E-01	1.50E-01	0.98	0.88	0.86
8.5	1.61E-01	9.00E-01	7.38E-07	5.22E-06	1.62E-02	1.11E-01	1.27E-01	0.98	0.89	0.88
9.0	1.91E-01	1.07E+00	5.99E-07	4.52E-06	1.31E-02	9.62E-02	1.09E-01	0.99	0.91	0.90
9.5	2.24E-01	1.26E+00	4.91E-07	3.95E-06	1.08E-02	8.39E-02	9.47E-02	0.99	0.92	0.91
10.0	2.62E-01	1.47E+00	4.07E-07	3.47E-06	8.91E-03	7.38E-02	8.27E-02	0.99	0.93	0.92

Table 3-3. Orbital Debris & Meteoroid Impacts on Phase II Space Station Nodes

Meteoroid density (g/cc)	0.5		
Debris density (g/cc)	2.8		
Ave. meteoroid velocity (km)	20		
Ave. debris velocity (km/s)	9.3		
Node Diameter (in)	3.7	(cm)	9.398
Node Area (m^2)	0.028		
Number Bays	93		
Number Nodes/Bay	4		
Number Nodes	372		
Truss area (m^2)	10.3		
Earth's radius (km)	6378.145		
Station orbital altitude (km)	500		
Earth defocusing factor	0.968596		
Earth shielding factor	0.668024		
Station Lifetime (yrs)	30		

Particle Diameter (mm)	Particle Mass Met. (g)	Particle Mass Debris (g)	Particle Flux Met. ($\#/m^2$-yr)	Particle Flux Debris	Number Impacts of given Diameter and greater Met. (#/30yr life)	Number Impacts Debris	Number Impacts Total	Probability of No Impact Met.	Probability of No Impact Deb.	Probability of No Impact Total
0.01	2.62E-10	1.47E-09	2.11E+02	1.26E+02	6.54E+04	3.90E+04	1.04E+05	0	0	0
0.05	3.27E-08	1.83E-07	1.85E+01	2.18E+00	5.72E+03	6.75E+02	6.40E+03	0	0	0
0.1	2.62E-07	1.47E-06	4.37E+00	3.80E-01	1.35E+03	1.18E+02	1.47E+03	0	0	0
0.5	3.27E-05	1.83E-04	2.35E-02	6.59E-03	7.29E+00	2.04E+00	9.33E+00	0	0	0
1.0	2.62E-04	1.47E-03	1.86E-03	1.15E-03	5.76E-01	3.56E-01	9.32E-01	0.55	0.70	0.39
1.5	8.84E-04	4.95E-03	4.22E-04	4.13E-04	1.31E-01	1.28E-01	2.59E-01	0.88	0.88	0.77
2.0	2.09E-03	1.17E-02	1.47E-04	2.00E-04	4.56E-02	6.20E-02	1.08E-01	0.96	0.94	0.90
2.5	4.09E-03	2.29E-02	6.51E-05	1.14E-04	2.01E-02	3.53E-02	5.55E-02	0.98	0.97	0.95
3.0	7.07E-03	3.96E-02	3.34E-05	7.21E-05	1.03E-02	2.23E-02	3.27E-02	0.99	0.98	0.97
3.5	1.12E-02	6.29E-02	1.90E-05	4.89E-05	5.88E-03	1.51E-02	2.10E-02	0.99	0.98	0.98
4.0	1.68E-02	9.38E-02	1.16E-05	3.49E-05	3.61E-03	1.08E-02	1.44E-02	1.00	0.99	0.99

Table 3-4. Truss Node Failure Analysis

NODE PROPERTIES

Type	Al 2024-T3	
Diameter (in)	3.7	9.398 (cm)
Density (g/cc)	2.712	
Brinell Hardness	145	

	Meteoroid	Debris
Particle Density (g/cc)	0.5	2.8
Particle Velocity (km/s)	20	9.3
Particle Min. Diameter (cm)	0.1	0.1
Particle Max. Diameter (cm)	0.3	0.3
Min. Crater Depth (in)	0.055	0.079
Max. Crater Depth (in)	0.186	0.263
(calc. from Cour-Palais penetration equation, Ref.24, p.265)		
Min. No Spall Depth (in)	0.166	0.235
Max. No Spall Depth (in)	0.557	0.788
Ratio of Min. No Spall Depth/Node Diameter	0.045	0.064
Ratio of Max. No Spall Depth/Node Diameter	0.150	0.213

Table 3-5. Predicted Perforations in Tube Coating (0.002" Al 2024-T3)

Coating Properties:				
Type	Al 2024-T3			
Thickness (in)	0.002	0.00508 (cm)		
Density (g/cc)	2.712			
Brinell Hardness	145			
Space Station Properties:			Meteoroid Flux Parameters:	
Operational Lifetime (yr)	30		Earth's radius (km)	6378.145
			Station orbital alt. (km)	500
Truss Properties:			Earth defocusing factor	0.968596
Tube thickness (in)	0.066	1.6764 (mm)	Earth shielding factor	0.688024
Tube O.D. (in)	2.1	5.334 (cm)		
Surface Area of 5m Long Struts (m^2)		0.84		
Surface Area of 7m Long Struts (m^2)		1.17		
Hole Diameter to Fail 5m Tube (cm)		2.6		
Atomic Oxygen Properties:				
Fluence on ram-facing surfaces (atoms/cm^2-yr)		1.091E+21		
G/E Reactivity Rate (cm^3/atom)		2.600E-24		
Recession Rate (cm/yr)		2.836E-03	0.001116 (in/yr)	
(for uncoated ram-facing surfaces)				
Percent of Unprotected Tube Thickness Erroded During Lifetime			50.8%	
		Meteoroid	Debris	
Particle Density (g/cc)		0.5	2.8	
Particle Velocity (km/s)		20	9.3	
Particle Critical Diameter (cm)		0.0049	0.0036	
above which crater depth exceeds coating thickness (from Cour-Palais, Ref.24, p.265)				
Particle Mass (g)		3.05E-08	6.60E-08	
Particle Energy (J)		0.006	0.003	
Particle Flux (#/m^2-yr)		19.9	5.14	
with critical diameter and greater that will perforate coating.				
Total Perforation Flux (#/m^2-yr)		25.02		
Lifetime Coating Perforations on 5m Strut		629		
Lifetime Coating Perforations on 7m Strut		881		
Lifetime Perforation Density (#/cm^2)		0.075		
Max. Size Particle On 5m Strut In Lifetime:				
Particle Mass (g)		2.18E-05	2.15E-05	
Particle Diameter (cm)		0.0437	0.0245	
Average Particle Dia (cm)		0.024	0.014	
Average Dia. G/E Exposed (cm)		0.059	0.046	
(assume hemispherical crater and no surface delamination)				
Exposed G/E area on 5m struts (cm^2/yr)		0.031	0.007	
Critical Area (cm^2)		5.40		
per 5m truss tube that must be exposed to atomic oxygen before failure possible				
Total Exposed area on 5m struts (cm^2/yr)		0.038		
Number of years before critical graphite/epoxy area is uncovered on 5m struts		143		

Table 3-6. Predicted Perforations in Tube Coating (0.006" Al 2024-T3)

Coating Properties:				
Type	Al 2024-T3			
Thickness (in)	0.006	0.01524 (cm)		
Density (g/cc)	2.712			
Brinell Hardness	145			
Space Station Properties:			Meteoroid Flux Parameters:	
Operational Lifetime (yr)	30		Earth's radius (km)	6378.145
			Station orbital alt. (km)	500
Truss Properties:			Earth defocusing factor	0.968596
Tube thickness (in)	0.066	1.6764 (mm)	Earth shielding factor	0.688024
Tube O.D. (in)	2.1	5.334 (cm)		
Surface Area of 5m Long Struts (m^2)		0.84		
Surface Area of 7m Long Struts (m^2)		1.17		
Hole Diameter to Fail 5m Tube (cm)		2.6		
Atomic Oxygen Properties:				
Fluence on ram-facing surfaces (atoms/cm^2-yr)		1.091E+21		
G/E Reactivity Rate (cm^3/atom)		2.600E-24		
Recession Rate (cm/yr)		2.836E-03	0.001116 (in/yr)	
(for uncoated ram-facing surfaces)				
Percent of Unprotected Tube Thickness Erroded During Lifetime			50.8%	
		Meteoroid	Debris	
Particle Density (g/cc)		0.5	2.8	
Particle Velocity (km/s)		20	9.3	
Particle Critical Diameter (cm)		0.0133	0.0097	
above which crater depth exceeds coating thickness (from Cour-Palais, Ref.24, p.265)				
Particle Mass (g)		6.10E-07	1.32E-06	
Particle Energy (J)		0.122	0.057	
Particle Flux (#/m^2-yr)		2.33	0.415	
with critical diameter and greater that will perforate coating.				
Total Perforation Flux (#/m^2-yr)		2.75		
Lifetime Coating Perforations on 5m Strut		69		
Lifetime Coating Perforations on 7m Strut		97		
Lifetime Perforation Density (#/cm^2)		0.0082		
Max. Size Particle On 5m Strut In Lifetime:				
Particle Mass (g)		2.18E-05	2.15E-05	
Particle Diameter (cm)		0.0437	0.0245	
Average Particle Dia (cm)		0.028	0.017	
Average Dia. G/E Exposed (cm)		0.071	0.057	
(assume hemispherical crater and no surface delamination)				
Exposed G/E area on 5m struts (cm^2/yr)		0.005	0.001	
Critical Area (cm^2)		5.40		
per 5m truss tube that must be exposed to atomic oxygen before failure possible				
Total Exposed area on 5m struts (cm^2/yr)		0.006		
Number of years before critical graphite/epoxy area is uncovered on 5m struts		902		

Table 3-7. Predicted Perforations in Tube Coating (0.002" Al 1100-0)

Coating Properties:				
Type	Al 1100-0			
Thickness (in)	0.002	0.00508 (cm)		
Density (g/cc)	2.712			
Brinell Hardness	27			
Space Station Properties:			Meteoroid Flux Parameters:	
Operational Lifetime (yr)	30		Earth's radius (km)	6378.145
			Station orbital alt. (km)	500
Truss Properties:			Earth defocusing factor	0.968596
Tube thickness (in)	0.066	1.6764 (mm)	Earth shielding factor	0.688024
Tube O.D. (in)	2.1	5.334 (cm)		
Surface Area of 5m Long Struts (m^2)		0.84		
Surface Area of 7m Long Struts (m^2)		1.17		
Hole Diameter to Fail 5m Tube (cm)		2.6		
Atomic Oxygen Properties:				
Fluence on ram-facing surfaces (atoms/cm^2-yr)		1.091E+21		
G/E Reactivity Rate (cm^3/atom)		2.600E-24		
Recession Rate (cm/yr)		2.836E-03	0.001116 (in/yr)	
(for uncoated ram-facing surfaces)				
Percent of Unprotected Tube Thickness Erroded During Lifetime			50.8%	
		Meteoroid	Debris	
Particle Density (g/cc)		0.5	2.8	
Particle Velocity (km/s)		20	9.3	
Particle Critical Diameter (cm)		0.0033	0.0024	
above which crater depth exceeds coating thickness (from Cour-Palais, Ref.24, p.265)				
Particle Mass (g)		9.69E-09	2.10E-08	
Particle Energy (J)		0.002	0.001	
Particle Flux (#/m^2-yr)		39.6	13.5	
with critical diameter and greater that will perforate coating.				
Total Perforation Flux (#/m^2-yr)		53.09		
Lifetime Coating Perforations on 5m Strut		1334		
Lifetime Coating Perforations on 7m Strut		1868		
Lifetime Perforation Density (#/cm^2)		0.159		
Max. Size Particle On 5m Strut In Lifetime:				
Particle Mass (g)		2.18E-05	2.15E-05	
Particle Diameter (cm)		0.0437	0.0245	
Average Particle Dia (cm)		0.023	0.013	
Average Dia. G/E Exposed (cm)		0.087	0.067	
(assume hemispherical crater and no surface delamination)				
Exposed G/E area on 5m struts (cm^2/yr)		0.132	0.040	
Critical Area (cm^2)		5.40		
per 5m truss tube that must be exposed to atomic oxygen before failure possible				
Total Exposed area on 5m struts (cm^2/yr)		0.171		
Number of years before critical		32		
graphite/epoxy area is uncovered on 5m struts				

Table 3-8. Predicted Perforations in Tube Coating (0.006" Al 1100-0)

Coating Properties:				
Type	Al 1100-0			
Thickness (in)	0.006	0.01524 (cm)		
Density (g/cc)	2.712			
Brinell Hardness	27			
Space Station Properties:			Meteoroid Flux Parameters:	
Operational Lifetime (yr)	30		Earth's radius (km)	6378.145
			Station orbital alt. (km)	500
Truss Properties:			Earth defocusing factor	0.968596
Tube thickness (in)	0.066	1.6764 (mm)	Earth shielding factor	0.688024
Tube O.D. (in)	2.1	5.334 (cm)		
Surface Area of 5m Long Struts (m^2)		0.84		
Surface Area of 7m Long Struts (m^2)		1.17		
Hole Diameter to Fail 5m Tube (cm)		2.6		
Atomic Oxygen Properties:				
Fluence on ram-facing surfaces (atoms/cm^2-yr)		1.091E+21		
G/E Reactivity Rate (cm^3/atom)		2.600E-24		
Recession Rate (cm/yr)		2.836E-03	0.001116 (in/yr)	
(for uncoated ram-facing surfaces)				
Percent of Unprotected Tube Thickness Erroded During Lifetime			50.8%	
		Meteoroid	Debris	
Particle Density (g/cc)		0.5	2.8	
Particle Velocity (km/s)		20	9.3	
Particle Critical Diameter (cm)		0.0090	0.0066	
above which crater depth exceeds coating thickness (from Cour-Palais, Ref.24, p.265)				
Particle Mass (g)		1.94E-07	4.20E-07	
Particle Energy (J)		0.039	0.018	
Particle Flux (#/m^2-yr)		5.61	1.09	
with critical diameter and greater that will perforate coating.				
Total Perforation Flux (#/m^2-yr)		6.70		
Lifetime Coating Perforations on 5m Strut		168		
Lifetime Coating Perforations on 7m Strut		236		
Lifetime Perforation Density (#/cm^2)		0.020		
Max. Size Particle On 5m Strut In Lifetime:				
Particle Mass (g)		2.18E-05	2.15E-05	
Particle Diameter (cm)		0.0437	0.0245	
Average Particle Dia (cm)		0.026	0.016	
Average Dia. G/E Exposed (cm)		0.099	0.078	
(assume hemispherical crater and no surface delamination)				
Exposed G/E area on 5m struts (cm^2/yr)		0.024	0.004	
Critical Area (cm^2)		5.40		
per 5m truss tube that must be exposed to atomic oxygen before failure possible				
Total Exposed area on 5m struts (cm^2/yr)		0.028		
Number of years before critical graphite/epoxy area is uncovered on 5m struts		190		

Table 3-9. Graphite-Epoxy Tube and Plate Characteristics

Target Serial Number	Vendor	Quan.	Len. (in)	Fiber Modulus (M psi)	Specimen Shape	Ply Orientation	Nominal Thick-ness (in)	Coating	Tube Manufact-uring Technique
6F1,2	Amoco	2	6	34	Flat	(+/-10,+/-30,+/-10)s	0.066	Bare	
6T1,2,3	Amoco	3	6	34	Tube	(+/-10,+/-30,+/-10)r	0.077	Bare	Roll Wrap
11F1,2	Amoco	2	6	75	Flat	(+/-10,+/-30,+/-10)s	0.066	Bare	
11T2,3,4	Amoco	3	6	75	Tube	(+/-10,+/-30,+/-10)r	0.077	Bare	Roll Wrap
6T4,5,6	Amoco	3	6	34	Tube	(+/-10,+/-30,+/-10)r	0.081	0.002" Al bonded	Roll Wrap
6T7,8,9	Amoco	2	6	34	Tube	(+/-10,+/-30,+/-10)r	0.089	0.006" Al bonded	Roll Wrap
6T10,11,12	Amoco	3	6	34	Tube	(+/-10,+/-30,+/-10)r	0.077	Al, Ion Assisted Vacuum Deposited (IVAD'ized)	Roll Wrap
9F1,2	Amoco	0	6	34	Flat	(+/-80,+/-30,+/-10)r	0.066	Bare	
9T1,2	Amoco	2	6	34	Tube	(+/-80,+/-30,+/-10)r	0.077	Bare	Roll Wrap
12F1,2	Amoco	2	6	75	Flat	(+/-80,+/-30,+/-10)s	0.066	Bare	
12T2	Amoco	1	6	75	Tube	(+/-80,+/-30,+/-10)r	0.077	Bare	Roll Wrap
10F1,2	Amoco	2	6	34	Flat	(+/-45,+/-10,+/-45)s	0.066	Bare	
10T1,2	Amoco	2	6	34	Tube	(+/-45,+/-10,+/-45)r	0.077	Bare	Roll Wrap
13F1,2	Amoco	2	6	75	Flat	(+/-45,+/-10,+/-45)s	0.066	Bare	
13T1,2	Amoco	0	6	75	Tube	(+/-45,+/-10,+/-45)r	0.077	Bare	Roll Wrap
7T1,2,3,4	Amoco	4	6	34	Tube	(+/-10,+/-30,+/-10)3r	0.110	Bare	Roll Wrap
8T1,2	Amoco	2	6	34	Tube	(+/-10,+/-30,+/-10)4r	0.143	Bare	Roll Wrap
6sT1,2	Amoco	2	6	34	Tube	(+/-10,+/-30,+/-10)s	0.077	Bare	Roll Wrap
11sT1,2	Amoco	2	6	75	Tube	(+/-10,+/-30,+/-10)s	0.077	Bare	Roll Wrap
9sT1,2	Amoco	2	6	34	Tube	(+/-80,+/-30,+/-10)s	0.077	Bare	Roll Wrap
9sF1,2,3,4	Amoco	4	6	34	Flat	(+/-80,+/-30,+/-10)s	0.066	Bare	
	Plate Total	--- 14							
	Tube Total	31							
	Total	45							
MT-1,2,3	Morton Thiokol	3	6	75	Tube	(+/-45,0,0,0,0)s	0.066	Bare	Roll Wrap
MT-4,5,6	Morton Thiokol	3	6	75	Tube	(+/-45,0,+/-15,0)s	0.066	Bare	Roll Wrap
MD-1,2	McDonnell Douglas	2	6	34	Tube	(+/-10,+/-30,+/-10)s	0.066	Bare	Tape Wound (Filament Wound)
UT-1	United Technology (Sikorsky Div.)	1	48	47.5	Tube	(+/-45,(0)5,-/+45)s	0.06	Bare	Roll Wrap
UT-2	United Technology (Sikorsky Div.)	1	48	46	Tube	(+/-30,0,0,+/-30,+/-30)	0.06	Bare	Tape Wound (Filament Wound)
UT-3	United Technology (Sikorsky Div.)	1	48	46	Tube	(((0)4,+/-8),+/-30)	0.06	Bare	Braided/-Filament Wound

Comments:
Ply orientation reference 0° down longitudinal axis of tube and 90° circumferentially around tube.
"s" stands for symmetric ply orientation, "r" ply orientation stands for repeating layup.
Tube I.D. ~2" and 6" long. Flat plates are 6" square (some trimmed prior to impact).
11-T-1 split at 30 angle in structural compression tests 8/28/86.
6-T-8 crushed while applying 6 mil Al coating.
6-T-10,11,12 tubes turned over to JSC structures group for IVADized aluminum coating.
9-F-1 and 9-F-2 plates were rejected due to manufacturing defects.
12-T-1 failed during compression tests @ 13,600 lbs. on 8/28/86 (unshot tube).
13-T-1 and 13-T-2 both rejected due to manufacturing defects.
Morton Thiokol tubes utilized high pressure cure.
UT-1 Manufactured with layed-up opaque glass and fiber optic cables.
UT-2 Four opaque glass fibers in composite.
UT-3 Six opaque glass fibers in composite.

Table 3-10. Target Dimensions and Mass

Tube ID	Ply Orientation	Fiber Modulus (M psi)	Length (in)	Avg. O.D. (in)	Avg. Thickness (in)	Avg. I.D. (in)	Mass (g)	Density (g/cc)
6F1	(+/-10,+/-30,+/-10)2s	34	6		0.0609		55.918	1.556
6F2	(+/-10,+/-30,+/-10)2s	34	6		0.0618		55.398	1.521
6T1	(+/-10,+/-30,+/-10)2r	34	6.019	2.124	0.0714	1.981	69.861	1.538
6T2	(+/-10,+/-30,+/-10)2r	34	6	2.14	0.0726	1.995	71.885	1.551
6T3	(+/-10,+/-30,+/-10)2r	34	5.975	2.130	0.0775	1.975	71.712	1.466
6sT1	(+/-10,+/-30,+/-10)2s	34	6	2.13	0.0686	1.993	67.611	1.549
6sT2	(+/-10,+/-30,+/-10)2s	34	6	2.15	0.0641	2.022	66.001	1.599
6T4	(+/-10,+/-30,+/-10)2r with 2 mil Al coating	34	6	2.1 2.15	0.0755 0.0797	1.949	72.085 80.469	1.527
6T5	(+/-10,+/-30,+/-10)2r with 2 mil Al coating	34	6	2.1	0.0764 0.0820	1.947	72.628 80.974	1.521
6T6	(+/-10,+/-30,+/-10)2r with 2 mil Al coating	34	6	2.1 2.15	0.0795 0.0808	1.941	72.363 80.651	1.458
6T7	(+/-10,+/-30,+/-10)2r with 6 mil Al coating	34	6	2.1	0.0720 0.0817	1.956	71.003 87.009	1.574
6T8	(+/-10,+/-30,+/-10)2r	34	6	2.1	0.0728	1.955	71.833	1.577
6T9	(+/-10,+/-30,+/-10)2r with 6 mil Al coating	34	6	2.1 2.16	0.0787 0.0788	1.943	72.344 88.374	1.472
6T10	(+/-10,+/-30,+/-10)2r	34	6	2.1	0.0766	1.947	72.425	1.512
6T11	(+/-10,+/-30,+/-10)2r	34	6	2.1	0.0675	1.965	72.086	1.702
6T12	(+/-10,+/-30,+/-10)2r	34	6	2.1	0.0763	1.948	71.986	1.510
7T1	(+/-10,+/-30,+/-10)3r	34	6	2.16	0.1029	1.954	103.568	1.585
7T2	(+/-10,+/-30,+/-10)3r	34	6	2.21	0.1063	1.997	103.896	1.504
7T3	(+/-10,+/-30,+/-10)3r	34	6	2.18	0.1045	1.971	100.150	1.495
7T4	(+/-10,+/-30,+/-10)3r	34	6	2.16	0.1050	1.950	103.006	1.546
8T1	(+/-10,+/-30,+/-10)4r	34	6	2.23	0.1303	1.969	135.141	1.599
8T2	(+/-10,+/-30,+/-10)4r	34	6	2.27	0.1334	2.006	135.038	1.532
9F1	Unknown	34	6		0.0615		56.146	1.548
9F2	Unknown	34	6		0.0618		55.002	1.509
9sF1	(+/-80,+/-30,+/-10)2s	34	6		0.0609		56.103	1.562
9sF2	(+/-80,+/-30,+/-10)2s	34	6		0.0602		54.777	1.544
9sF3	(+/-80,+/-30,+/-10)2s	34	6		0.0604		55.500	1.558
9sF4	(+/-80,+/-30,+/-10)2s	34	6		0.0598		54.341	1.542
9T1	(+/-80,+/-30,+/-10)2r	34	5.983	2.136	0.0695	1.997	68.337	1.545
9T2	(+/-80,+/-30,+/-10)2r	34	5.981	2.140	0.0707	1.999	69.547	1.544
9sT1	(+/-80,+/-30,+/-10)2s	34	6	2.14	0.0694	2.001	68.878	1.551
9sT2	(+/-80,+/-30,+/-10)2s	34	6	2.14	0.0678	2.004	67.829	1.564
10F1	(+/-45,+/-10,+/-45)2s	34	6		0.0611		55.459	1.539
10F2	(+/-45,+/-10,+/-45)2s	34	6		0.0627		55.211	1.494
10T1	(+/-45,+/-10,+/-45)2r	34	5.981	2.143	0.0721	1.999	71.114	1.548
10T2	(+/-45,+/-10,+/-45)2r	34	5.988	2.140	0.0770	1.986	69.599	1.421
11F1	(+/-10,+/-30,+/-10)2s	75	6		0.0726		69.266	1.618
11F2	(+/-10,+/-30,+/-10)2s	75	6		0.0723		69.092	1.620
11T1	(+/-10,+/-30,+/-10)2r	75	6.001	2.154	0.0829	1.988	89.033	1.679
11T2	(+/-10,+/-30,+/-10)2r	75	6	2.17	0.0885	1.993	89.065	1.565
11T3	(+/-10,+/-30,+/-10)2r	75	6.001	2.156	0.0817	1.993	89.438	1.709
11T4	(+/-10,+/-30,+/-10)2r	75	6	2.14	0.0765	1.987	86.912	1.782
11sT1	(+/-10,+/-30,+/-10)2s	75	6	2.13	0.0601	2.010	68.339	1.778
11sT2	(+/-10,+/-30,+/-10)2s	75	6	2.1	0.0645	1.971	71.374	1.761

Table 3-10 (Cont). Target Dimensions and Mass

Tube ID	Ply Orientation	Fiber Modulus (M psi)	Length (in)	Avg. O.D. (in)	Avg. Thickness (in)	Avg. I.D. (in)	Mass (g)	Density (g/cc)
12F1	(+/-80,+/-30,+/-10)2s	75	6		0.0722		69.847	1.640
12F2	(+/-80,+/-30,+/-10)2s	75	6		0.0714		68.565	1.629
12T1	(+/-80,+/-30,+/-10)2r	75	6.005	2.158	0.0807	1.997	87.816	1.695
12T2	(+/-80,+/-30,+/-10)2r	75	5.999	2.155	0.0795	1.996	86.008	1.688
13F1	(+/-45,+/-10,+/-45)2s	75	6		0.0723		69.560	1.631
13F2	(+/-45,+/-10,+/-45)2s	75	6		0.0723		69.699	1.634

Table 3-11. Target Sonic Velocity and Elastic Modulus

Tube ID	Ply Orientation	Fiber Modulus (M psi)	Sonic Velocity (km/s) Long.	Radial	TTT	Sonic Modulus (M psi) Long.	Radial	TTT	Compression Modulus (M psi) Long.	Vendor Modulus (M psi) Long.	Radial
6F1	(+/-10,+/-30,+/-10)2s	34	8.11	2.69	1.79	14.8	1.6	0.7		14.1	1.66
6F2	(+/-10,+/-30,+/-10)2s	34	8.12	2.67	1.79	14.8	1.6	0.7			
6T1	(+/-10,+/-30,+/-10)2r	34	7.97			14.3			13.5		
6T2	(+/-10,+/-30,+/-10)2r	34	8.02			14.5					
6T3	(+/-10,+/-30,+/-10)2r	34	7.86			13.9			12.3		
6sT1	(+/-10,+/-30,+/-10)2s	34	7.95			14.2			13.0		
6sT2	(+/-10,+/-30,+/-10)2s	34	8.07			14.6					
6T4	(+/-10,+/-30,+/-10)2r	34	7.87			13.9					
6T5	(+/-10,+/-30,+/-10)2r	34	7.79			13.6					
6T6	(+/-10,+/-30,+/-10)2r	34	7.78			13.6					
6T7	(+/-10,+/-30,+/-10)2r	34	7.90			14.0					
6T8	(+/-10,+/-30,+/-10)2r	34	8.07			14.6					
6T9	(+/-10,+/-30,+/-10)2r	34	7.82			13.7					
6T10	(+/-10,+/-30,+/-10)2r	34	7.78			13.6					
6T11	(+/-10,+/-30,+/-10)2r	34	7.83			13.8					
6T12	(+/-10,+/-30,+/-10)2r	34	7.90			14.0					
7T1	(+/-10,+/-30,+/-10)3r	34	7.95			14.2				13.6	1.59
7T2	(+/-10,+/-30,+/-10)3r	34	7.87			13.9					
7T3	(+/-10,+/-30,+/-10)3r	34	8.08			14.7					
7T4	(+/-10,+/-30,+/-10)3r	34	7.90			14.0					
8T1	(+/-10,+/-30,+/-10)4r	34	7.96			14.2				14.0	1.63
8T2	(+/-10,+/-30,+/-10)4r	34	7.94			14.2					
9F1	Unknown	34	5.51	7.26	1.60	6.8	11.9	0.6		6.77	12.1
9F2	Unknown	34	5.53	7.40	1.57	6.9	12.3	0.6			
9sF1	(+/-80,+/-30,+/-10)2s	34	6.69	5.69	1.61	10.1	7.3	0.6			
9sF2	(+/-80,+/-30,+/-10)2s	34	6.71	5.70	1.66	10.1	7.3	0.6			
9sF3	(+/-80,+/-30,+/-10)2s	34	6.68	5.67	1.60	10.0	7.2	0.6			
9sF4	(+/-80,+/-30,+/-10)2s	34	6.67	5.61	1.63	10.0	7.1	0.6			
9T1	(+/-80,+/-30,+/-10)2r	34	6.52			9.6			9.2		
9T2	(+/-80,+/-30,+/-10)2r	34	6.43			9.3			9.1		
9sT1	(+/-80,+/-30,+/-10)2s	34	6.57			9.7					
9sT2	(+/-80,+/-30,+/-10)2s	34	6.68			10.0					
10F1	(+/-45,+/-10,+/-45)2s	34	7.12	3.74	1.57	11.4	3.1	0.6		9.13	2.53
10F2	(+/-45,+/-10,+/-45)2s	34	7.10	3.74	1.57	11.3	3.1	0.6			
10T1	(+/-45,+/-10,+/-45)2r	34	6.44			9.3			7.1		
10T2	(+/-45,+/-10,+/-45)2r	34	6.77			10.3			6.6		
11F1	(+/-10,+/-30,+/-10)2s	75	10.85	2.53	1.66	27.8	1.5	0.7		27.3	1.40
11F2	(+/-10,+/-30,+/-10)2s	75	10.90	2.55	1.64	28.1	1.5	0.6			
11T1	(+/-10,+/-30,+/-10)2r	75	10.89			28.0			20.9		
11T2	(+/-10,+/-30,+/-10)2r	75	10.58			26.5					
11T3	(+/-10,+/-30,+/-10)2r	75	10.44			25.8			22.4		
11T4	(+/-10,+/-30,+/-10)2r	75	10.66			26.9					
11sT1	(+/-10,+/-30,+/-10)2s	75	10.78			27.5					
11sT2	(+/-10,+/-30,+/-10)2s	75	10.51			26.1					
12F1	(+/-80,+/-30,+/-10)2s	75	9.03	7.48	1.66	19.3	13.2	0.7		19.0	12.9
12F2	(+/-80,+/-30,+/-10)2s	75	8.98	7.40	1.66	19.1	13.0	0.7			
12T1	(+/-80,+/-30,+/-10)2r	75	8.66			17.7			15.9		
12T2	(+/-80,+/-30,+/-10)2r	75	9.23			20.1			17.0		
13F1	(+/-45,+/-10,+/-45)2s	75	8.38	5.11	1.66	16.6	6.2	0.7		15.2	4.90
13F2	(+/-45,+/-10,+/-45)2s	75	8.48	5.12	1.66	17.0	6.2	0.7			

Table 3-11 (Cont). Target Sonic Velocity and Elastic Modulus

Tube ID	Ply Orientation	Fiber Modulus (M psi)	Sonic Velocity (km/s) Long.	Radial	TTT	Sonic Modulus (M psi) Long.	Radial	TTT	Compression Modulus (M psi) Long.	VendorModulus (M psi) Long.	Radial
MD-2	(+/-10,+/-30,+/-10)s	34	7.78			13.6				13.7	
MD-3	(+/-10,+/-30,+/-10)s	34	7.83			13.8				13.7	
MT-1	(+/-45,0,0,0,0)2s	75	9.73			22.4				20.6	
MT-2	(+/-45,0,0,0,0)2s	75	10.42			25.7				20.4	
MT-3	(+/-45,0,0,0,0)2s	75	10.28			25.0					
MT-4	(+/-45,0,+/-15,0)2s	75	10.35			25.3				24.1	
MT-5	(+/-45,0,+/-15,0)2s	75	10.15			24.4				24.3	
MT-6	(+/-45,0,+/-15,0)2s	75	10.30			25.1					

Table 3-12. Predicted Tube Specimen Ultimate Compressive Loads

Test Number	Serial Number	Repetitions	Tube Ult. Compression Strength (lbs)	Test Load (lbs)	Test Purpose
1	6-T-1	10	19,300	7,500	Test repeatability of procedure.
2	6-T-1	8	19,300	7,500	Test different strain gage positions.
3	6-T-3	4	19,300	15,000	Determine modulus, test load machine setup.
4	11-T-1	2	17,800	14,000	Determine modulus of elasticity.
5	11-T-3	2	17,800	14,000	Determine modulus of elasticity.
6	9-T-1	2	13,500	10,000	Determine modulus of elasticity.
7	9-T-2	2	13,500	10,000	Determine modulus of elasticity.
8	12-T-1	2	12,600	10,000	Determine modulus of elasticity.
9	12-T-2	2	12,600	10,000	Determine modulus of elasticity.
10	10-T-1	2	10,100	7,500	Determine modulus of elasticity.
11	10-T-2	2	10,100	7,500	Determine modulus of elasticity.
12	6s-T-1	2	19,300	15,000	Determine modulus of elasticity.

Table 3-13. Results of Compression Tests on Undamaged Tubes

Test No.	1
Date	25-Aug-86
Tube S/N	6-T-1
Len. (in)	6.019
I.D. (in)	1.981
O.D. (in)	2.124
Thick (in)	0.071
Area (in^2)	0.4604
Gage L (in)	2.1

Test Cycle No.	Point 1 Load (lb)	Point 1 Defl.(in)	Point 2 Load (lb)	Point 2 Defl.(in)	Del Load (lb)	Del Defl. (in)	Calc. Modulus (psi)
1	2700	0.00054	6720	0.00196	4020	0.00142	1.29E+07
2	3000	0.00054	7000	0.00188	4000	0.00134	1.36E+07
3	4030	0.00188	6350	0.00271	2320	0.00083	1.27E+07
4	3820	0.002	7490	0.00334	3670	0.00134	1.25E+07
5	4010	0.00061	7500	0.00176	3490	0.00115	1.38E+07
6	3990	-.0001	6940	0.00085	2950	0.00095	1.42E+07
7	2620	0.00045	6950	0.00192	4330	0.00147	1.34E+07
8	3050	0.00186	7000	0.00322	3950	0.00136	1.32E+07
9	5240	0.00093	7800	0.0018	2560	0.00087	1.34E+07
10	4100	0.00101	7820	0.00232	3720	0.00131	1.30E+07
						Mean	1.328E+07
						Std. Dev.	4.898E+05 3.69% (delta from mean)
						Avg. Abs. Deviation from mean	4.124E+05 3.10% (delta from mean)

Test No.	2
Date	26-Aug-86
Tube S/N	6-T-1
Len. (in)	6.019
I.D. (in)	1.981
O.D. (in)	2.124
Thick (in)	0.071
Area (in^2)	0.4604
Gage L (in)	2.1

Orientation (deg)	Point 1 Load (lb)	Point 1 Defl.(in)	Point 2 Load (lb)	Point 2 Defl.(in)	Del Load (lb)	Del Defl. (in)	Calc. Modulus (psi)
0	1960	0.0007	6310	0.00228	4350	0.00158	1.26E+07
45	4000	0.00125	6860	0.00228	2860	0.00103	1.27E+07
90	2500	0.00077	6100	0.00204	3600	0.00127	1.29E+07
135	2170	0.00069	5420	0.0018	3250	0.00111	1.34E+07
180	2820	0.000615	6510	0.0018	3690	0.001185	1.42E+07
225	2700	0.00054	6020	0.00156	3320	0.00102	1.48E+07
270	2100	0.00069	6500	0.002125	4400	0.001435	1.40E+07
315	1890	0.00069	6730	0.002355	4840	0.001665	1.33E+07
						Mean	1.347E+07
						Std. Dev.	7.523E+05 5.58% (delta from mean)
						Avg. Abs. Deviation from mean	6.524E+05 4.84% (delta from mean)

Table 3-13 (Cont). Results of Compression Tests on Undamaged Tubes

Test No.	3
Date	25-Aug-86
Tube S/N	6-T-3
Len. (in)	5.975
I.D. (in)	1.975
O.D. (in)	2.130
Thick (in)	0.078
Area (in^2)	0.4997
Gage L (in)	2.1

Orientation (deg)	Point 1 Load (lb)	Point 1 Defl.(in)	Point 2 Load (lb)	Point 2 Defl.(in)	Del Load (lb)	Del Defl. (in)	Calc. Modulus (psi)	
0-h.lock	5650	0.00212	13800	0.0050	8150	0.00288	1.19E+07	
180-lock	3900	0.00062	12100	0.00338	8200	0.00276	1.25E+07	
0-unlock	4000	0.000462	6700	0.0014	2700	0.000938	1.21E+07	
180-unlck	2400	0.000935	8100	0.002825	5700	0.00189	1.27E+07	
						Mean	1.229E+07	
						Std. Dev.	3.087E+05	2.51% (delta from mean)
						Avg. Abs. Deviation from mean	2.926E+05	2.38% (delta from mean)

Test No.	4
Date	25-Aug-86 & 28-Aug-86
Tube S/N	11-T-1
Len. (in)	6.001
I.D. (in)	1.988
O.D. (in)	2.154
Thick (in)	0.083
Area (in^2)	0.5394
Gage L (in)	2.1

Orientation (deg)	Point 1 Load (lb)	Point 1 Defl.(in)	Point 2 Load (lb)	Point 2 Defl.(in)	Del Load (lb)	Del Defl. (in)	Calc. Modulus (psi)	
0-end dam	3700	0.00046	6800	0.00109	3100	0.00063	1.92E+07	
0-split	1800	0.000219	9150	0.001485	7350	0.001266	2.26E+07	
						Mean	2.088E+07	
						Std. Dev.	1.723E+06	8.25% (delta from mean)
						Avg. Abs. Deviation from mean	1.712E+06	8.25% (delta from mean)

Test No.	5
Date	28-Aug-86
Tube S/N	11-T-3
Len. (in)	6.001
I.D. (in)	1.993
O.D. (in)	2.156
Thick (in)	0.082
Area (in^2)	0.5324
Gage L (in)	2.1

Orientation (deg)	Point 1 Load (lb)	Point 1 Defl.(in)	Point 2 Load (lb)	Point 2 Defl.(in)	Del Load (lb)	Del Defl. (in)	Calc. Modulus (psi)
0	5700	0	13700	0.00165	8000	0.00165	1.91E+07
180	4200	0.0003	9800	0.00116	5600	0.00086	2.57E+07

Table 3-13 (Cont). Results of Compression Tests on Undamaged Tubes

Test. No. 5 (Cont.)

Mean	2.240E+07	
Std. Dev.	3.280E+06	14.6% (delta from mean)
Avg. Abs. Deviation from mean	3.280E+06	14.6% (delta from mean)

Test No.	6
Date	27-Aug-86
Tube S/N	9-T-1
Len. (in)	5.983
I.D. (in)	1.997
O.D. (in)	2.136
Thick (in)	0.070
Area (in^2)	0.4512
Gage L (in)	2.1

Orientation (deg)	Point 1 Load (lb)	Point 1 Defl.(in)	Point 2 Load (lb)	Point 2 Defl.(in)	Del Load (lb)	Del Defl. (in)	Calc. Modulus (psi)
0	3400	0.00045	7400	0.0023	4000	0.00185	1.01E+07
180	3600	0.0031	6000	0.00445	2400	0.00135	8.27E+06

Mean	9.169E+06	
Std. Dev.	8.945E+05	9.76% (delta from mean)
Avg. Abs. Deviation from mean	8.945E+05	9.76% (delta from mean)

Test No.	7
Date	27-Aug-86
Tube S/N	9-T-2
Len. (in)	5.981
I.D. (in)	1.999
O.D. (in)	2.140
Thick (in)	0.071
Area (in^2)	0.4596
Gage L (in)	2.1

Orientation (deg)	Point 1 Load (lb)	Point 1 Defl.(in)	Point 2 Load (lb)	Point 2 Defl.(in)	Del Load (lb)	Del Defl. (in)	Calc. Modulus (psi)
0	4000	0.00316	9000	0.0060	5000	0.00284	8.04E+06
180	2000	0.000625	9500	0.0040	7500	0.003375	1.02E+07

Mean	9.099E+06	
Std. Dev.	1.055E+06	11.6% (delta from mean)
Avg. Abs. Deviation from mean	1.055E+06	11.6% (delta from mean)

Table 3-13 (Cont). Results of Compression Tests on Undamaged Tubes

Test No.	8
Date	28-Aug-86
Tube S/N	12-T-1
Len. (in)	6.005
I.D. (in)	1.997
O.D. (in)	2.158
Thick (in)	0.081
Area (in^2)	0.5267
Gage L (in)	2.1

Orientation (deg)	Point 1 Load (lb)	Point 1 Defl.(in)	Point 2 Load (lb)	Point 2 Defl.(in)	Del Load (lb)	Del Defl. (in)	Calc. Modulus (psi)	
0	2200	0.00045	8800	0.002115	6600	0.001665	1.58E+07	
0	2000	0.00037	9000	0.00212	7000	0.00175	1.59E+07	
						Mean	1.588E+07	
						Std. Dev.	7.185E+04	0.45% (delta from mean)
						Avg. Abs. Deviation from mean	7.185E+04	0.45% (delta from mean)

Test No.	9
Date	27-Aug-86
Tube S/N	12-T-2
Len. (in)	5.999
I.D. (in)	1.996
O.D. (in)	2.155
Thick (in)	0.080
Area (in^2)	0.5184
Gage L (in)	2.1

Orientation (deg)	Point 1 Load (lb)	Point 1 Defl.(in)	Point 2 Load (lb)	Point 2 Defl.(in)	Del Load (lb)	Del Defl. (in)	Calc. Modulus (psi)	
0	1900	0.000532	8000	0.002200	6100	0.001668	1.48E+07	
180	3225	0.0003	8500	0.001410	5275	0.00111	1.93E+07	
						Mean	1.703E+07	
						Std. Dev.	2.218E+06	13.0% (delta from mean)
						Avg. Abs. Deviation from mean	2.218E+06	13.0% (delta from mean)

Test No.	10
Date	27-Aug-86
Tube S/N	10-T-1
Len. (in)	5.981
I.D. (in)	1.999
O.D. (in)	2.143
Thick (in)	0.072
Area (in^2)	0.4691
Gage L (in)	2.1

Orientation (deg)	Point 1 Load (lb)	Point 1 Defl.(in)	Point 2 Load (lb)	Point 2 Defl.(in)	Del Load (lb)	Del Defl. (in)	Calc. Modulus (psi)	
0	1000	0.00063	7000	0.004590	6000	0.00396	6.78E+06	
180	2000	0.00105	7000	0.004100	5000	0.00305	7.34E+06	
						Mean	7.061E+06	
						Std. Dev.	2.780E+05	3.94% (delta from mean)
						Avg. Abs.	2.780E+05	3.94% (delta from mean)

Table 3-13 (Cont). Results of Compression Tests on Undamaged Tubes

Test No.	11
Date	27-Aug-86
Tube S/N	10-T-2
Len. (in)	5.988
I.D. (in)	1.986
O.D. (in)	2.140
Thick (in)	0.077
Area (in^2)	0.4990
Gage L (in)	2.1

Orientation (deg)	Point 1 Load (lb)	Point 1 Defl.(in)	Point 2 Load (lb)	Point 2 Defl.(in)	Del Load (lb)	Del Defl. (in)	Calc. Modulus (psi)	
0	2000	0.00032	7000	0.003500	5000	0.00318	6.62E+06	
180	2000	0.0021	7000	0.005285	5000	0.003185	6.61E+06	
						Mean	6.611E+06	
						Std. Dev.	5.193E+03	0.08% (delta from mean)
						Avg. Abs. Deviation from mean	5.193E+03	0.08% (delta from mean)

Table 3-14. Impacts on Phase I Truss having same Diameter as Test Projectiles

Phase I Space Station Truss area (m^2)	224.6
Station Lifetime (yrs)	30
Meteoroid density (g/cc)	0.5
Ave. meteoroid velocity (km/s)	20
Debris density (g/cc)	2.8
Ave. debris velocity (km/s)	9.3

Proj. Dia. (mm)	Particle Mass (g) Met.	Particle Mass (g) Debris	Particle Flux (#/m^2-yr) Met.	Particle Flux (#/m^2-yr) Debris	Particle Flux (#/m^2-yr) Total	Impacts of given Diameter and greater (#/30 yr life) Met.	Impacts of given Diameter and greater (#/30 yr life) Debris	Impacts of given Diameter and greater (#/30 yr life) Total	Probability of No Impact Met.	Probability of No Impact Debris	Probability of No Impact Total
0.55	4.36E-05	2.44E-04	1.66E-02	5.18E-03	2.18E-02	112	34.9	146.8	0	0	0
0.77	1.20E-04	6.69E-04	4.84E-03	2.22E-03	7.06E-03	32.7	15.0	47.6	0	0	0
0.95	2.24E-04	1.26E-03	2.25E-03	1.31E-03	3.55E-03	15.1	8.81	23.9	0	0	0
1.55	9.75E-04	5.46E-03	3.74E-04	3.81E-04	7.55E-04	2.52	2.56	5.09	0.08	0.08	0.01
2.37	3.49E-03	1.95E-02	7.91E-05	1.31E-04	2.10E-04	0.53	0.88	1.41	0.59	0.41	0.24
3.14	8.11E-03	4.54E-02	2.83E-05	6.42E-05	9.25E-05	0.19	0.43	0.62	0.83	0.65	0.54
4.39	2.21E-02	1.24E-01	8.29E-06	2.76E-05	3.59E-05	0.06	0.19	0.24	0.95	0.83	0.79

4.0 Test Results

The following sections document the results of impact tests to examine the effect of projectile characteristics (size, velocity, impact obliquity) and target properties (layup, modulus, thickness, coatings, shape) on impact damage severity. Data from 32 light gas gun shots performed at JSC and 26 made at NDE Technology were used in the comparisons and to develop correlations between damage and certain projectile/target variables.

A summary of the shot conditions and resulting target damage for all 58 data shots is given in Table 4-1. Data describing the impact conditions includes projectile material, spherical diameter, mass, velocity, impact obliquity angles, and kinetic energy. The projectile velocity (speed) and kinetic energy normal to the target was calculated from the obliquity angles. Target damage information includes separate entries for the tube first and second wall through hole shape, size, equivalent circular diameter to projectile diameter ratio, crater size (crater defined as deep delamination area surrounding the through hole), area of surface peelings, and ultrasonic C-scan area. Damage to witness plates positioned behind the targets is also recorded.

Projectiles used in the JSC shots included 2 sizes of glass spheres (0.55 mm and 0.95 mm), 3 aluminum spheres (1.58 mm, 2.38 mm, and 3.18 mm) and a nylon slug (4.4 x 4.4 mm). JSC projectile velocities ranged from 6.1 - 7.8 km/sec and impact obliquity angles varied from 0° - 15°. Two intentional 45° oblique impacts were also performed. As indicated in Figure 4-1, for all tube shots, there were two impact angles relative to the target that were derived from measurements: a radial and longitudinal obliquity angle (for flat plates they are the same angle which was 0° for all shots). The radial obliquity angle is the angle between the normal to the target surface and the projectile flight path line in the plane perpendicular to the longitudinal tube axis (equal to the arcsin of the ratio of measured distance from the longitudinal tube centerline to the impact divided by the tube radius). The longitudinal obliquity is the angle between the projectile flight path and the tube longitudinal axis.

Shots at NDE involved impacts of glass (0.55 mm and 0.77 mm) and aluminum (1.58 mm and 2.38 mm) projectiles traveling at 3.3 to 7.3 km/sec, with radial impact obliquity angles of 0 - 40°. All NDE projectiles impacted normal to the longitudinal axis.

Appendix A contains a detailed description of all shots (including 12 NDE shots not used in the data analysis portion of the study) done for this study ordered by shot number.

Figure 4-1. Definition of Encounter Parameters

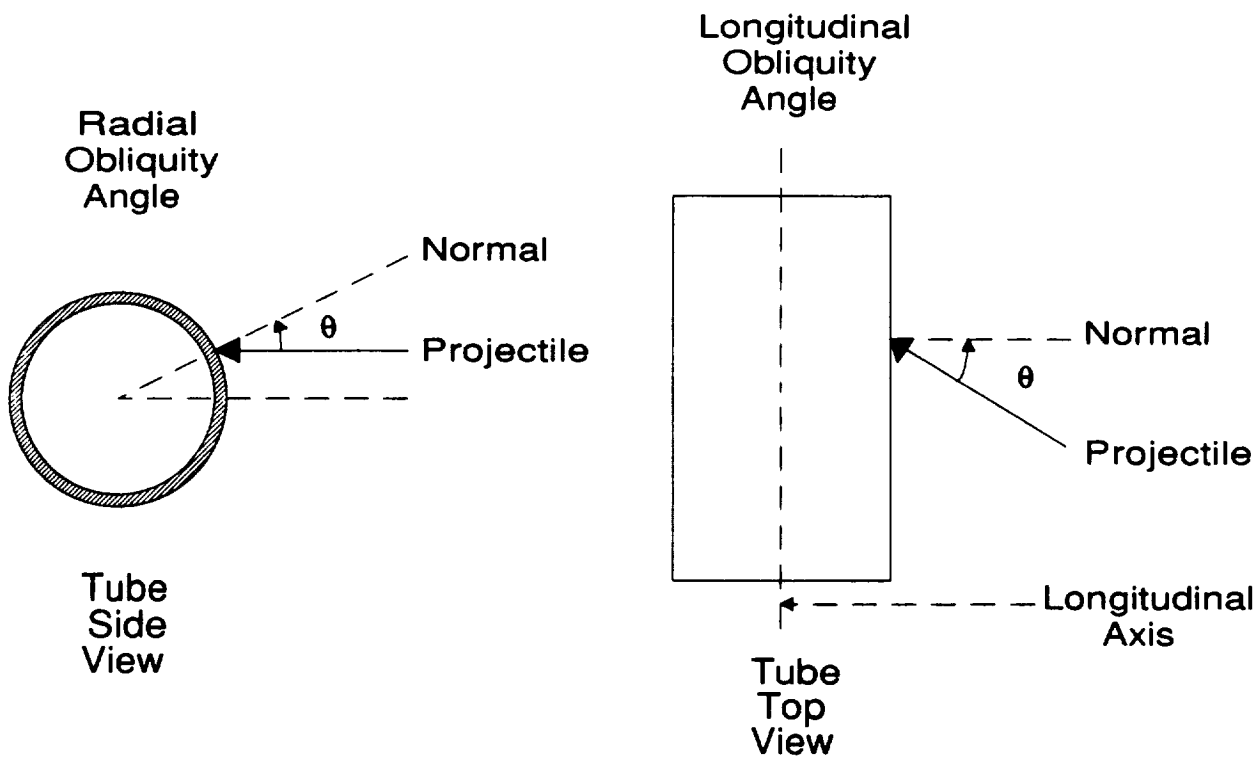

Table 4-1. Shot Data Summary (Ordered by Target Serial Number)

Shot	Date	Target S/N	Type	Layup	Nominal Thickness (in)	Fiber Modulus (Mpsi)	Proj. Mat'l	Proj. Dia. (mm)	Proj. Mass (mg)	Proj. Vel. (km/s)	Proj. Dens. (g/cc)	Proj. Energy (J)	Proj. Obliquity Angle Radially (on curve) (deg) 0=normal	Obliquity to Longitud. Axis (deg) 0=normal	Normal Proj. Vel. (km/s)	Normal Proj. Energy (J)	Target Mass Before (g)	Target Mass After (g)
							Shot Conditions											
JSC-A333	03-Sep-87	6-F-1	Plate	10,30,10	0.061	34	Al2024-T4	1.55	5.49	7.19	2.796	141.9	0	0	7.19	141.9	55.95	55.85
NDE-33	25-Aug-87	6-F-1	Plate	10,30,10	0.061	34	Al2024-T4	1.55	5.41	6.10	2.796	100.5	0	0	6.10	100.5		
JSC-A411	06-Nov-87	9s-F-1	Plate	80,30,10	0.061	34	Al2024-T4	1.56	5.51	6.97	2.796	133.8	0	0	6.97	133.8	55.93	55.82
NDE-35	20-Oct-87	9s-F-1	Plate	80,30,10	0.061	34	Al2024-T4	1.54	5.39	5.79	2.796	90.4	0	0	5.79	90.4		
NDE-7	15-Apr-87	9s-F-2	Plate	80,30,10	0.060	34	Glass	0.55	0.21	5.49	2.45	3.2	0	0	5.49	3.2	54.78	
JSC-A181	10-Apr-87	9s-F-3	Plate	80,30,10	0.0604	34	Glass	0.55	0.21	7.23	2.45	5.6	0	0	7.23	5.6	55.42	55.23
JSC-A410	05-Nov-87	10-F-1	Plate	45,10,45	0.061	34	Al2024-T4	1.55	5.50	7.68	2.796	162.2	0	0	7.68	162.2	52.78	52.66
NDE-37	20-Oct-87	10-F-1	Plate	45,10,45	0.061	34	Al2024-T4	1.54	5.36	6.71	2.796	120.5	0	0	6.71	120.5		
JSC-A346	16-Sep-87	11-F-1	Plate	10,30,10	0.073	75	Al2024-T4	1.55	5.44	6.89	2.796	129.1	0	0	6.89	129.1	66.87	68.67
JSC-A352	21-Sep-87	11-F-1	Plate	10,30,10	0.073	75	Al2024-T4	1.55	5.45	6.83	2.796	127.1	0	0	6.83	127.1	62.08	61.86
NDE-34	25-Aug-87	11-F-1	Plate	10,30,10	0.073	75	Al2024-T4	1.54	5.37	5.79	2.796	90.0	0	0	5.79	90.0		
NDE-2	02-Feb-87	11-F-2	Plate	10,30,10	0.072	75	Glass	0.55	0.21	6.89	2.45	5.1	0	0	6.89	5.1	69.09	69.08
JSC-A409	05-Nov-87	12-F-1	Plate	80,30,10	0.072	75	Al2024-T4	1.56	5.51	7.30	2.796	146.8	0	0	7.30	146.8	67.71	67.50
NDE-36	20-Oct-87	12-F-1	Plate	80,30,10	0.072	75	Al2024-T4	1.55	5.45	3.96	2.796	42.8	0	0	3.96	42.8		
NDE-3	06-Feb-87	12-F-2	Plate	80,30,10	0.071	75	Glass	0.55	0.21	6.40	2.45	4.4	0	0	6.40	4.4	68.57	
JSC-A413	09-Nov-87	13-F-1	Plate	45,10,45	0.072	75	Al2024-T4	1.55	5.40	7.29	2.796	143.5	0	0	7.29	143.5	68.95	68.77
NDE-38	20-Oct-87	13-F-1	Plate	45,10,45	0.072	75	Al2024-T4	1.54	5.38	5.18	2.796	72.2	0	0	5.18	72.2		
JSC-A204	19-May-87	6-T-1	Tube	10,30,10	0.0714	34	Glass	0.89	0.89	7.05	2.45	22.1	7	0	7.00	21.8	69.98	69.95
JSC-A292	05-Aug-87	6-T-2	Tube	10,30,10	0.073	34	Al2024-T4	1.55	5.48	7.78	2.796	165.8	10	0	7.65	160.5	72.15	71.93
JSC-A308	17-Aug-87	6-T-2	Tube	10,30,10	0.073	34	Al2024-T4	3.14	45.20	6.10	2.796	840.9	3	0	6.09	838.8	71.96	69.61
JSC-A313	19-Aug-87	6-T-3	Tube	10,30,10	0.078	34	Al2024-T4	1.54	5.37	7.08	2.796	134.6	6	45	4.98	66.6	71.57	71.39
JSC-A329	01-Sep-87	6-T-3	Tube	10,30,10	0.078	34	Al2024-T4	1.55	5.43	7.33	2.796	145.9	42	0	5.44	80.4	71.38	71.16
NDE-22	04-Aug-87	6-T-3	Tube	10,30,10	0.078	34	Al2024-T4	1.58	5.72	4.57	2.796	59.8	41	0	3.43	33.7	71.71	
JSC-A249	02-Jul-87	6s-T-1	Tube	10,30,10	0.066	34	Al2024-T4	2.38	19.70	7.48	2.796	551.1	5	0	7.46	547.7	66.72	66.27
JSC-A334	08-Sep-87	6s-T-2	Tube	10,30,10	0.064	34	Nylon	4.39	72.84	6.68	1.1	1625.1	9	0	6.59	1583.5	66.00	61.60
NDE-11	11-Jun-87	6s-T-2	Tube	10,30,10	0.064	34	Glass	0.77	0.59	4.21	2.45	5.2	2	0	4.20	5.2	66.11	66.11
NDE-32	25-Aug-87	6s-T-2	Tube	10,30,10	0.064	34	Al2024-T4	1.54	5.35	7.01	2.796	131.5	4	0	6.99	130.8		
JSC-A206	20-May-87	6-T-4	Tube	10,30,10	0.082	34	Glass	0.93	1.02	6.45	2.45	21.2	10	0	6.34	20.5	80.48	80.43
JSC-A250	06-Jul-87	6-T-4	Tube	10,30,10	0.078	34	Al2024-T4	2.37	19.60	7.15	2.796	501.0	5	0	7.13	497.8	80.56	79.73
JSC-A307	14-Aug-87	6-T-6	Tube	10,30,10	0.086	34	Al2024-T4	1.54	5.39	7.35	2.796	145.6	0	0	7.35	145.6	80.66	80.45
NDE-12	11-Jun-87	6-T-6	Tube	10,30,10	0.086	34	Glass	0.77	0.59	3.29	2.45	3.2	0	0	3.29	3.2		80.68
NDE-23	04-Aug-87	6-T-6	Tube	10,30,10	0.086	34	Al2024-T4	1.57	5.70	7.01	2.796	140.1	27	0	6.22	110.4		
NDE-13	11-Jun-87	6-T-9	Tube	10,30,10	0.089	34	Glass	0.77	0.59	4.69	2.45	6.5	21	0	4.38	5.6		88.39
NDE-24	04-Aug-87	6-T-9	Tube	10,30,10	0.089	34	Al2024-T4	1.58	5.77	6.71	2.796	129.7	24	0	6.15	109.0		
NDE-28	25-Aug-87	7-T-2	Tube	10,30,10	0.106	34	Al2024-T4	1.58	5.72	4.27	2.796	52.1	12	0	4.18	50.0		
JSC-A211	28-May-87	7-T-3	Tube	10,30,10	0.105	34	Glass	0.95	1.11	7.32	2.45	29.7	0	0	7.32	29.7	100.21	100.14
NDE-21	30-Jul-87	8-T-2	Tube	10,30,10	0.133	34	Al2024-T4	2.37	19.58	4.57	2.796	204.6	14	0	4.43	191.9	135.04	
NDE-29	25-Aug-87	8-T-2	Tube	10,30,10	0.133	34	Al2024-T4	1.57	5.66	4.88	2.796	67.3	20	0	4.59	59.5		
JSC-A293	06-Aug-87	9-T-1	Tube	80,30,10	0.070	34	Al2024-T4	1.55	5.41	7.47	2.796	150.9	10	0	7.36	146.6	68.47	68.27
NDE-30	25-Aug-87	9-T-2	Tube	80,30,10	0.071	34	Al2024-T4	1.57	5.68	5.49	2.796	85.5	4	0	5.47	85.1		
JSC-A208	22-May-87	9s-T-1	Tube	80,30,10	0.0694	34	Glass	0.94	1.06	6.67	2.45	23.6	5	0	6.64	23.4	69.05	68.99
NDE-31	25-Aug-87	9s-T-2	Tube	80,30,10	0.068	34	Al2024-T4	1.54	5.37	4.27	2.796	48.9	15	0	4.12	45.6		
JSC-A209	26-May-87	10-T-1	Tube	45,10,45	0.072	34	Glass	0.94	1.07	7.16	2.45	27.4	4	0	7.14	27.3	71.20	71.12
JSC-A294	06-Aug-87	10-T-2	Tube	45,10,45	0.077	34	Al2024-T4	1.55	5.45	7.33	2.796	146.4	3	0	7.32	145.9	69.70	69.47
NDE-19	30-Jul-87	10-T-2	Tube	45,10,45	0.077	34	Glass	0.77	0.59	6.40	2.45	12.0	35	0	5.21	8.0	69.60	
JSC-A196	11-May-87	11-T-2	Tube	10,30,10	0.0885	75	Glass	0.55	0.21	7.60	2.45	6.2	7	0	7.54	6.1	89.29	89.16

Table 4-1 (Cont). Shot Data Summary (Ordered by Target Serial Number)

Shot Conditions

Shot	Date	Target S/N	Type	Layup	Nominal Thickness (in)	Fiber Modulus (Mpsi)	Proj. Mat'l	Proj. Dia. (mm)	Proj. Mass (mg)	Proj. Vel. (km/s)	Proj. Dens. (g/cc)	Proj. Energy (J)	Proj. Obliquity Angle Radially (on curve) (deg) 0=normal	Obliquity to Longitud. Axis (deg) 0=normal	Normal Proj. Vel. (km/s)	Normal Proj. Energy (J)	Target Mass Before (g)	Target Mass After (g)
JSC-A246	01-Jul-87	11-T-2	Tube	10,30,10	0.089	75	Al2024-T4	2.38	19.66	7.38	2.796	535.4	12	0	7.23	513.3	89.47	86.80
JSC-A201	14-May-87	11-T-4	Tube	10,30,10	0.0765	75	Glass	0.55	0.21	7.07	2.45	5.3	5	0	7.04	5.3	86.91	86.85
JSC-A291	05-Aug-87	11-T-4	Tube	10,30,10	0.077	75	Al2024-T4	1.55	5.47	7.55	2.796	155.9	10	0	7.43	150.9	87.64	87.32
JSC-A212	29-May-87	11s-T-1	Tube	10,30,10	0.060	75	Glass	0.94	1.06	6.68	2.45	23.6	9	0	6.60	23.1	68.44	68.34
JSC-A302	12-Aug-87	12-T-2	Tube	80,30,10	0.080	34	Al2024-T4	1.55	5.45	7.16	2.796	139.7	7	0	7.10	137.3	86.01	85.71
NDE-18	28-Jul-87	12-T-2	Tube	80,30,10	0.080	75	Glass	0.77	0.59	3.96	2.45	4.6	0	0	3.96	4.6	86.01	
JSC-A261	11-Jul-87	MB-02	Tube	10,30,10	0.066	34	Al2024-T4	2.37	19.53	7.25	2.796	513.3	13	0	7.07	488.4	72.87	71.80
JSC-A305	13-Aug-87	MB-03	Tube	10,30,10	0.066	34	Al2024-T4	1.54	5.38	7.25	2.796	141.4	0	0	7.25	141.4	73.40	73.14
NDE-26	04-Aug-87	MB-03	Tube	10,30,10	0.066	34	Al2024-T4	1.57	5.70	6.10	2.796	105.9	15	0	5.89	98.7		
JSC-A245	30-Jun-87	MT-02	Tube	45,0,0	0.063	75	Al2024-T4	2.37	19.60	7.08	2.796	491.2	13	0	6.91	468.2	68.15	65.97
NDE-27	04-Aug-87	MT-03	Tube	45,0,0,0	0.066	75	Al2024-T4	1.57	5.71	4.88	2.796	67.9	24	0	4.47	57.0		
NDE-25	04-Aug-87	MT-04	Tube	45,0,15,0	0.066	75	Al2024-T4	1.58	5.73	7.32	2.796	153.3	28	0	6.46	119.4		

Table 4-1 (Cont). Shot Data Summary (Ordered by Target Serial Number)

Target Front Side Conditions: (outside of tube's 1st wall)

Shot	Date	Target S/N	1st wall Hole Shape	Hole Dimensions Length (mm)	Hole Dimensions Width (mm)	Hole Equiv. Circular Diameter (mm)	Hole to Proj. Dia. Ratio	Crater (if evident) Dia. (mm)	Crater to Proj. Dia. Ratio	Surface Peel Total Area (mm^2)	Coated Tube Exposed Area (mm^2)	Coated Tube Additional Peel Area (mm^2)	Peel Equiv. Circular Diameter (mm)	Peel to Proj. Dia. Ratio	C-Scan Dimensions Area (mm^2)	C-Scan Dimensions Equiv. Circular Diameter (mm)	C-scan to Proj. Dia. Ratio	Actual Shape: Approx. Axial Length (mm)	Actual Shape: Overall (Circumf) Width (mm)
JSC-A333	03-Sep-87	6-F-1	Oval	5.1	4.6	4.8	3.1	6.1	3.9	83			10.3	6.6	537.1	26.1	16.8	40	13
NBE-33	25-Aug-87	6-F-1	Circ.	4.1		4.1	2.6	5.1	3.3	114			12.0	7.8	396.7	22.5	14.5	30	13
JSC-A411	06-Nov-87	9s-F-1	Rect.	5.2	4.8	5.6	3.6	6.7	4.3	108			11.7	7.5	513.3	25.6	16.4	25	21
NBE-35	20-Oct-87	9s-F-1	Circ.	4.6		4.6	3.0	5.6	3.6	111			11.9	7.7					
NBE-7	15-Apr-87	9s-F-2	Circ.	1.1		1.1	2.1	1.9	3.4	44			7.5	13.6	99.2	11.2	20.4	7	13
JSC-A181	10-Apr-87	9s-F-3	Circ.	1.93		1.93	3.5	2.48	4.5	13			4.1	7.4					
JSC-A410	05-Nov-87	10-F-1	Oval	5.2	4.4	4.7	3.1	6.3	4.0	141			13.4	8.6	813.0	32.2	20.7	35	23
NBE-37	20-Oct-87	10-F-1	Circ.	4.3		4.3	2.8	5.6	3.6	98			11.1	7.2					
JSC-A346	16-Sep-87	11-F-1	Circ.	6.7		6.7	4.4	9.5	6.1	0			0.0	0.0	666.3	29.1	18.8	33	20
JSC-A352	21-Sep-87	11-F-1	Circ.	7.1		7.1	4.6	9.5	6.1	0			0.0	0.0	725.3	30.4	19.6	29	25
NBE-34	25-Aug-87	11-F-1	Circ.	5.8		5.8	3.8	6.6	4.3	5			2.5	1.6					
NBE-2	02-Feb-87	11-F-2	Rect.	1.9	1.5	1.9	3.4	2.7	4.9	0			0.0	0.0	78.0	10.0	18.1	12	6.8
JSC-A409	05-Nov-87	12-F-1	Circ.	7.1		7.1	4.6	9.5	6.1	20			5.1	3.3	368.3	21.7	13.9	16	23
NBE-36	20-Oct-87	12-F-1	Circ.	4.6		4.6	2.9	5.8	3.8	10			3.6	2.3	194.8	15.7	10.2	10	19
NBE-3	06-Feb-87	12-F-2	Circ.	2.7		2.7	4.8	3.3	6.0	0			0.0	0.0					
JSC-A413	09-Nov-87	13-F-1	Circ.	7.5		7.5	4.9	10.3	6.7	0			0.0	0.0	253.5	18.0	11.6	14	18
NBE-38	20-Oct-87	13-F-1	Circ.	5.5		5.5	3.6	7.5	4.9	21			5.2	3.4					
JSC-A204	19-May-87	6-T-1	Rect.	2.1	1.5	2.0	2.3	3.3	3.7	80			10.1	11.4	278.4	18.8	21.3	28	10
JSC-A292	05-Aug-87	6-T-2	Rect.	3.8	4.8	4.8	3.1	5.7	3.7	114			12.1	7.8	372.2	21.8	14.0	24	15
JSC-A308	17-Aug-87	6-T-2	Circ.	7.9		7.9	2.5	10.4	3.3	378			21.9	7.0	656.9	28.9	9.2	42	16
JSC-A313	19-Aug-87	6-T-3	Oval	5.8	4.6	5.2	3.4	7.1	4.6	75			9.8	6.3	355.1	21.3	13.8	25	14
JSC-A329	01-Sep-87	6-T-3	Rect.	4.8	4.3	5.2	3.3	6.2	4.0	103			11.5	7.4	330.7	20.5	13.3	22	15
NBE-22	04-Aug-87	6-T-3	Circ.	3.3		3.3	2.1	4.8	3.1	45			7.6	4.8	139.2	13.3	8.5	18	8
JSC-A249	02-Jul-87	6s-T-1	Rect.	7.1	5.3	6.9	2.9	11.3	4.7	315			20.0	8.4	546.9	26.4	11.1	25	22
JSC-A334	08-Sep-87	6s-T-2	Oval	10.7	9.7	10.1	2.3	12.7	2.9	348			21.0	4.8	606.1	27.8	6.3	40	15
NBE-11	11-Jun-87	6s-T-2	Rect.	0.3	0.9	0.6	0.8	1.6	2.1	21			5.2	6.7	66.4	9.2	11.9	10	7
NBE-32	25-Aug-87	6s-T-2	Rect.	3.0	3.0	3.4	2.2	4.9	3.2	128			12.8	8.3	306.0	19.7	12.8	24	13
JSC-A206	20-May-87	6-T-4	Rect.	2.3	1.7	2.2	2.4	3.7	4.0	38			6.9	7.5	118.3	12.3	13.2	12	10
JSC-A250	06-Jul-87	6-T-4	Circ.	6.9		6.9	2.9	9.7	4.1	359	248	111	21.4	9.0	641.1	28.6	12.0	33	19
JSC-A307	14-Aug-87	6-T-6	Circ.	4.3		4.3	2.8	5.8	3.8	173	67	106	14.8	9.6	279.9	18.9	12.2	21	13
NBE-12	11-Jun-87	6-T-6	Rect.	1.6	1	1.4	1.9	3.3	4.3	2	2		1.7	2.2	91.7	10.8	14.0	16	6
NBE-23	04-Aug-87	6-T-6	Oval	2.5	3.3	2.9	1.8	4.9	3.1	48	23	26	7.8	5.0	134.9	13.1	8.3	13	10
NBE-13	11-Jun-87	6-T-9	Circ.	1.0		1.0	1.3	1.7	2.2	10	10		3.5	4.6	58.7	8.6	11.2	8	7
NBE-24	04-Aug-87	6-T-9	Oval	3.6	3.3	3.4	2.2	5.5	3.5	24	24		5.5	3.5	118.5	12.3	7.8	13	9
NBE-28	25-Aug-87	7-T-2	Rect.	2.7	2.3	2.8	1.8	4.8	3.1	38			7.0	4.4	130.6	12.9	8.2	12	11
JSC-A211	28-May-87	7-T-3	Rect.	2.3	1.8	2.3	2.4	3.1	3.3	99			11.2	11.8	325.9	20.4	21.4	9	36
NBE-21	30-Jul-87	8-T-2	Rect.	3.0	2.5	3.1	1.3	5.0	2.1	214			16.5	6.9	579.3	27.2	11.4	30	19
NBE-29	25-Aug-87	8-T-2	Rect.	2.8	2.8	3.2	2.0	4.6	2.9	130			12.9	8.2	343.2	20.9	13.3	24	14
JSC-A293	06-Aug-87	9-T-1	Rect.	3.8	3.8	4.3	2.8	6.1	3.9	123			12.5	8.1	418.4	23.1	14.9	28	15
NBE-30	25-Aug-87	9-T-2	Circ.	4.0		4.0	2.5	4.6	2.9	165			14.5	9.2	460.9	24.2	15.4	28	16
JSC-A208	22-May-87	9s-T-1	Circ.	2.1		2.1	2.2	3.7	3.9	44			7.5	8.0	220.3	16.7	17.8	7	30
NBE-31	25-Aug-87	9s-T-2	Rect.	2.5	2.5	2.9	1.9	4.3	2.8	45			7.6	4.9	138.5	13.3	8.6	9	15
JSC-A209	26-May-87	10-T-1	Circ.	2.2		2.2	2.3	3.6	3.8	71			9.5	10.1	189.8	15.5	16.5	13	14
JSC-A294	06-Aug-87	10-T-2	Circ	4.3		4.3	2.8	5.8	3.8	178			15.0	9.7	161.3	14.3	9.2	12	13
NBE-19	30-Jul-87	10-T-2	Oval	1.1	0.9	1.0	1.3	2.2	2.8	17			4.7	6.0	64.1	9.0	11.7	8	8
JSC-A196	11-May-87	11-T-2	Rect.	2.1	1.7	2.1	3.9	3.0	5.5	0			0.0	0.0					

Table 4-1 (Cont). Shot Data Summary (Ordered by Target Serial Number)

Target Front Side Conditions: (outside of tube's 1st wall)

Shot	Date	Target S/N	1st wall Hole Shape	Hole Dimensions Length (mm)	Hole Dimensions Width (mm)	Hole Equiv. Circular Diameter (mm)	Hole to Proj. Dia. Ratio	Crater (if evident) Dia. (mm)	Crater to Proj. Dia. Ratio	Surface Peel Total Area (mm^2)	Coated Tube Exposed Area (mm^2)	Coated Tube Additional Peel Area (mm^2)	Peel Equiv. Circular Diameter (mm)	Peel to Proj. Dia. Ratio	C-Scan Dimensions Area (mm^2)	C-Scan Dimensions Equiv. Circular Diameter (mm)	C-scan to Proj. Dia. Ratio	Actual Shape: Approx. Axial Length (mm)	Actual Shape: Overall (Circumf) Width (mm)
JSC-A246	01-Jul-87	11-T-2	Oval	9.1	10.3	9.7	4.1	14.7	6.2	0			0.0	0.0	298.3	19.5	8.2	15	20
JSC-A201	14-May-87	11-T-4	Rect.	2.2	1.7	2.2	4.0	3.6	6.5	0			0.0	0.0	67.9	9.3	16.9	7	10
JSC-A291	05-Aug-87	11-T-4	Oval	8.4	6.9	7.6	4.9	9.5	6.1	0			0.0	0.0	312.9	20.0	12.9	20	15
JSC-A212	29-May-87	11s-T-1	Rect.	3.9	3.2	4.0	4.2	6.4	6.8	0			0.0	0.0	138.1	13.3	14.1	14	10
JSC-A302	12-Aug-87	12-T-2	Circ	7.6		7.6	4.9	10.9	7.0	0			0.0	0.0	409.0	22.8	14.7	24	17
NDE-18	28-Jul-87	12-T-2	Circ.	3.3		3.3	4.3	4.5	5.8	3			1.9	2.4	119.6	12.3	16.0	13	9
JSC-A261	11-Jul-87	MD-02	Square	5.3	5.3	6.0	2.5	9.5	4.0	444			23.8	10.0	679.7	29.4	12.4	33	20
JSC-A305	13-Aug-87	MD-03	Circ.	3.8		3.8	2.5	5.6	3.6	261			18.2	11.8	434.3	23.5	15.2	31	14
NDE-26	04-Aug-87	MD-03	Oval	2.8	2.3	2.5	1.6	3.0	1.9	164			14.5	9.2	295.1	19.4	12.3	33	9
JSC-A245	30-Jun-87	MT-02	Rect.	9.5	8.25	8.9	3.7	11.7	4.9	0			0.0	0.0	251.1	17.9	7.5	15	16
NDE-27	04-Aug-87	MT-03	Oval	5.8	4.3	5.0	3.2	8.1	5.1	1			1.3	0.8	284.0	19.0	12.1	16	18
NDE-25	04-Aug-87	MT-04	Rect.	4.3	5.3	5.4	3.4	7.3	4.6	58			8.6	5.5	257.2	18.1	11.5	17	15

Table 4-1 (Cont). Shot Data Summary (Ordered by Target Serial Number)

Target Second Side Conditions: (outside of tube's 2nd wall, or back side of plate)

Shot	Date	Target S/N	2nd wall Hole Shape	Hole Dimensions Length (mm)	Hole Dimensions Width (mm)	Equiv. Circular Diameter (mm)	2nd Hole to Proj. Dia. Ratio	Surface Peel Total Area (mm^2)	Coated Tube Exposed Area (mm^2)	Coated Tube Additional Peel Area (mm^2)	Equiv. Circular Diameter (mm)	2nd Peel to Proj. Dia. Ratio	C-Scan Dimensions Area (mm^2)	C-Scan Dimensions Equiv. Circular Diameter (mm)	2nd C-scan to Proj. Dia. Ratio	Actual Shape: Approx. Length (mm)	Actual Shape: Overall Width (mm)	Both Sides (for tubes) or Single Side (plates): Hole to Proj. Dia. Ratio	Peel to Proj. Dia. Ratio	C-scan to Proj. Dia. Ratio
JSC-A333	03-Sep-87	6-F-1																3.1	5.6	16.8
NDE-33	25-Aug-87	6-F-1																2.6	7.8	14.5
JSC-A411	06-Nov-87	9s-F-1																3.6	7.5	16.4
NDE-35	20-Oct-87	9s-F-1																3.0	7.7	
NDE-7	15-Apr-87	9s-F-2																2.1	13.6	20.4
JSC-A181	10-Apr-87	9s-F-3						18.1			4.8	8.7						3.5	11.4	
JSC-A410	05-Nov-87	10-F-1																3.1	8.6	20.7
NDE-37	20-Oct-87	10-F-1																2.8	7.2	
JSC-A346	16-Sep-87	11-F-1																4.4	0.0	18.8
JSC-A352	21-Sep-87	11-F-1																4.6	0.0	19.6
NDE-34	25-Aug-87	11-F-1																3.8	1.6	
NDE-2	02-Feb-87	11-F-2																3.4	0.0	18.1
JSC-A409	05-Nov-87	12-F-1																4.6	3.3	13.9
NDE-36	20-Oct-87	12-F-1																2.9	2.3	10.2
NDE-3	06-Feb-87	12-F-2																4.8	0.0	
JSC-A413	09-Nov-87	13-F-1																4.9	0.0	11.6
NDE-38	20-Oct-87	13-F-1																3.6	3.4	
JSC-A204	19-May-87	6-T-1																2.3	11.4	21.3
JSC-A292	05-Aug-87	6-T-2						9			3.3	2.1	290	19	12.4	20	14	3.1	8.1	18.7
JSC-A308	17-Aug-87	6-T-2	Rect	20.3	22.9	24.8	7.9	1080			37.1	11.8	2278	54	17.2	58	40	8.3	13.7	19.5
JSC-A313	19-Aug-87	6-T-3																3.4	6.3	13.8
JSC-A329	01-Sep-87	6-T-3						55			8.4	5.4	142	13	8.7	14	10	3.3	9.2	15.9
NDE-22	04-Aug-87	6-T-3						2			1.6	1.0	63.3	9.0	5.7	12	5	2.1	4.9	10.2
JSC-A249	02-Jul-87	6s-T-1	Rect.	16.0	11.0	15.0	6.3	1015			35.9	15.1	1706	47	19.6	60	28	6.9	17.3	22.5
JSC-A334	08-Sep-87	6s-T-2	Rect.	33.0	22.9	31.0	7.1	3350			65.3	14.9	3814	70	15.9	109	35	7.4	15.6	17.1
NDE-11	11-Jun-87	6s-T-2																0.8	6.7	11.9
NDE-32	25-Aug-87	6s-T-2						164			14.5	9.4	314.8	20.0	13.0	26	12	2.2	12.5	18.3
JSC-A206	20-May-87	6-T-4																2.4	7.5	13.2
JSC-A250	06-Jul-87	6-T-4						720			30.3	12.8	1505	44	18.4	50	30	2.9	15.6	22.0
JSC-A307	14-Aug-87	6-T-6						7.5			3.1	2.0	134	13	8.5	13	10	2.8	9.8	14.9
NDE-12	11-Jun-87	6-T-6																1.9	2.2	14.0
NDE-23	04-Aug-87	6-T-6																1.8	5.0	8.3
NDE-13	11-Jun-87	6-T-9																1.3	4.6	11.2
NDE-24	04-Aug-87	6-T-9																2.2	3.5	7.8
NDE-28	25-Aug-87	7-T-2																1.8	4.4	8.2
JSC-A211	28-May-87	7-T-3																2.4	11.8	21.4
NDE-21	30-Jul-87	8-T-2						3			1.8	0.8	308.0	19.8	8.3	28	11	1.3	7.0	14.2
NDE-29	25-Aug-87	8-T-2																2.0	8.2	13.3
JSC-A293	06-Aug-87	9-T-1						31			6.3	4.1	500	25	16.3	25	20	2.8	9.0	22.1
NDE-30	25-Aug-87	9-T-2						90			10.7	6.8	249.9	17.8	11.4	24	10	2.5	11.5	19.1
JSC-A208	22-May-87	9s-T-1																2.2	8.0	17.8
NDE-31	25-Aug-87	9s-T-2						62			8.9	5.7	259.3	18.2	11.8	15	17	1.9	7.6	14.6
JSC-A209	26-May-87	10-T-1																2.3	10.1	16.5
JSC-A294	06-Aug-87	10-T-2						45			7.6	4.9	431	23	15.1	20	22	2.8	10.9	17.7
NDE-19	30-Jul-87	10-T-2																1.3	6.0	11.7
JSC-A196	11-May-87	11-T-2																3.9	0.0	

Table 4-1 (Cont). Shot Data Summary (Ordered by Target Serial Number)

Target Second Side Conditions: (outside of tube's 2nd wall, or back side of plate)

				Hole Dimensions								C-Scan Dimensions					Both Sides (for tubes) or Single Side (plates):		
Shot	Date	Target S/N	2nd wall Hole Shape	Length (mm)	Width (mm)	Equiv. Circular Diameter (mm)	2nd Hole to Proj. Dia. Ratio	Surface Peel Total Area (mm^2)	Coated Tube Exposed Area (mm^2)	Coated Tube Additional Peel Area (mm^2)	Equiv. Circular Diameter (mm)	2nd Peel to Proj. Dia. Ratio	Area (mm^2)	Equiv. Circular Diameter (mm)	2nd C-scan to Proj. Dia. Ratio	Actual Shape: Approx. Overall Length (mm)	Actual Shape: Approx. Overall Width (mm)	Hole to Proj. Dia. Ratio	Peel to Proj. Dia. Ratio	C-scan to Proj. Dia. Ratio
JSC-A246	01-Jul-87	11-T-2	Rect.	21.4	19.1	22.8	9.6						1889	49.0	20.6	48	39	10.4	0.0	22.2
JSC-A201	14-May-87	11-T-4																4.0	0.0	16.9
JSC-A291	05-Aug-87	11-T-4						36			6.8	4.4	653	29	18.6	25	26	4.9	4.4	22.6
JSC-A212	29-May-87	11s-T-1																4.2	0.0	14.1
JSC-A302	12-Aug-87	12-T-2						82			10.2	6.6	684	30	19.0	28	25	4.9	6.6	24.1
NBE-18	28-Jul-87	12-T-2																4.3	2.4	16.0
JSC-A261	11-Jul-87	MB-02	Rect.	13.0	3.0	7.0	3.0	1040			36.4	15.3	1650	46	19.3	59	28	3.9	18.3	23.0
JSC-A305	13-Aug-87	MB-03						17			4.6	3.0	297	19	12.6	18	17	2.5	12.2	19.8
NBE-26	04-Aug-87	MB-03											102.7	11.4	7.3	17	6	1.6	9.2	14.3
JSC-A245	30-Jun-87	MT-02	Rect.	25.5	23	24.2	10.2						2085	51.5	21.7	47	44	10.9	0.0	23.0
NBE-27	04-Aug-87	MT-03	Rect.	3.0	2.1	2.9	1.8	55			8.4	5.3	601.6	27.7	17.6	20	30	3.7	5.4	21.3
NBE-25	04-Aug-87	MT-04	Oval	5.3	2.0	3.3	2.1	55			8.4	5.3	807.0	32.1	20.3	29	28	4.0	7.6	23.4

Table 4-1 (Cont). Shot Data Summary (Ordered by Target Serial Number)

Witness Plate Conditions

Shot	Date	Target S/N	Material	Thickness (in)	Dist. from Target (in)	Number of Impact Perfor-ations	Maximum Hole Dia. (mm)	Dia. of Dispersion Area of Conc. hits/perf (in)	half-angle of Conc. Hits (deg)	Dia. of all impacts (in)	Max. Disp. half-angle of any impact (deg)
JSC-A333	03-Sep-87	6-F-1	Al 3003-0	0.016	2	50	1.2	1	27	3	56
NDE-33	25-Aug-87	6-F-1	Al6061-T6	0.032	0.25	1	4.6	0.18	36	0.49	63
JSC-A411	06-Nov-87	9s-F-1	Al 3003-0	0.016	2	43	2.0	1.3	32	3.0	56
NDE-35	20-Oct-87	9s-F-1	Al6061-T6	0.032	0.25	1	5.2	0.20	39	0.20	39
NDE-7	15-Apr-87	9s-F-2	Al6061-T6	0.032	0.25					0.3	50
JSC-A181	10-Apr-87	9s-F-3	Al6061-T6	0.032	2	0					
JSC-A410	05-Nov-87	10-F-1	Al 3003-0	0.016	2	33	2.5	1.1	29	2.8	54
NDE-37	20-Oct-87	10-F-1	Al6061-T6	0.016	0.25	1	5.5	0.22	41	0.22	41
JSC-A346	16-Sep-87	11-F-1	Al 3003-0	0.016	2	26	0.9	1.2	31	3.25	58
JSC-A352	21-Sep-87	11-F-1	Al 3003-0	0.016	2	23	0.9	1.5	37	3.5	60
NDE-34	25-Aug-87	11-F-1	Al6061-T6	0.032	0.25	1	2	0.22	41	0.59	67
NDE-2	02-Feb-87	11-F-2	Al6061-T6	0.032	0.25						
JSC-A409	05-Nov-87	12-F-1	Al 3003-0	0.016	2	18	1.4	1.4	35	3.0	56
NDE-36	20-Oct-87	12-F-1	Al6061-T6	0.032	0.25			0.16	32	0.45	61
NDE-3	06-Feb-87	12-F-2	Al6061-T6	0.032	0.25						
JSC-A413	09-Nov-87	13-F-1	Al 3003-0	0.016	2	38	1.2	1.4	35	2.8	54
NDE-38	20-Oct-87	13-F-1	Al6061-T6	0.032	0.25						
JSC-A204	19-May-87	6-T-1									
JSC-A292	05-Aug-87	6-T-2									
JSC-A308	17-Aug-87	6-T-2									
JSC-A313	19-Aug-87	6-T-3									
JSC-A329	01-Sep-87	6-T-3									
NDE-22	04-Aug-87	6-T-3									
JSC-A249	02-Jul-87	6s-T-1	Al 3003-0	0.016	2						
JSC-A334	08-Sep-87	6s-T-2	Al 3003-0	0.008	2						
NDE-11	11-Jun-87	6s-T-2									
NDE-32	25-Aug-87	6s-T-2									
JSC-A206	20-May-87	6-T-4									
JSC-A250	06-Jul-87	6-T-4	Al 3003-0	0.016	2						
JSC-A307	14-Aug-87	6-T-6									
NDE-12	11-Jun-87	6-T-6									
NDE-23	04-Aug-87	6-T-6									
NDE-13	11-Jun-87	6-T-9									
NDE-24	04-Aug-87	6-T-9									
NDE-28	25-Aug-87	7-T-2									
JSC-A211	28-May-87	7-T-3									
NDE-21	30-Jul-87	8-T-2									
NDE-29	25-Aug-87	8-T-2									
JSC-A293	06-Aug-87	9-T-1									
NDE-30	25-Aug-87	9-T-2									
JSC-A208	22-May-87	9s-T-1									
NDE-31	25-Aug-87	9s-T-2									
JSC-A209	26-May-87	10-T-1									
JSC-A294	06-Aug-87	10-T-2									
NDE-19	30-Jul-87	10-T-2									
JSC-A196	11-May-87	11-T-2									

Table 4-1 (Cont). Shot Data Summary (Ordered by Target Serial Number)

Witness Plate Conditions

Shot	Date	Target S/N	Material	Thickness (in)	Dist. from Target (in)	Number of Impact Perfor-ations	Maximum Hole Dia. (mm)	Dia. of Dispersion Area of Conc. hits/perf (in)	half-angle of Conc. Hits (deg)	Dia. of all impacts (in)	Max. Disp. half-angle of any impact (deg)
JSC-A246	01-Jul-87	11-T-2	Al 3003-0	0.016	2						
JSC-A201	14-May-87	11-T-4									
JSC-A291	05-Aug-87	11-T-4									
JSC-A212	29-May-87	11s-T-1									
JSC-A302	12-Aug-87	12-T-2									
NDE-18	28-Jul-87	12-T-2									
JSC-A261	11-Jul-87	MD-02	Al 3003-0	0.016	2						
JSC-A305	13-Aug-87	MD-03									
NDE-26	04-Aug-87	MD-03									
JSC-A245	30-Jun-87	MT-02	Al 3003-0	0.016	2						
NDE-27	04-Aug-87	MT-03									
NDE-25	04-Aug-87	MT-04									

4.1 Effect of Projectile Size/Mass

Photographic documentation given in Figures 4-2 through 4-7 of a series of shots on the 6T series of uncoated tubes (Amoco, 0.07" nominal thickness, 34M psi fiber modulus) illustrates the effect of projectile size on tube damage. All of these shots impacted essentially normal to the tube's first wall (all impact obliquity angles <10° in radial direction). Glass projectiles less than 1mm in diameter created a hole on one side of the target tubes. Peeling in the 10° direction of the surface ply was evident in all shots. Peeled area is summarized in Table 4-1 and broken down into detailed measurements in Appendix A.

Transition to more significant damage to the second wall of the tube was evident by external delamination of the second wall caused by 1.6 mm (0.063") diameter aluminum projectiles (Figure 4-4). As shown in Figure 4-5, the expanding debris plume from impact of a 2.4 mm (0.094") on the front wall of the tube produces several holes in the second wall and a large delamination area. A 3.1 mm (0.125") aluminum sphere produced a nearly circular hole in the second wall ~8 times larger than the projectile. Figure 4-7 depicts the results of an impact by the largest particle shot during the test: a 73 mg, 4.4 mm diameter by 4.4 mm long nylon cylinder. This projectile was shot in an attempt to find a particle that would completely break a representative test tube specimen. However, although the second wall hole was larger and more irregular in this case, its equivalent circular diameter was just over 7 times larger than projectile, and the tube was not broken.

The first wall through-hole diameter size for all NDE and JSC data shots on the 6T series tubes are shown in Figure 4-8. Regression analysis was used to find the best correlation of hole size with projectile density, size, velocity, and impact obliquity. For the 10 data points in the set, the diameter of a circular hole with an area equivalent to the actual measured hole area, D_{h1} (mm), was found to be related to the cube root of projectile energy, E (J):

$$D_{h1} = 0.907 * (E)^{0.33} - 0.388$$

The correlation coefficient, r, for this expression is 0.98 (1.00 is a perfect fit). Hole size was found to be independent of the projectile impact obliquity angle. As will be discussed

in Section 4.7, although the shape of the hole changed as a function of impact obliquity, the total area of the hole, and thus the equivalent circular hole diameter, remained essentially constant for the same impact particle size and velocity (for the impact obliquity angles tested; with no impact angles greater than 45°). Since projectile diameter d (mm), density p (g/cc), and velocity V (km/sec), can be related to projectile energy by:

$$E = \pi/12 * d^3 * p * V^2$$

The first wall hole diameter correlation becomes:

$$D_{h1} = 0.58 * d * p^{0.33} * V^{0.67} - 0.388$$

Ultrasonic C-scan diameter of the damage in the first wall for the ten 6T uncoated tubes is given in given in Figure 4-9. The equivalent circular C-scan diameter, D_{c1} (mm), was correlated with the cube root of the product of projectile energy and tube wall thickness to projecile diameter ratio, t/d, with a correlation coefficient of 0.95:

$$D_{c1} = 3\,(E * t/d)^{0.33} + 4.0$$

The standard deviation in the measured and estimated C-scan diameters for this equation is 2.1 mm. The form of this equation was suggested after extensive analysis of previously reported C-scan area data for hypervelocity impacts into generic graphite-epoxy targets (20). Data from over 40 impacts of 5 mg aluminum and nylon cylinders at 4.5-7 km/sec into low modulus G/E flat plate targets (with and without cloth covering surface coating) ranging in thickness from 2.4 mm to 17.1 mm were correlated with the following equation (r = 0.97):

$$D_c/d = 2.72\, V^{0.67}\, p^{0.33}\, (t/d)^{0.33} + 0.26$$

The data and correlation curve are given in Figure 4-10. Rearranged and neglecting the y-intercept, this equation becomes:

$$D_c = 4.2\, E^{0.33}\, (t/d)^{0.33}$$

The combined first and second wall hole diameter, D_{hb} (mm), given in Table 4-1 was calculated from the equivalent circular first wall hole diameter, D_{h1}, and second wall hole diameter, D_{h2}, simply by:

$$D_{hb} = (D_{h1}^2 + D_{h2}^2)^{0.5}$$

For the ten 6T series tube data points, the combined hole diameter is plotted in Figure 4-11 with the following correlation:

For projectiles with an energy less than 127 J ($D_{hb} < 4.4$ mm),

$$D_{hb} = 1.14\ E^{0.33} - 1.29 \qquad r = 0.95$$

And for projectiles with an energy greater than 127 J ($D_{hb} > 4.4$ mm),

$$D_{hb} = 4.32\ E^{0.33} - 17.25 \qquad r = 0.96$$

This implies that for this particular type tube (10,30,10 layup, 34 M psi modulus fibers, 0.07" thick walls) projectiles with energies more than 125 joules will produce increasingly more damage to the second wall. This is because the projectile fragments upon impact with the first wall, producing a plume (bubble) of debris particles that expands as it is projected onto a large area of the tube's second wall. The half-angle (measured from the surface normal at the impact point) of the most concentrated debris in the expanding plume is ~15° for the impacts studied.

The combined diameter of the ultrasonic C-scan region (internal delamination and through holes) for the 6T series tubes is described by (Figure 4-12):

For projectiles with $(E * t/d) < 180$ J, or for $D_{cb} < 26$ mm,

$$D_{cb} = 4.64\ (E * t/d)^{0.33} - 0.39 \qquad r = 0.89$$

And for projectiles with $(E * t/d) > 180$ J, or for $D_{cb} > 26$ mm,

$$D_{cb} = 16.90\ (E * t/d)^{0.33} - 69.8 \qquad r = 0.99$$

Figure 4-2. Projectile Size Effects: Photographic Documentation of Shot NDE-11
NDE-11, Tube 6s-T-2, 0.77 mm glass sphere, 4.21 km/sec, 10° radial obliquity.

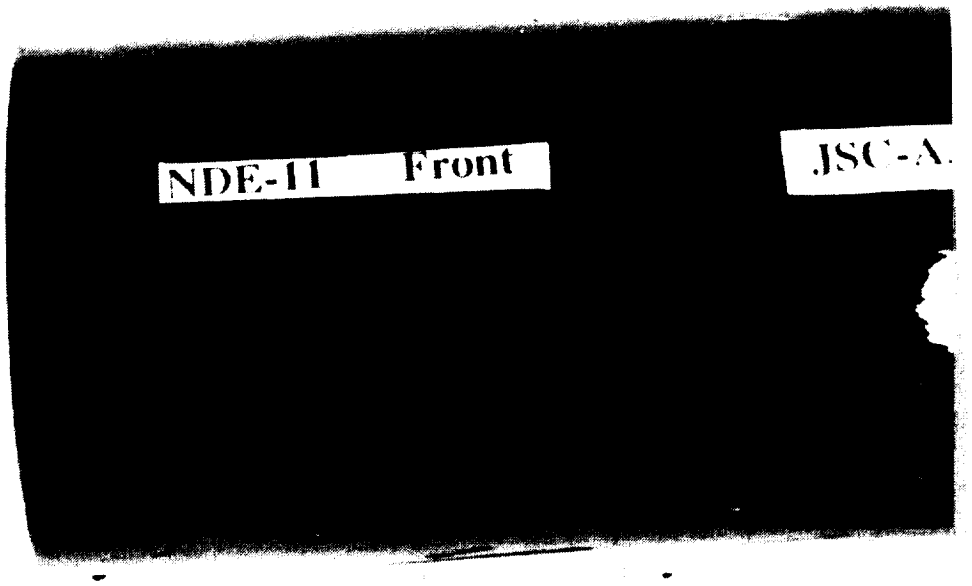

Figure 4-3. Projectile Size Effects: Photographic Documentation of Shot JSC-A204
JSC-A204, Tube 6-T-1, 0.938 mm Glass sphere, 7.05 km/sec, 7° radial obliquity.

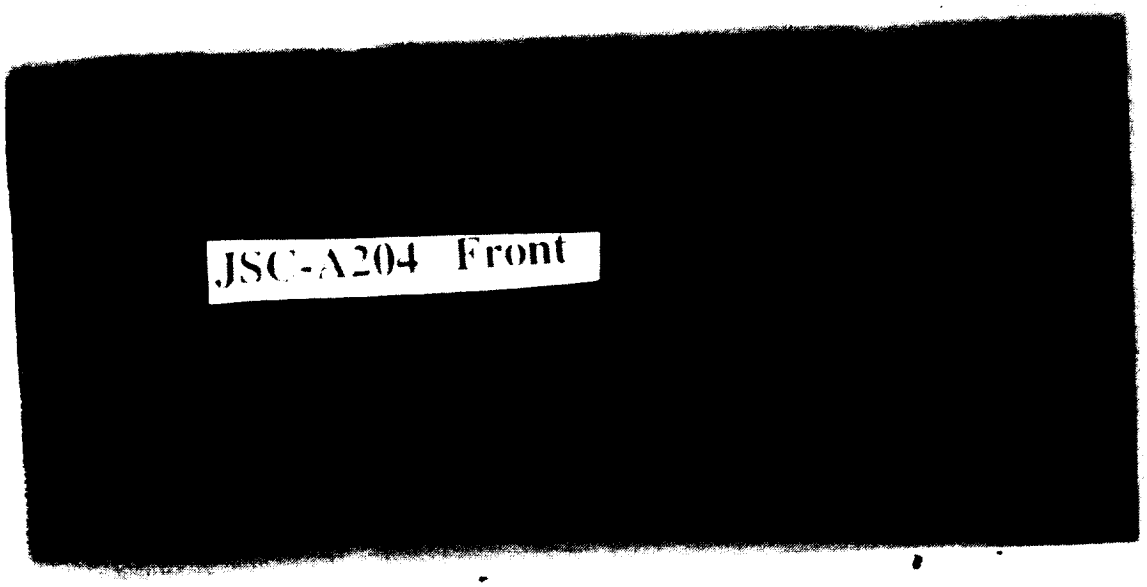

Figure 4-4. Projectile Size Effects: Photographic Documentation of Shot JSC-A292
JSC-A292, Tube 6-T-2, 1.55 mm Al 2024-T4 sphere, 7.78 km/sec, 10° radial obliquity.

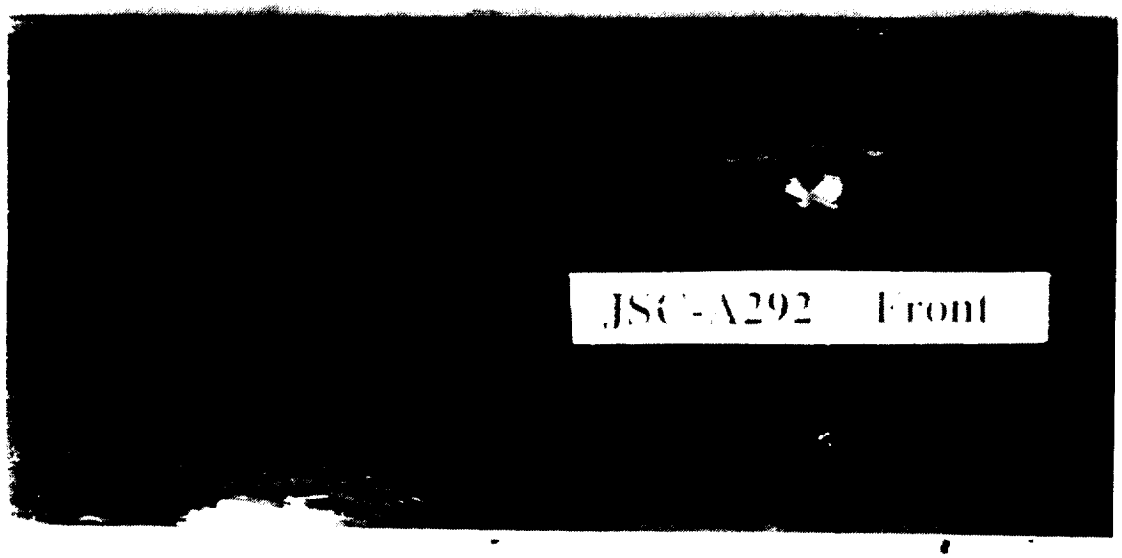

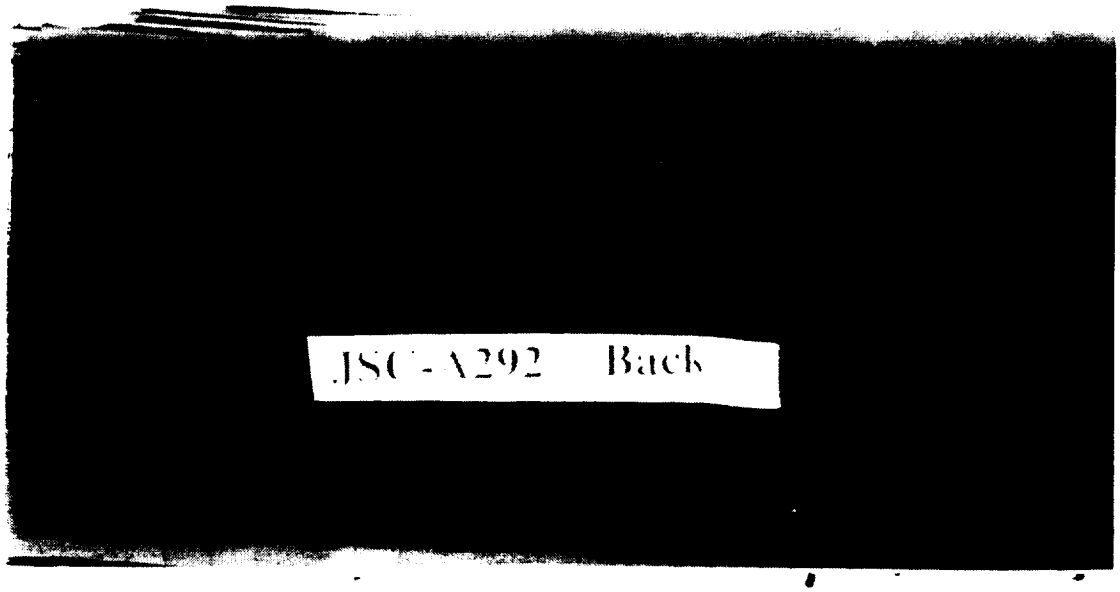

Figure 4-5. Projectile Size Effects: Photographic Documentation of Shot JSC-A249
JSC-A249, Tube 6s-T-1, 2.38 mm Al 2024-T4 sphere, 7.48 km/sec, 5° radial obliquity.

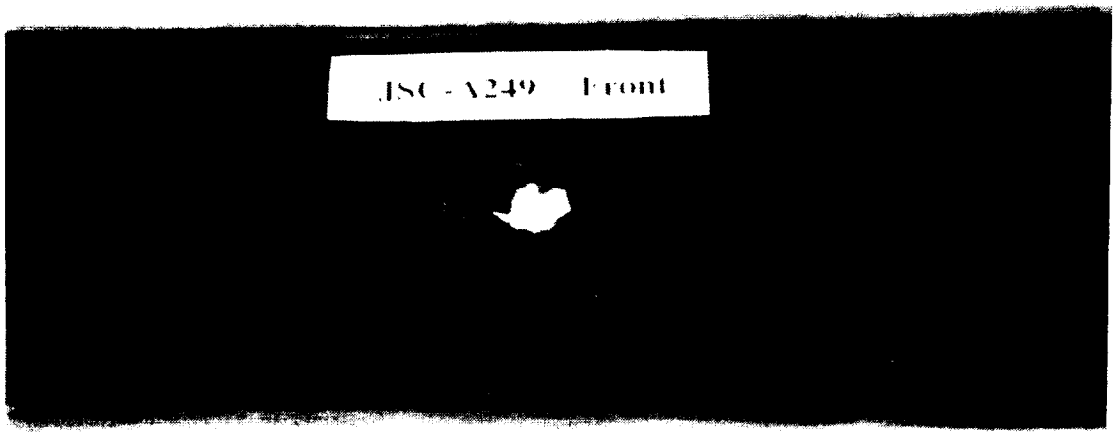

Figure 4-6. Projectile Size Effects: Photographic Documentation of Shot JSC-A308
JSC-A308, Tube 6-T-2, 3.14 mm Al 2024-T4 sphere, 6.10 km/sec, 3° radial obliquity.

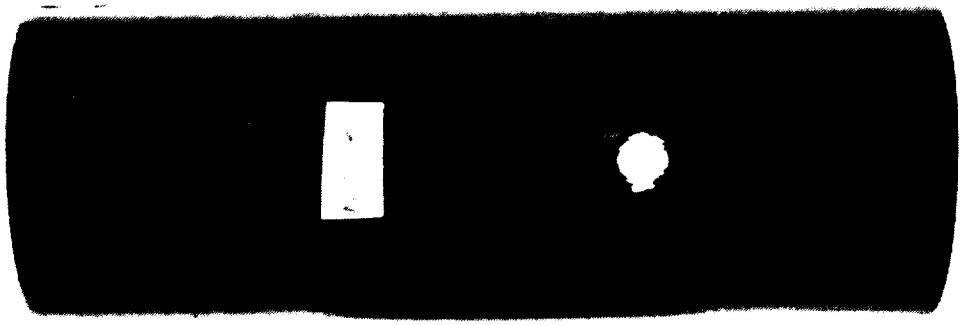

JSC-A308 Front

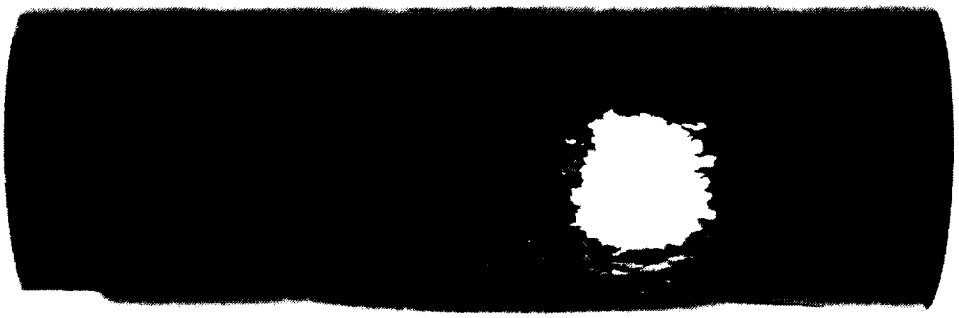

JSC-A308 Back

Figure 4-7. Projectile Size Effects: Photographic Documentation of Shot JSC-A334
JSC-A334, Tube 6s-T-2, 4.4 mm Nylon Slug (L/D=1), 6.68 km/sec, 9° radial obliquity.

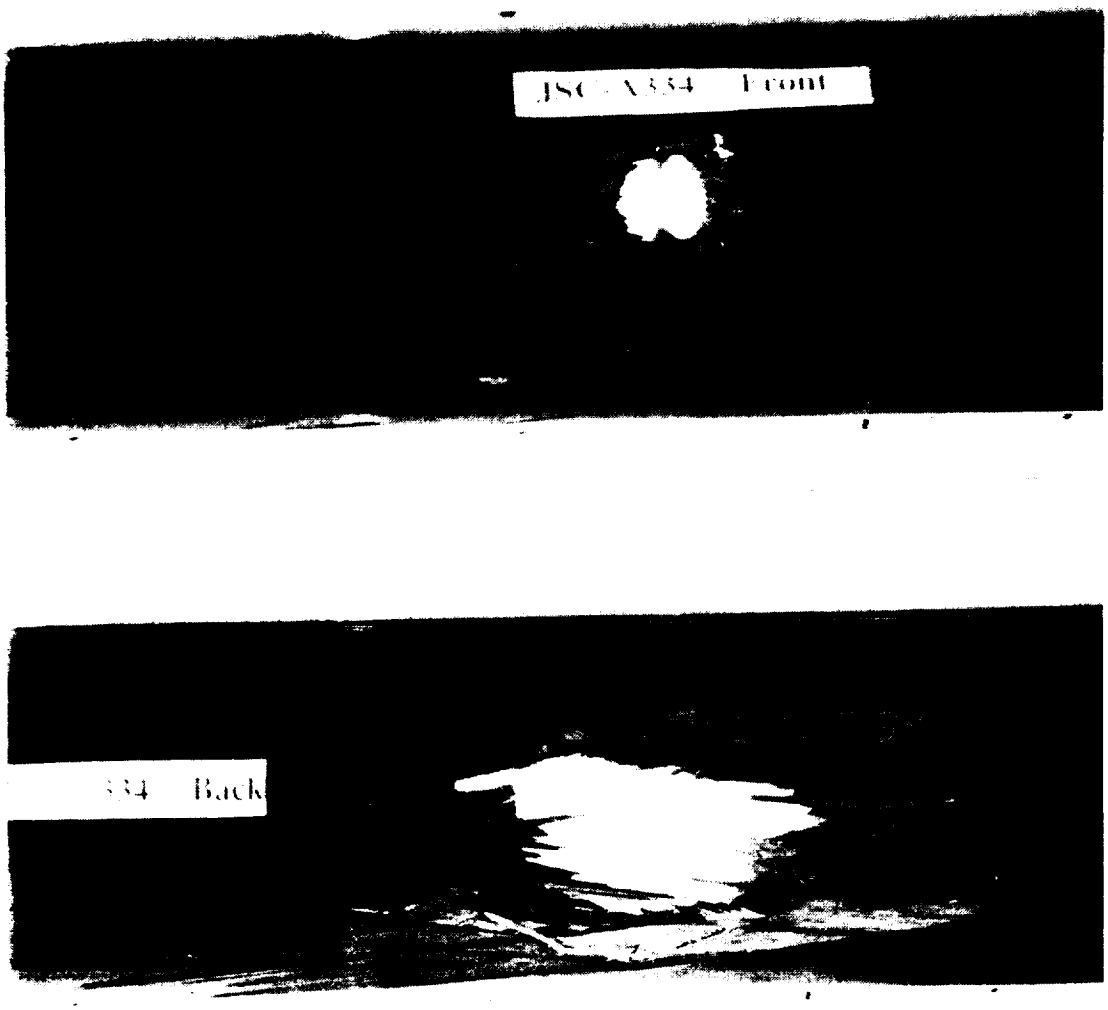

Figure 4-8. First Wall Hole Size for 6T Series Tubes

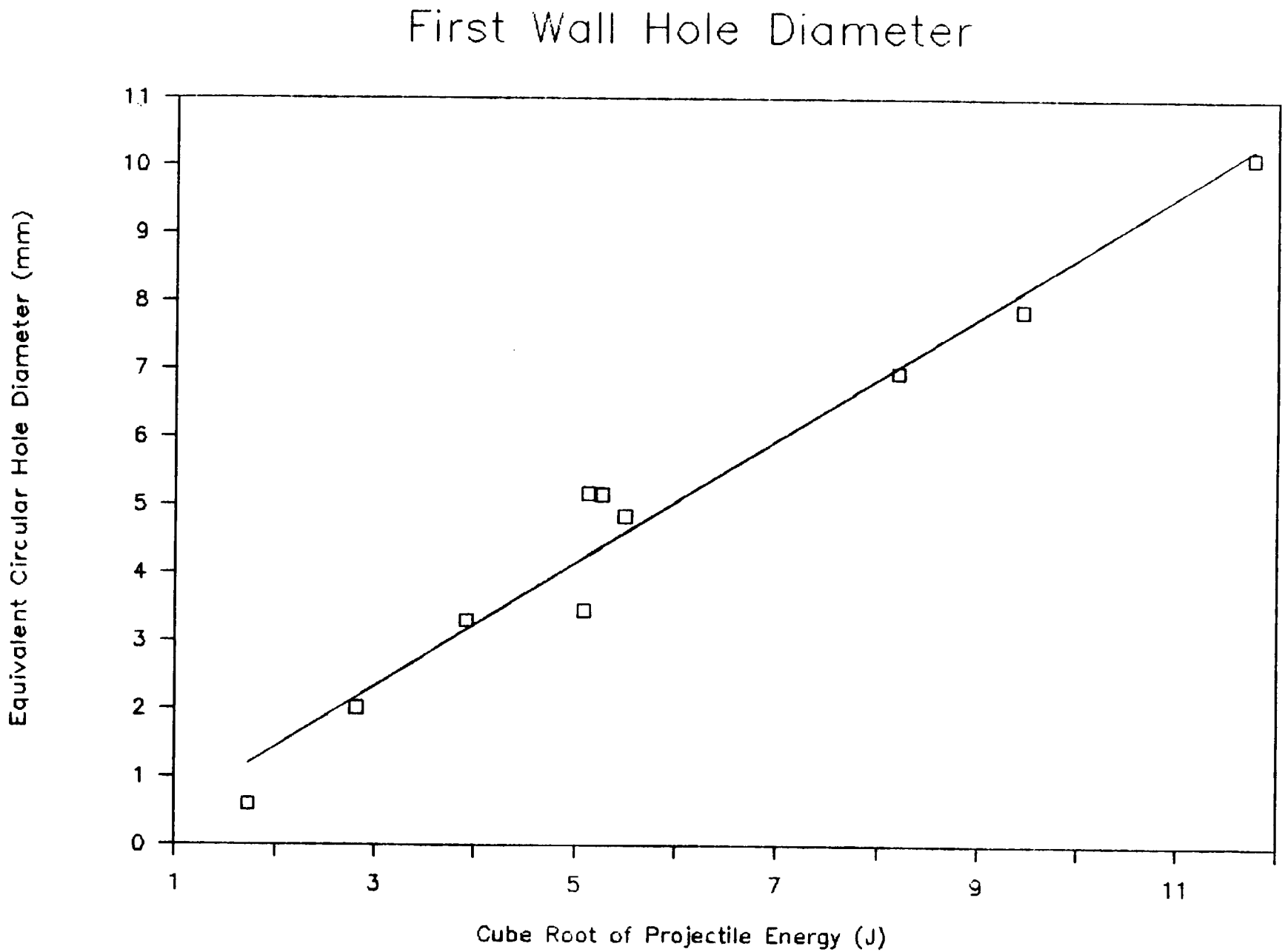

Figure 4-9. First Wall C-Scan Size for 6T Series Tubes

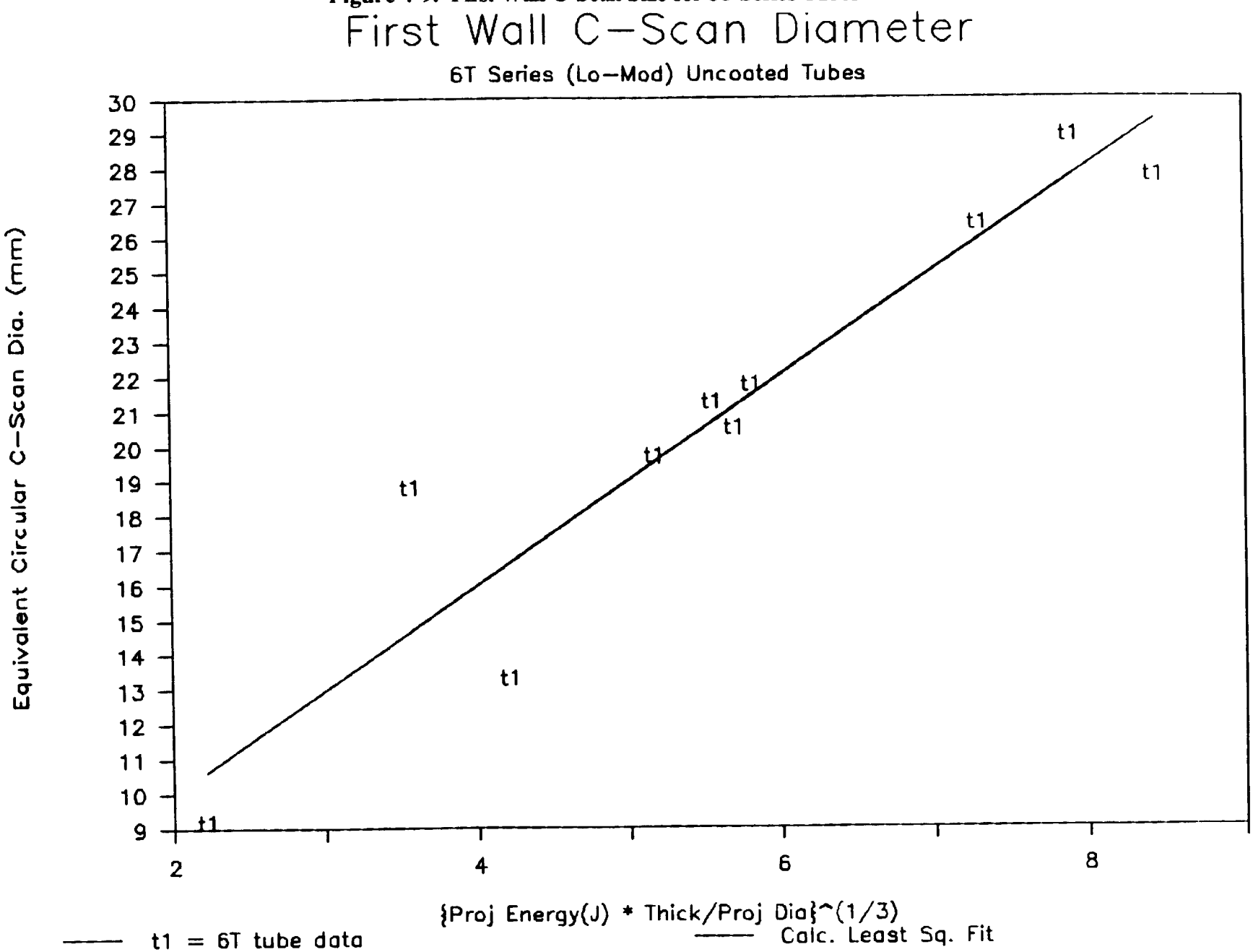

Figure 4-10. C-Scan Size Correlation for Data from Previous Study

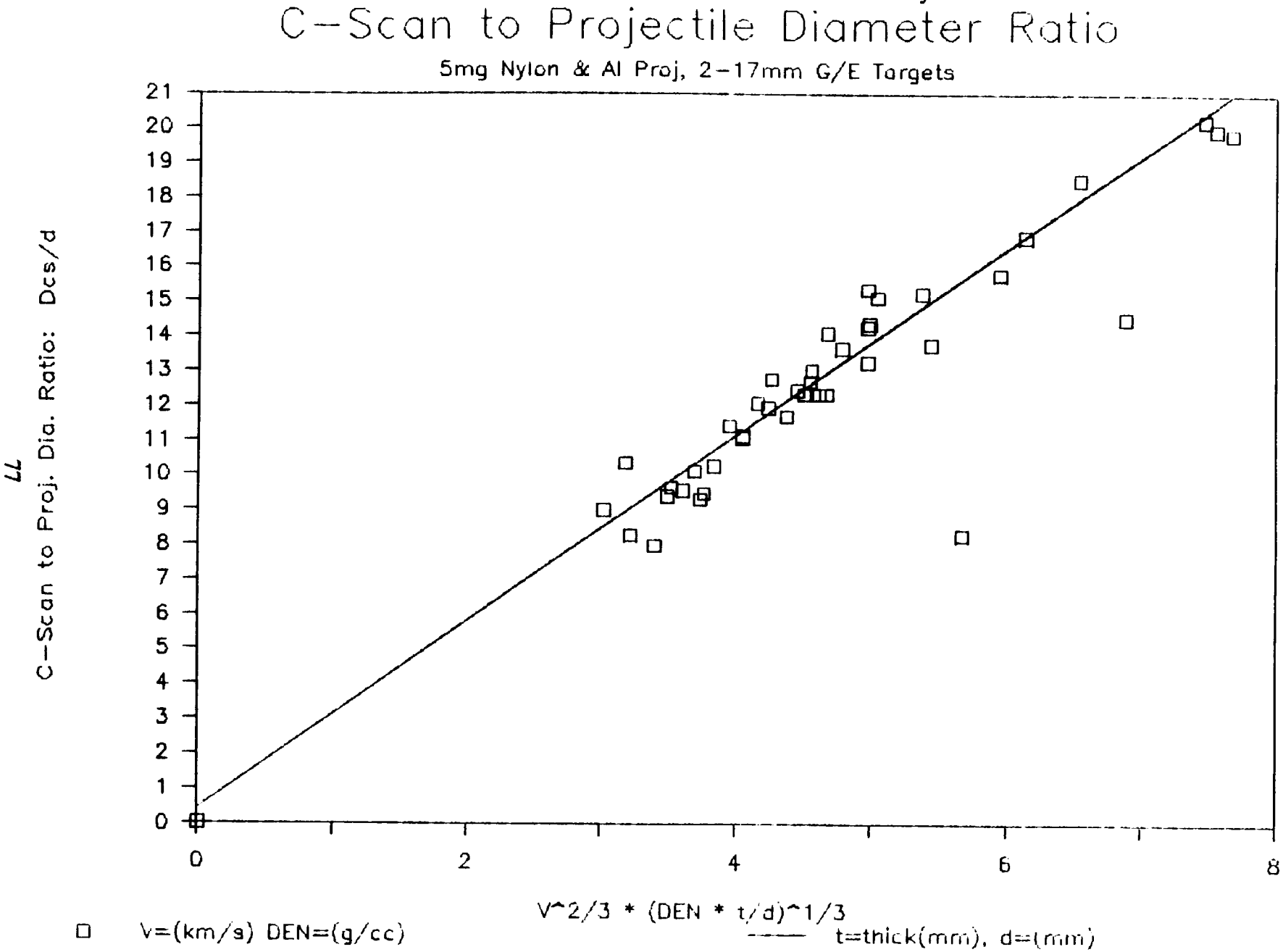

Figure 4-11. Combined First and Second Wall Hole Size for 6T Series Tubes

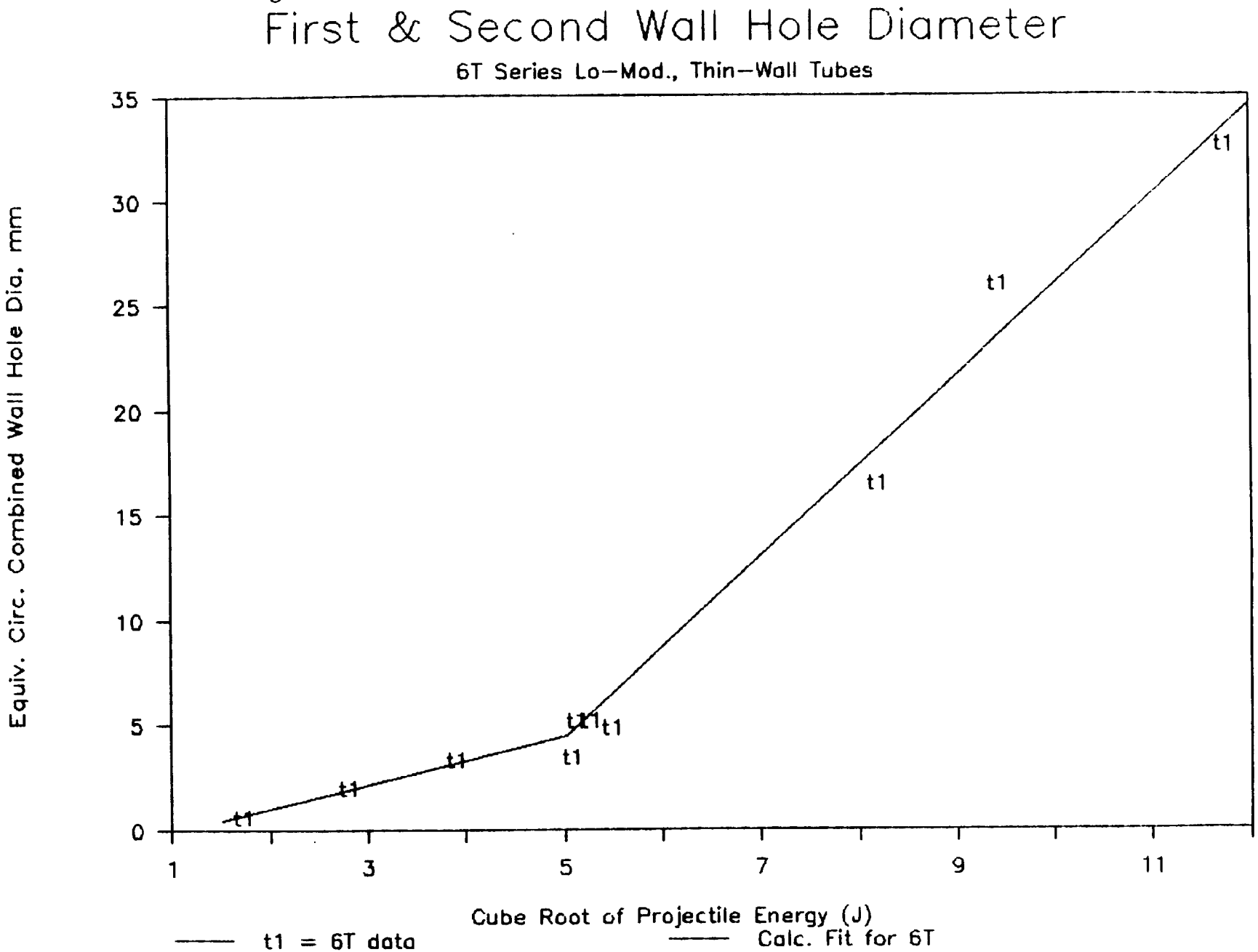

Figure 4-12. Combined First and Second Wall C-Scan Size for 6T Series Tubes

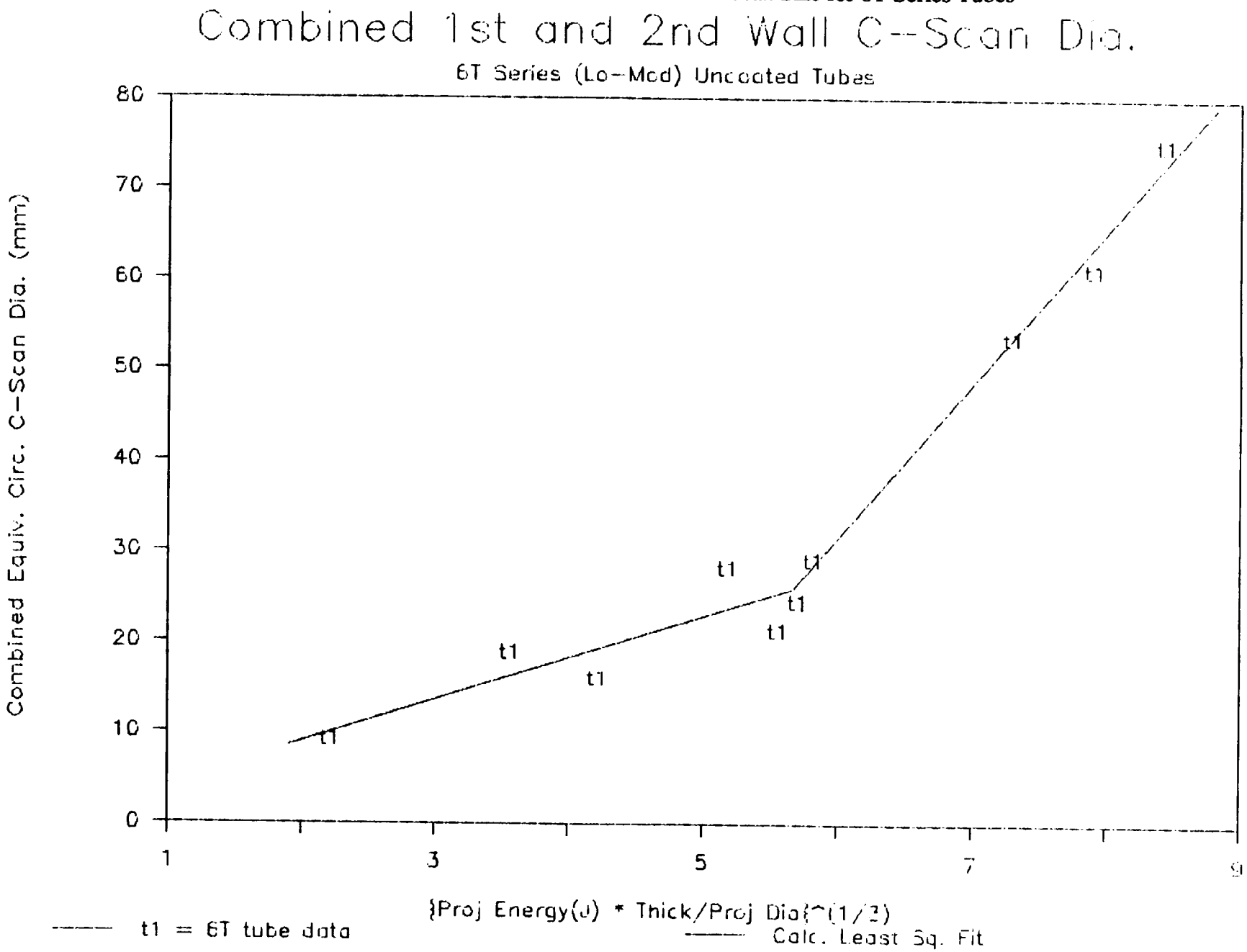

4.2 Effect of Ply Orientation

A series of impact tests were conducted to study the effect of ply layup on the extent of impact damage. Low-modulus, uncoated tubes were tested (9T and 10T series) and compared with the results of the 6T series tests given in the previous section. Damage illustrated in Figures 4-13 and 4-14 (for 9T and 10T tubes respectively) should be compared with Figure 4-4. Although the orientation of the surface peeling varied between the different ply layups (6T peeled in 10°, 9T peeled on interior surfaces in 80°, and 10T peeled in 45° direction to the longitudinal axis of the tube), the damage hole or C-scan size did not appreciably vary as a function of layup. Hole diameters for the seven 9T and 10T data points are compared in Figure 4-15 with the 6T first wall hole size correlation given in the previous section. A new formulation for all uncoated, low-modulus, Amoco tubes (17 data points) is shown in Figure 4-16 and is given by the following equation:

$$D_{h1} = 0.927\ E^{0.33} - 0.536 \qquad r = 0.98$$

where D_{h1} is the hole diameter (mm), E is projectile energy (J), and r is a measure of the goodness of fit for the correlation (r = 1 is a prefect fit). Differences were small for the low and high modulus tube first-wall C-scan size as a function of projectile parameters, therefore a combined expression was formulated as described in Section 4.3.

As given in Figure 4-17, little change to the 6T combined hole diameter correlation was indicated to account for the 9T and 10T data:

For projectiles with an energy less than 155 J ($D_{hb} < 4.8$ mm),

$$D_{hb} = 1.14\ E^{0.33} - 1.29 \qquad r = 0.95$$

And for projectiles with an energy greater than 155 J ($D_{hb} > 4.8$ mm),

$$D_{hb} = 4.54\ E^{0.33} - 19.54 \qquad r = 0.99$$

where D_{hb} is the combined hole diameter (mm) and E is projectile energy (J). Figure 4-18 presents the correlations for the combined wall C-scan diameter for all low-modulus Amoco tubes:

For projectiles with $(E * t/d) < 200$ J, or for $D_{cb} < 30$ mm,

$$D_{cb} = 5.60\,(E * t/d)^{0.33} - 3.32 \qquad r = 0.83$$

And for projectiles with $(E * t/d) > 200$ J, or for $D_{cb} > 30$ mm,

$$D_{cb} = 16.90\,(E * t/d)^{0.33} - 69.8 \qquad r = 0.99$$

where D_{cb} is the combined C-scan diameter (mm), E is projectile energy (J), t is the tube thickness (mm), and d is projectile diameter (mm). No significant difference between symmetric and repetitive layups was noted. With the data in Table 4-1, a nearly direct comparison of impact damage can be made for the 6T tubes with shots JSC-A292 and NDE-32, and for 9T tubes with shots NDE-30 and NDE-31.

Figure 4-13. Ply Orientation Effects: Photographic Documentation of Shot JSC-A293
JSC-A293, Tube 9-T-1, 1.55 mm Al 2024-T4 sphere, 7.47 km/sec, 10° radial obliquity.

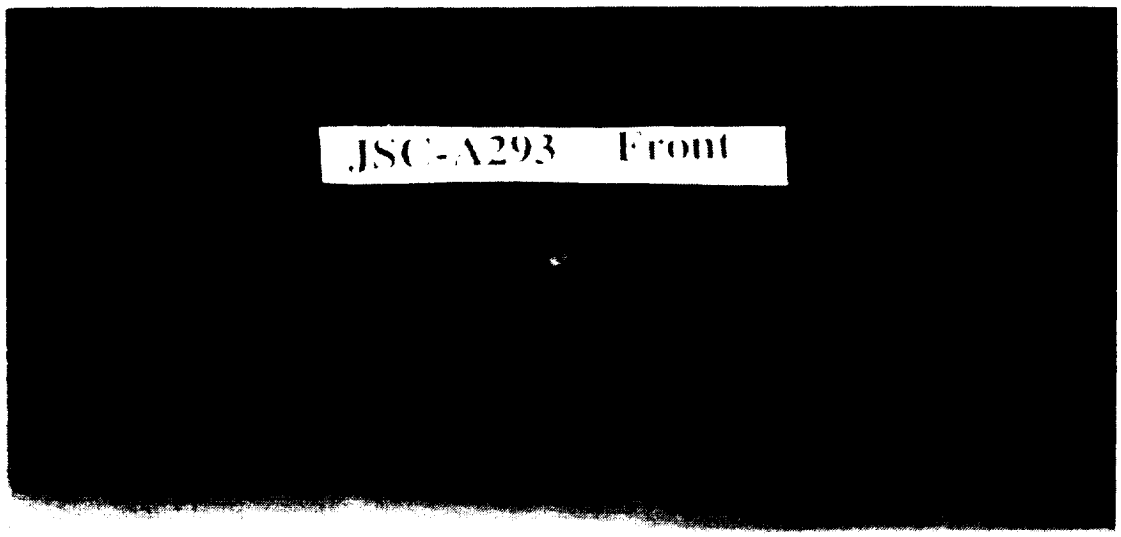

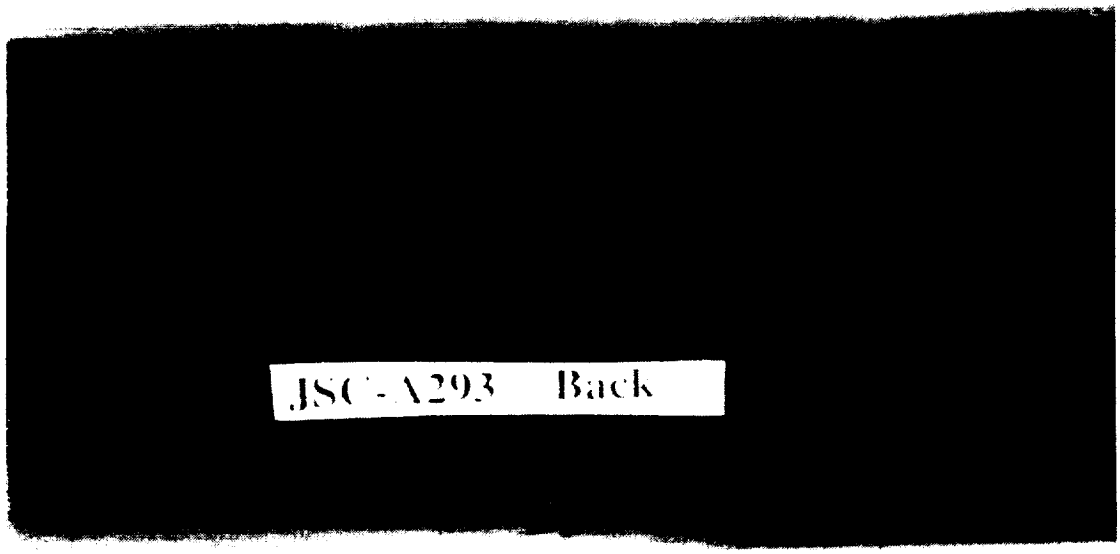

Figure 4-14. Ply Orientation Effects: Photographic Documentation of Shot JSC-A294
JSC-A294, Tube 10-T-2, 1.55 mm Al 2024-T4 sphere, 7.33 km/sec, 3° radial obliquity.

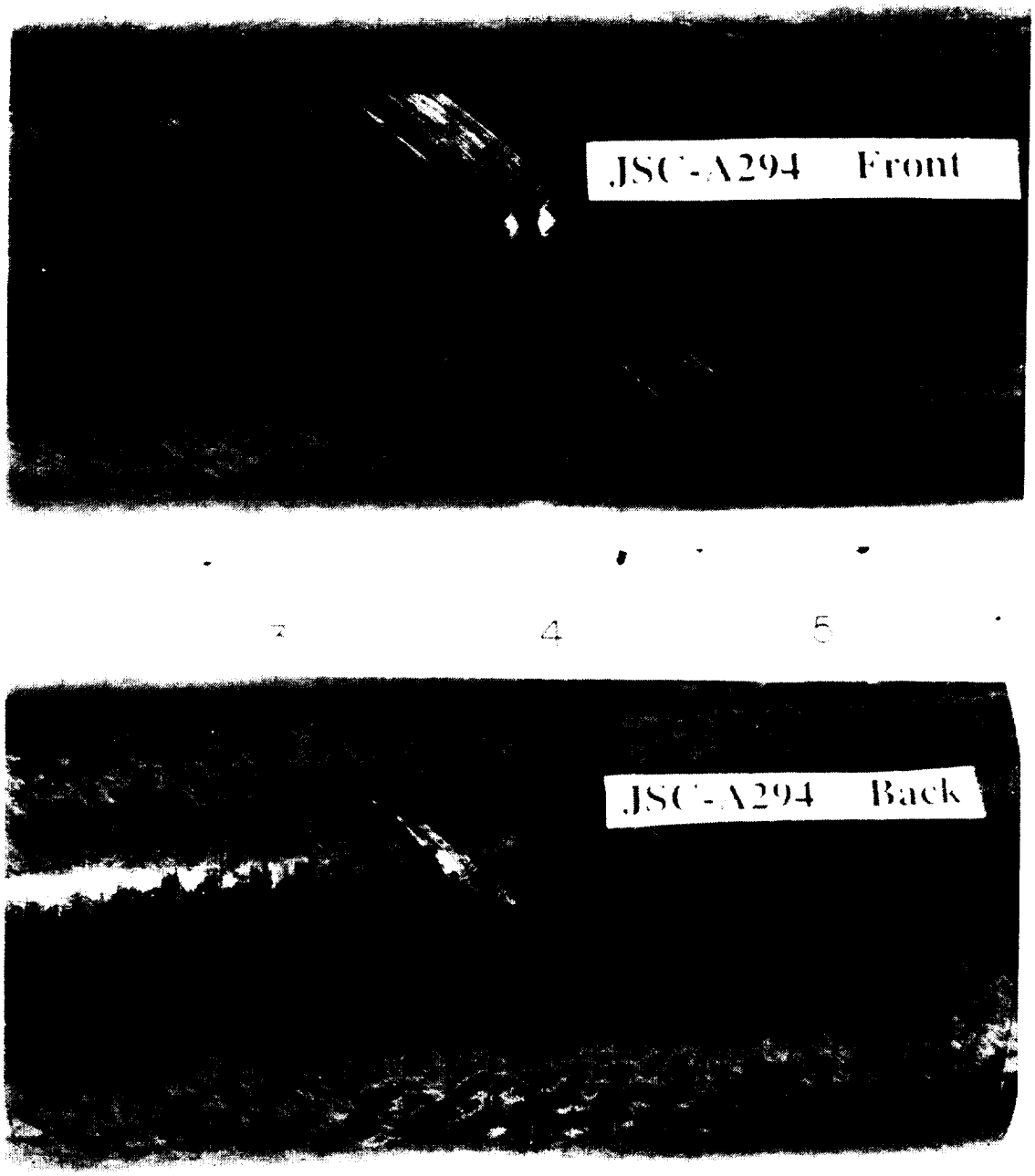

Figure 4-15. 9T and 10T Tube First Wall Hole Diameter Versus 6T Correlation

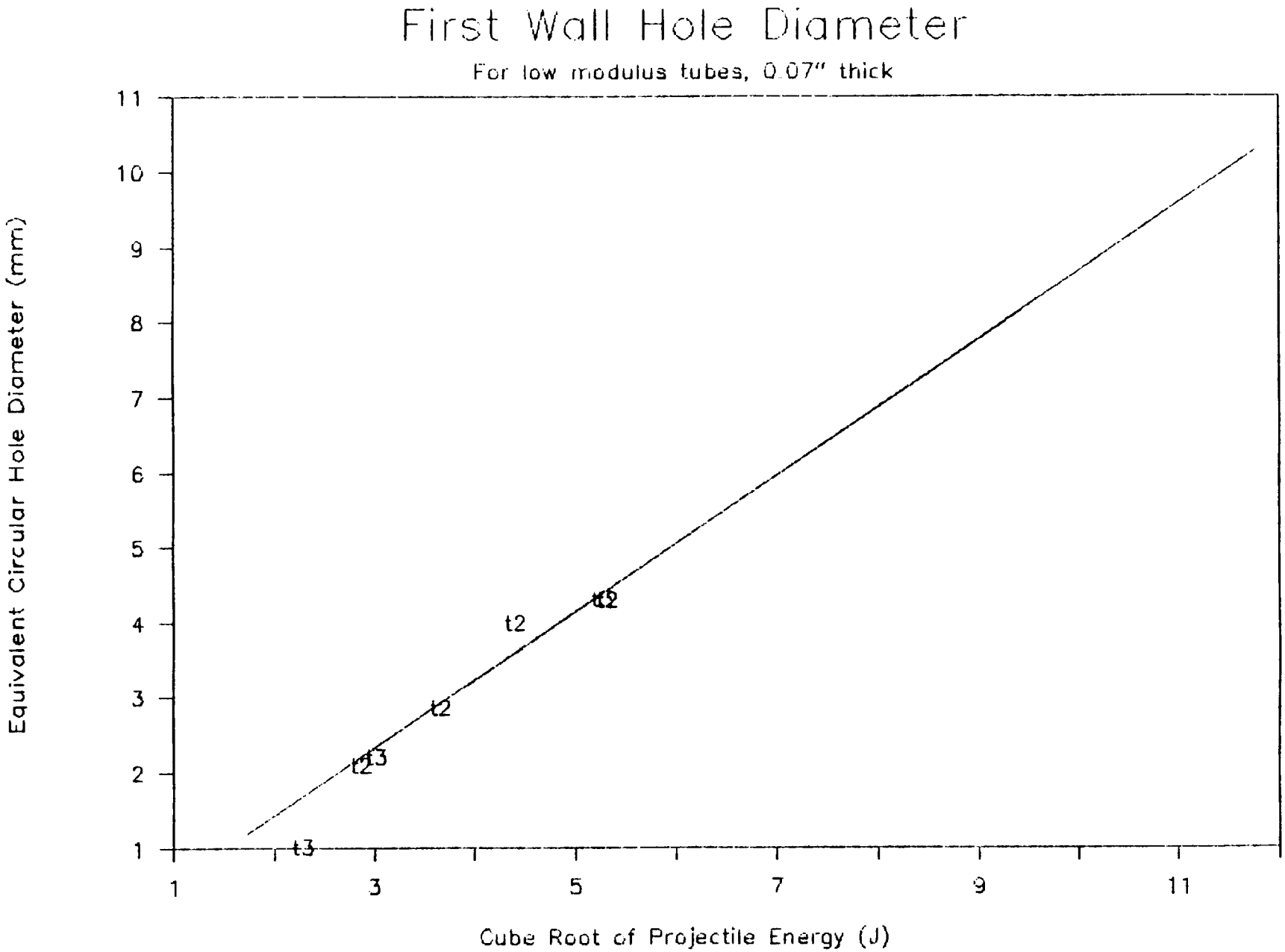

Figure 4-16. First Wall Hole Diameter for all Amoco, Uncoated, Low-Modulus Tubes

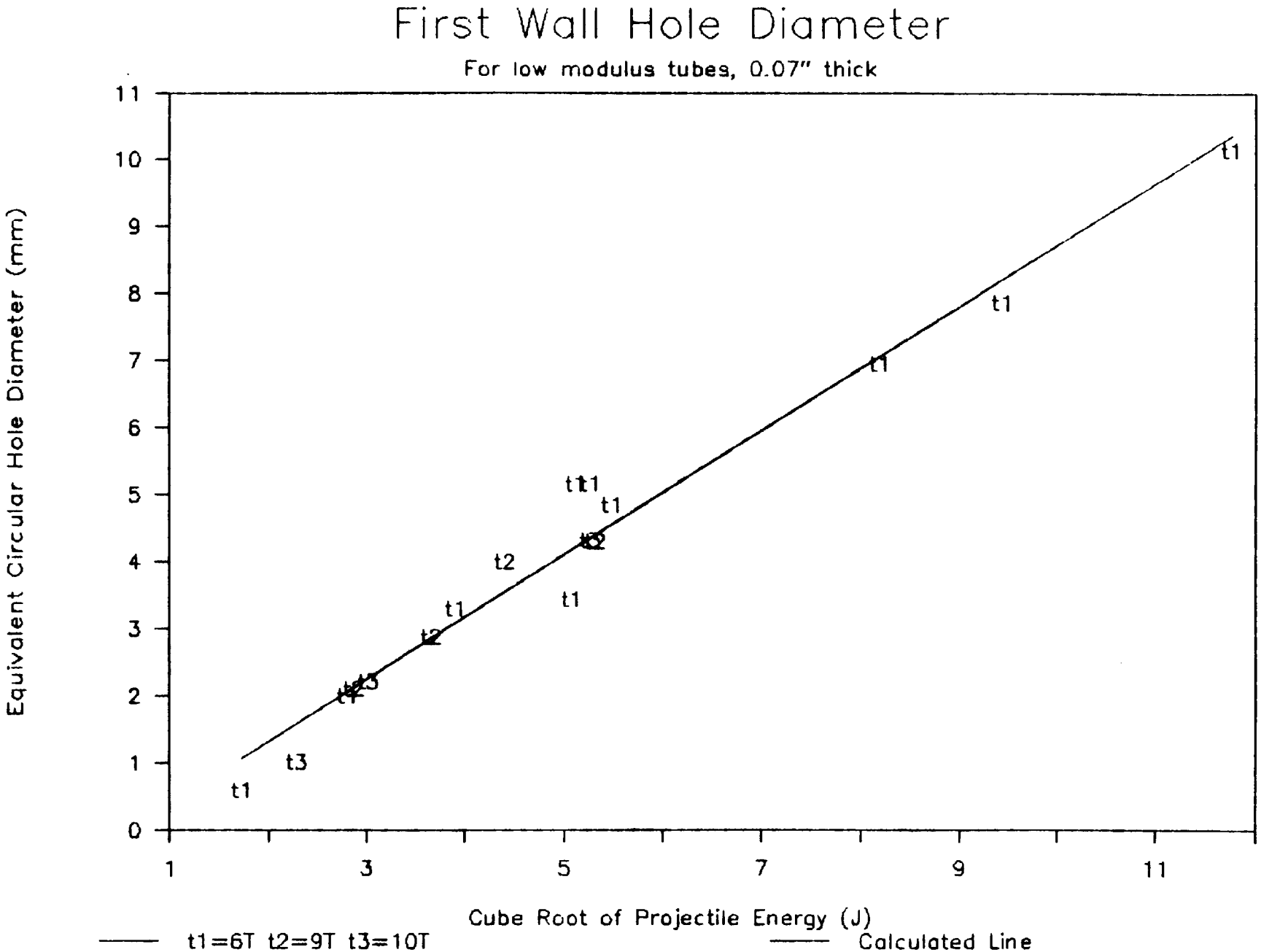

Figure 4-17. 9T and 10T Tube Data for Combined Wall Hole Diameter

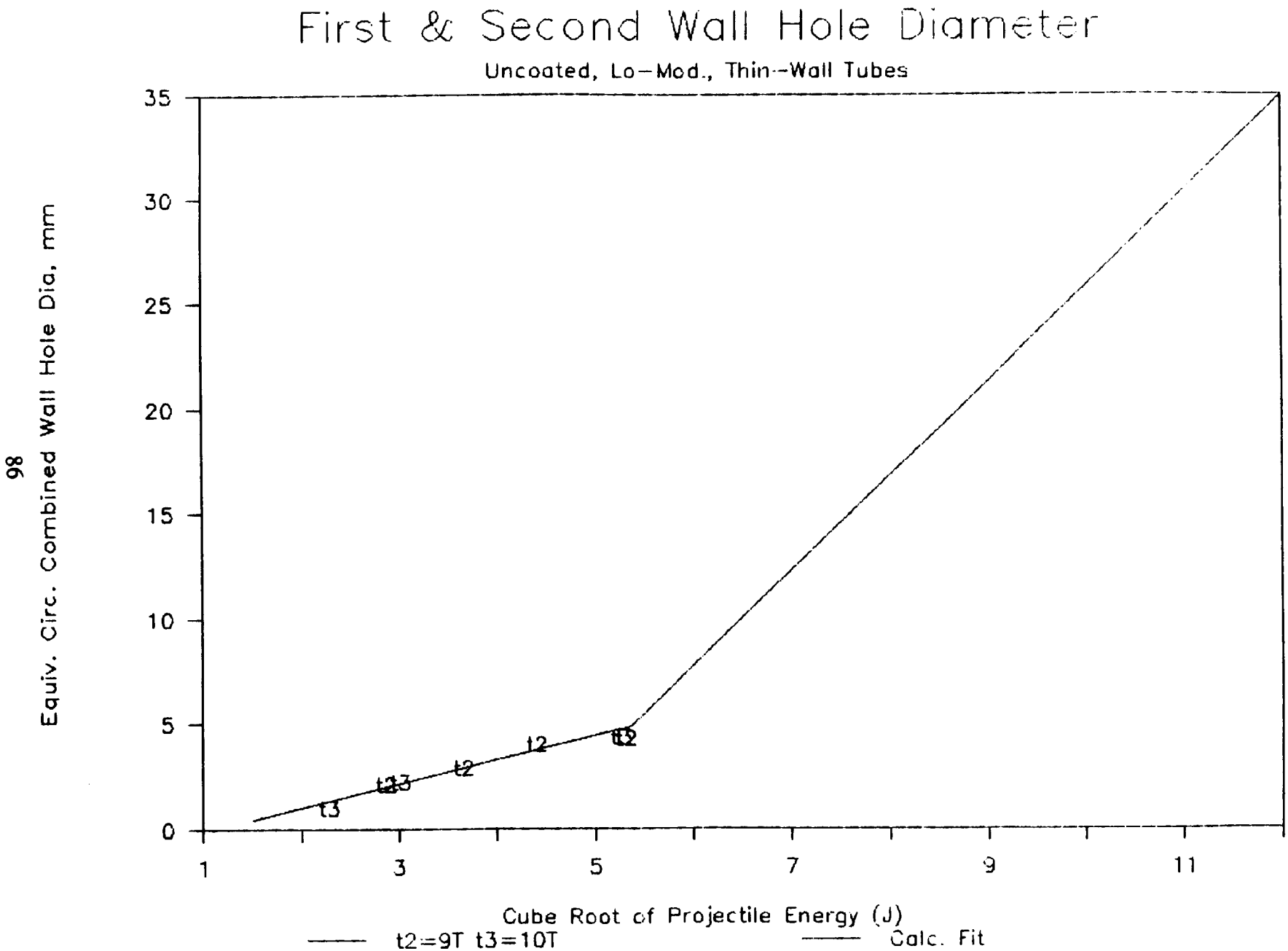

Figure 4-18. Combined Wall C-Scan Diameter for Low Modulus, Amoco Tubes

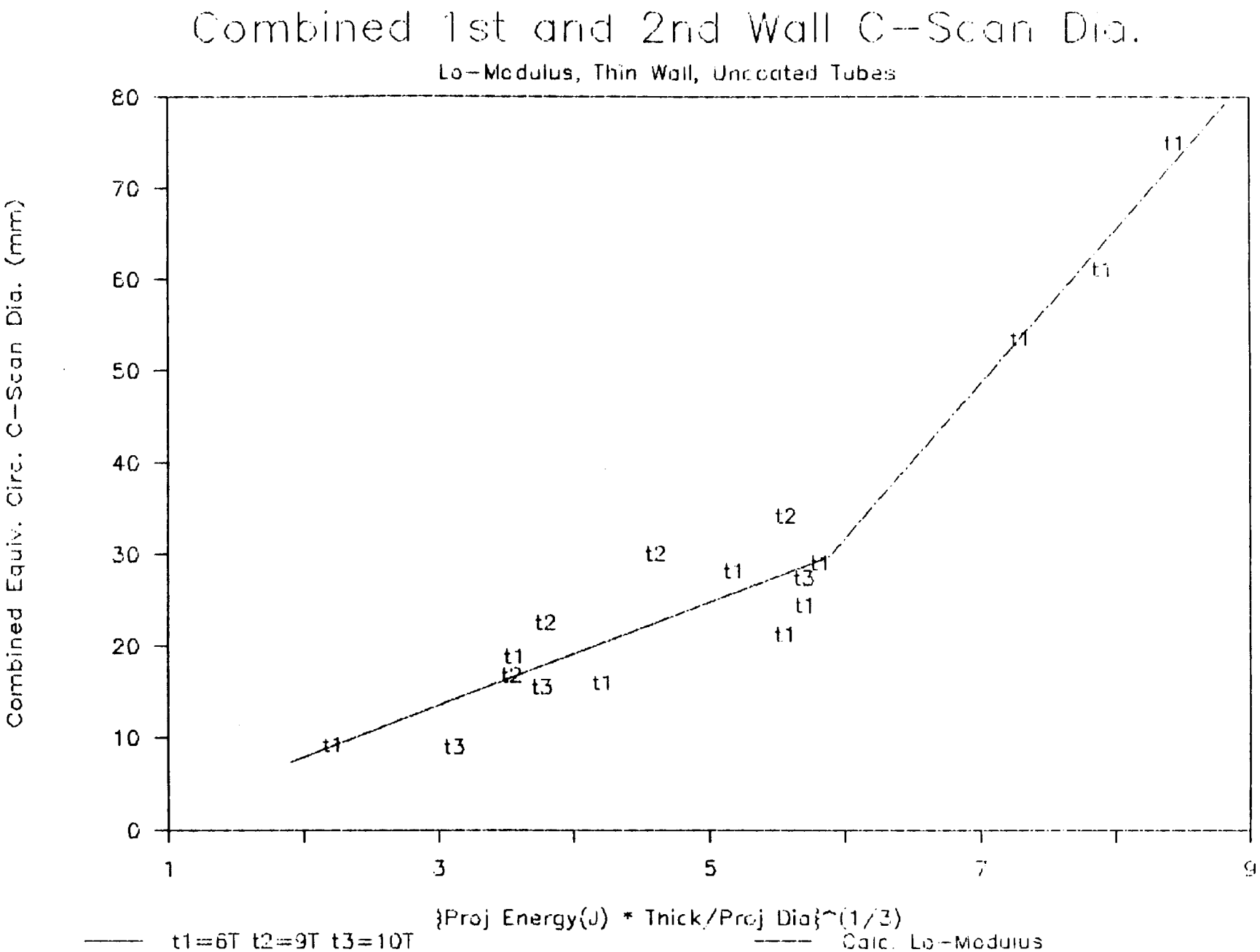

4.3 Effect of Fiber Elastic Modulus

Larger holes but similar sized C-scan areas resulted from impact testing on tube specimens with 75M psi modulus fibers as indicated by comparing Figures 4-19 and 4-20 with Figures 4-4 and 4-13. The high modulus tubes also did not exhibit surface ply delamination and peeling that occured with the low modulus tubes. Figure 4-21 illustrates that the least-squares fit for the first wall hole size in high modulus fiber tubes is greater for a given projectile energy than the low modulus fiber data fit. The high modulus curve was fit for 7 data points (11T and 12T tube series) to the equation:

$$D_{h1} = 1.202\ E^{0.33} + 0.612 \qquad r = 0.98$$

where D_{h1} is the equivalent circular first wall hole diameter (mm) and E is the projectile energy (J). The first wall C-scan size correlation (23 data points) is combined for both low and high modulus fiber tubes:

$$D_{c1} = 2.72\ (E * t/d)^{0.33} + 4.86 \qquad r = 0.84$$

where D_{c1} is the equivalent circular C-scan diameter, E is the projectile energy (J), t is the tube wall thickness (mm), and d is the projectile diameter (mm). This correlation and all data are displayed in Figure 4-22. Figure 4-23 shows the correlation for the equivalent circular diameter for the through hole in both walls of high modulus tube targets, D_{hb} (mm). For projectiles with an energy less than 158 J ($D_{hb} < 7.7$ mm),

$$D_{hb} = 1.424\ E^{0.33} + 0.034 \qquad r = 0.98$$

And for projectiles with an energy greater than 158 J ($D_{hb} > 7.7$ mm),

$$D_{hb} = 6.281\ E^{0.33} - 26.22$$

Little difference was found between low and high modulus fiber tubes for the size of the combined wall ultrasonic C-scan zone as a function of projectile conditions. Figure 4-24 illustrates this by plotting all high modulus tube data versus the low modulus tube correlation presented in the previous section. Figure 4-25 shows all data plotted against an updated correlation developed by least squares fit of the data. The formulas for

the equivalent circular combined wall ultrasonic C-scan diameter, D_{cb} (mm), for both high and low modulus tube data are:

For projectiles with (E * t/d) < 230 J, or for D_{cb} < 30 mm,

$$D_{cb} = 6.31\ (E * t/d)^{0.33} - 5.72 \qquad r = 0.88$$

And for projectiles with (E * t/d) > 230 J, or for D_{cb} > 30 mm,

$$D_{cb} = 15.50\ (E * t/d)^{0.33} - 61.8 \qquad r = 0.94$$

Rearranging this last equation to solve for projectile diameter, d (mm) in terms of projectile density, p (g/cc), and velocity, V (km/sec):

$$d = [(D_{cb} + 61.8)/15.5]^{1.5} * (12/\pi)^{0.5} * p^{-0.5} * V^{-1} * t^{-0.5}$$

Figure 4-19. Target Fiber Modulus Effects: Photographic Documentation of Shot JSC-A291
JSC-A291, Tube 11-T-4, 1.55 mm Al 2024-T4 sphere, 7.55 km/sec, 10° radial obliquity.

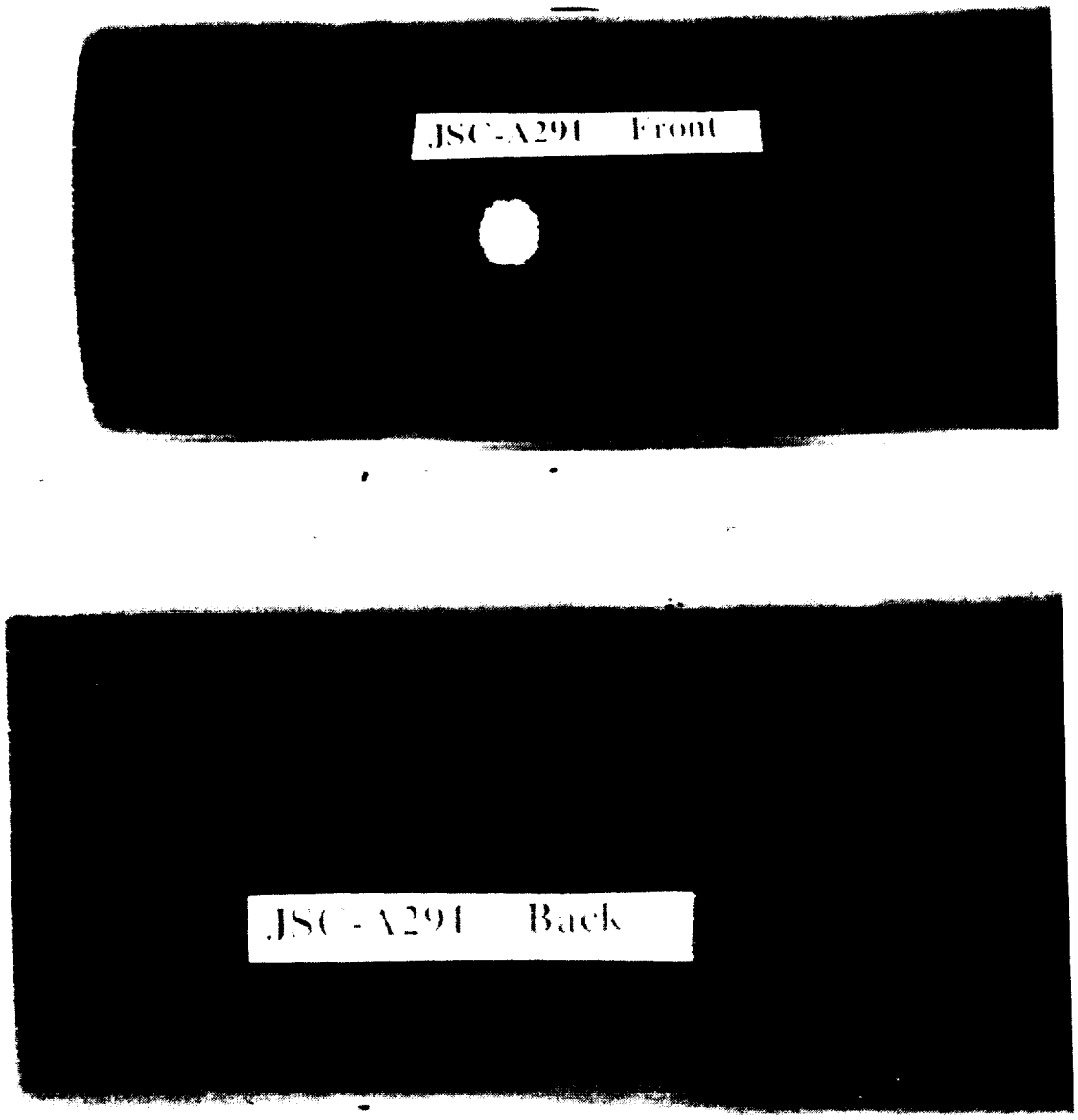

Figure 4-20. Target Fiber Modulus Effects: Photographic Documentation of Shot JSC-A302
JSC-A302, Tube 12-T-2, 1.55 mm Al 2024-T4 sphere, 7.16 km/sec, 7° radial obliquity.

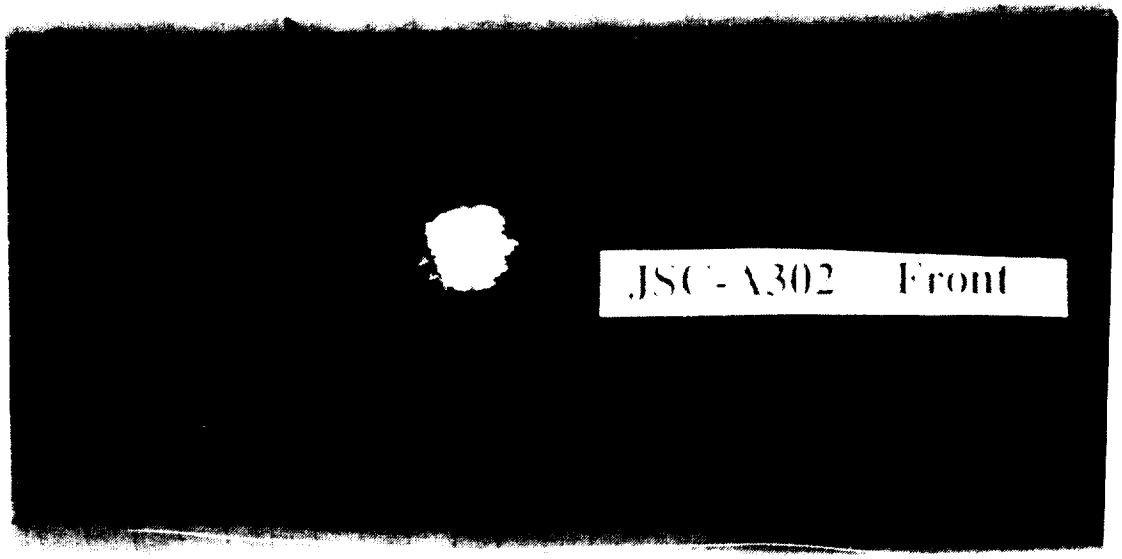

Figure 4-21. First Wall Hole Diameter for Low and High Modulus Amoco Tubes

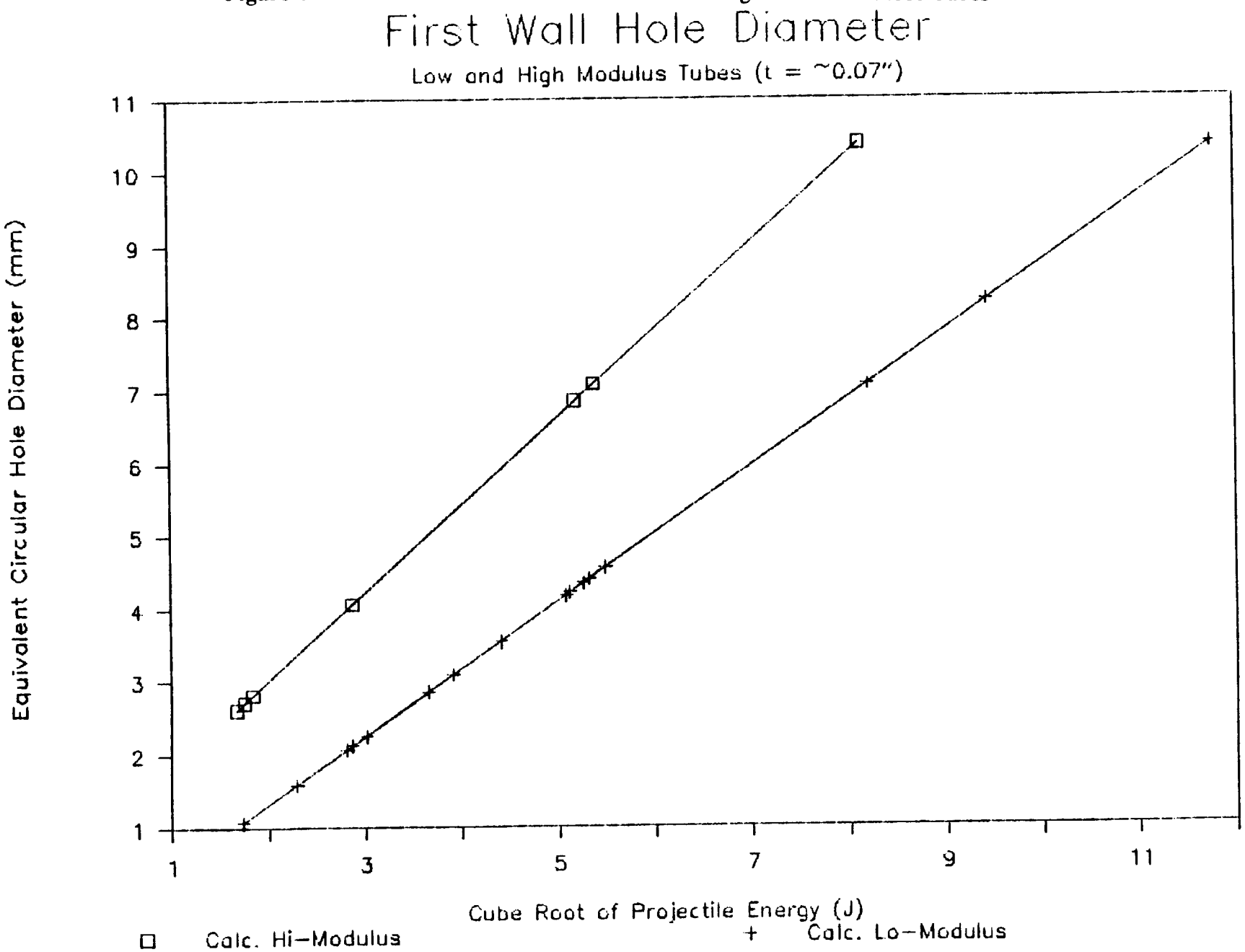

Figure 4-22. First Wall C-Scan Diameter for Low and High Modulus Amoco Tubes

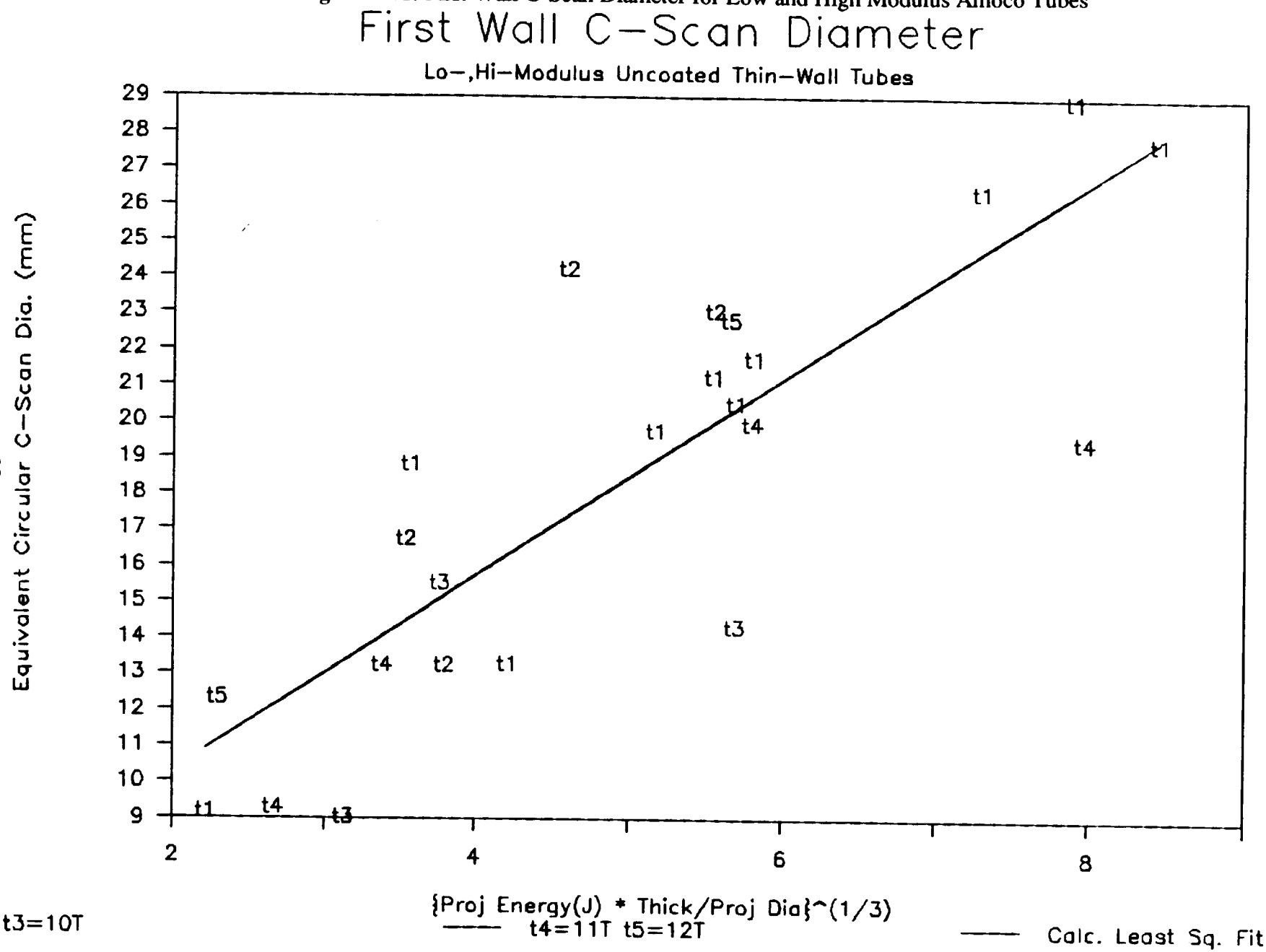

Figure 4-23. Combined Wall Hole Diameter for High Modulus Amoco Tubes

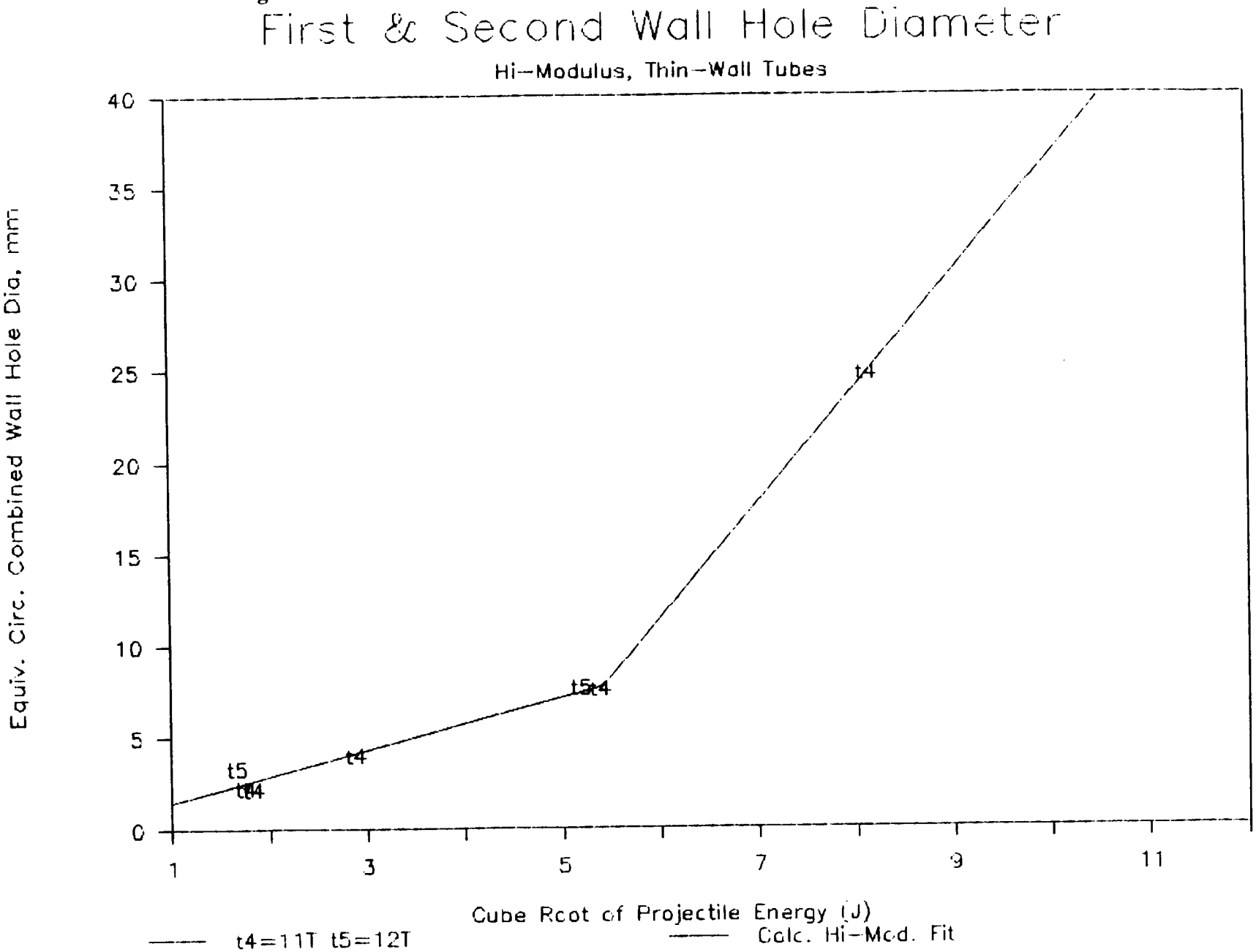

Figure 4-24. High Modulus Combined Wall C-Scan Diameter Vs. Low Modulus Correlation

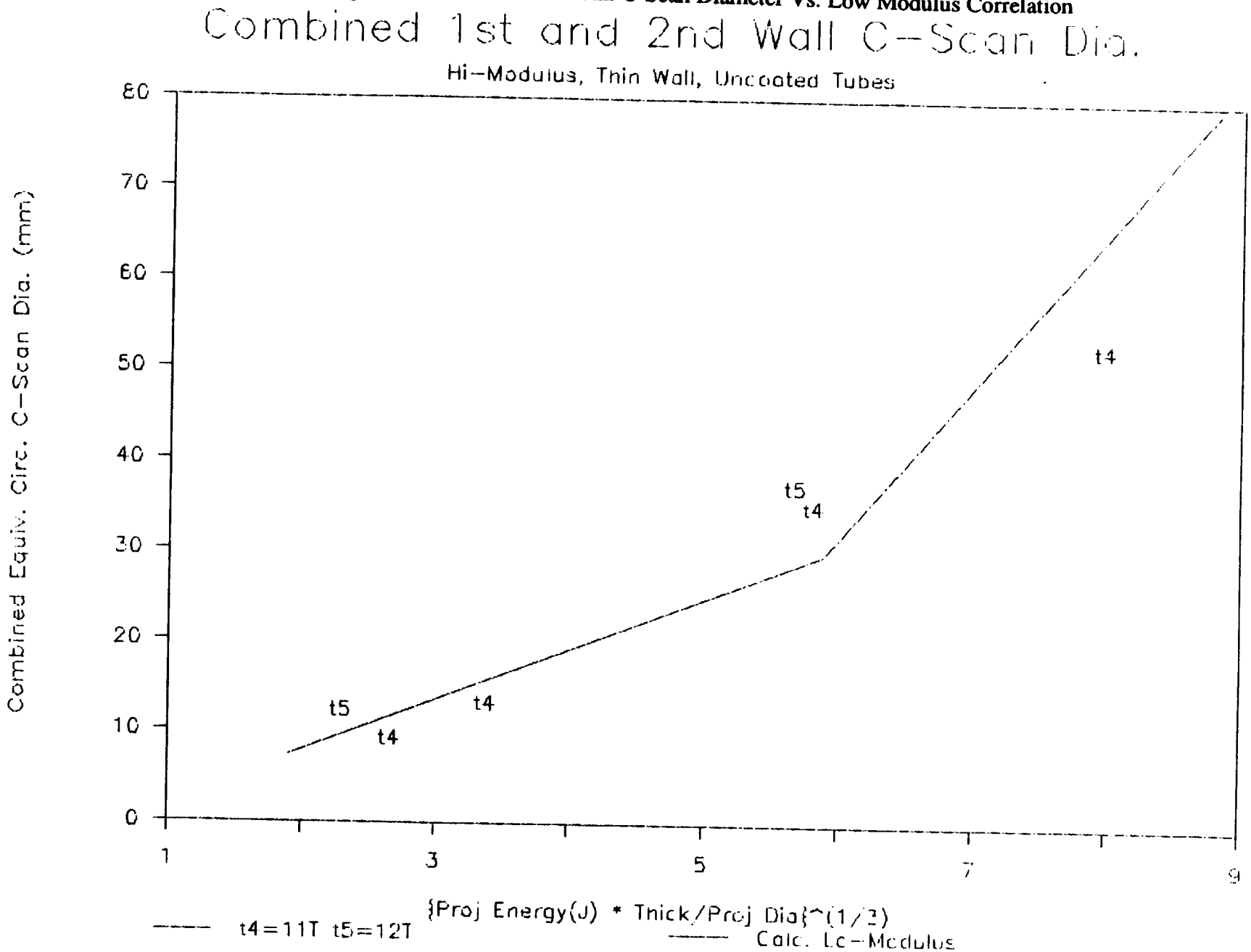

Figure 4-25. Combined Wall C-Scan Diameter for Low and High Modulus Amoco Tubes

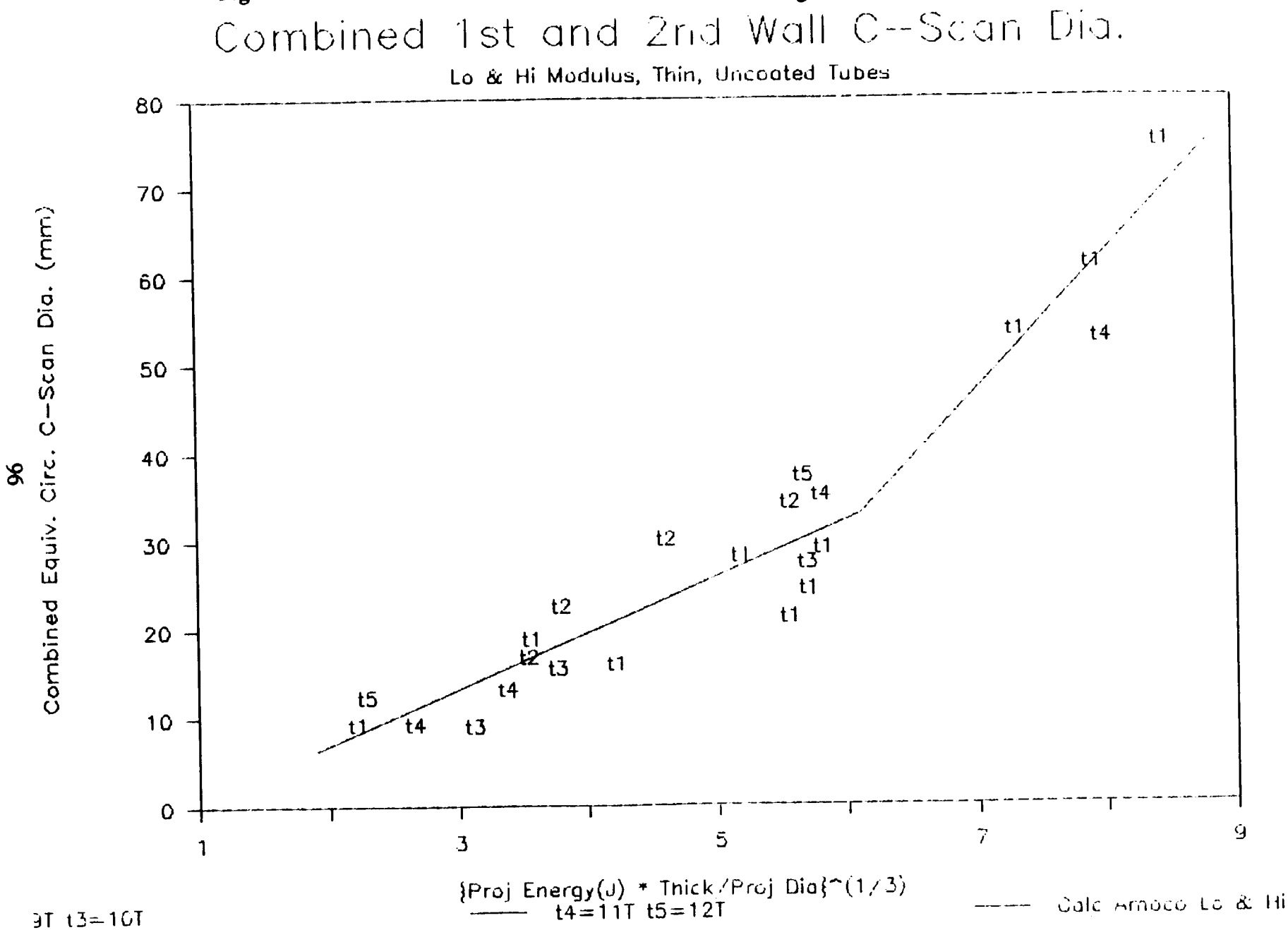

4.4 Effect of Surface Coatings

Several 6T series tubes with 0.002" and 0.006" thick aluminum bonded to the tube exterior were included in the test program. The 6T series are thin-walled (nominally 0.07" thick) tubes containing low modulus fibers (34M psi) in a [10,30,10] ply layup (see Section 3.4). Thus, the impact effects on coated tubes reported in this section can be directly compared to the impact results described in Section 4.1.

The results of an impact on tube with a 2 mil aluminum coating by a 2.4 mm aluminum ball at 7 km/sec are shown in Figure 4-26 (JSC Shot #A250). The impact peeled the low modulus tube's surface ply and, along with it, the 2 mil aluminum in the 10° direction. The first wall external ply peeling was generally similar (in direction and width, although not as long) to the response of an uncoated tube from a similar impact (JSC Shot #A249, see Figure 4-5). The first wall hole size was also essentially the same in both cases. First wall hole size produced by a 1.6 mm aluminum ball impacting at 7 km/sec on 2 mil and 6 mil aluminum bonded targets (JSC Shot #A307 and NDE Shot #24, respectively) shown in Figures 4-27 and 4-28 can be compared with a similar impact in an uncoated tube (JSC-A292 in Figure 4-4). As illustrated in Figure 4-29, first wall hole size, for the two aluminum coatings tested, did not vary significantly from the previously derived equation for uncoated low modulus tubes. However, as given in Figure 4-30, C-scan diameter was less in most coated tube cases compared to the uncoated correlation. As projectile energy increases, the coating would probably become less significant in reducing impact damage and the C-scan data would be expected to more closely track the uncoated tube C-scan correlation.

While the 2 mil aluminum peeled away from the impact point, the 6 mil aluminum did not significantly peel, although the largest projectile shot at the 6 mil coated targets was a 1.6 mm diameter aluminum sphere. Peeling of 0.006" thick aluminum might take place with impacts by larger projectiles.

Figure 4-26 shows the second wall of the 2 mil aluminum coated tube as severly delaminated as the corresponding uncoated tube shot (Figure 4-5) although no second wall through hole resulted. Similarly for the smaller projectile shots, the second wall exterior surface of the 2 mil aluminum coated tube was dimpled in several places (see Figure 4-27 and numerical details in Appendix A) while the uncoated tube was more severely delaminated

(Figure 4-4). No damage at all was apparent on the second wall exterior surface for the 6 mil aluminum coated tube (Figure 4-27). Thus, as given in Figure 4-31, the combined first and second wall hole damage for coated tubes falls well below the uncoated tube curve after the break, indicating increasing second wall tube damage for uncoated tubes. It would be expected that a coated tube curve for combined hole size would eventually break upward also (at a higher projectile energy) when the second wall starts to be perforated. Although this limit was nearly reached for the 2 mil aluminum coated tubes, a correlation was not formulated due to lack of data.

Because second wall damage was apparent with the coated tubes at practically the same impact conditions that caused damage to the second wall of uncoated tubes, the internal damage reflected by ultrasonic C-scans of both sides of the tube essentially duplicated the results from just the impact side. Figure 4-32 shows the combined wall equivalent C-scan diameter for all coated tube data points versus the combined wall C-scan correlation presented in the previous section. At higher impact energies, the coated wall data is expected to track the uncoated data because the coating will represent insignificant damage resistance.

An equation was developed to relate the area peeled back from the impact point and exposed to atomic oxygen attack for a 2 mil coated tube to impact conditions:

$$P/d = 1.827\,(E_n)^{0.33} - 0.0989$$

where P (mm) is the equivalent circular diameter of the exposed region (not including the perforation or crater area), d (mm) is the projectile diameter, and E_n (J) is the projectile energy determined from the velocity normal to the target surface. The data and resulting least squares data fit is shown in Figure 4-33.

Figure 4-26. Target Surface Coating Effects: Photographic Documentation of Shot JSC-A250 JSC-A250, Tube 6-T-4, 2 mil aluminum bonded coating, 2.37 mm Al 2024-T4 sphere, 7.15 km/sec, 5° radial obliquity.

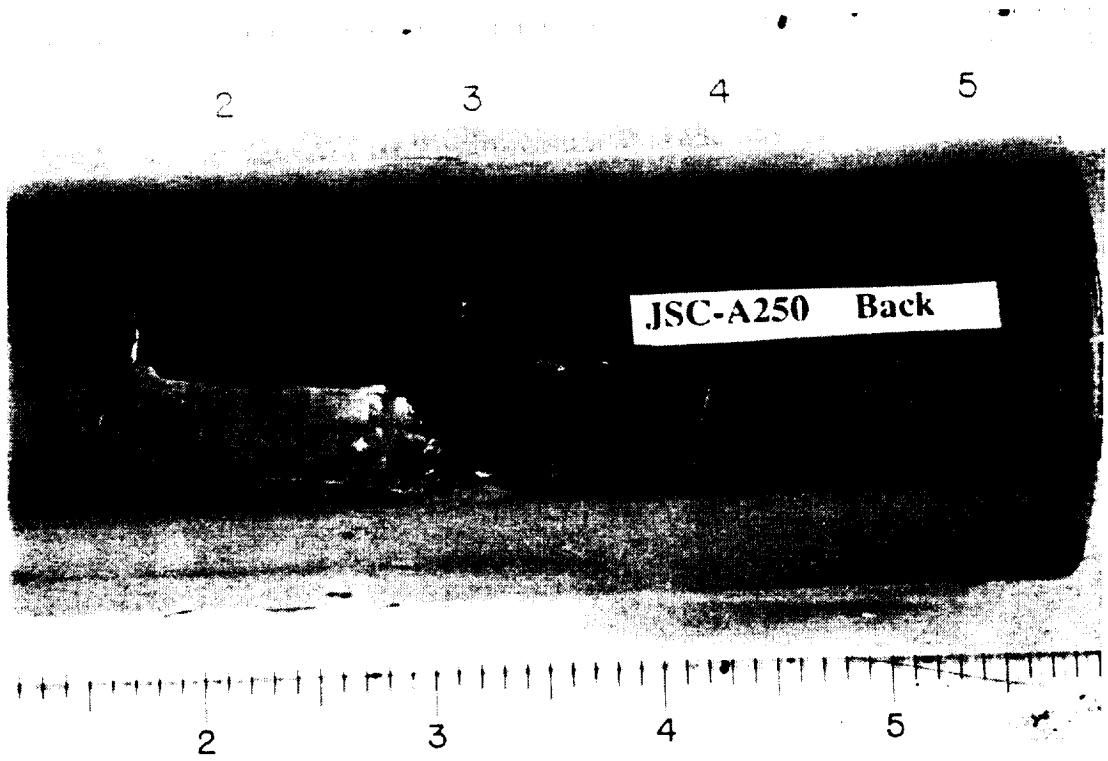

Figure 4-27. Target Surface Coating Effects: Photographic Documentation of Shot JSC-A307

JSC-A307, Tube 6-T-6, 2 mil aluminum bonded coating, 1.54 mm Al 2024-T4 sphere, 7.35 km/sec, 0° radial obliquity.

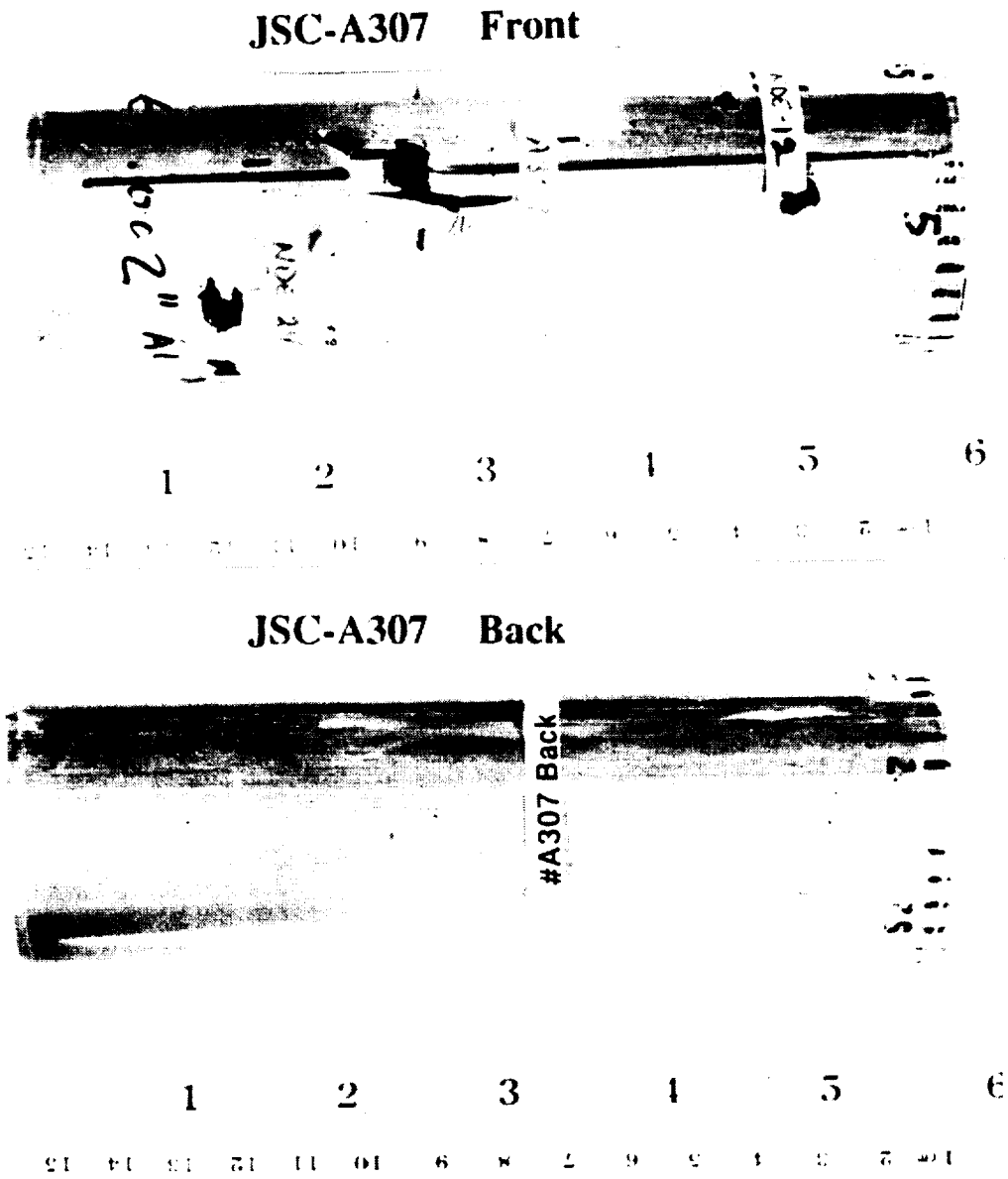

Figure 4-28. Target Surface Coating Effects: Photographic Documentation of Shot NDE-24
NDE-24, Tube 6-T-9, 6 mil aluminum bonded coating, 1.58 mm Al 2024-T4 sphere, 6.71 km/sec, 24° radial obliquity.

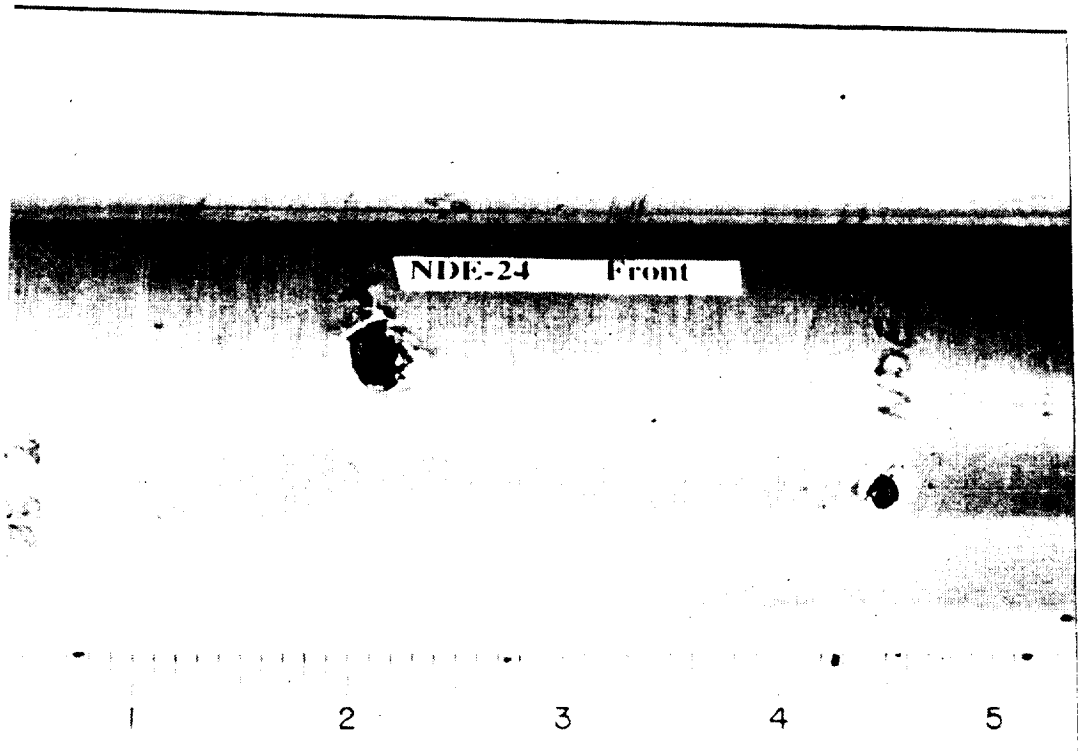

Figure 4-29. First Wall Hole Diameter for 2 mil and 6 mil Aluminum Coated Tubes

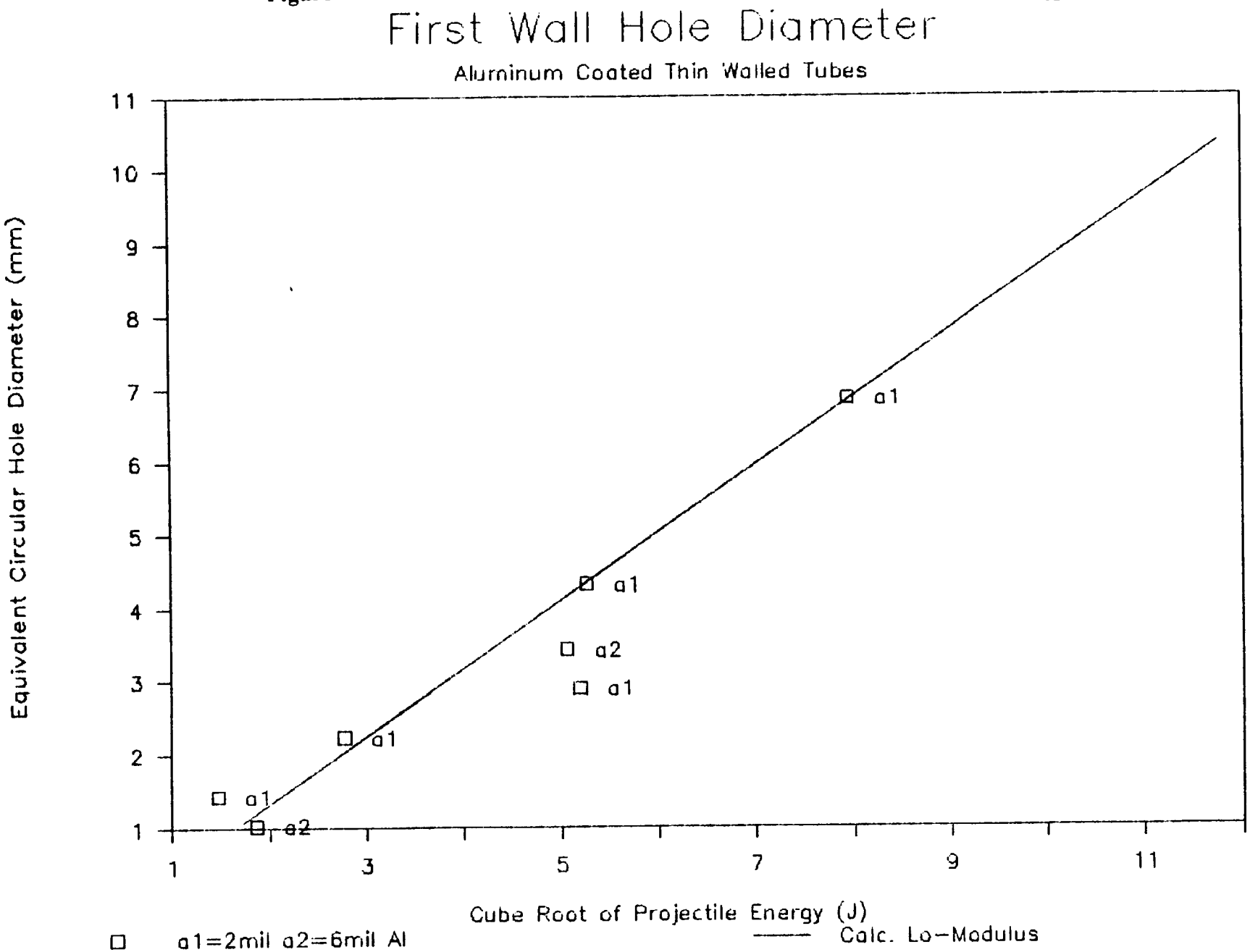

Figure 4-30. First Wall C-Scan Diameter for Aluminum Coated Tubes

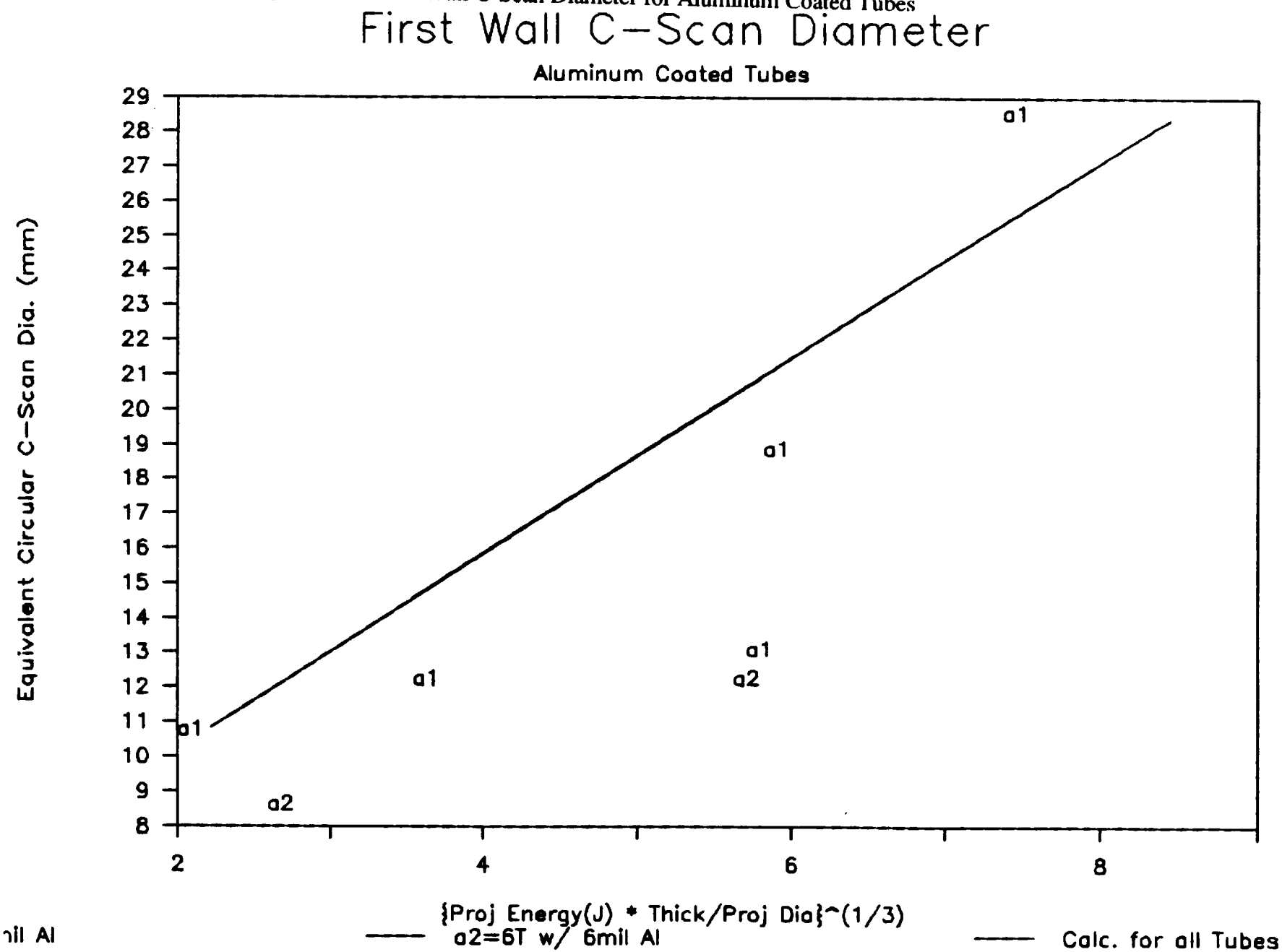

Figure 4-31. Combined Wall Equivalent Circular Hole Diameter for Aluminum Coated Tubes

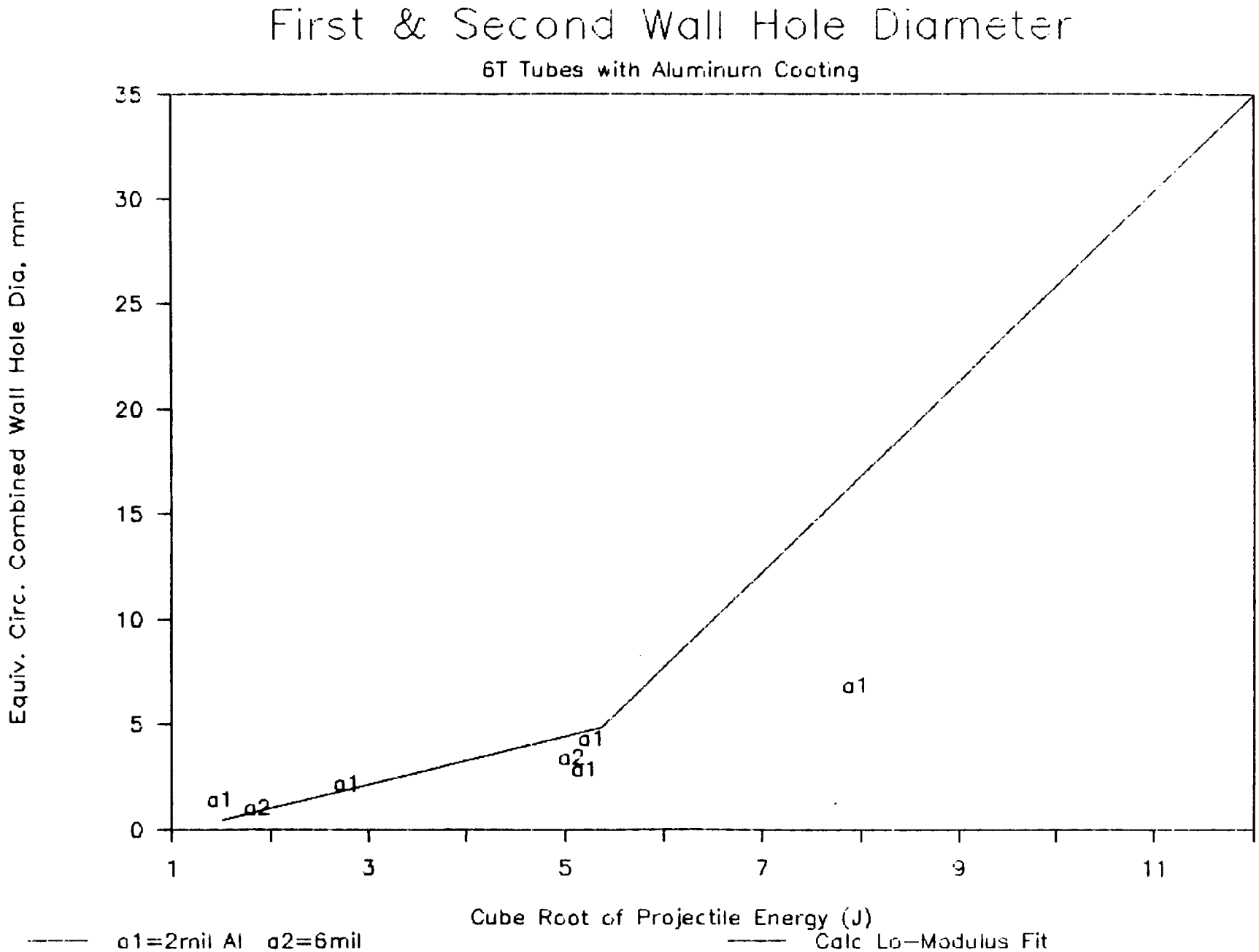

Figure 4-32. Combined Wall C-Scan Diameter for Aluminum Coated Tubes

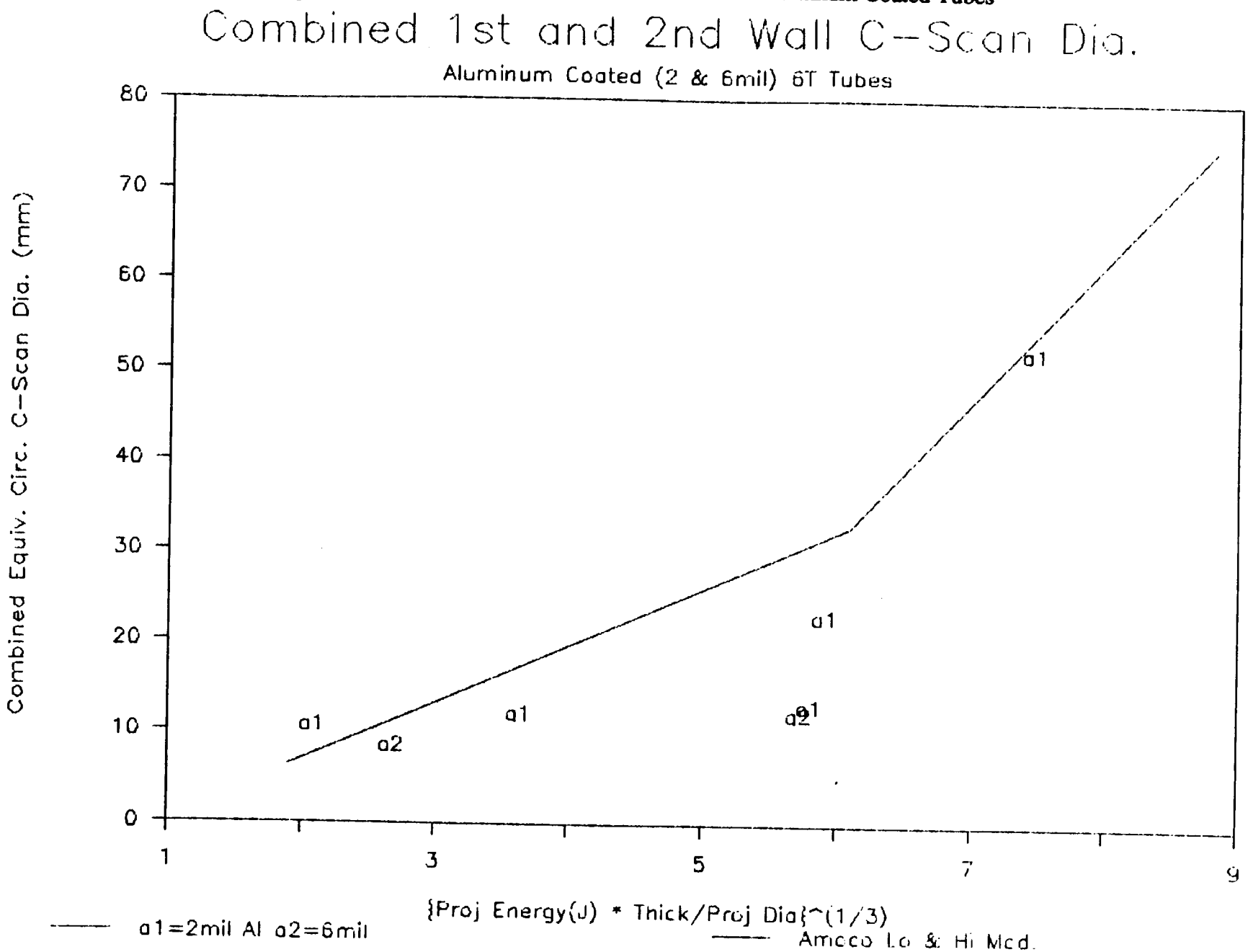

Figure 4-33. Exposed Area for 2 mil Aluminum Coated Tubes

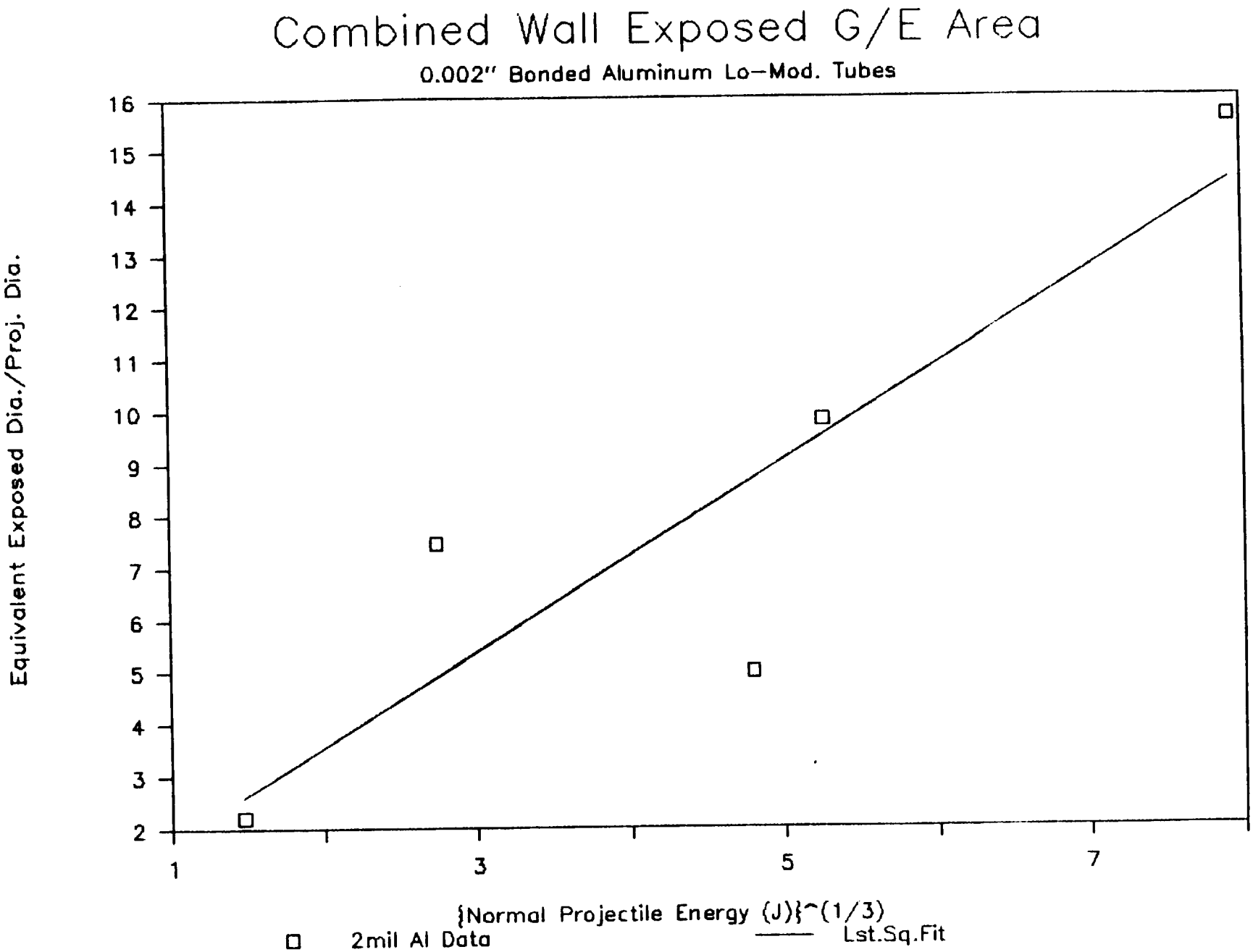

4.5 Effect of Target Thickness

In the few successful data shots on thick walled tubes completed during this study (Table 4-1), little significant difference between the three tube thicknesses was optically observed (hole and crater size, extent of surface peeling) in the damage on the first wall of the tubes for similar impact conditions. As illustrated in Figures 4-34 through 4-36, front surface damage is similar on tubes having wall thicknesses nominally 0.07", 0.11", and 0.14" for impacts of a 1.6 mm aluminum projectile at 4.5 km/sec. Hole diameter from four shots on thick tubes is plotted on Figure 4-37 with the correlation for all Amoco, thin, low modulus tubes given in Section 4.2 ($D_{h1} = 0.927\ E^{0.33} - 0.536$). As indicated, at the projectile energies tested, the front wall hole size closely matches the correlation. It is expected that the thicker the tube, the more projectile energy is required to perforate the first wall. Thus, it would seem that at lower energies than tested, the first wall hole size should decrease quicker than the thin wall corrrelation. However, not enough data is available to substantiate this supposition.

Front wall C-scan size is a function of tube wall thickness as given in Figure 4-38 which shows the four thick wall data points versus the first wall C-scan correlation given in Section 4.3. As tube wall thickness increases, the C-scan area also increases for the same projectile impact conditions. The new first wall C-scan correlation, for all Amoco thin and thick, low and high modulus tubes is:

$$D_{c1} = 2.82\ (E * t/d)^{0.33} + 4.58 \qquad r = 0.83$$

where D_{c1} is the equivalent circular C-scan diameter, E is the projectile energy (J), t is the tube wall thickness (mm), d is the projectile diameter (mm), and r is the coefficient of correlation (a measure of the goodness of fit of the correlation to the measured values of D_{c1}; r=1 would be a perfect fit). All data for this correlation are plotted in Figure 4-39.

The equivalent circular hole size for the combined first and second wall for the four data points is plotted with the curve for thin, low modulus tubes in Figure 4-40. Because none of the projectiles fired in these tests had sufficient energy to break through the second wall, the data is basically confined to the lower portion of the curve corresponding to front wall damage. With sufficient data, a family of curves could be developed

that would show the transition to second wall damage shifting to the right on the graph with increasing tube wall thickness.

Figure 4-41 shows the combined wall C-scan diameter for the four thick wall data points plotted against the curve given in Section 4.3 for the thin wall, high and low modulus Amoco tubes. The points fell near the previously derived equations. More thick wall data shots would be necessary to confirm the exponent on the tube wall thickness to projectile diameter ratio (t/d) was adequately correlating the results. However, the correlation does correctly indicate C-scan size trends with changes in projectile diameter, density, velocity, and tube wall thickness.

Figure 4-34. Tube Wall Thickness Effects: Photographic Documentation of Shot NDE-22
NDE-22, Tube 6-T-3, t=0.073", 1.58 mm Al 2024-T4 sphere, 4.57 km/sec, 41° radial obliquity.

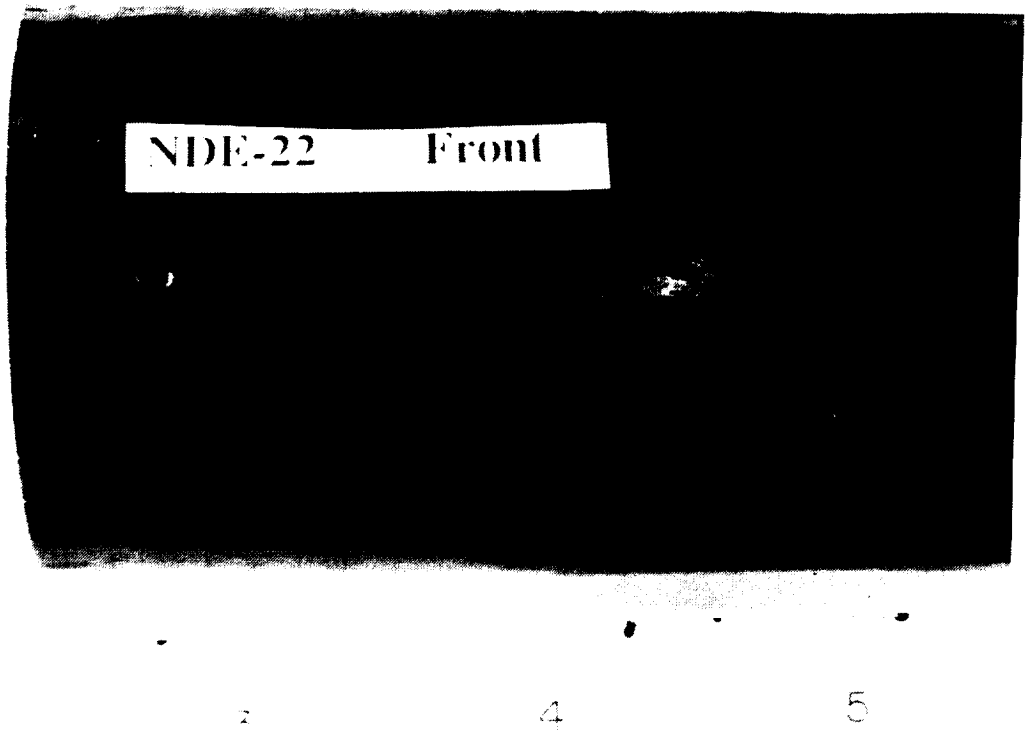

Figure 4-35. Tube Wall Thickness Effects: Photographic Documentation of Shot NDE-28
NDE-28, Tube 7-T-2, t=0.106", 1.58 mm Al 2024-T4 sphere, 4.27 km/sec, 12° radial obliquity.

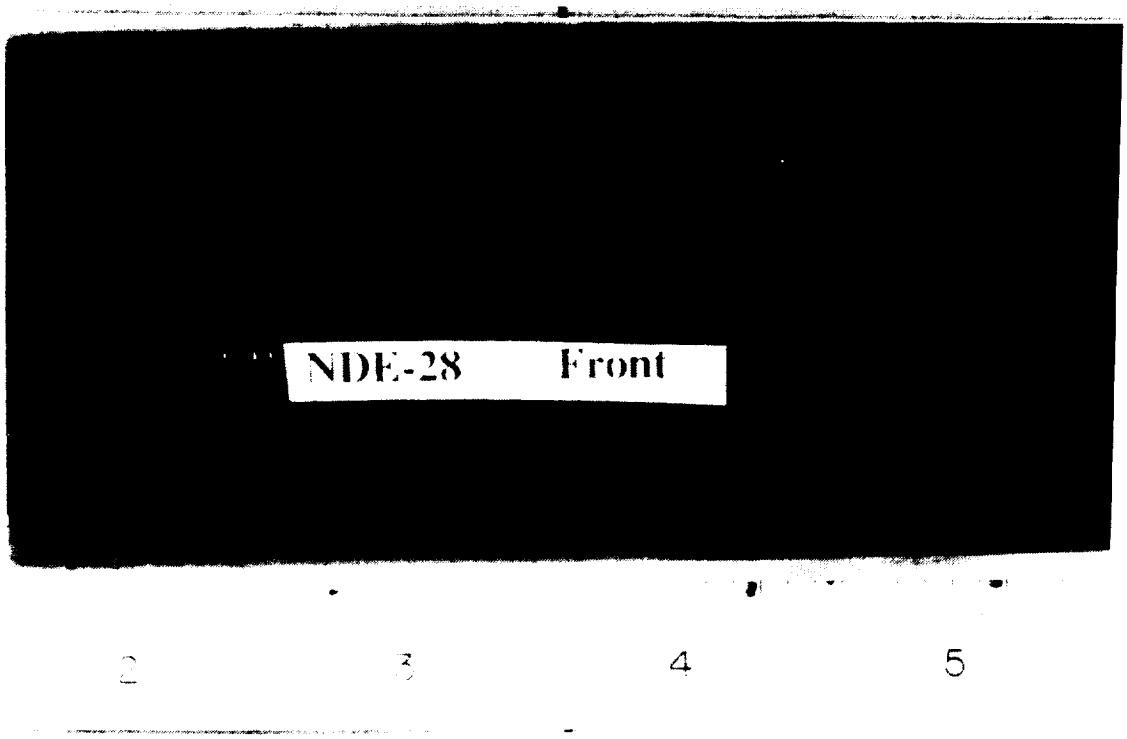

Figure 4-36. Tube Wall Thickness Effects: Photographic Documentation of Shot NDE-29
NDE-29, Tube 8-T-2, t=0.133", 1.58 mm Al 2024-T4 sphere, 4.88 km/sec, 20° radial obliquity.

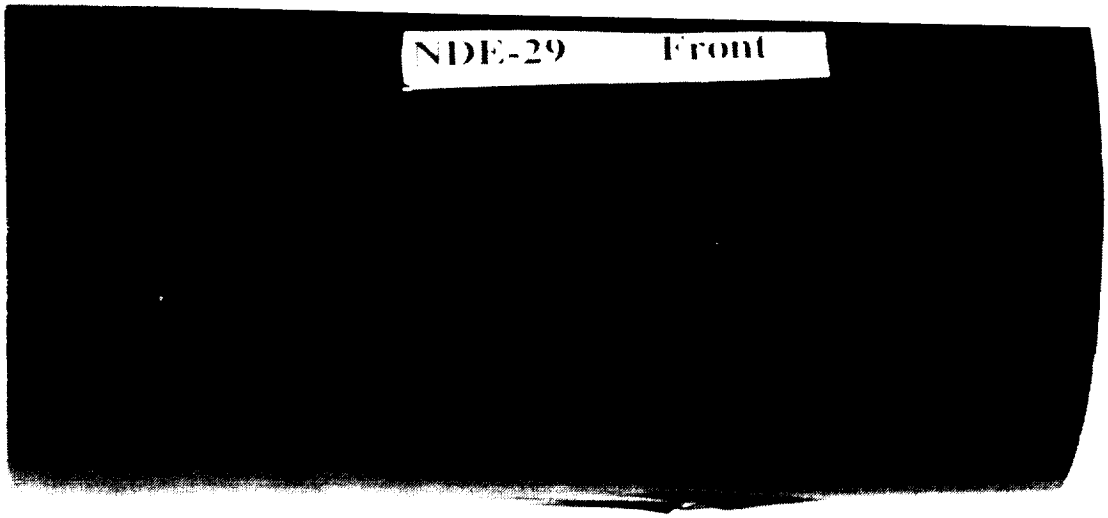

Figure 4-37. First Wall Hole Diameter Data for Thick Wall Tubes

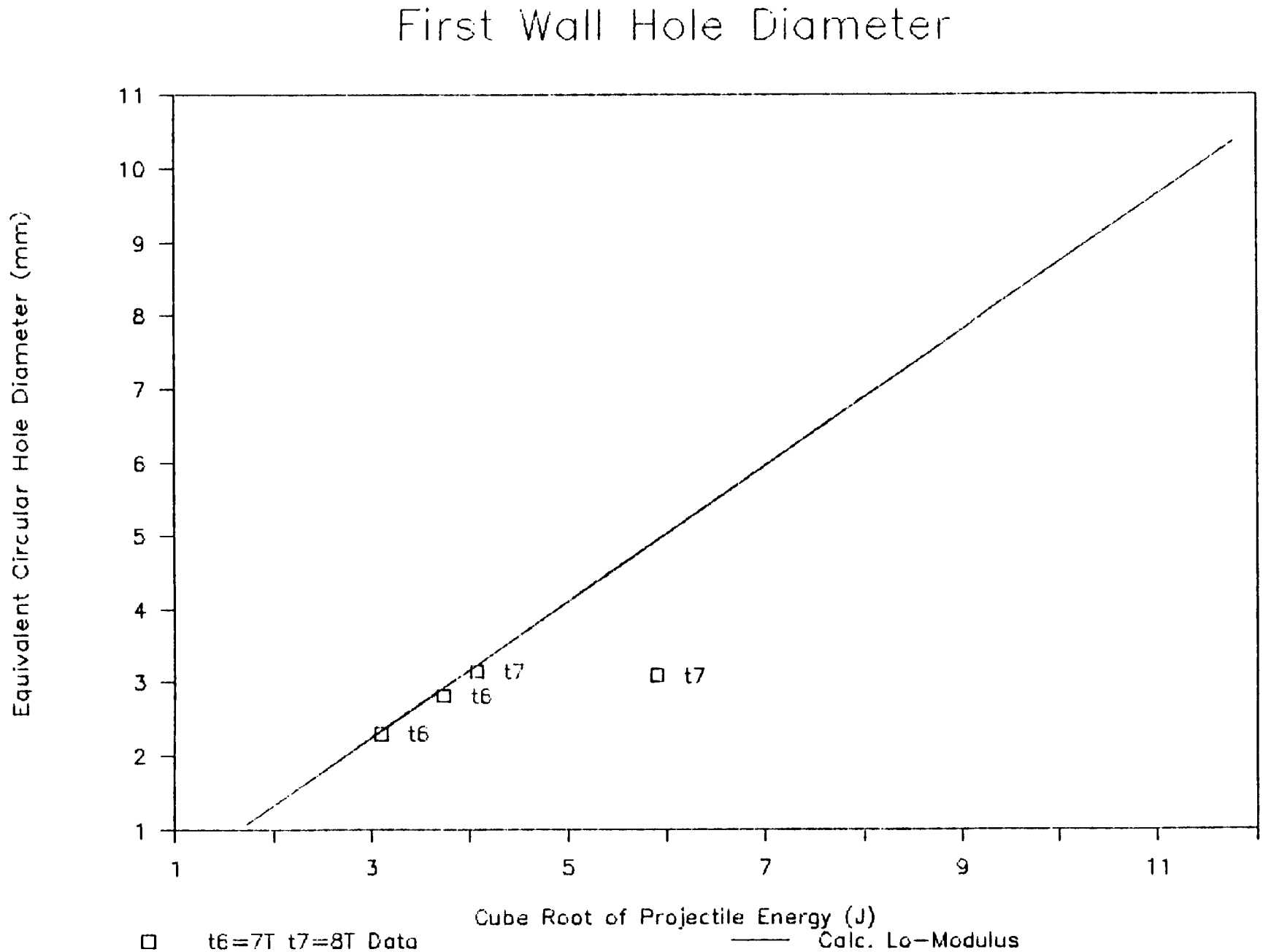

Figure 4-38. First Wall C-Scan Diameter Data for Thick Wall Tubes vs. Thin Wall Curve

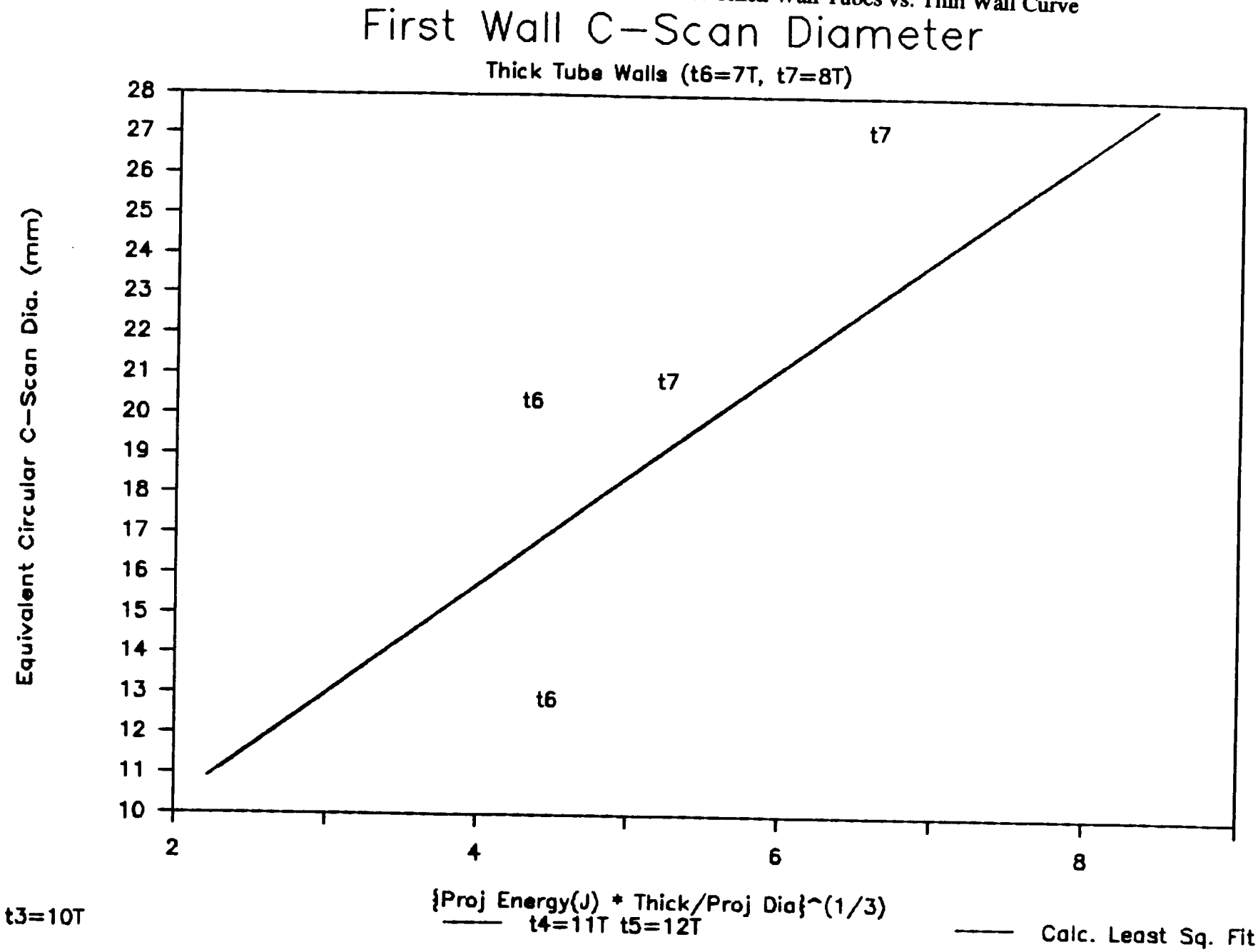

Figure 4-39. First Wall C-Scan Diameter Data for Thick and Thin Wall Tubes

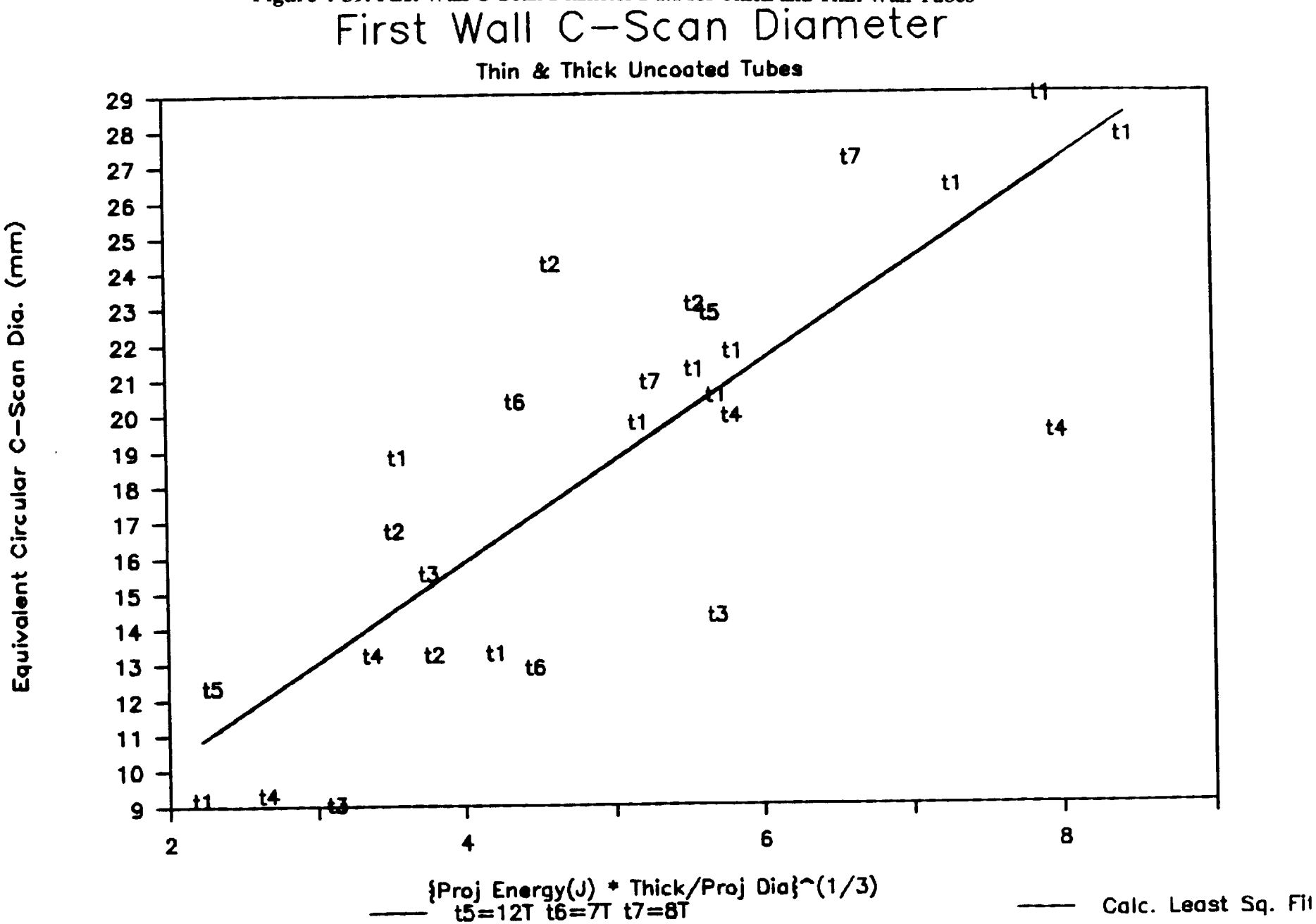

Figure 4-40. Combined Wall Hole Diameter for Thick Wall Tubes

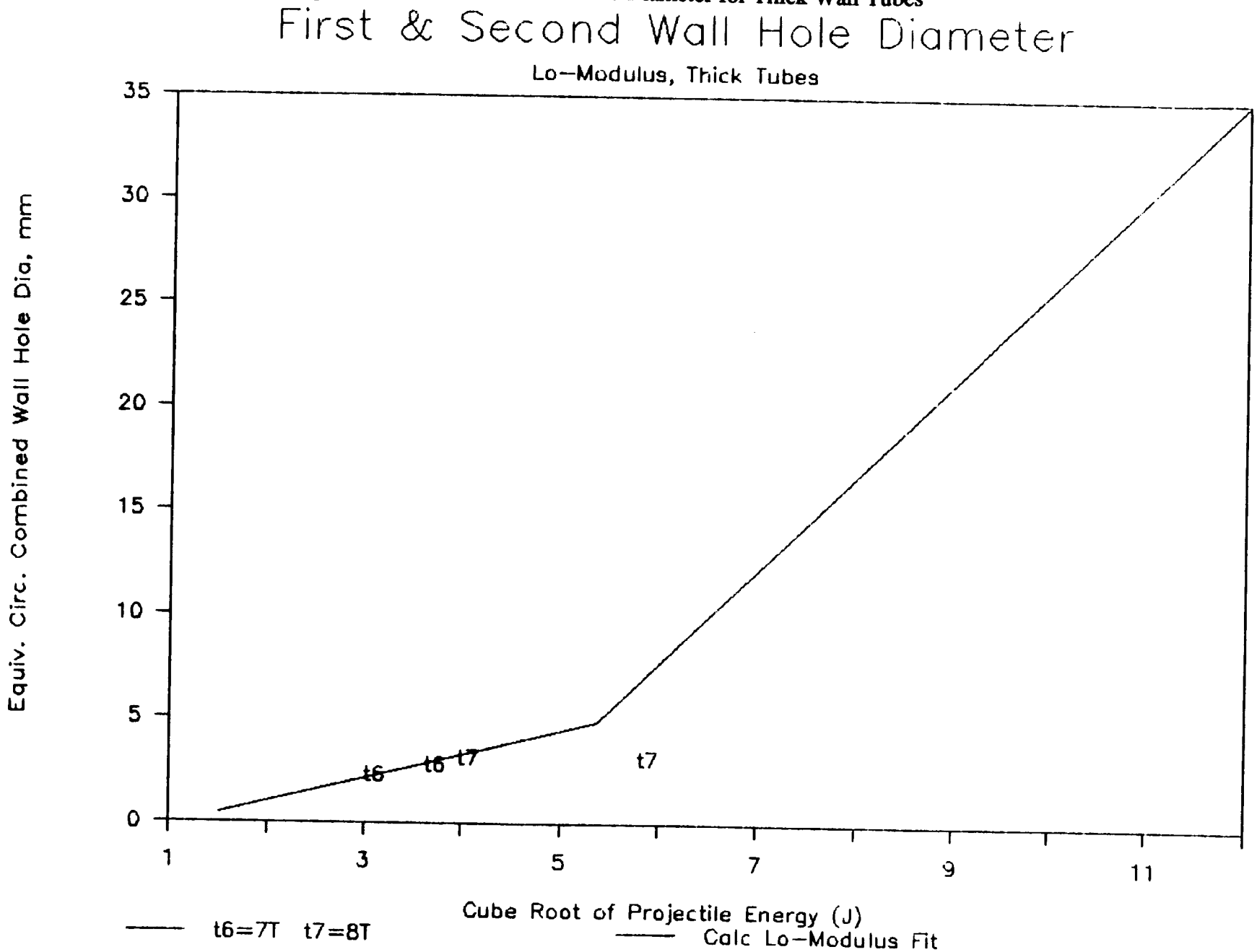

Figure 4-41. Combined C-Scan Diameter for Thick Wall Tubes

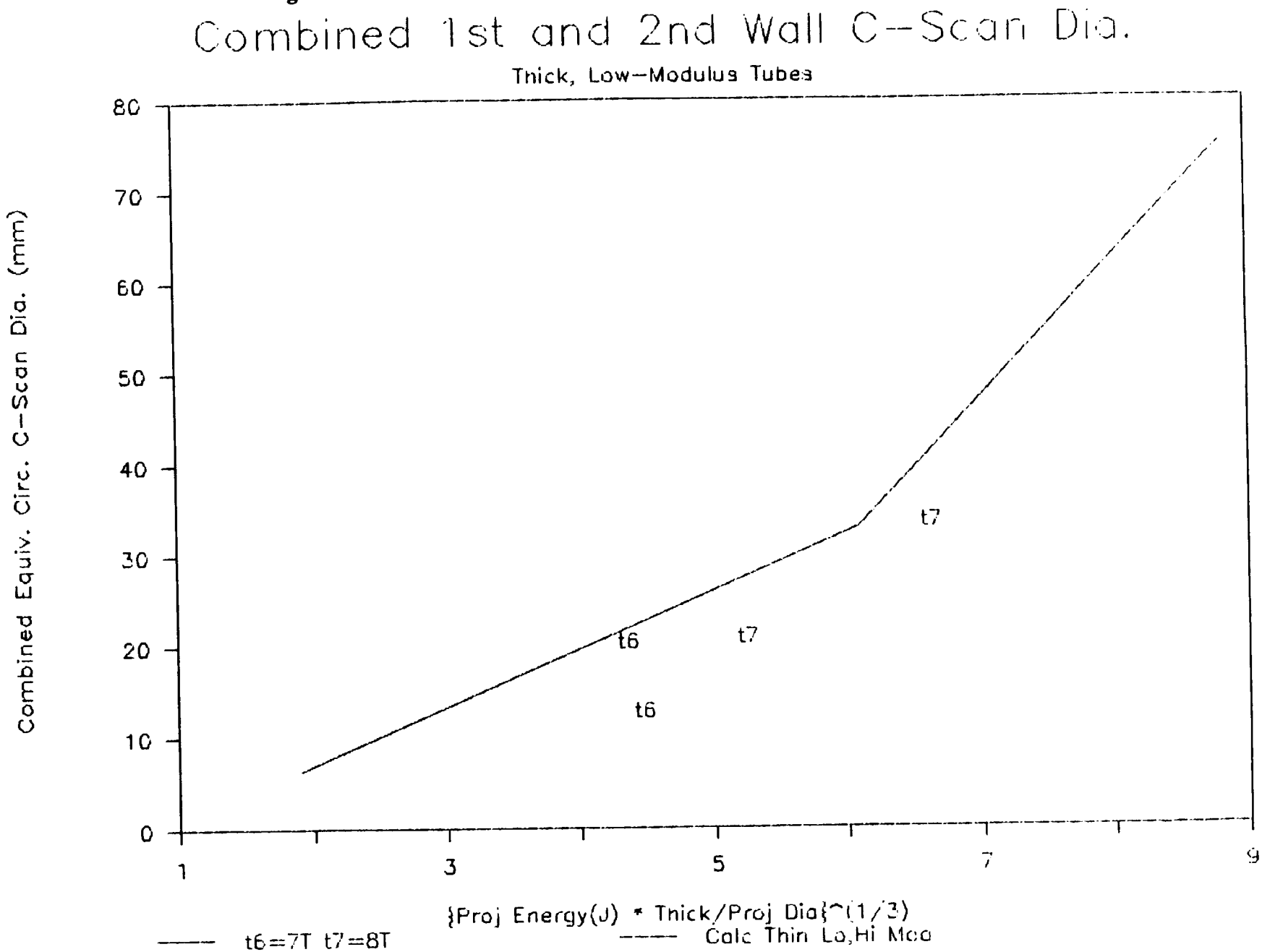

4.6 Flat Plates

Flat plates having similar fiber and layup characteristics as the tube specimens were impacted to determine if flat plate tests can be used in-place of or to supplement tube data. This is important since a substantial data base of graphite/epoxy flat plate data already exists.

Figures 4-42 through 4-47 present photographic documentation of flat plates impacted with a 1.6 mm diameter aluminum sphere at approximately 7 km/sec. As with the tubes, the low modulus fiber plates peeled in the direction of the surface ply on either side of the impact point while the high modulus fiber plates did not. The high modulus plates had larger holes at the same impact conditions than low modulus plates. No difference in C-scan diameter was apparent for different ply orientations.

Generally, as given in Figure 4-48, hole sizes for the low modulus plates (6f, 9f, and 10f series) were similar to the corresponding low modulus tube correlation:

$$D_{h1} = 0.927\ E^{0.33} - 0.536 \qquad r = 0.98$$

where D_{h1} is the hole diameter (mm), E is projectile energy (J), and r is a measure of the goodness of fit for the correlation (r = 1 is a prefect fit). Figure 4-49 likewise indicates the close match between the high modulus plate data (11f, 12f, and 13f) and the previously defined high modulus tube correlation:

$$D_{h1} = 1.202\ E^{0.33} + 0.612 \qquad r = 0.98$$

where D_{h1} is the equivalent circular first wall hole diameter (mm) and E is the projectile energy (J). However, as presented in Figure 4-50, the flat plates' C-scan diameter data scatter was obviously much greater than recorded for the tubes, although the general trend was evident. Thus, sets of flat plate data should be useful in determining the effect changes in composite properties would have on tube damage response trends. Confirmation shots on tubes would be necessary to actually quantify the results, especially for assessments of delamination area size.

Figure 4-42. Flat Plate Effects: Photographic Documentation of Shot JSC-A333
JSC-A333, Plate 6-F-1, [10,30,10], 34M psi, 1.55 mm Al 2024-T4 sphere, 7.19 km/sec.

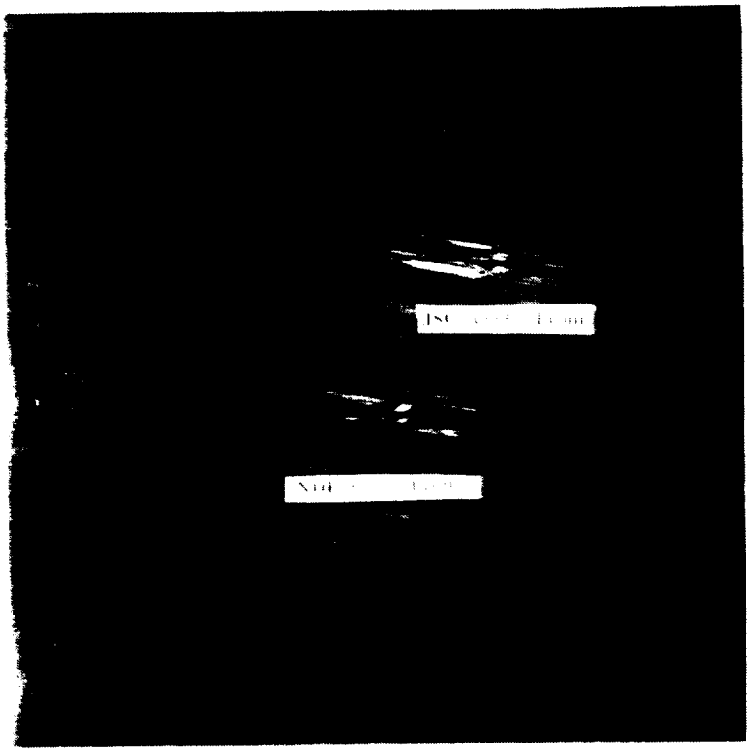

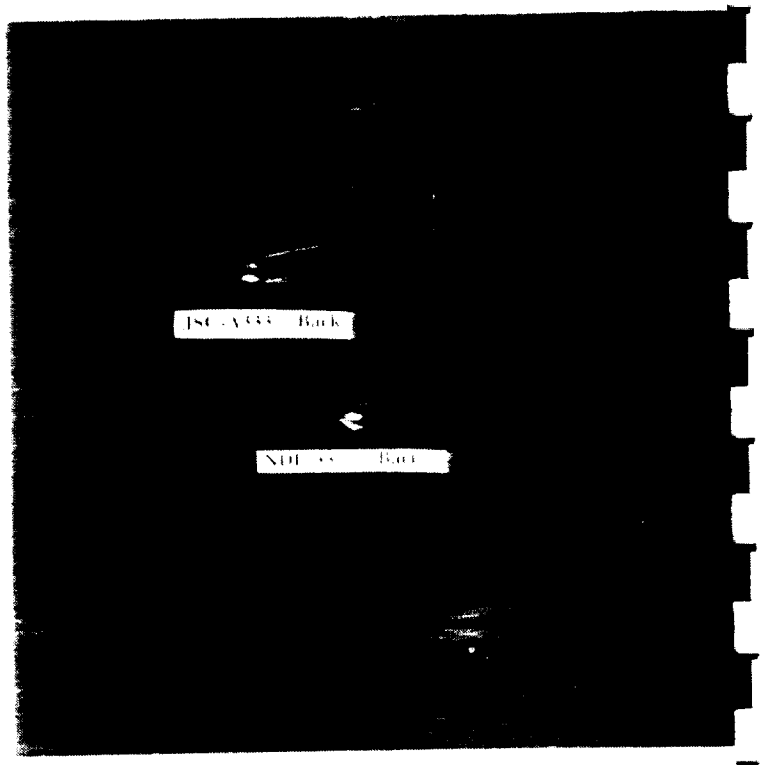

Figure 4-43. Flat Plate Effects: Photographic Documentation of Shot JSC-A411
JSC-A411, Plate 9s-F-1, [80,30,10], 34M psi, 1.56 mm Al 2024-T4 sphere, 6.97 km/sec.

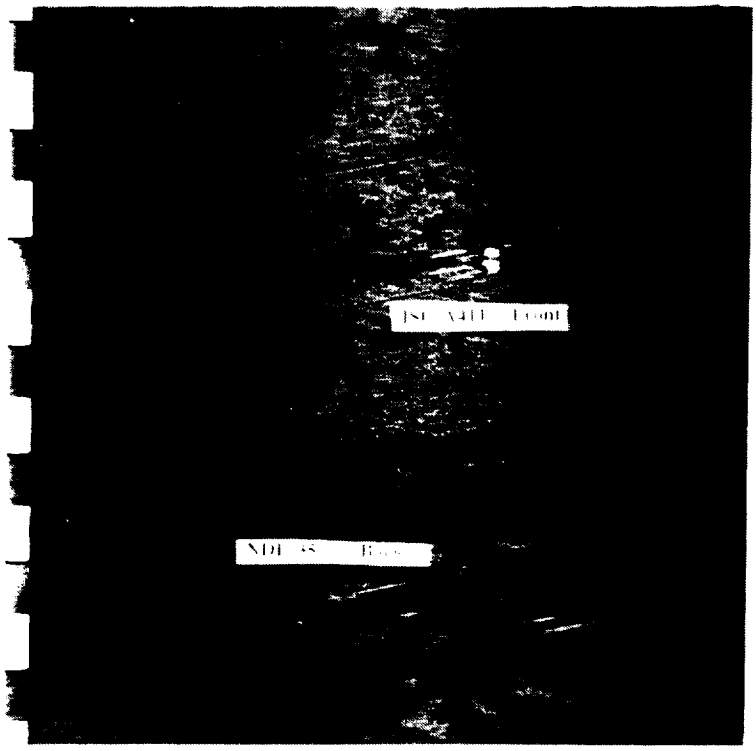

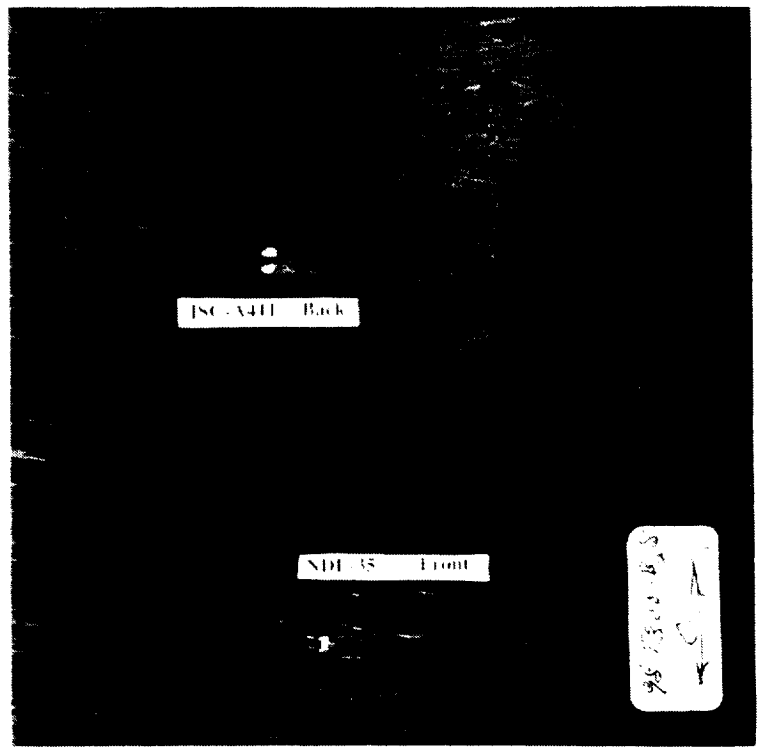

Figure 4-44. Flat Plate Effects: Photographic Documentation of Shot JSC-A410
JSC-A410, Plate 10-F-1, [45,10,45], 34M psi, 1.55 mm Al 2024-T4 sphere, 7.68 km/sec.

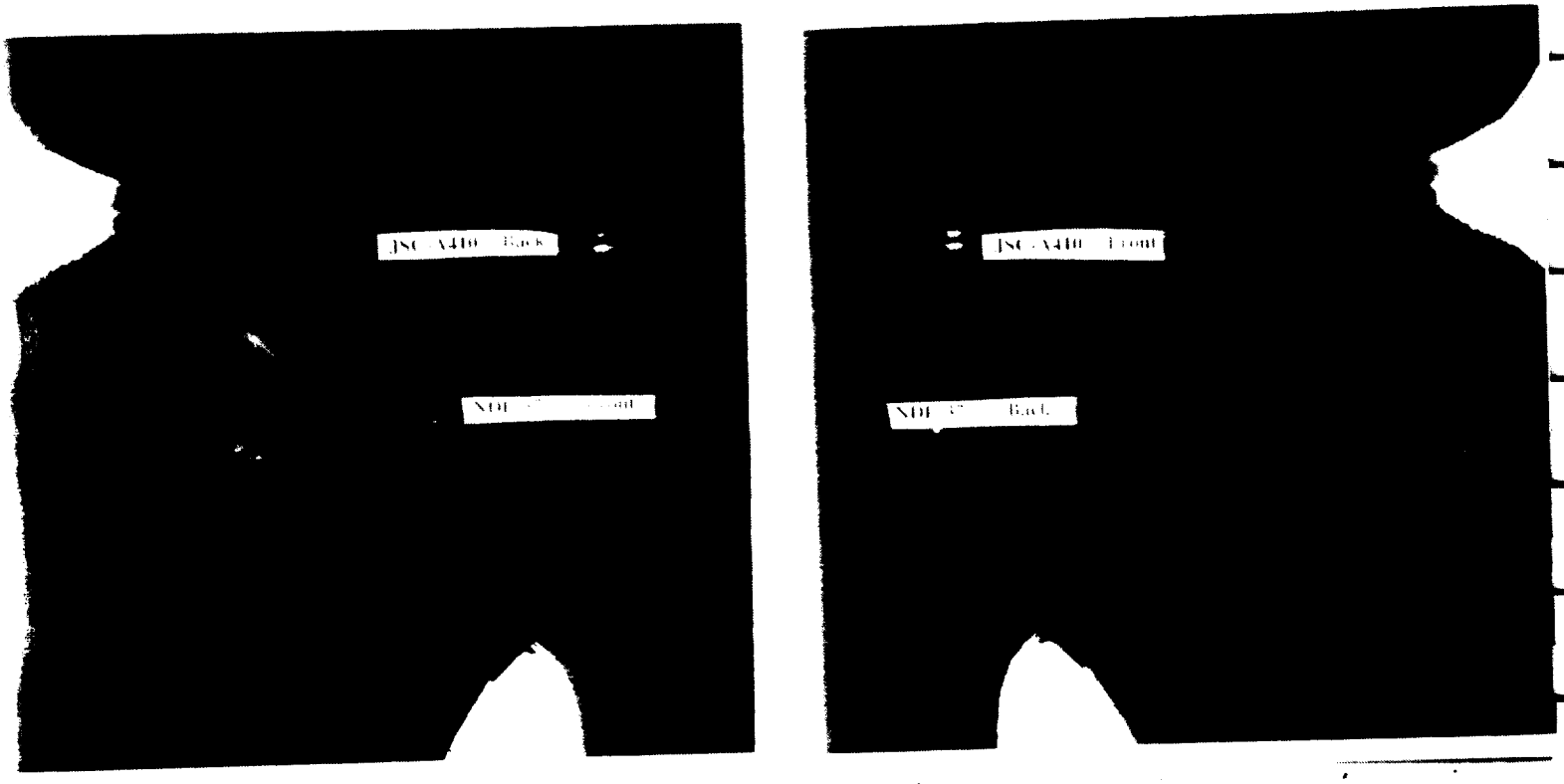

Figure 4-45. Flat Plate Effects: Photographic Documentation of Shot JSC-A352
JSC-A352, Plate 11-F-1, [10,30,10], 75M psi, 1.55 mm Al 2024-T4 sphere, 6.83 km/sec.

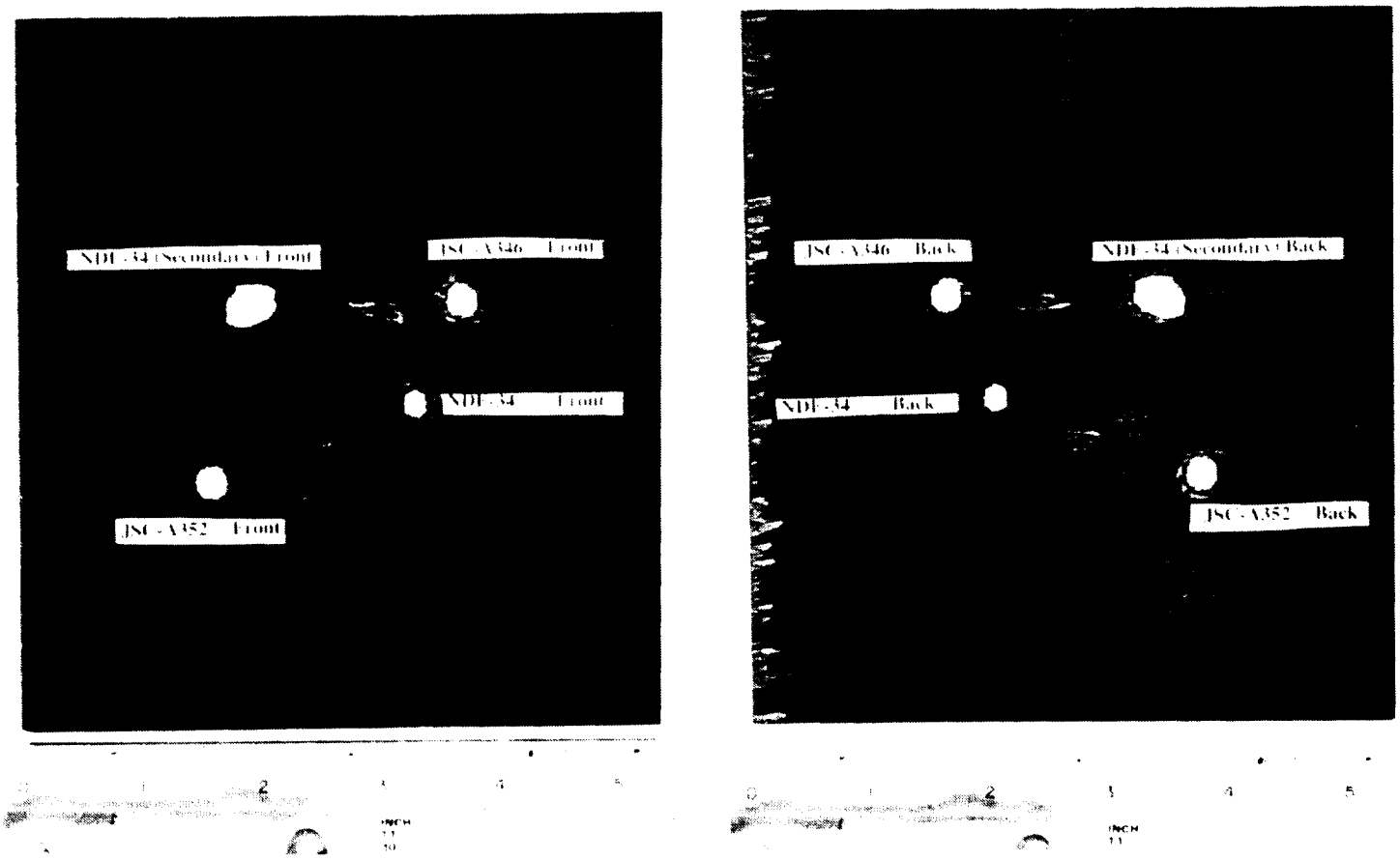

Figure 4-46. Flat Plate Effects: Photographic Documentation of Shot JSC-A407
JSC-A407, Plate 12-F-1, [80,30,10], 75M psi, 1.56 mm Al 2024-T4 sphere, 7.30 km/sec.

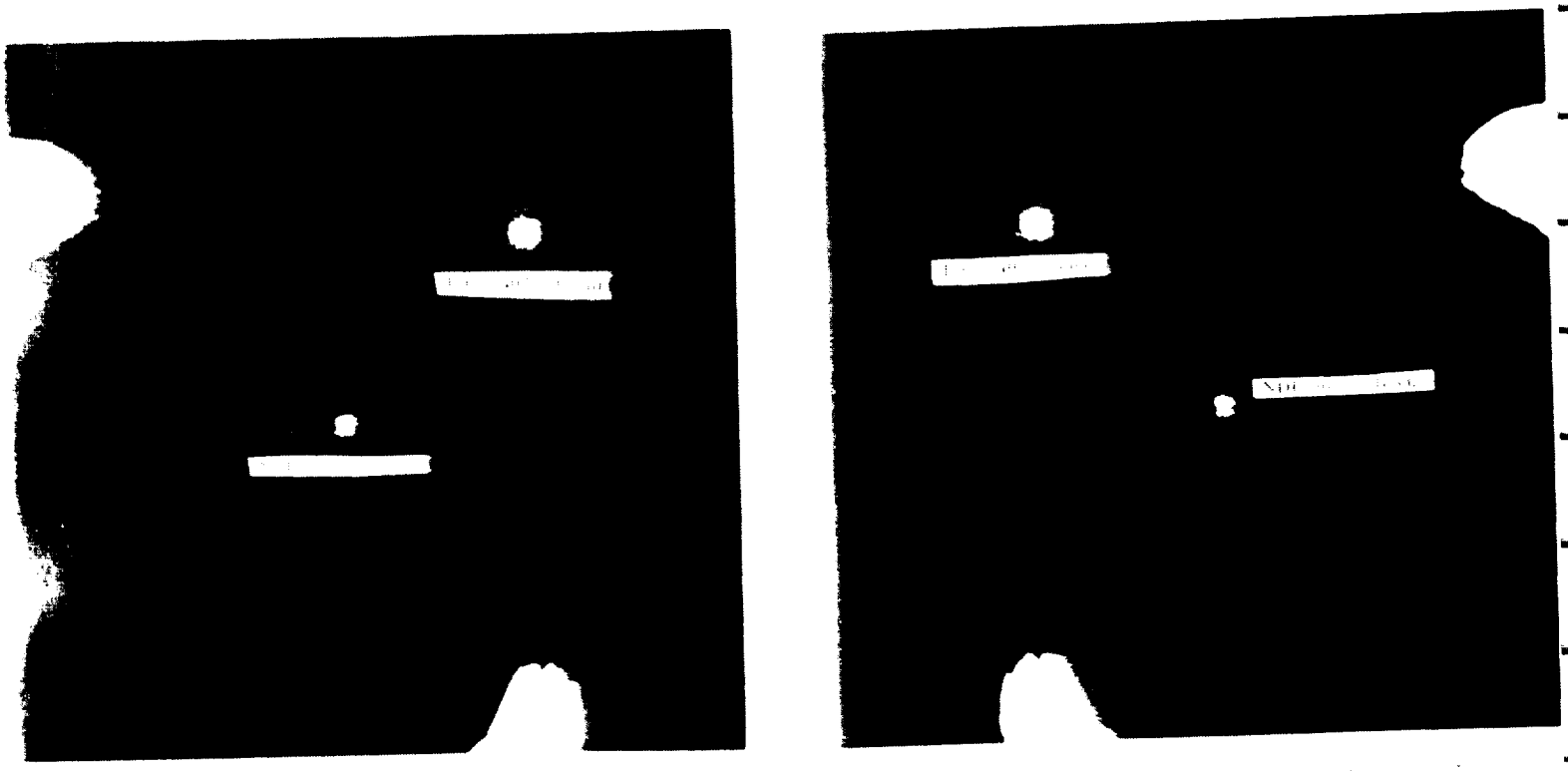

ORIGINAL PAGE IS
OF POOR QUALITY

Figure 4-47. Flat Plate Effects: Photographic Documentation of Shot JSC-A413
JSC-A413, Plate 13-F-1, [45,10,45], 75M psi, 1.55 mm Al 2024-T4 sphere, 7.29 km/sec.

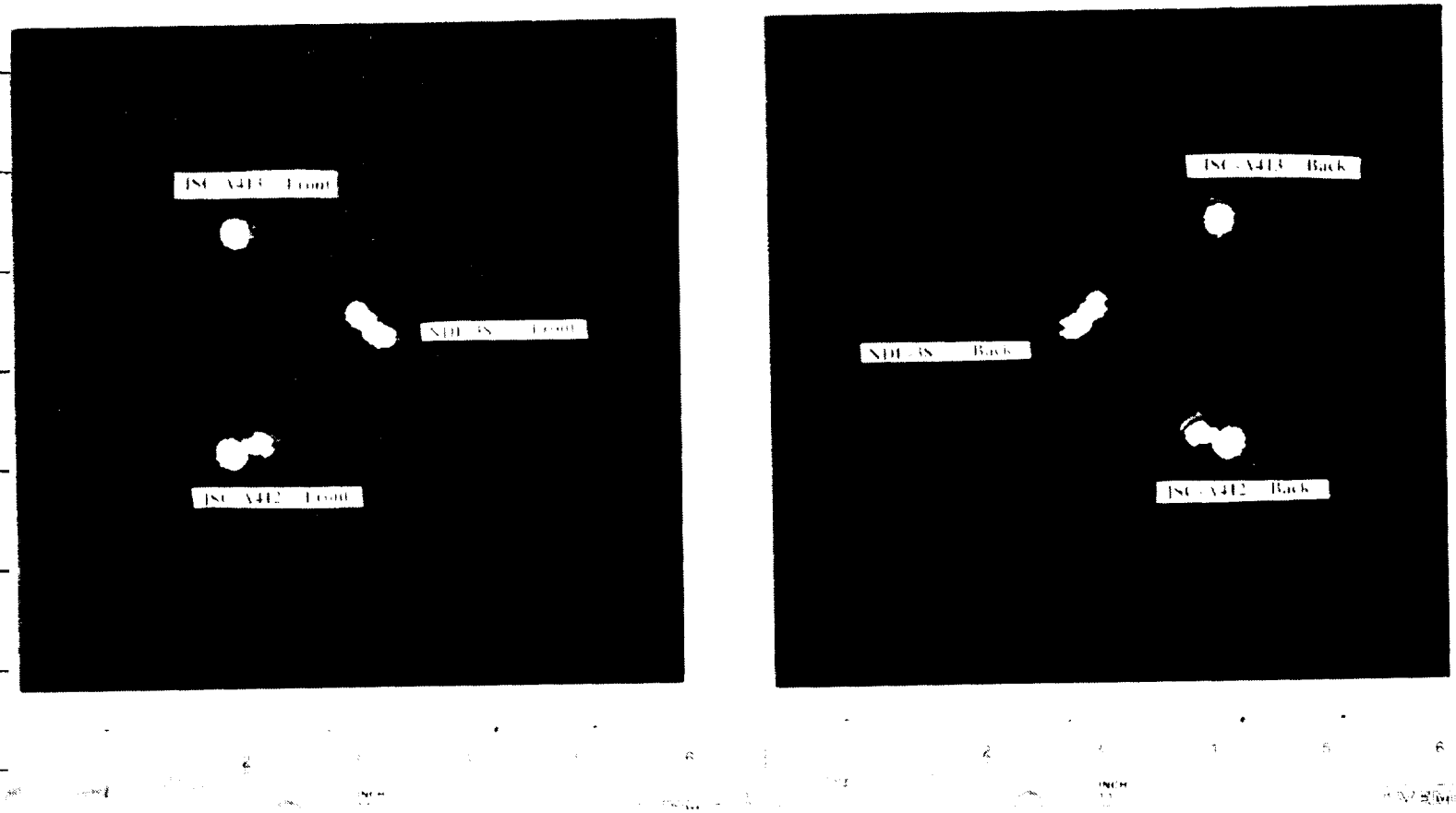

Figure 4-48. Hole Diameter Data for Low Modulus Flat Plates

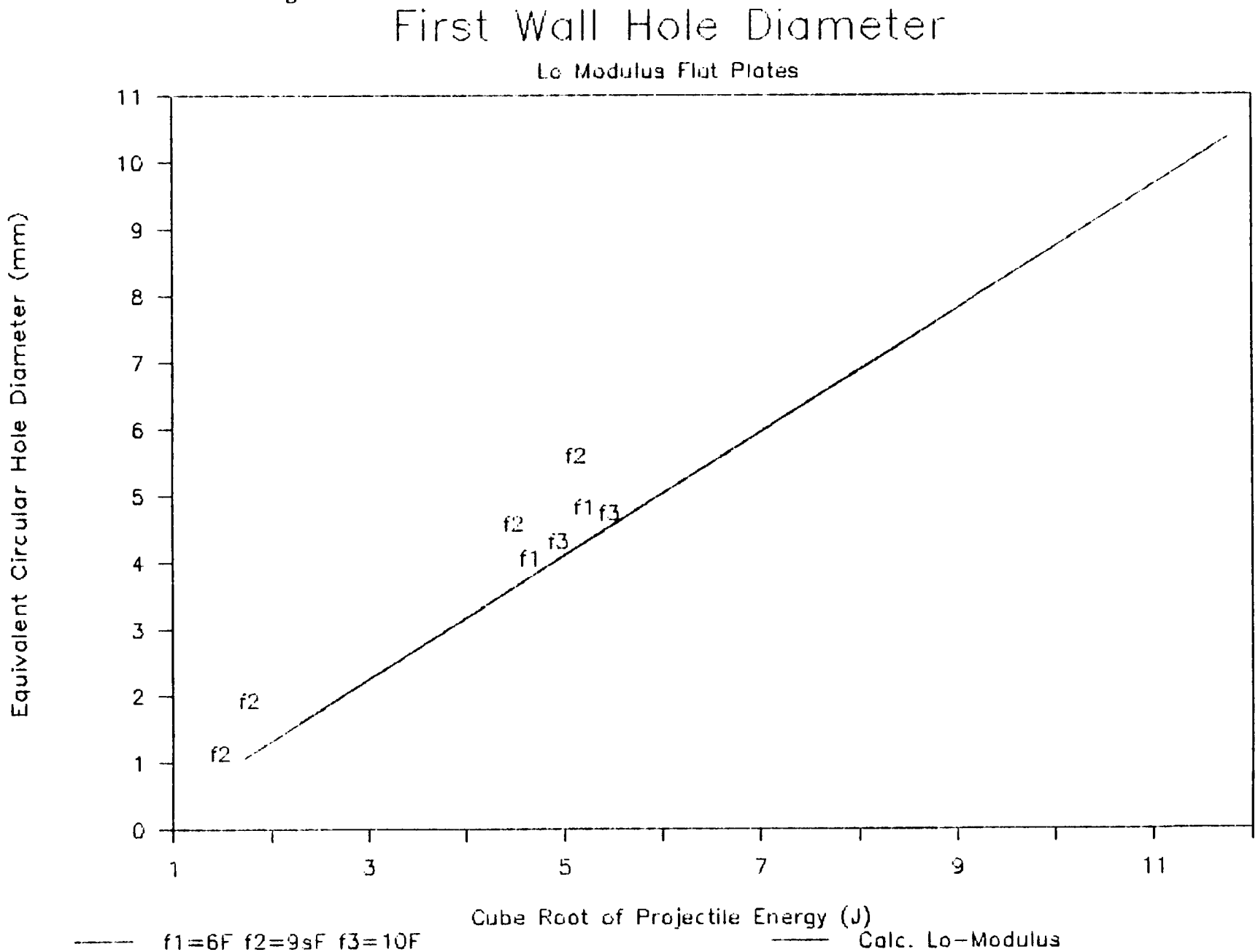

Figure 4-49. Hole Diameter Data for High Modulus Flat Plates

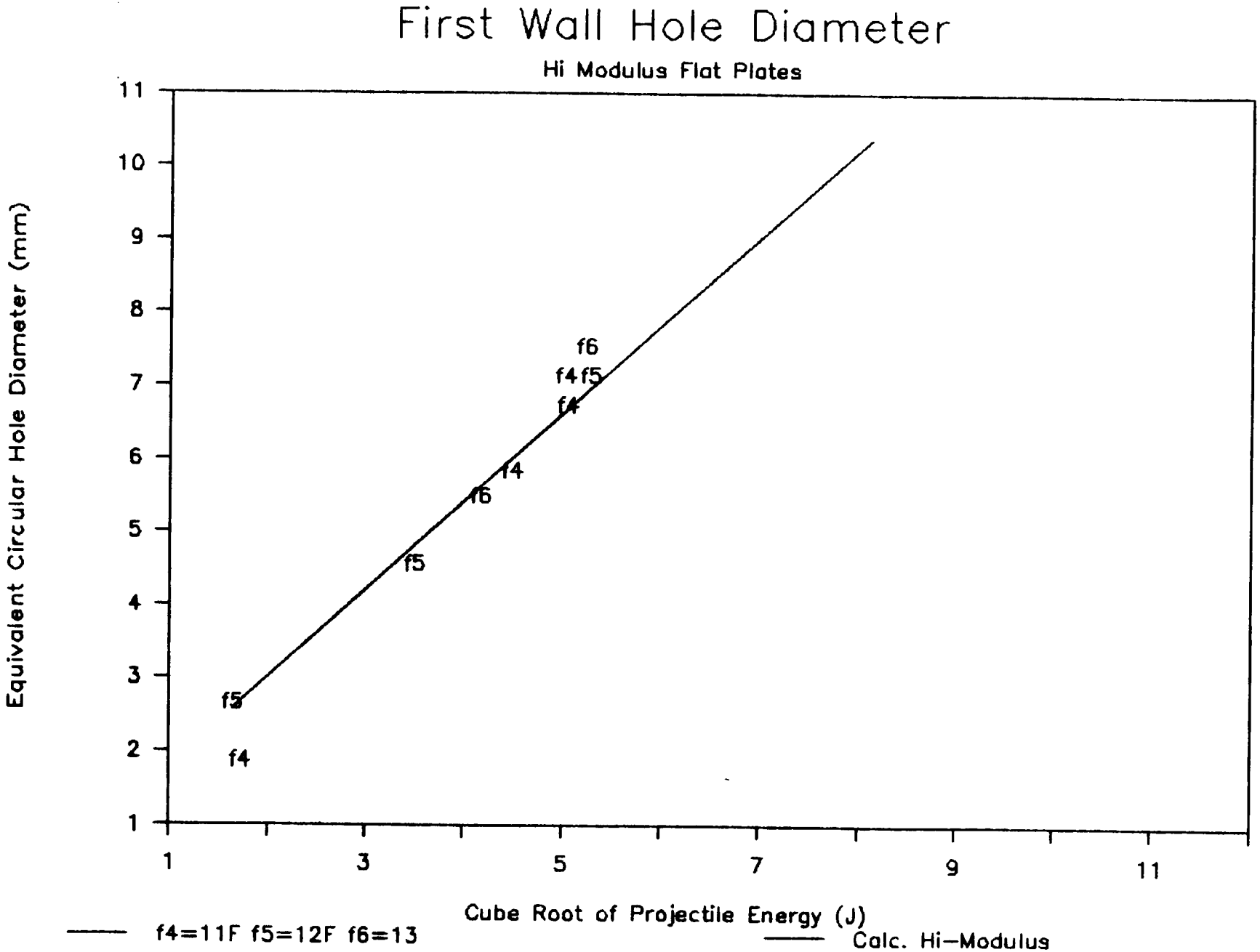

Figure 4-50. C-Scan Diameter Data for Low and High Modulus Flat Plates

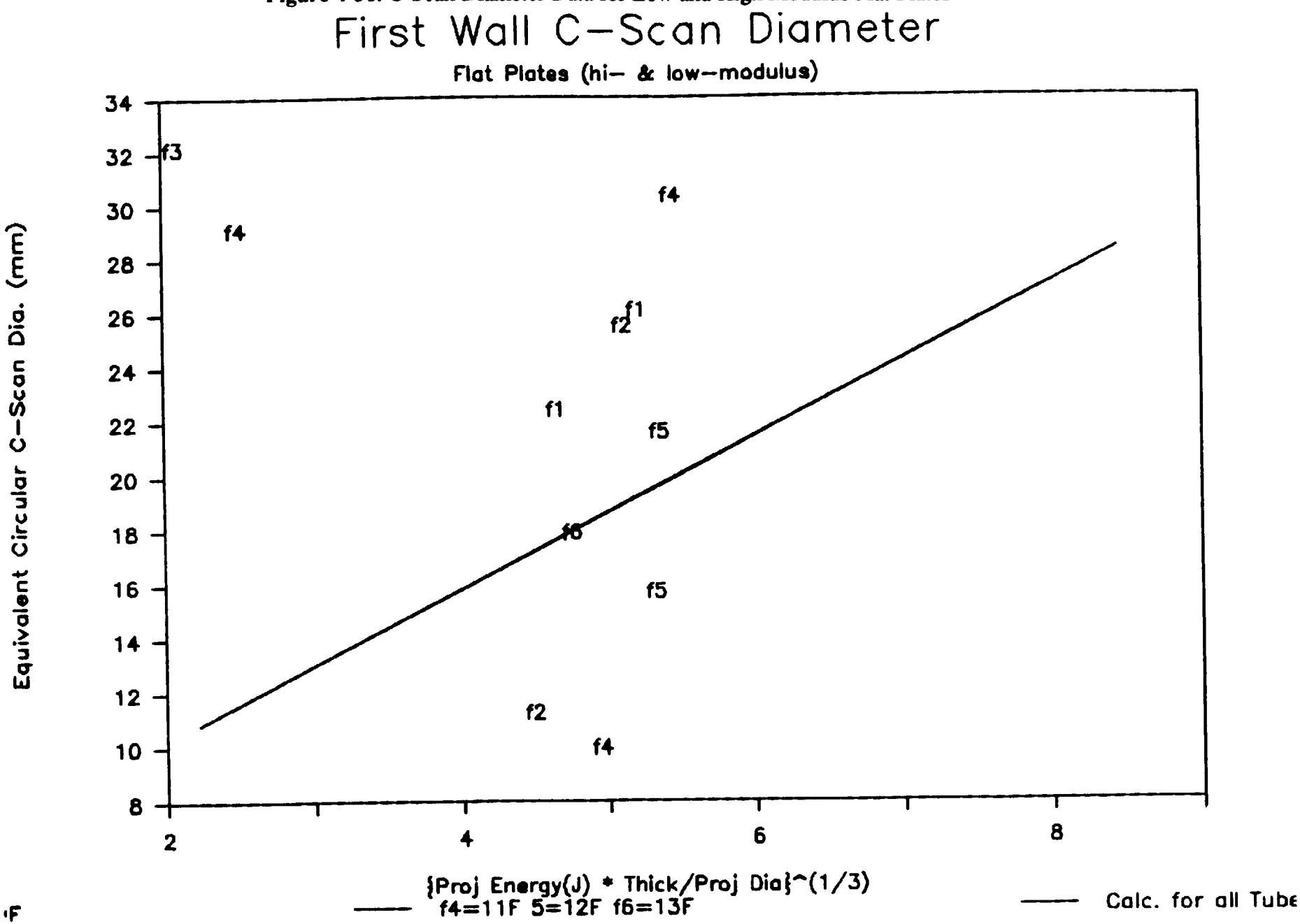

4.7 Effect of Projectile Obliquity

Space Station tubes will be exposed to projectiles impacting at oblique angles in two planes. Projectiles can impact at an angle to the longitudinal axis of the tube (along the length of the tube), and/or at an angle to the radius of the tube (see Figure 4-1). These two impact obliquity situations will be described by the "longitudinal" and "radial" obliquity impact angles, respectively. A 0° obliquity angle is defined as normal to the tube surface. Thus, a 0° longitudinal obliquity means the projectile impacts perpendicular to the longitudinal axis of the tube while a 0° radial obliquity means the projectile impacts parallel to a radial line connecting the tube center and the impact point.

Almost all impact tests were conducted perpendicular to the longitudinal axis. Because of the dispersion inherent in the ballistic ranges, radial obliquity angles up to 40° occured during the testing (longitudinal obliquity angle remained at 0°). Intentional obliquity testing was conducted to provide additional data. Photographs of the results of intentional tests at 45° radial and longitudinal impact obliquity angles are given in Figures 4-51 and 4-52. Direct comparisons can be made with Figure 4-4 for impact results on the same type tube and projectile at a near zero impact obliquity.

The amount of peeling around the front wall perforation did not appear to be a function of impact obliquity (Table 4-1), however, hole shape was. As indicated in the detailed descriptions of the damage in Appendix A, the larger the obliquity angle, the more elliptical the surface hole. The longest axis of the elliptical hole is parallel to the projectile flight path. It was thought that hole size would vary with the velocity normal to the tube surface; however, this did not turn out to be the case. The equivalent circular hole size of the front wall perforation to projectile diameter ratio is plotted against the normal velocity in Figure 4-53 for the impact tests on all uncoated, low-modulus Amoco tubes (6T series). The "t1" data points are the low obliquity data points (<10° radial obliquity) with the least squares data fit of:

$$D_{h1}/d = 0.605\ V_n - 1.67 \qquad r = 0.93$$

where D_{h1} is the first wall hole diameter (mm), d is the projectile diameter (mm), V_n is the normal velocity (km/sec) calculated from the direction cosine of the impact obliquity:

$V_n = V * \cos(\theta)$ where V is the projectile velocity (km/sec) and θ is the impact angle. The "o1" data points are the high obliquity data (40-50°) having a least squares fit of:

$$D_{h1}/d = 0.664\ V_n - 0.14 \qquad r = 0.97$$

For the obliquity angles tested (up to 45°), hole area was not a function of obliquity angle. As described in Section 4.1 (Figure 4-8), all the above data was correlated by the expression:

$$D_{h1} = 0.907 * (E)^{0.33} - 0.388 \qquad r = 0.98$$

where the diameter of a circular hole with an area equivalent to the actual measured hole area, D_{h1} (mm), was found to be related to the cube root of projectile energy, E (J), and where projectile energy is related to projectile diameter d (mm), density p (g/cc), and velocity V (km/sec):

$$E = \pi/12 * d^3 * V^2 * p$$

Second wall damage was not a function of radial obliquity angle. Comparing Figures 4-52 (45° radial obliquity) and 4-4 (10° radial obliquity), the back wall delamination extent and C-scan area was nearly the same. Typically, damage to the second wall of a dual wall structure increases as the spacing between the two walls decreases. Thus, it is expected that the second wall damage would increase with larger radial obliquity angles, but would decrease with larger longitudinal obliquity angles. In these tests, with radial obliquity angles less than 45°, second wall damage extent was not a function of radial impact angle. However, second wall exterior surface peeling or internal C-scan delamination was not evident for the 45° longitudinal obliquity impact test (Figure 4-51). Thus, impacts with longitudinal obliquities of 45° or more are demonstrably less damaging than normal angle impacts.

Figure 4-51. Impact Obliquity Effects: Photographic Documentation of Shot JSC-A313
JSC-A313, Tube 6-T-3, 1.54 mm Al 2024-T4 sphere, 7.29 km/sec, 6° radial, 45° longitudinal obliquity impact angles.

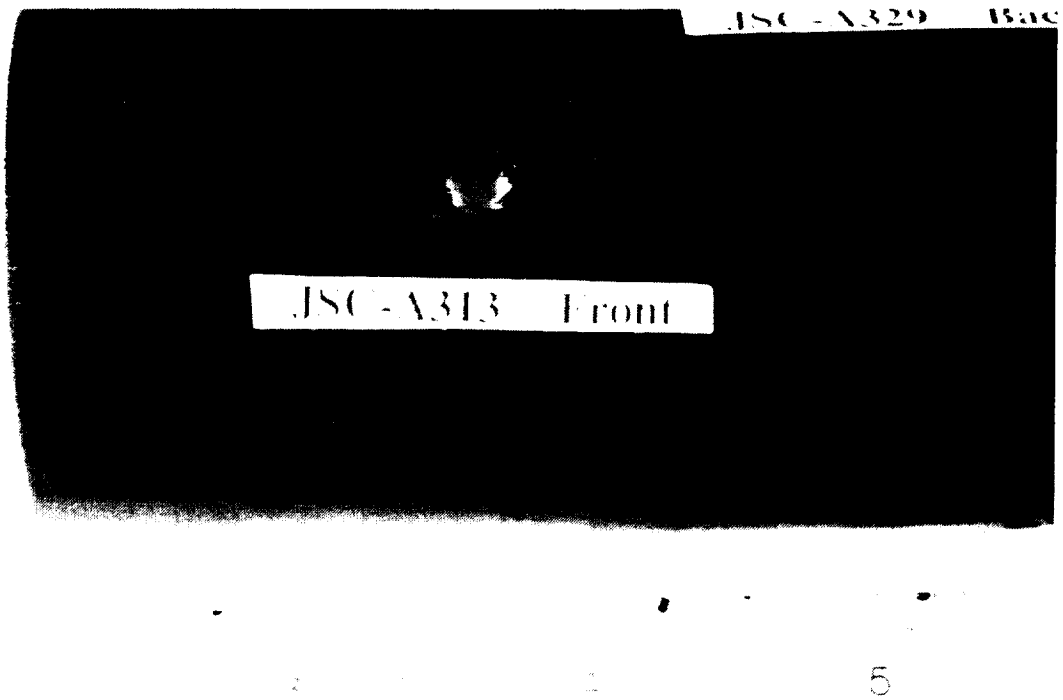

Figure 4-52. Impact Obliquity Effects: Photographic Documentation of Shot JSC-A329
JSC-A329, Tube 6-T-3, 1.55 mm Al 2024-T4 sphere, 7.33 km/sec, 42° radial obliquity.

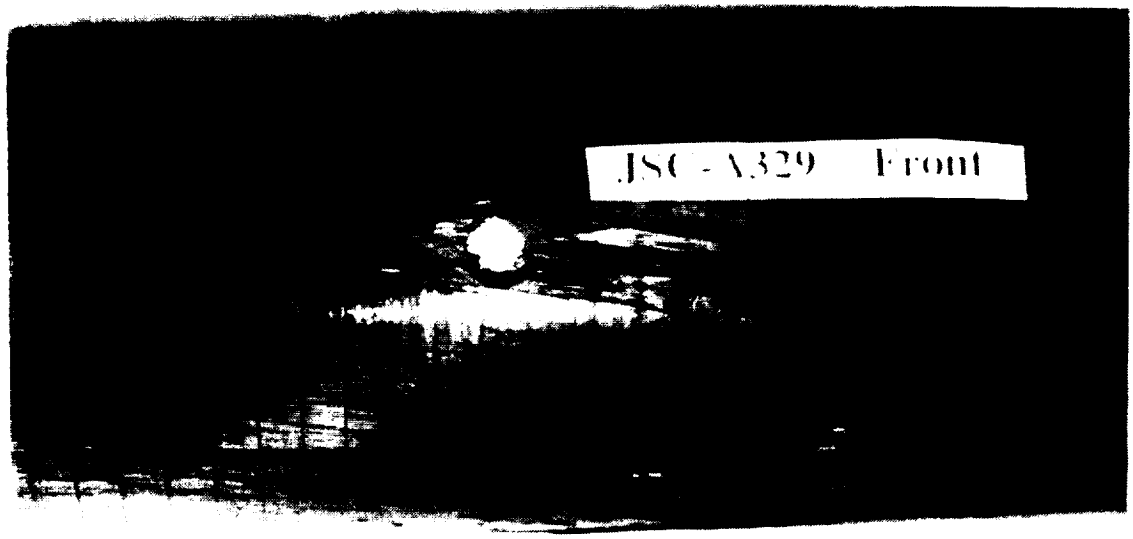

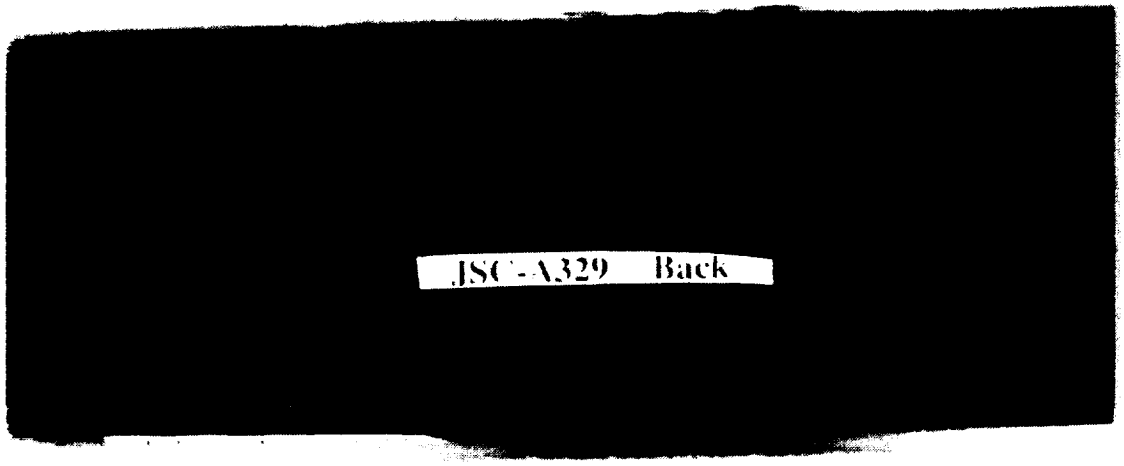

Figure 4-53. First Wall Hole Size for Oblique Impacts on Tubes

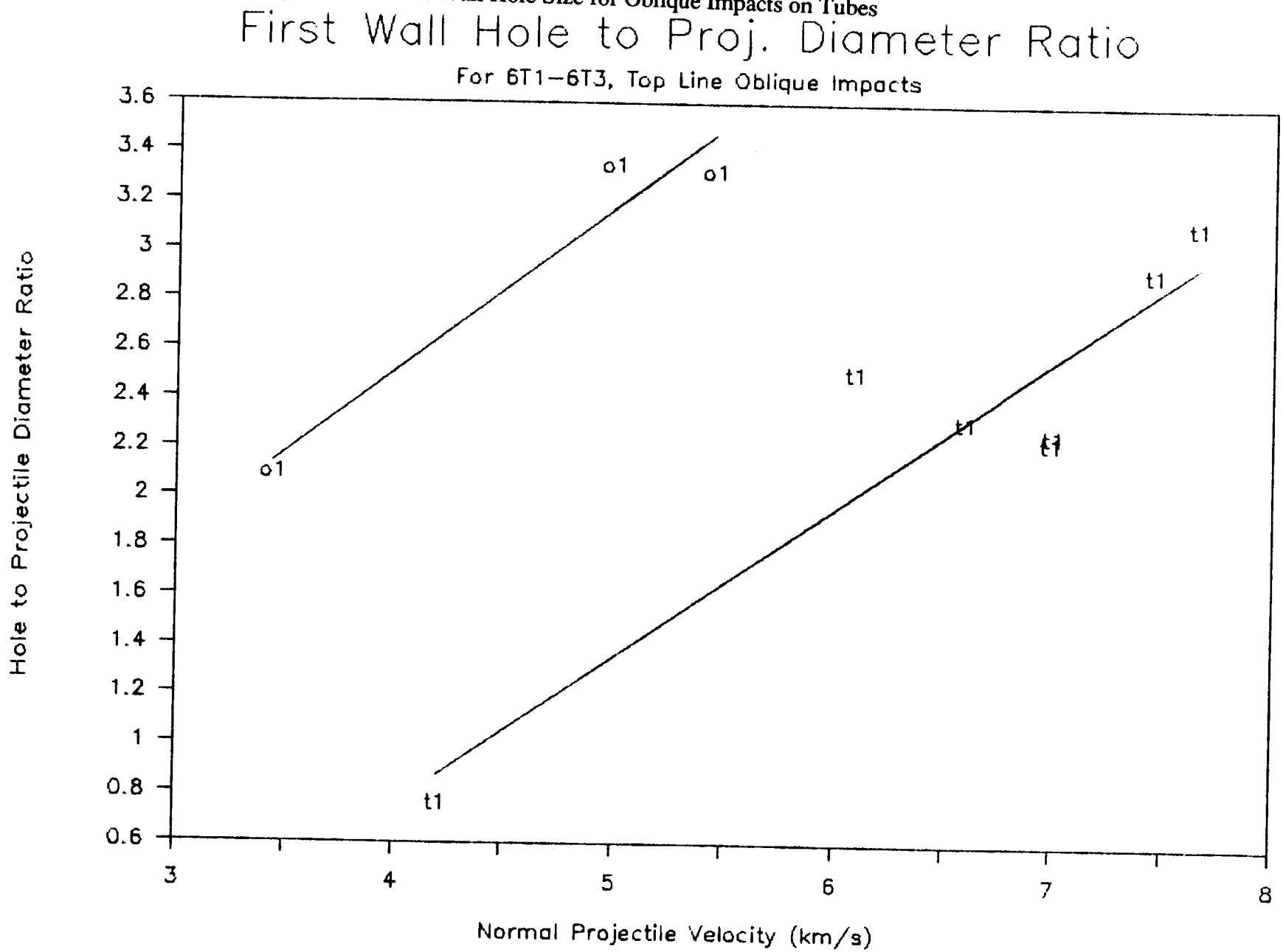

4.8 Effect of Tube Manufacturing Technique

The Amoco tubes used for the principal part of the tests were made by wrapping uni-directional plies around a mandrel in the proper orientation. Tubes made by Morton Thiokol and McDonnell Douglas were also included in the testing for a preliminary comparison of alternative manufacturing techniques. As given in Table 3-9, the Morton Thiokol tubes were also roll-wrapped. They had two different layups with 75M psi fibers, closely resembling the Amoco 11T series tubes. A filament winding process was used to make the McDonnell Douglas tubes. Because the 3 mm wide rovings used in the [10,30,10] oreintation winding contained 34M psi modulus fibers, the McDonnell Douglas closely resembled the Amoco 6T series tubes.

Figure 4-54 shows the results of a 2.37 mm aluminum impact on a McDonnell Douglas tube. It can be directly compared to Figure 4-5 for a similar impact on an uncoated, low-modulus Amoco tube. The McDonnell tube exhibited peeling in an X pattern on the front wall while the Amoco tube peels in a linear pattern. However, the McDonnell tube did not have a clear perforation of the second wall although significant peeling resulted, while the Amoco tube did have holes in the second wall. Apparently, the filament winding reduces second wall damage to some extent.

Figures 4-55 and 4-56 show a comparison of a similar impact on a high modulus Amoco tube and a Morton Thiokol tube. The holes in first and second walls appear superficially nearly equal in these two cases. Figure 5-57 plots all Thiokol and McDonnell tube data against the previously derived first wall correlations for the high and low modulus Amoco tubes. The first wall hole diameter was slightly lower for both McDonnell and Thiokol data than the correlations. The low modulus first wall hole size was given in Section 4.2 as:

$$D_{h1} = 0.927\ E^{0.33} - 0.536 \qquad r = 0.98$$

where D_{h1} is the hole diameter (mm), E is projectile energy (J), and r is a measure of the goodness of fit for the correlation (r = 1 is a prefect fit). A least squares fit for the McDonnell first wall hole size data is given in Figure 5-58 as:

$$D_{h1} = 0.971\ E^{0.33} - 1.688 \qquad r = 0.97$$

However, the McDonnell Douglas tubes' first wall C-scan diameter was, if anything, slightly greater than the curve for the Amoco tubes as indicated in Figure 5-59. The combined first and second wall hole size for all McDonnell Douglas and Morton Thiokol data is presented in Figure 5-60 plotted against the Amoco tube data (top curve for Amoco high modulus tubes and bottom curve for low modulus tubes). The Morton Thiokol combined hole data matched closely the correlation for the Amoco high modulus tubes. The data in Figure 5-60 for the McDonnell Douglas shows that the filament wound tubes have somewhat greater resistance to second wall perforation damage than the Amoco low modulus roll-wrap tubes. However, the data in Figure 5-61 indicates that the filament wound tubes had slightly greater combined wall ultrasonic C-scan areas than the roll-wrap tubes. There was little difference between the Morton Thiokol combined wall C-scan data and the Amoco tubes' correlation.

Figure 4-54. Tube Manufacturing Effects: Photographic Documentation of Shot JSC-A261
JSC-A261, Tube MD-2, 2.37 mm Al 2024-T4 sphere, 7.25 km/sec, 13° radial obliquity.

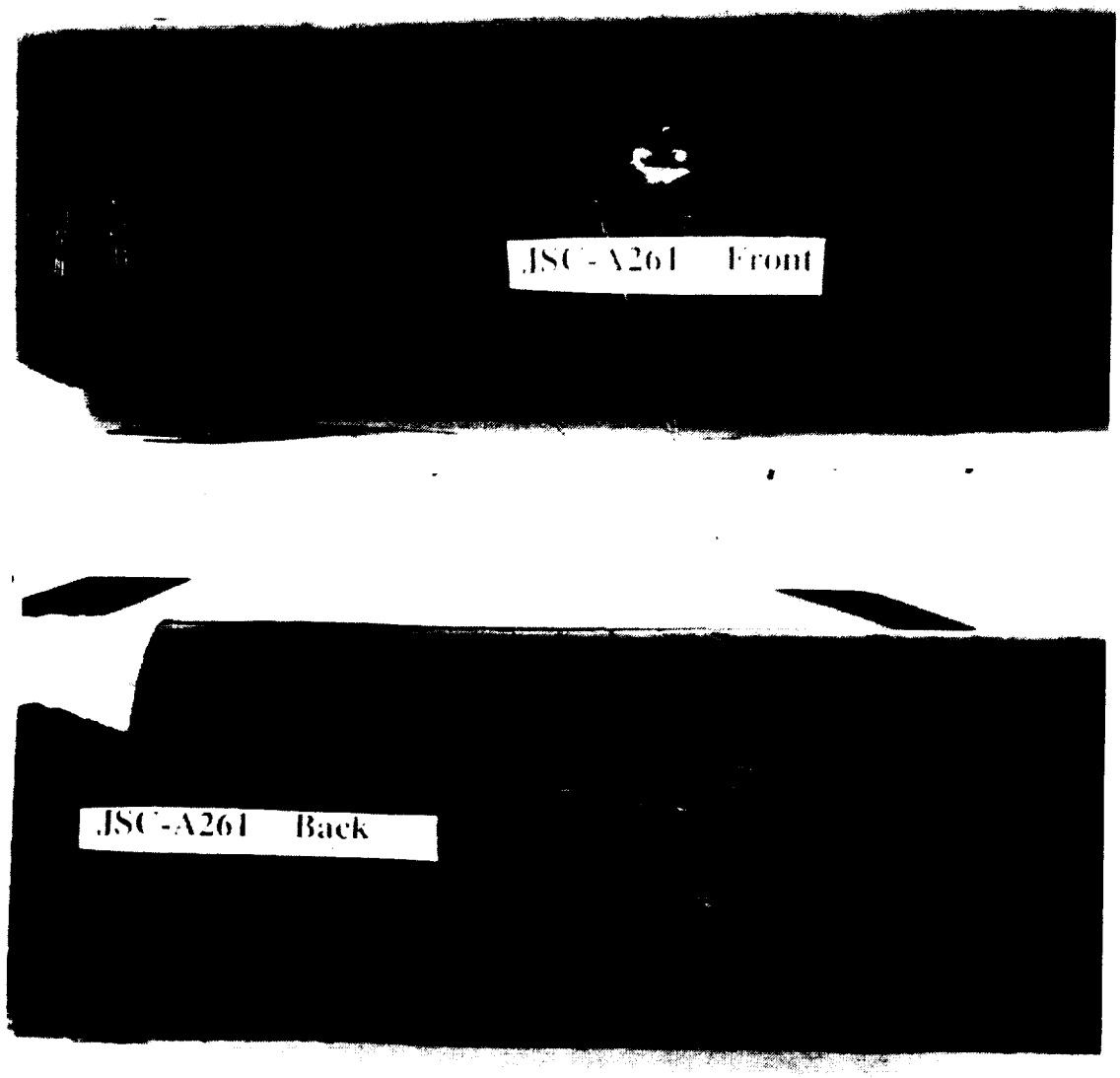

Figure 4-55. Tube Manufacturing Effects: Photographic Documentation of Shot JSC-A246
JSC-A246, Tube 11-T-2, 2.38 mm Al 2024-T4 sphere, 7.38 km/sec, 12° radial obliquity.

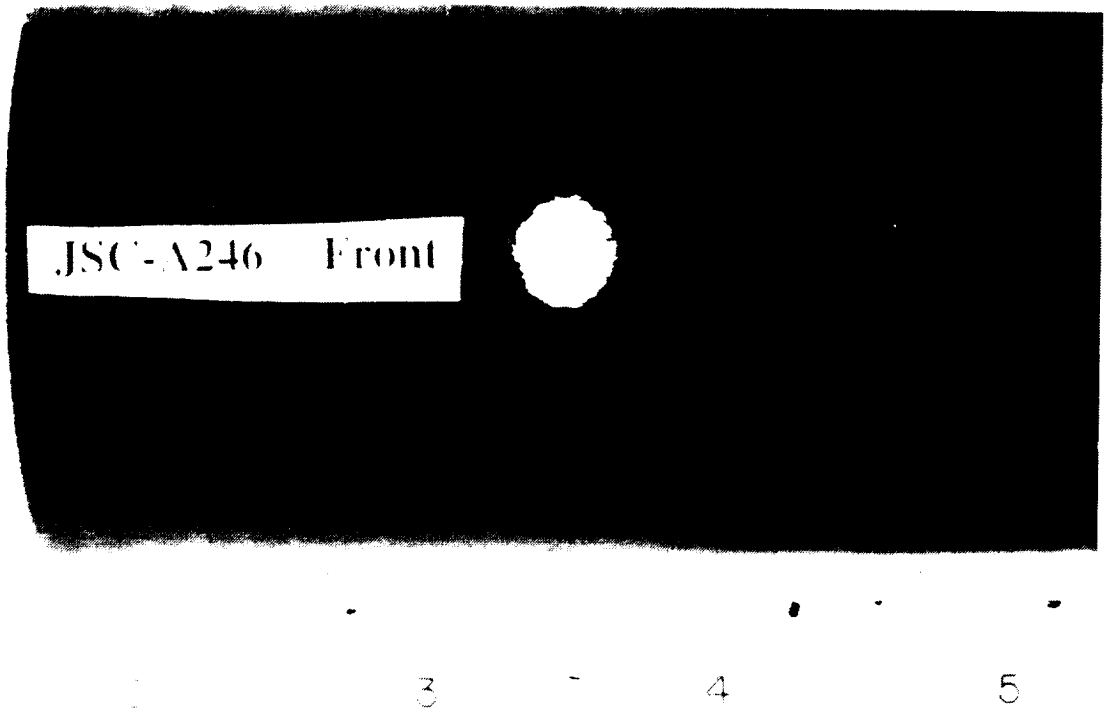

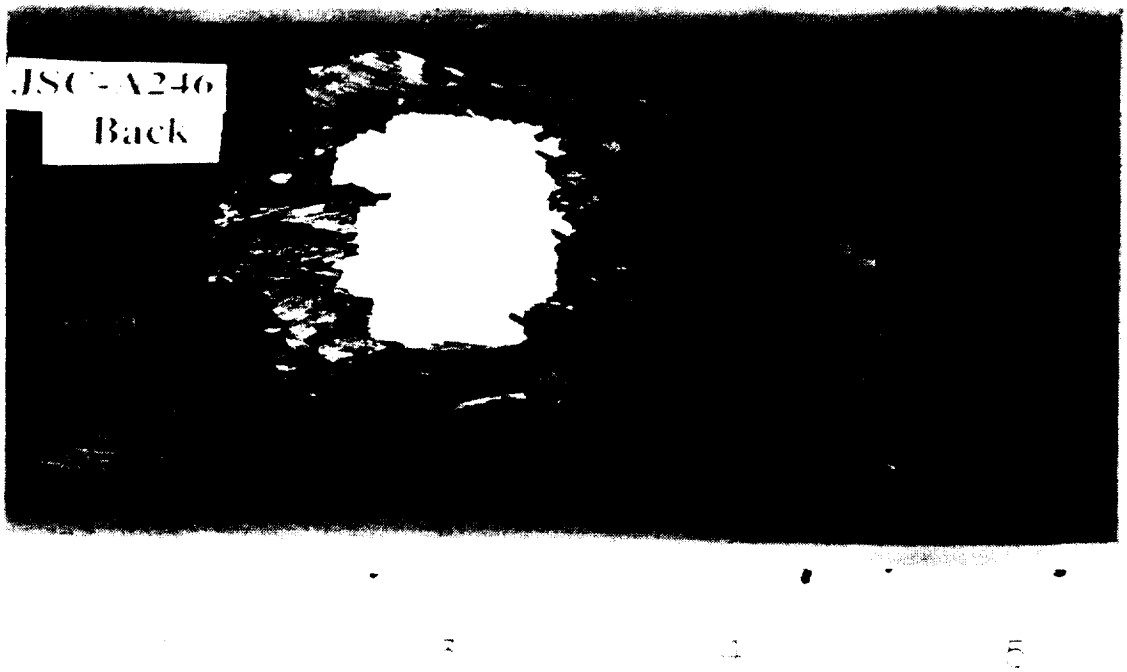

Figure 4-56. Tube Manufacturing Effects: Photographic Documentation of Shot JSC-A245
JSC-A245, Tube MT-2, 2.34 mm Al 2024-T4 sphere, 7.08 km/sec, 13° radial obliquity.

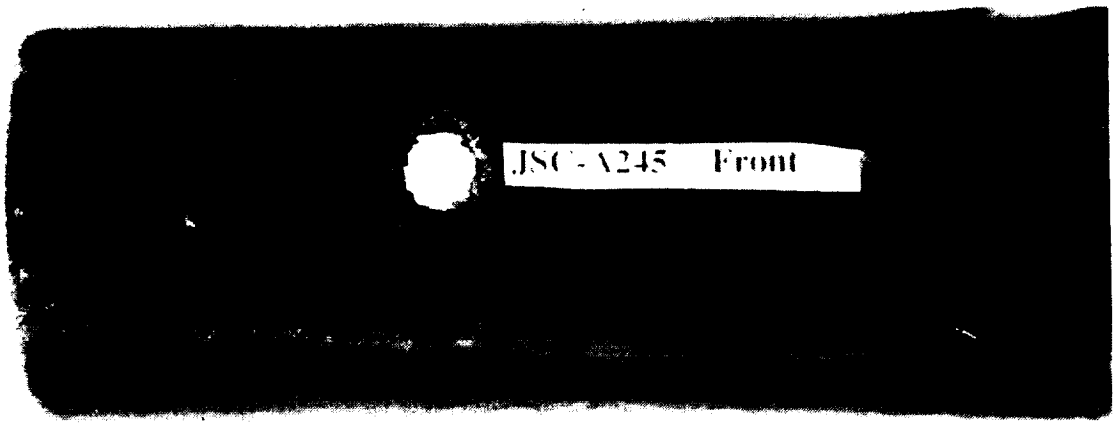

Figure 4-57. First Wall Hole Diameter for McDonnell Douglas and Morton Thiokol Tubes

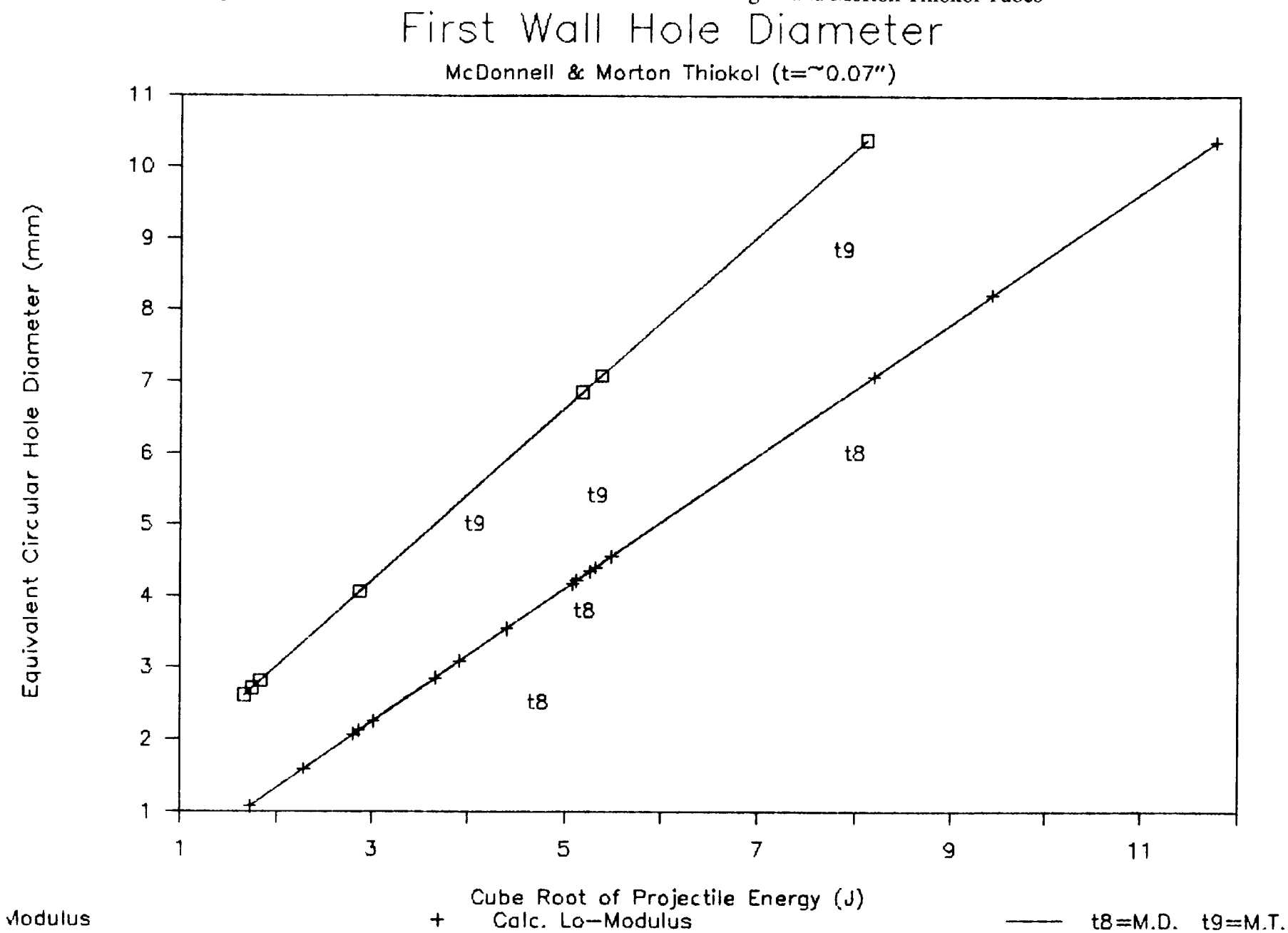

Figure 4-58. First Wall Hole Diameter Correlation for McDonnell Douglas Tubes

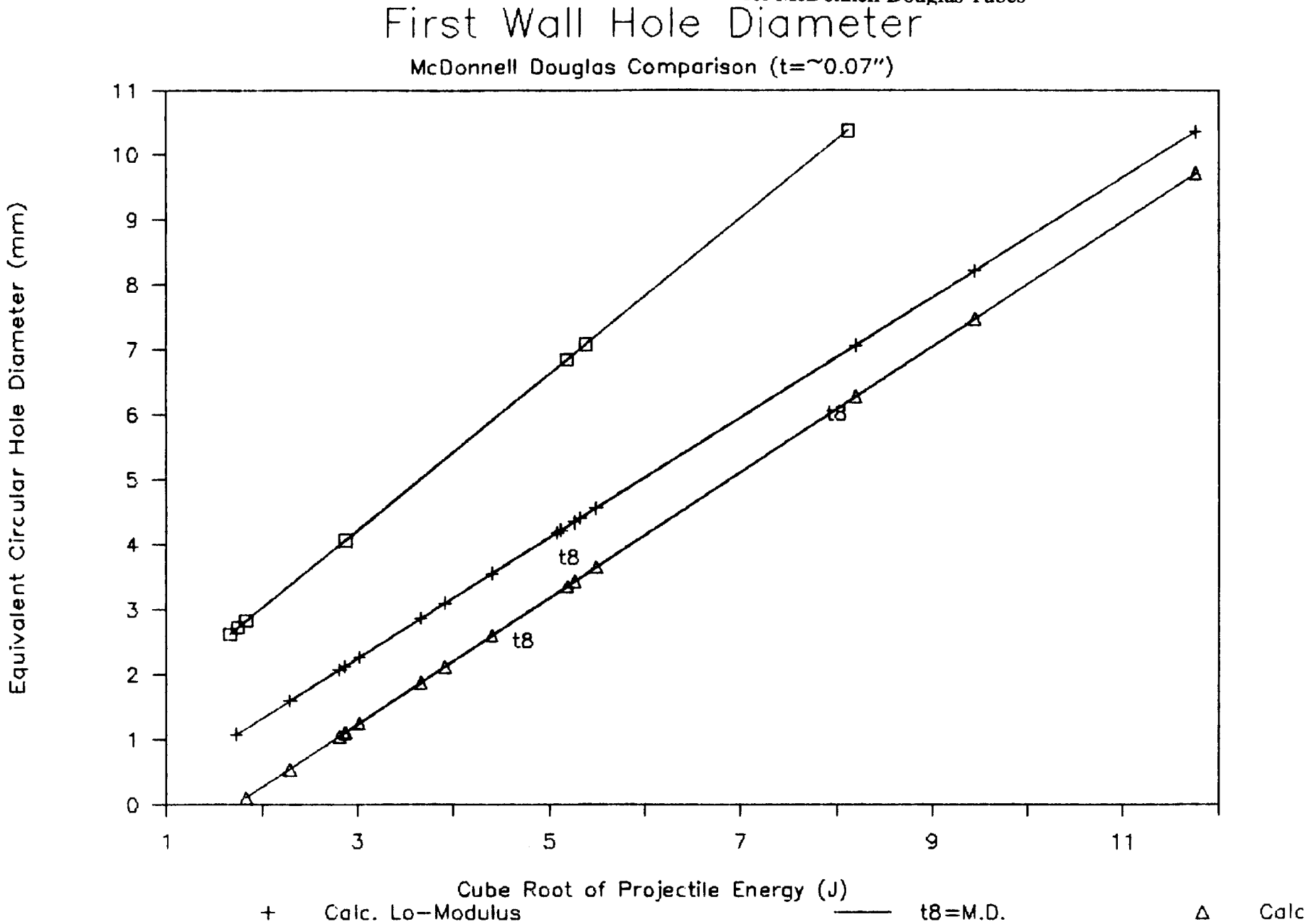

Figure 4-59. First Wall C-Scan Diameter for McDonnell Douglas and Morton Thiokol Tubes

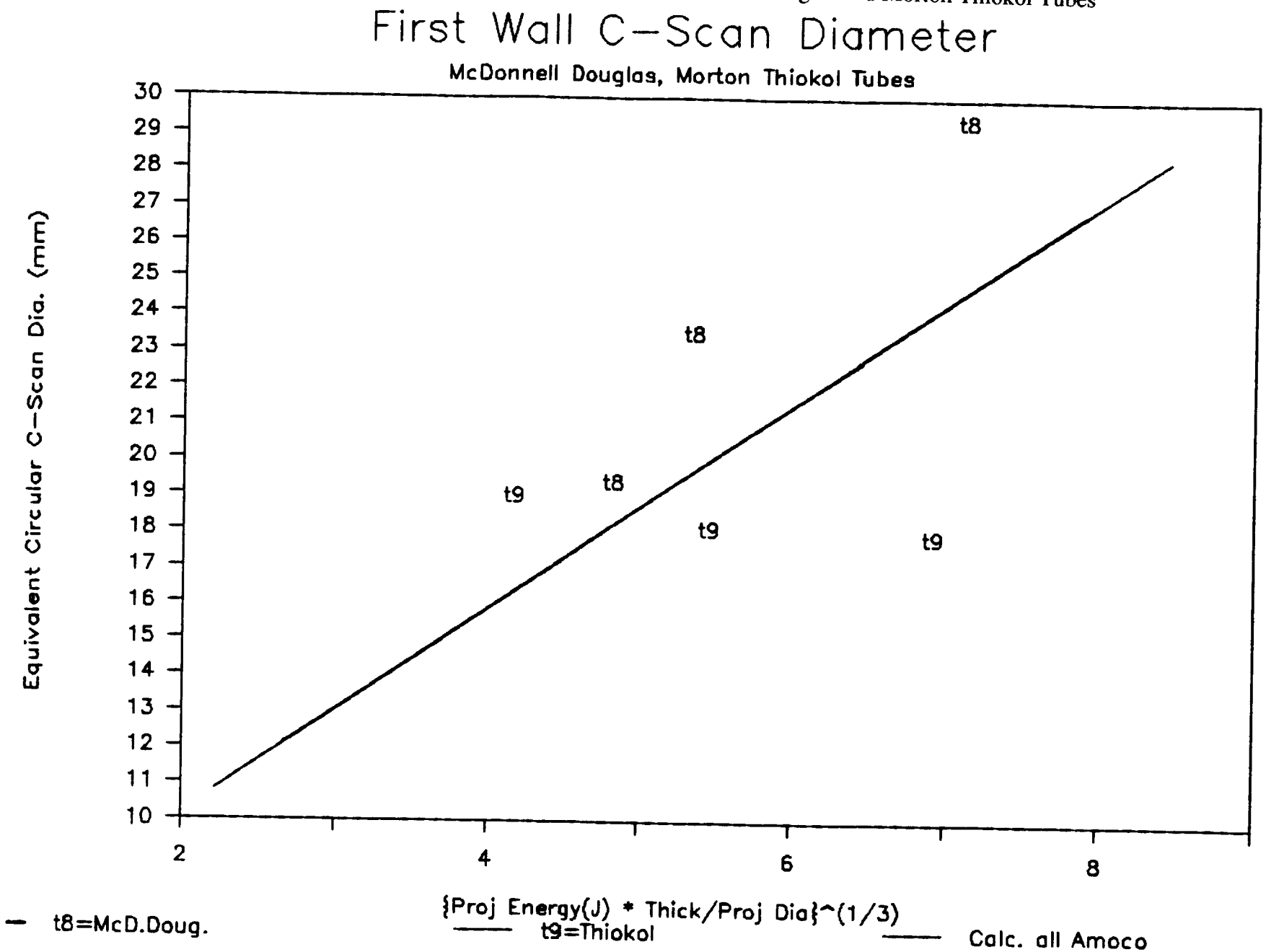

Figure 4-60. Combined Wall Hole Diameter for McDonnell Douglas and Morton Thiokol Tubes

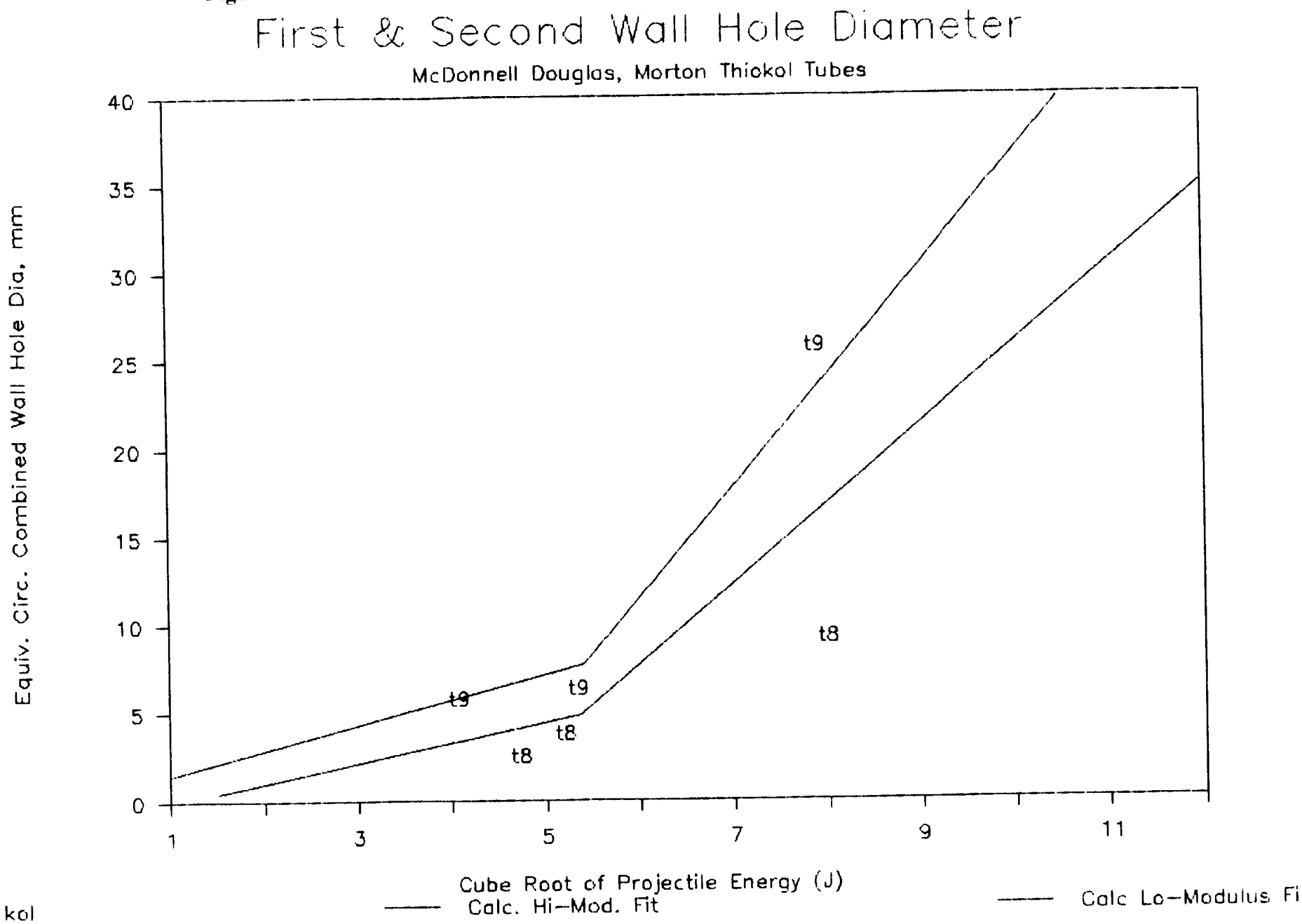

kol

Figure 4-61. Combined Wall C-Scan Diameter for McDonnell and Thiokol Tubes

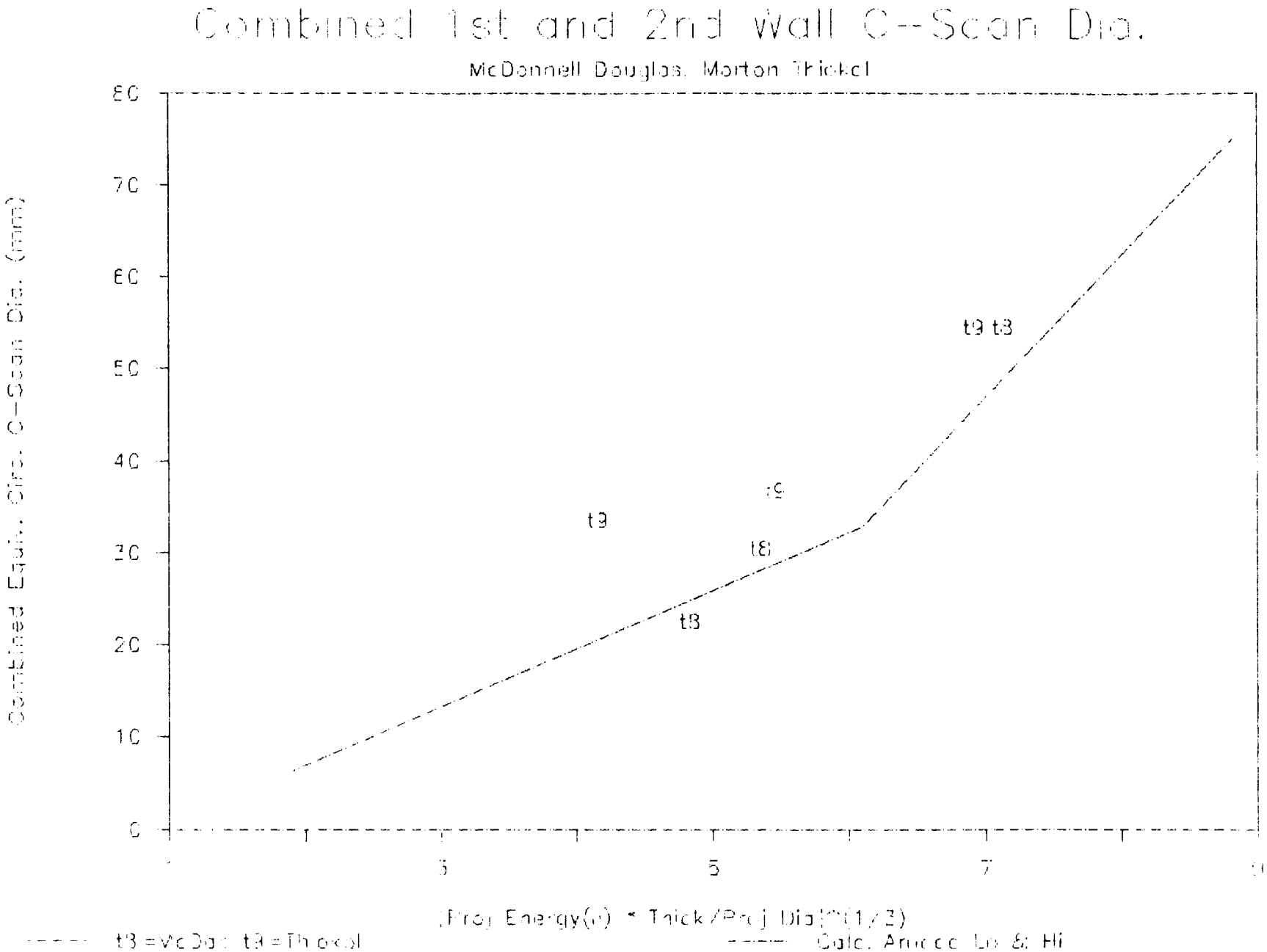

ORIGINAL PAGE IS
OF POOR QUALITY

4.9 Summary of Derived Equations

The impact testing resulted in the following correlations between damage extent and projectile parameters. Symbols used in the equations include:

D_{h1} = Tube first wall equivalent circular hole diameter (mm).
D_{hb} = Combined first and second wall equivalent circular hole diameter (mm).
D_{c1} = First wall equivalent circular C-scan diameter, including hole (mm).
D_{cb} = Combined first and second wall equivalent circular C-scan diameter, including any holes (mm).
D_c = Diameter of C-scan zone for flat plates (mm).
P = Equivalent circular diameter of exposed region of 2mil aluminum coated tubes, not including the perforated/crater area (mm).
d = Projectile diameter (mm).
p = Projectile density (g/cc).
V = Projectile velocity (km/sec).
V_n = Projectile velocity normal to target surface (km/sec).
E = Projectile kinetic energy (J).
E_n = Projectile kinetic energy normal to target surface (km/sec).
t = Target wall thickness (mm).
r = Correlation coefficient (perfect fit = 1).

<u>Uncoated tubes, 0.07" thick walls, [10,30,10] layup, 34M psi modulus fibers (Amoco 6T Series):</u>

$$D_{h1} = 0.907 * (E)^{0.33} - 0.388 \qquad r = 0.98$$

$$D_{h1} = 0.58 * d * p^{0.33} * V^{0.67} - 0.388$$

$$D_{c1} = 3\,(E * t/d)^{0.33} + 4.0 \qquad r = 0.95$$

For E < 127J (or D_{hb} < 4.4 mm):

$$D_{hb} = 1.14\,E^{0.33} - 1.29 \qquad r = 0.95$$

For E > 127J (or D_{hb} > 4.4 mm):

$D_{hb} = 4.32\ E^{0.33} - 17.25$ $\quad r = 0.96$

For $(E * t/d) < 180J$ (or $D_{cb} < 26$ mm):

$D_{cb} = 4.64\ (E * t/d)^{0.33} - 0.39$ $\quad r = 0.89$

For $(E * t/d) > 180J$ (or $D_{cb} > 26$ mm):

$D_{cb} = 16.90\ (E * t/d)^{0.33} - 69.8$ $\quad r = 0.99$

For low obliquity impacts (<10°):

$D_{h1}/d = 0.605\ V_n - 1.67$ $\quad r = 0.93$

For high obliquity impacts (40°-50°):

$D_{h1}/d = 0.664\ V_n - 0.14$ $\quad r = 0.97$

<u>Uncoated tubes; 0.07" thick walls; [10,30,10], [80,30,10], and [45,10,45] layups; 34M psi modulus fibers (Amoco 6T, 9T, and 10T Series)</u>:

$D_{h1} = 0.927 * (E)^{0.33} - 0.536$ $\quad r = 0.98$

For $E < 155J$ (or $D_{hb} < 4.8$ mm):

$D_{hb} = 1.14\ E^{0.33} - 1.29$ $\quad r = 0.95$

For $E > 155J$ (or $D_{hb} > 4.8$ mm):

$D_{hb} = 4.54\ E^{0.33} - 19.54$ $\quad r = 0.95$

For $(E * t/d) < 200J$ (or $D_{cb} < 30$ mm):

$D_{cb} = 5.60\ (E * t/d)^{0.33} - 3.32$ $\quad r = 0.83$

For $(E * t/d) > 200J$ (or $D_{cb} > 30$ mm):

$D_{cb} = 16.90\ (E * t/d)^{0.33} - 69.8$ $\quad r = 0.99$

Uncoated tubes; 0.07" thick walls; [10,30,10] and [80,30,10] layups; 75M psi modulus fibers (Amoco 11T and 12T Series):

$$D_{h1} = 1.202 * (E)^{0.33} + 0.612 \qquad r = 0.98$$

For E < 158J (or D_{hb} < 7.7 mm):

$$D_{hb} = 1.424\ E^{0.33} + 0.034 \qquad r = 0.98$$

For E > 158J (or D_{hb} > 7.7 mm):

$$D_{hb} = 6.281\ E^{0.33} - 26.22$$

Uncoated tubes; 0.07" thick walls; [10,30,10], [80,30,10], and [45,10,45] layups; 34M and 75M psi modulus fibers (Amoco 6T, 9T, 10T, 11T and 12T Series):

$$D_{c1} = 2.72\ (E * t/d)^{0.33} + 4.86 \qquad r = 0.84$$

For (E * t/d) < 230J (or D_{cb} < 30 mm):

$$D_{cb} = 6.31\ (E * t/d)^{0.33} - 5.72 \qquad r = 0.88$$

For (E * t/d) > 230J (or D_{cb} > 30 mm):

$$D_{cb} = 15.50\ (E * t/d)^{0.33} - 61.8 \qquad r = 0.94$$

Also for (E * t/d) > 230J (or D_{cb} > 30 mm):

$$d = [(D_{cb} + 61.8)/15.5]^{1.5} * (12/\pi)^{0.5} * p^{-0.5} * V^{-1} * t^{-0.5}$$

Coated tube, 0.002" thick aluminum bonded coating, 0.07" thick G/E walls, [10,30,10] layup, 34M psi modulus fibers (2mil Al Coated Amoco 6T Series):

$$P/d = 1.827\ (E_n)^{0.33} - 0.0989$$

Uncoated tubes; 0.07", 0.11", and 0.14" thick walls; [10,30,10], [80,30,10], and [45,10,45] layups; 34M and 75M psi modulus fibers (Amoco 6T, 7T, 8T, 9T, 10T, 11T and 12T Series):

$$D_{c1} = 2.82\,(E * t/d)^{0.33} + 4.58 \qquad r = 0.83$$

Uncoated McDonnell Douglas tubes, filament wound, 0.07" thick walls, [10,30,10] layup, 34M psi modulus fibers:

$$D_{h1} = 0.971 * (E)^{0.33} - 1.688 \qquad r = 0.97$$

Derived from data in previous study (20), 5mg Al & Nylon projectiles, 2 mm to 17 mm thick generic flat plate Graphite/Epoxy targets:

$$D_c/d = 2.72\,V^{0.67}\,p^{0.33}\,(t/d)^{0.33} + 0.26 \qquad r = 0.97$$

rearranging and neglecting constant:

$$D_c = 4.2\,(E * t/d)^{0.33}$$

5.0 Impact Damage Estimates for Space Station Truss Tubes

The following sections describe the preliminary assessment made in this study of the damage potential of orbital debris and meteoroid impact on the truss structure. This analysis uses the correlations for hole and delamination area sizes presented in Section 4.

5.1 Groundrules for Space Station Truss Failure Study

Studies have predicted that the maximum loads experienced by the truss will occur during station orbit-keeping reboost and orbiter docking operations (10, p.63; 31, p.d-26). These distrubance forces cause bending and torsional moments on the truss which result in axial loads on the individual longeron, batten, and diagonal elements of the truss structure (truss diagram and element nomenclature given in Figure 3-6). Shear forces and moments in the truss elements (struts) are negligible. Maximum axial loads in the individual truss tubes are not expected to exceed 1,067 lb_f in the longerons/battens and 600 lb_f in the face diagonals (9, p.155). Loads in the batten diagonals are negligible. Maximum loads are not experienced in all similar truss members. For instance, reaction control system and orbiter docking distrubances create highest stresses near the transverse boom and keel intersections of the phase II dual-keel space station (10). Thus, some truss struts will always be more suspectible to impact damage because they are exposed to the highest loads. Other struts may never be exposed to the maximum loads anytime during the station lifetime and will thus be able to sustain more (larger) impact damage without failing than the fully loaded struts.

A 1.4 factor of safety is required for nonmetallic flight structures (11, p.3-162). This factor is multiplicatively applied to the maximum expected service loads to account for uncertainties in load definition, material properties, dimensional discrepancies, etc. The tube design loads then become 1,500 lb_f for the longerons and 850 lb_f for the face diagonals. However, the truss tubes are also required to withstand the maximum loads that would result from the redistribution of forces through the truss structure with one strut removed from the structure (a strut may be removed to install or remove payloads or stored cargo from within the truss, or for repair purposes, etc.). Removing a longeron, batten, or face diagonal will redistribute the loads in the remaining struts. Redistributed loads peak in the bay with the missing strut (10, p.70) with the maximum redistributed load

about double the original load (8, 10). The redistributed loads remain primarily axial in the individual truss elements. Thus, the truss tubes must be capable of reacting twice the maximum no-strut-out load, 2,100 lb_f for the 5m longerons and 1,200 lb_f for the 7m face diagonals.

The axial loads in the struts will be in both compression and tension. However, it will be more critical for the tube to withstand compressive loads than tensile. The long composite tubes (5m - 7m) will fail by buckling from compressive loads well before the ultimate tensile strength of the graphite-epoxy is exceeded. Graphite-epoxy composites typically have 60 percent by volume graphite fibers which have high tensile strength. For instance, low modulus AS4/3501-6 prepreg tape has a tensile strength of 310,000 psi along the axis of the fibers. For a 0.066" thick, 2" diameter tube with 45° plies, about 500,000 lb_f in tension would be required to fail the tube. However, an undamaged longeron with the same physical parameters will buckle by applying an axial compressive load of approximately 3,000 lb_f. Thus, there is a critical amount of damage that a tube can sustain before it will fail under the design compressive load.

The space station tubes are essentially fixed-end columns, rigidly attached to truss nodes at either end. For a fixed-end column, the middle third and very ends of the tube are subject to the greatest buckling stresses. Other sections of the tube could thus sustain more damage without failing than the tube middle and ends.

A study was conducted to determine the critical damage size that would result in failure of a representative space station truss tube under the maximum compressive load that is likely to be experienced on-orbit. The focus of the study was a 5m longeron tube with an ultimate axial load of 2,100 lb_f. For purposes of the tube, the baseline tube was defined as graphite-epoxy material in a [+/-10,+/-30,+/-10]s layup, 0.066" wall thickness, and using low modulus (34M psi) fibers (AS4/3501-6 fiber/resin system). Results of this study, which was carried out by Hercules Inc., are described in the following section.

5.2 Truss Failure Criteria Study

Hercules applied finite-element analyses to predict the amount of damage that causes a stability failure in a truss tube under compression. The Hercules report included in Appendix B presents details of their approach, analysis, and conclusions. Damage to only

one side of a tube was modelled. Because the residual mechanical properties of the delamination area were not known, it was assumed that the damage area represented both the hole and delamination area and that the delamination area was equivalent to the hole (having no residual stiffness or mechanical properties). A finite element analysis of a short (6") damaged tube was conducted to determine flexural rigidity (EI) as a function of damage size. A second finite element used the results from the first to predict the critical buckling load for a full-length (5m) tube as a function of the amount of damage. The damage was always located at mid-column as the worst case. A model check was made for an undamaged tube. The model predicted a critical buckling load that favorably compared to the closed form Euler solution to column buckling.

For the ultimate load, a 5.4 in^2 (2.6" diameter) hole/delamination area was predicted to result in buckling failure of a longeron. It was suggested that although it was conservative to assume the delamination area did not contribute to tube stiffness, the modeling approach was unconservative in another respect by not accounting for the local moment generated at the damage point in the full-length tube model by the eccentric loading caused by the shift in the tube's neutral axis. Further study was recommended to ascertain the contribution of the induced moment to stability failure of a tube. Bending tests were also recommended for the impacted test elements to determine the effect of the delamination area on tube EI. Unfortunately, the 6" test specimens were too short to effectively conduct this structural test (see Section 3.5).

5.3 Lifetime Impact Damage Projections

The most obvious failure mode for truss elements associated with hypervelocity impact is the case in which a particle impacts a truss element and damages it such that it subsequently fails in buckling. This studies experimental results were applied to project the lifetime failure rate of truss members from meteoroids and debris large enough to cause immediate failure. Hercules' predicted 5.4 in^2 damage area that results in buckling failure was used in this analysis. Thin, low modulus tube properties (0.066" wall thickness, 34M psi fibers, [10,30,10] layup) are used in this analysis. It is assumed that the coating does not provide any penetration resistance. Because the Hercules analysis was for the 5m tubes only, it was also assumed that the lower ultimate load experienced by the 7m diagonals would exactly offset the lower critical buckling load and, therefore, a 5.4 in^2 critical damage area is a good approximation for the diagonals as well. The number of

truss falures over the 30 year design life range from zero to less than 5 depending on the assumptions made. This is not many. However, this is not calculated as a 5% probability of failure, but a 100% probability. A 95% reliability against meteoroid and debris failure is suggested in one reference for non-critical (or redundant) hardware (25, p.13-2). Table 5-1 shows the predicted strut replacements for the phase I space station and Table 5-2 shows the same thing for the phase II space station. To summarize:

Assuming that the mechanical properties of the delamination area are totally degraded and contribute zero flexural rigidity (EI) for resisting buckling, the meteoroid and debris sizes that will produce the 5.4 in^2 critical damage size are:

Particle Diameter (mm)		Mass (mg)		Flux ($\#/m^2/yr$)	
Meteor.	Debris	Meteor.	Debris	Meteor.	Debris
2.5	2.3	4.3	18.1	6.10E-5	1.39E-4

Since in this case the delamination zone is assumed to provide zero structural support (the same as a hole), the particle sizes shown above represent the smallest size that could possibly cause failure of a strut (with the properties given above). The critical particle diameter was calculated by applying the equation developed for correlating projectile energy E (J), diameter d (mm), tube wall thickness t (mm), to the total C-scan equivalent circular diameter, D_{cb} (mm), for both walls:

$$D_{cb} = 15.5\,(E * t/d)^{0.33} - 61.8$$

Which was valid for predicting projectile parameters that result in C-scan diameters greater than 33 mm. In this case, D_{cb} = 66.6 mm. Rearranging this equation to solve for projectile diameter, d (mm) in terms of projectile density, p (g/cc), and velocity, V (km/sec):

$$d = [(D_{cb} + 61.8)/15.5]^{1.5} * (12/\pi)^{0.5} * p^{-0.5} * V^{-1} * t^{-0.5}$$

For purposes of this calculation, average meteoroid velocity was assumed to be 20 km/sec and density to be 0.5 g/cc. Average orbital debris velocity was assumed 9.3 km/sec and density 2.8 g/cc. Tube thickness was 1.676 mm.

If half of the delamination area represents total loss of stiffness/mechanical properties, then the following particle sizes would cause the critical damage area of 5.4 in^2:

Particle Diameter (mm)		Mass (mg)		Flux ($\#/m^2/yr$)	
Meteor.	Debris	Meteor.	Debris	Meteor.	Debris
3.9	3.6	16.0	67.3	1.23E-5	4.61E-5

These critical particle sizes were determined from the following equation and assuming a through hole to delamination diameter ratio of 4/15:

$$d = [(\{19\ D_{cb}/(19 - 15\ CF)\} + 61.8)/15.5]^{1.5} * (12/\pi)^{0.5} * p^{-0.5} * V^{-1} * t^{-0.5}$$

where the C-scan factor, CF = 0.5, was used to describe the fraction of the delamination region that represented good material.

If no flexural rigidity is lost in the delamination zone, than only through holes contribute to structural instability. This is unlikely, but it is the boundary condition that describes the particle sizes that would certainly produce the critical amount of tube damage. The meteoroid and orbital debris particle sizes that produce holes in the first and second tube walls with a combined area equal to the critical damage area are:

Particle Diameter (mm)		Mass (mg)		Flux ($\#/m^2/yr$)	
Meteor.	Debris	Meteor.	Debris	Meteor.	Debris
5.1	4.8	34.2	158	4.89E-6	2.25E-5

These sizes were calculated by applying the equation relating hole diameter (equivalent circular hole diameter for all holes in both tube walls), D_{hb} (mm), to projectile energy, E (J):

$$D_{hb} = 4.54\ (E)^{0.33} - 19.54$$

As explained in Section 4, this is a correlation developed from all low-modulus (34M psi) uncoated tube data with $D_{hb} > 5$ mm. In this case, $D_{hb} = 66.6$ mm. The equation is rearranged to determine the critical projectile diameter, d (mm), as a function of projectile density, p (g/cc), and velocity, V (km/sec):

$$d = [(D_{hb} + 19.54)/4.54] * (12/\pi)^{0.33} * p^{-0.33} * V^{-0.667}$$

The flux of meteoroid and orbital debris particles of the indicated diameter and larger was calculated from the equations given in Section 3. As given in Table 5-2, the phase II station has a truss surface area of 710 m^2. If only one half of the total number of tubes are assumed to be subjected to loads at or near the maximums used in this analysis, the truss area of interest drops to 355 m^2. The finite element analysis indicates a tube with fixed ends is more susceptible to buckling failure when damaged in the middle or a either end, but not 1/4 of the way from either end. If it is assumed that only 1/3 of the tubes loaded to the maximum are susceptible to this kind of damage, the truss area of concern for damage decreases to 120 m^2. As discussed in Section 3, the total number of impacts over the 30 year design life is directly related to surface area. Thus, the number of impacts that would cause tube failure decreases with reduction of the vulnerable surface area. Similar arguments can be applied to the total phase I truss surface area of 225 m^2. Summarizing the calculations of the expected number of tube failures (rounded up) from the combined meteoroid and debris impact flux on the entire truss, on 1/2 of the truss, and on 1/6 of the truss, over the 30 year lifetime:

Station	Percent of C-Scan That has Failed	Number of Impacts From Met. & Debris with Critical Diameter and Greater on: Full Truss	1/2 Truss	1/6 Truss
Phase II	100%	5	3	1
	50%	2	1	<1
	0%	1	<1	<1
Phase I	100%	2	1	<1
	50%	<1	<1	<1
	0%	<1	<1	0

It should be kept in mind that although only a certain fraction (whether 1/6 or 1/2 or more) of the truss is the most vulnerable to impact damage, depending on replacement procedures, all tubes with the critical damage area will prehaps need to be replaced, regardless of the location of the damage on the tube or the location of the tube in the truss. A truss diagram showing loads in several configurations could be used to derive a better estimate of the percentage of tubes exposed to the ultimate load and whether certain truss areas on the station should be designated as "critical" places to inspect for damage. Segregated truss areas might make it practical to schedule and perform an

inspection of these critical tube areas for damage and possible replacement prior to events that generate ultimate loads in the truss (reboost or shuttle docking).

Another difficulty might be in distinguishing critical damage that requires tube replacement from non-threatening damage. Damage observed optically is only a fraction of the total damage revealed by ultrasonic scanning. Thus, more tubes than indicated by the above analysis might be replaced in practice unless (or even if) ultrasonic or other non-destructive test equipment is designed and used on-orbit.

The amount of delaminated area around a penetration that actually represents failed tube and reduced stiffness needs additional study. A bending test on impacted specimens and more analysis will allow a better determination of the effect of the delaminated area. A related question concerns how the delaminated area on the tension side of a buckling tube should be treated. In this analysis, it was assumed that the delaminated area on the tension side was essentially equivalent to the delaminated area on the compressed side of the tube in terms of mechanical properties of stiffness and rigidity. However, the delaminated area in tension may be less "failed" then in compression. This assumption requires more study.

The damage size that results in failure also deserves more study. Finite element model predictions should be compared to actual buckling tests of shorter or full-scale tubes. This analysis was for low modulus fiber tubes. High modulus fiber tubes are stiffer, more resistant to buckling, and will require larger damage areas to fail. Because delaminated (C-scan) areas for high modulus tubes were similar to low modulus, the number of failures could be reduced by a factor of two or more. However, the through-hole size for high modulus tubes were ~1.5 times low modulus tube holes for the same impact conditions, indicating that the residual stiffness of the hole/delaminated damage area may be less for high modulus tubes. Bending tests would provide substantiating data.

5.4 Atomic Oxygen Protective Coating Considerations

The equation presented in Section 4 that correlates exposed graphite epoxy area (where 2 mil thick aluminum coating peeled away from a perforation) to projectile conditions was:

$$P/d = 1.827\,(E_n)^{0.33} - 0.0989$$

where P (mm) is the equivalent circular diameter of the exposed region (not including the perforation or crater area), d (mm) is the projectile diameter, and E_n (J) is the projectile energy determined from the velocity normal to the target surface. Table 5-3 gives the results of compensating the exposed area for peeling as calculated in the above equation to determine how long all tubes of the phase I space station will each have an area equal to 5.4 in^2 exposed to atomic oxygen. The results of this analysis for a 2 mil soft aluminum coating (Al 1100-0) are similar to that obtained in Section 3.2, indicating that a 2 mil soft coating provides borderline protection against atomic oxygen attack over the entire 30 year period. A 2 mil coating made with a harder aluminum alloy would probably be adequate.

Table 5-1. Failure Frequency for Phase I Space Station Truss Tubes

Meteoroid density (g/cc)	0.5		
Debris density (g/cc)	2.8		
Ave. meteoroid velocity (km/s)	20		
Ave. debris velocity (km/s)	9.3		
Strut Diameter (in)	2.1	(cm)	5.334
Tube Thickness (in)	0.066	(mm)	1.6764
Longeron/Batten Length (m)	5	SA (m^2)	0.838
Diagonal Length (m)	7	SA (m^2)	0.184
Number Bays	29		
Number Longerons & Battens	236	SA (m^2)	197.7
Number Diagonals	146	SA (m^2)	26.9
Truss area (m^2)	224.6		
Earth's radius (km)	6378.145		
Station orbital altitude (km)	500		
Earth defocusing factor	0.968596		
Earth shielding factor	0.668024		
Station Lifetime (yrs)	30		
Critical Damage Area (in^2)	5.4		
Critical Damage Diameter (mm)	66.6		

Truss Area (m^2)	Met. Particle Diameter (cm)	Debris Particle Diameter (cm)	Particle Mass Met. (g)	Particle Mass Debris (g)	Particle Flux (incl. SF,DF) Met. (#/m^2-yr)	Particle Flux (incl. SF,DF) Debris	Number Impacts of given Diameter and greater (#/30yr life) Met.	Deb.	Total	Probability of No Impact Met.	Deb.	Total
For C-Scan Having 0% Mechanical Properties:												
Entire truss area:												
224.6	0.2545	0.2313	4.32E-03	1.81E-02	6.10E-05	1.39E-04	0.4	0.9	1.3	0.66	0.39	0.26
1/2 tubes w/ ult.load:												
112.3	0.2545	0.2313	4.32E-03	1.81E-02	6.10E-05	1.39E-04	0.2	0.5	0.7	0.81	0.63	0.51
1/2 tubes + 1/3 tube susceptible:												
37.4	0.2545	0.2313	4.32E-03	1.81E-02	6.10E-05	1.39E-04	0.1	0.2	0.2	0.93	0.86	0.80
For C-Scan Having 50% Bending Rigidity and Mechanical Properties:												
Entire truss area:												
224.6	0.3940	0.3581	1.60E-02	6.73E-02	1.23E-05	4.61E-05	0.1	0.3	0.4	0.92	0.73	0.67
1/2 tubes w/ ult.load:												
112.3	0.3940	0.3581	1.60E-02	6.73E-02	1.23E-05	4.61E-05	0.0	0.2	0.2	0.96	0.86	0.82
1/2 tubes + 1/3 tube susceptible:												
37.4	0.3940	0.3581	1.60E-02	6.73E-02	1.23E-05	4.61E-05	0.0	0.1	0.1	0.99	0.95	0.94
For C-Scan Having 100% Mechanical Properties:												
Entire truss area:												
224.6	0.5072	0.4758	3.42E-02	1.58E-01	4.89E-06	2.25E-05	0.0	0.2	0.2	0.97	0.86	0.83
1/2 tubes w/ ult.load:												
112.3	0.5072	0.4758	3.42E-02	1.58E-01	4.89E-06	2.25E-05	0.0	0.1	0.1	0.98	0.93	0.91
1/2 tubes + 1/3 tube susceptible:												
37.4	0.5072	0.4758	3.42E-02	1.58E-01	4.89E-06	2.25E-05	0.0	0.0	0.0	0.99	0.98	0.97

Table 5-2. Failure Frequency for Phase II Space Station Truss Tubes

Meteoroid density (g/cc)	0.5		
Debris density (g/cc)	2.8		
Ave. meteoroid velocity (km/s)	20		
Ave. debris velocity (km/s)	9.3		
Strut Diameter (in)	2.1	(cm)	5.334
Tube Thickness (in)	0.066	(mm)	1.6764
Longeron/Batten Length (m)	5	SA (m^2)	0.838
Diagonal Length (m)	7	SA (m^2)	0.184
Number Bays	93		
Number Longerons & Battens	744	SA (m^2)	623.4
Number Diagonals	465	SA (m^2)	85.7
Truss area (m^2)	709.0		
Earth's radius (km)	6378.145		
Station orbital altitude (km)	500		
Earth defocusing factor	0.968596		
Earth shielding factor	0.668024		
Station Lifetime (yrs)	30		
Critical Damage Area (in^2)	5.4		
Critical Damage Diameter (mm)	66.6		

Truss Area (m^2)	Met. Particle Diameter (cm)	Debris Particle Diameter (cm)	Particle Mass Met. (g)	Particle Mass Debris (g)	Particle Flux (incl. SF,DF) Met. (#/m^2-yr)	Particle Flux (incl. SF,DF) Debris	Number Impacts of given Diameter and greater Met. (#/30yr life)	Number Impacts Deb.	Number Impacts Total	Probability of No Impact Met.	Probability of No Impact Deb.	Probability of No Impact Total
For C-Scan Having 0% Mechanical Properties:												
Entire truss area:												
709.0	0.2545	0.2313	4.32E-03	1.81E-02	6.10E-05	1.39E-04	1.3	3.0	4.2	0.27	0.05	0.01
1/2 tubes w/ ult.load:												
354.5	0.2545	0.2313	4.32E-03	1.81E-02	6.10E-05	1.39E-04	0.6	1.5	2.1	0.52	0.23	0.12
1/2 tubes + 1/3 tube susceptible:												
118.2	0.2545	0.2313	4.32E-03	1.81E-02	6.10E-05	1.39E-04	0.2	0.5	0.7	0.81	0.61	0.49
For C-Scan Having 50% Bending Rigidity and Mechanical Properties:												
Entire truss area:												
709.0	0.3940	0.3581	1.60E-02	6.73E-02	1.23E-05	4.61E-05	0.3	1.0	1.2	0.77	0.37	0.29
1/2 tubes w/ ult.load:												
354.5	0.3940	0.3581	1.60E-02	6.73E-02	1.23E-05	4.61E-05	0.1	0.5	0.6	0.88	0.61	0.54
1/2 tubes + 1/3 tube susceptible:												
118.2	0.3940	0.3581	1.60E-02	6.73E-02	1.23E-05	4.61E-05	0.0	0.2	0.2	0.96	0.85	0.81
For C-Scan Having 100% Mechanical Properties:												
Entire truss area:												
709.0	0.5072	0.4758	3.42E-02	1.58E-01	4.89E-06	2.25E-05	0.1	0.5	0.6	0.90	0.62	0.56
1/2 tubes w/ ult.load:												
354.5	0.5072	0.4758	3.42E-02	1.58E-01	4.89E-06	2.25E-05	0.1	0.2	0.3	0.95	0.79	0.75
1/2 tubes + 1/3 tube susceptible:												
118.2	0.5072	0.4758	3.42E-02	1.58E-01	4.89E-06	2.25E-05	0.0	0.1	0.1	0.98	0.92	0.91

Table 5-3. Exposure of 2 mil Aluminum Coating Compensated for Peeling

Coating Properties:				
Type	Al 2024-T3			
Thickness (in)	0.002	0.00508 (cm)		
Density (g/cc)	2.712			
Brinell Hardness	145			
Space Station Properties:			Meteoroid Flux Parameters:	
Operational Lifetime (yr)	30		Earth's radius (km)	6378.145
			Station orbital alt. (km)	500
Truss Properties:			Earth defocusing factor	0.968596
Tube thickness (in)	0.066	1.6764 (mm)	Earth shielding factor	0.688024
Tube O.D. (in)	2.1	5.334 (cm)		
Surface Area of 5m Long Struts (m^2)		0.84		
Surface Area of 7m Long Struts (m^2)		1.17		
Hole Diameter to Fail 5m Tube (cm)		2.6		
Atomic Oxygen Properties:				
Fluence on ram-facing surfaces (atoms/cm^2-yr)		1.091E+21		
G/E Reactivity Rate (cm^3/atom)		2.600E-24		
Recession Rate (cm/yr)		2.836E-03	0.001116 (in/yr)	
(for uncoated ram-facing surfaces)				
Percent of Unprotected Tube Thickness Erroded During Lifetime			50.8%	
		Meteoroid	Debris	
Particle Density (g/cc)		0.5	2.8	
Particle Velocity (km/s)		20	9.3	
Particle Critical Diameter (cm)		0.0049	0.0036	
above which crater depth exceeds coating thickness (from Cour-Palais, Ref.24, p.265)				
Particle Mass (g)		3.05E-08	6.60E-08	
Particle Energy (J)		0.006	0.003	
Particle Flux (#/m^2-yr)		19.3	5.14	
with critical diameter and greater that will perforate coating.				
Total Perforation Flux (#/m^2-yr)		24.47		
Lifetime Coating Perforations on 5m Strut		615		
Lifetime Coating Perforations on 7m Strut		861		
Lifetime Perforation Density (#/cm^2)		0.073		
Max. Size Particle On 5m Strut In Lifetime:				
Particle Mass (g)		2.13E-05	2.15E-05	
Particle Diameter (cm)		0.0433	0.0245	
Average Particle Dia (cm)		0.024	0.014	
Average Dia. G/E Exposed (cm)		0.096	0.059	
(assume hemispherical crater and no surface delamination)				
Exposed G/E area on 5m struts (cm^2/yr)		0.076	0.012	
Critical Area (cm^2)		5.40		
per 5m truss tube that must be exposed to atomic oxygen before failure possible				
Total Exposed area on 5m struts (cm^2/yr)		0.088		
Number of years before critical graphite/epoxy area is uncovered on 5m struts		62		

6.0 Conclusions

From Section 3:

1. The number of impacts from the combined meteoroids and debris flux on the space station truss tubes is summarized below:

	Truss Area (m^2)	Combined Number of Impacts on Truss Struts Per Year From Particles With Given Diameter (mm) And Greater: 0.01	0.1	0.5	1.0	2.0
Phase I	225	75,900	1,068	6.8	0.68	0.078
Phase II	710	239,400	3,369	21.4	2.14	0.247

2. Every year, meteoroids and debris will create ~25/m^2 perforations in a 2 mil thick aluminum (alloy 2024-T3) used for protecting the graphite-epoxy tube from atomic oxygen erosion. The number of perforations can be substantially decreased by thicker coatings or by using a harder aluminum. Increasing the aluminum coating thickness from 2 mils to 6 mils will decrease perforations by a factor of 8, but will add weight. A hard Al 2024-T3 coating reduces complete penetration by a factor of 2 over a soft Al 1100-0 coating, without an increase in weight.

3. Structural compressive tests of selected 6" tube specimens were successful in determining the tubes' elastic modulus in compression and axial rigidity (EA). The derived modulus compared favorably with a modulus determined from ultrasonic testing and a vendor supplied modulus.

4. Holes less than 0.5" in diameter could not be detected by changes in EA or elastic modulus in compression.

5. The Phase I Space Station truss tubes will be impacted by approximately 5 meteoroid and debris particles over a 30 year lifetime with a diameter equal to or greater than the size of the projectile used most often in the impact testing, a 1.6 mm aluminum sphere. The largest particle used in the study (4.4 mm nylon slug) did not break a tube specimen having a [10,30,10] layup, 34M psi modulus fibers, 0.07" tube wall thickness. There is only a 1 in 5 chance that a particle of this size or greater will impact the Phase I station tubes in 30 years.

From Section 4:

1. From impact experiments, it was determined that fiber modulus influenced the magnitude of hypervelocity impact damage to a greater extent than the ply orientation of the graphite-epoxy layup. Low modulus (34M psi) fiber tubes and flat plates exhibited peeling of the surface plies near the impact point. High modulus (75M psi) did not peel. Larger holes (in both walls of tube specimens) were created in the high modulus targets compared to similar impacts into low modulus targets. Low and high modulus targets experience generally the same area of internal delaminations and damage around the impact point (and the far wall of a tube across from the impact point) revealed by ultrasonic C-scans of the composite. Differences in ply orientation made no notable difference in the overall area of the impact induced holes, craters, and C-scan damage.

2. The following equation relating projectile energy and the equivalent circular hole diameter for combined first and second walls was developed for tubes with low modulus fibers (34M psi) and 0.07" thick walls. For projectile energy, E (J), less than 155J or for a combined-wall hole diameter, D_{hb} (mm), less than 4.8 mm:

$$D_{hb} = 1.14\ E^{0.33} - 1.29$$

And for E greater than 155J, or D_{hb} greater than 4.8 mm:

$$D_{hb} = 4.54\ E^{0.33} - 19.5$$

The transition at E=155J to a steeper slope curve results from the greater damage to the second wall of the tube due to expansion of projectile and target debris behind the first wall. The above equations were found to adequately fit low modulus tube data regardless of ply orientation. Thicker tube data (0.11" and 0.14") generally matched the above equations for E < 155 J, but data was unavailable to determine the transition point to a steeper sloped curve. A similar equation was developed for tubes with high modulus fibers (75M psi) and 0.07" thick walls. For projectile energy less than 158J, or combined-hole diameter less than 7.7 mm:

$D_{hb} = 1.424\ E^{0.33} + 0.034$

And for E greater than 158J, or D_{hb} greater than 7.7 mm:

$D_{hb} = 6.281\ E^{0.33} - 26.22$

3. For all high and low modulus tubes, a correlation was developed that relates the diameter of the ultrasonic C-scan region for both walls, D_{cb} (mm), with projectile energy, E (J), projectile diameter, d (mm), and tube wall thickness, t (mm):

   For $(E * t/d) < 230J$, or $D_{cb} < 30$ mm:

   $D_{cb} = 6.31\ (E * t/d)^{0.33} - 5.72$

   For $(E * t/d) > 230J$, or $D_{cb} > 30$ mm:

   $D_{cb} = 15.50\ (E * t/d)^{0.33} - 61.8$

   Projectile energy can be substituted with parameters such as velocity, V (km/sec), density, p (g/cc), and diameter, d (mm). Thus, the previous equation would become:

   $d = [(D_{cb} + 61.8)/15.5]^{1.5} * (12/\pi)^{0.5} * p^{-0.5} * V^{-1} * t^{-0.5}$

4. The above correlations are valid for projectile impact obliquity angles up to 45° from the target surface normal. Greater obliquity angles were not tested. Damage to the second wall of the tube did not vary significantly with changes in radial obliquity impacts. Impacts at a 45° angle to the longitudinal axis of the tube also resulted in similar damage areas on the first wall as with normal impacts. However, less damage to the second wall of the tube resulted for high longitudinal obliquity shots (at 45° and greater) due to the greater distance between first and second wall at this angle. More data would be needed to quantify the effect of longitudinal obliquity impacts, but all are expected to result in less damage to the second wall than a normal angle impact.

5. Data for flat plates corresponded well with the correlations developed for the first wall hole of the tubes. For tubes and plates with low modulus (34M psi) fibers, projectile energy, E (J), and hole diameter, D_{h1} (mm), were related by:

$$D_{h1} = 0.927 * (E)^{0.33} - 0.536$$

A similar relationship was developed for high modulus tubes and plates:

$$D_{h1} = 1.202 * (E)^{0.33} + 0.612$$

The low modulus tube targets prone to surface ply peeling around the impact point were also susceptible to peeling as flat plates. C-scan data between tubes and flat plates showed similar trends with projectile energy, however, the flat plate C-scan data was substantially more variable (see Section 4). Thus, impact testing of flat plates could probably be substituted for tubes as long as only the effects on first wall damage was required. The flat plate C-scan data should only be used in comparison with other flat plate data. Because the flat plate C-scan data in this study were so variable, extrapolation to tube first wall C-scan size should be confirmed with actual testing of representative tube targets.

6. Peeling of a 2 mil Al 1145-H19 layer bonded to a low modulus tube occured in the direction of the underlying surface ply orientation. An equation was developed that related the equivalent circular diameter of the underlying exposed graphite-epoxy region of the 2 mil aluminum coated tubes, P (mm) which does not including the perforated/crater area, to the projectile diameter, d (mm), and energy normal to the surface, E_n (J).

$$P/d = 1.827 (E_n)^{0.33} - 0.0989$$

The 6 mil aluminum coating did not peel at the largest projectile tested (1.6 mm aluminum sphere), but is expected to for larger projectiles. The hole size in the first wall of coated tubes was essentially equivalent to the hole size in uncoated tubes for the same impact conditions. C-scan diameter was less for the coated tubes in comparison to uncoated tubes at lower projectile energies ($E*t/d < 250J$), but approached more closely uncoated tube results as projectile energy increased.

7. Tubes containing high modulus fibers (75M psi) manufactured by Morton Thiokol performed similarly to the high modulus tubes used in most of the testing (made by Amoco). Front wall damage to filament wound tubes made by McDonnell Douglas (with 34M psi fibers) closely matched results from tests on low modulus Amoco tubes. However, the filament wound tubes were less likely to sustain perforation of the second wall. More filament wound tubes and data would be needed to exactly quantify the advantage.

8. Regardless of ply layup or fiber modulus, the truss tubes appear to be resilient to complete failure from hypervelocity impact. The largest particles used in the study (a 3.2 mm aluminum sphere and a 4.4 mm nylon slug) did not break a low modulus tube. The probability of impact from 3.2 mm and 4.4 mm particles and greater on the Phase I truss tubes over 30 years is only 0.45 and 0.21, respectively. The impact probability for the Phase II truss tubes over 30 years from 3.2 mm particles and greater is 0.85, and 0.53 from 4.4 mm particles and greater.

9. Additional derived correlations are given in Section 4.9.

From Section 5:

1. A finite element model study concluded that a 5.4 in^2 hole/delamination area was required (2.6" diameter) to cause failure of a 5 m space station tube under the ultimate compressive load expected on-orbit. Important groundrules for the study were that the struts would be exposed to primarily axial loads, that the tubes would fail by buckling in compression prior to a tensile failure, and that 2,100 lb_f is the maximum compressive load experienced by a 5 m tube (and 1,200 lb_f for a 7 m diagonal strut) on-orbit for a one-strut out condition. Tube properties were baselined for a [10,30,10] layup, 34M psi modulus fibers, and 0.066" thick tube walls. The residual mechanical properties of the delamination zone were conservatively set to zero for the study. This approach was taken since the effect of the delamination zone on tube flexural rigidity (EI) was not known. The critical buckling load of the tube is related to EI. It was suggested that bending tests of the impacted tests elements would be useful in determining the effect of the delamination area on EI. Unfortunately, the 6" test specimens were too short to conduct this structural test.

2. The study assumed that the damage occured at the midpoint of a loaded strut. The most damage-sensitive portions of a fixed end tube in compression are in the middle and at either end. A quarter of the tube's length from either end are low stress points in buckling and could sustain more damage without failure. Not all of the tubes of the Space Station will be subjected to the maximum loads. Charts of the loads in the truss elements for a number of cases would be needed to determine the number of tubes subjected to loads at or near the maximums used in the finite element study. Thus, the critical damage size that would result in truss tube failure varies with damage location along the tube and location of the tube in the truss structure.

3. Assuming worst case conditions-that all truss tubes and all locations along the tubes are equally susceptible to failure from damage, that failure requires a 5.4 in^2 hole/-delamination damage area, and that the entire delamination area represents zero compressive strength or stiffness-the combined number of meteoroid and debris impacts that would result in strut failure over a 30 year lifetime was calculated as:

Truss	Strut Area (m^2)	Critical Diameter (mm) Resulting in Failure Meteoroids	Debris	Total Number of Impacts from Particles With Critical Diameter & >
Phase I	225	2.5	2.3	2
Phase II	710	2.5	2.3	5

Thus, a worst case estimate of the number of tube failures is 5 for the Phase II station truss (approximately 1,200 struts) over the 30 year station lifetime. Note that this calculation does not involve any probabilities, there is an essentially 100 percent probability that impacts on truss tubes from the given particle sizes will happen. Fortunately, the failure number is not expected to be large. However, means and procedures must be developed to find and identify tubes with the critical damage (many others will have lesser damage), and to develop repair or replacement procedures.

4. It was calculated to take several times the 30 year station lifetime for the combined flux of small meteoroid and debris particles to expose an area equal to the critical damage size (5.4 in^2) from all the truss tubes, given protection from a 2 mil hard

aluminum coating. If it is assumed that atomic oxygen only attacks exposed graphite-epoxy surfaces (and does not create cavities beneath the coating), a 2 mil thick hard aluminum coating should provide sufficient protection against both atomic oxygen attack and small meteoriod/debris erosion.

7.0 Recommendations

1. Additional finite element modelling is needed to confirm the predicted critical damage size resulting in strut failure. Either scaled or full-scale (5m-7m long) buckling tests of damaged graphite/epoxy tubes are recommended to confirm the modelling results.

2. Appropriate structural tests of impacted test specimens are needed to develop an understanding of the effect of delamination zone on tube mechanical properties. Four 6" tube specimens (6-T-1, 6s-T-1, 9-T-1, and 10-T-1) with a single hypervelocity impact can be made available for compression tests. Section 3.5.3 describes how the results could be used to determine the effect of delamination on the axial rigidity (EA) within the damage zone.

3. If a bonded aluminum foil is selected for atomic oxygen protection, a hard aluminum alloy is recommended to reduce the number of perforations by small meteoroid and debris particles.

4. Low-modulus filament wound tubes looked promising in suppressing perforation of the second wall. Therefore, use of filament wound tubes for Space Station should be further explored. However, the delamination region for damaged filament wound tubes was slightly greater than the roll-wrap baseline. Thus, an unqualified recommendation for filament wound tubes can not be made until a comparison test of the mechanical properties of the damaged tubes is complete.

5. The hypervelocity impact characteristics of the final selected graphite-epoxy tube/atomic oxygen coating combination should be ascertained in a short impact test program. In particular, the impact induced delamination properties of the coating should be studied.

6. Impacted tubes should be thermally and mechanically cycled to determine if the delamination zone grows under cyclical loadings.

7. The predicted number of tube replacements should be recalculated with any future

changes in the orbital debris environment model. Updates are also needed with new information on critical damage size.

8. Procedures for on-orbit truss inspection and identification of critically damaged tubes should be developed. Development of portable hand-held non-destructive testing equipment and tools (ultrasonic C-scanners, etc.) may be required. A visually obvious clue (such as obvious damage to both sides of a tube) may simplify the task of indentifing those tubes damaged enough to require replacement, but the implications on the predicted number of tube replacements should be assessed.

8.0 References

1. Christiansen, E.L., and Stump, W.R.: "Composite Truss Test Preparation Notebook," Eagle Engineering, July 3, 1986.

2. Baker, J., Personal Communication, Amoco Danbury Connecticut Office, (203)794-3718, May, 1986.

3. Santos-Mason, B., Personal Communication, JSC Structures, December, 1986.

4. Hercules Incorporated: "Hercules Composite Structures," 1981.

5. Space Station Control Board Directive, No. BB000311, "Initialization/Integration Revision of JSC 30000, Section 2, Part 6, Rev. B, Space Station Program Schedules," November 16, 1987.

6. Space Station Control Board Directive, No. BB000293, "Initialization/Integration Revision of JSC 30255, Baseline Configuration Document (BCD)," November 16, 1987.

7. "Space Station Work Package 2 Design, Development, Test, and Evaluation Request For Proposal," Solicitation No. 9-BF2-51-7-1P, NASA Johnson Space Center, April 1987.

8. "Space Station Definition and Preliminary Design, Work Package No. 2, Preliminary Analysis and Design Document (DR-02), Book 4, Structural, Mechanical and Fluid Systems," McDonnell Douglas Astronautics Company, December 1986.

9. "Space Station Definition and Preliminary Design, Work Package No. 2, Preliminary Analysis and Design Document (DR-02), Book 4, Assembly Trusses and Structure," McDonnell Douglas Astronautics Company, June 1986.

10. "Space Station Definition and Preliminary Design, Work Package No. 2, Preliminary Analysis and Design Document (DR-02), Book 4, Assembly Truss and Structure," McDonnell Douglas Astronautics Company, December 1985.

11. Space Station Projects Office: "Space Station Projects Requirements Document," JSC 31000, Rev. C, March 6, 1987.

12. Space Station Control Board Directive, No. BB000291, "Initialization/Integration Revision of JSC 30000, Section 3, Rev. D, Space Station Systems Requirements," November 16, 1987.

13. Leger, L. J.: "Oxygen Atom Reaction with Shuttle Materials at Orbital Altitudes," NASA TM-58246, May 1982.

14. Leger, L. J.: "Oxygen Atom Reaction with Shuttle Materials at Orbital Altitudes," AIAA-83-0073, AIAA 21st Aerospace Sciences Meeting, January 1983.

15. Visentine, J.T., Leger, L.J., Schomburg, C., and Jones, W.B.: "Atomic Oxygen Effects on Surfaces in Low Earth Orbit," Second Solar Dynamic Power Systems Workshop, JSC, August 1984.

16. Leger, L.J., Visentine, J.T., and Schliesing, J.A.: "A Consideration of Atomic Oxygen Interactions with Space Station," AIAA-85-0476, AIAA 23rd Aerospace Sciences Meeting, January 1985.

17. Whitaker, A.F., Burka, J.A., Coston, J.E., Dalins, I., Little, S.A., and DeHaye, R.F.: "Protective Coatings for Atomic Oxygen Susceptible Spacecraft Materials - STS 41G Results," AIAA Shuttle Environment and Operations II Conference, November 1985.

18. Kessler, D.J.: "Orbital Debris Environment for Space Station," JSC-20001, 1984.

19. Vaughan, W.W. and Green, C.E.: "Natural Environment Design Criteria Guidelines for the Space Station Definition and Preliminary Design (Second Revision)," NASA TM-86498, 1985.

20. Yew, C.H. and Wang, C.Y. (University of Texas), and Crews, J.L. (NASA JSC): "A Phenomenological Study of the Effect of Hypervelocity Impacts on Graphite-Epoxy Plates," NASA Johnson Space Center, 1987.

21. Parker, V.C. (Cordin Co.) and Crews, J.L. (NASA JSC): "Hypervelocity Impact Studies Using a Rotating Mirror Framing Laser Shadowgraph Camera," Paper 832-13, presented at the Optical and Optoelectronic Applied Science and Engineering Technical Symposium, San Diego, California, August 16-21, 1987.

22. Stump, W.R. and Christiansen, E.L.: "Secondary Impact Hazard Assessment," Eagle Engineering Report No. 86-128, June 1986.

23. Christiansen, E.L.: "Evaluation of Space Station Meteoroid/Debris Shielding Materials," Eagle Engineering Report No. 87-163, September 30, 1987.

24. Cour-Palais, B.G.: "Hypervelocity Impact Investigations and Meteoroid Shielding Experience Related to Apollo and Skylab," NASA CP-2360, July 1982.

25. Space Station Program Office: "Space Station Program Natural Environment Definition for Design," JSC-30425, January 15, 1987.

26. Zook, H. and Kessler, D.J.: "Meteoroid Velocity Distribution on a 500 km high Earth Orbiting Spacecraft," NASA JSC Memo SN3-86-82, March 1986.

27. Gere, J.M. and Timoshenko, S.P.: Mechanics of Materials, 2nd ed., PWS Publishers, Boston Massachusetts, 1984.

28. Tenney, D.R. (NASA LaRC): "Materials and Structures for Space Applications," AIAA Invited Lecture Series, Houston Texas, April 8, 1986.

29. Wolff, E.G.: "Microcracking in Graphite-Epoxy Composites," The Aerospace Corp., Report SD-TR-80-65, September 1980.

30. Wolff, E.G.: "Dimensional Stability of Carbon Fiber Reinforced Plastic Tubes," SAMPE Quarterly, pp.26-33, October 1984.

31. "Space Station Work Package 2, Definition and Preliminary Design Phase, Time-

Phased SE&I Study Products, Data Package 2.2," Rockwell International Corporation, NAS9-17365, August 16, 1985.

Appendix A - Shot Data

Shot Conditions

Shot	Date	Target S/N	Type	Layup	Nominal Thickness (in)	Fiber Modulus (Mpsi)	Proj. Mat'l	Proj. Dia. (mm)	Proj. Mass (mg)	Proj. Vel. (km/s)	Proj. Dens. (g/cc)	Dist. From C/L hole to C/L tube (mm)	Proj. Obliquity Angle Radially (on curve) (deg) 0=normal	Obliquity to Longitud. Axis (deg) 0=normal	Comments on Hi-speed Film &/or Shot (clean impact unless stated)
JSC Shots:															
JSC-A181	10-Apr-87	9s-F-3	Plate	80,30,10	0.0604	34	Glass	0.55	0.21	7.23	2.45	NA	0	0	No picture of impact. Sabot quarter hit plate (nylon, ~12mg, 3.75mm long x 2mm dia.) creating 7mm dia. hole.
JSC-A196	11-May-87	11-T-2	Tube	10,30,10	0.0885	75	Glass	0.55	0.21	7.60	2.45	3.3	7	0	Small secondary impact (0.3mm hole).
JSC-A201	14-May-87	11-T-4	Tube	10,30,10	0.0765	75	Glass	0.55	0.21	7.07	2.45	2.3	5	0	
JSC-A204	19-May-87	6-T-1	Tube	10,30,10	0.0714	34	Glass	0.89	0.89	7.05	2.45	3.0	7	0	
JSC-A206	20-May-87	6-T-4	Tube w/2 mil Al coating	10,30,10	0.082	34	Glass	0.93	1.02	6.45	2.45	4.6	10	0	Hi-speed film showed 2 additional particles following ball (2&3 micro sec). Suspect styrofoam from sabot/ barrel backing since no apparent damage to tube front or back walls resulted.
JSC-A208	22-May-87	9s-T-1	Tube	80,30,10	0.0694	34	Glass	0.94	1.06	6.67	2.45	2.4	5	0	
JSC-A209	26-May-87	10-T-1	Tube	45,10,45	0.072	34	Glass	0.94	1.07	7.16	2.45	1.8	4	0	Hi-speed film showed an additional secondary impact from particle app. same size as projectile, 4 microsec behind proj. Suspect piece of styro foam since no apparent damage to backwall or additional frontwall damage.
JSC-A211	28-May-87	7-T-3	Tube	10,30,10	0.105	34	Glass	0.95	1.11	7.32	2.45	0.0	0	0	Clean impact by hi-speed film.
JSC-A212	29-May-87	11s-T-1	Tube	10,30,10	0.060	75	Glass	0.94	1.06	6.68	2.45	3.9	9	0	Small secondary 1 microsec behind

Target Front Side Conditions: (outside of tube's 1st wall)

Shot JSC Shots:	Date	Target S/N	Target Mass Before (g)	Target Mass After (g)	1st wall Hole Shape	Hole Dimensions Length (mm)	Hole Dimensions Width (mm)	Equiv. Circular Diameter (mm)	Crater (if evident) Dia. (mm)	Surface Peeling Number	Surface Peeling Length (mm)	Surface Peeling Width (mm)	Total Area (mm^2)	C-Scan Dimensions Area (mm^2)	C-Scan Dimensions Equiv. Circular Diameter (mm)	C-Scan Dimensions Actual Shape: Approx. Axial Length (mm)	C-Scan Dimensions Actual Shape: Overall (Circumf) width (mm)	Comments on Target Condition (1st wall condition)
JSC-A181	10-Apr-87	9s-F-3	55.42	55.23	Circ.	1.93		1.93	2.48	2	14 12	0.5 0.5	13					C-scans overlapped due to sec. impact from sabot quarter.
JSC-A196	11-May-87	11-T-2	89.29	89.16	Rect.	2.1	1.7	2.1	3.0	0								C-scans overlapped due to sec. impact.
JSC-A201	14-May-87	11-T-4	86.91	86.85	Rect.	2.2	1.7	2.2	3.6	0				67.9	9.3	7	10	
JSC-A204	19-May-87	6-T-1	69.98	69.95	Rect.	2.1	1.5	2.0	3.3	4	30 33 6 27	1 0.75 0.75 0.75	80	278.4	18.8	28	10	Surface plys peeled on interior also.
JSC-A206	20-May-87	6-T-4	80.48	80.43	Rect.	2.3	1.7	2.2	3.7	2	3 4.5	5 5	38	118.3	12.3	12	10	Surface plys peeled on interior 2-3 times as far as outside surface.
JSC-A208	22-May-87	9s-T-1	69.05	68.99	Circ.	2.1		2.1	3.7	2	13 20	1.5 1.25	44	220.3	16.7	7	30	Interior surface peeling also.
JSC-A209	26-May-87	10-T-1	71.20	71.12	Circ.	2.2		2.2	3.6	4	8 15 23 10	2 0.75 1.5 1	71	189.8	15.5	13	14	Surface plys peeled on 45 deg angle and C-scan shape similar to surface damage. Interior peeling stopped on one side of hole at interface where plys initially were laid on mandril. This indicates peeling not due to shock wave/rarefaction wave, but initiated at perforation and peels back from initial impulse.
JSC-A211	28-May-87	7-T-3	100.21	100.14	Rect.	2.3	1.8	2.3	3.1	4	29 29 27 16	1 1 1.25 0.5	99	325.9	20.4	9	36	Surface plys peeled in direction of outer layup (+10 deg.). Surface plys peeled on interior of first wall " same length as on outside.
JSC-A212	29-May-87	11s-T-1	68.44	68.34	Rect.	3.9	3.2	4.0	6.4	0				138.1	13.3	14	10	Hole longer in circumferential

Target Second Side Conditions: (outside of tube's 2nd wall, or back side of plate)

Shot	Date	Target S/N	Hole Dimensions: 2nd wall Hole Shape	Hole Dimensions: Length (mm)	Hole Dimensions: Width (mm)	Hole Dimensions: Equiv. Circular Diameter (mm)	Surface Peelings: Number	Surface Peelings: Length (mm)	Surface Peelings: Width (mm)	Surface Peelings: Total Area (mm^2)	Surface Peelings: Equiv. Circular Diameter (mm)	C-Scan Dimensions: Area (mm^2)	C-Scan Dimensions: Equiv. Circular Diameter (mm)	C-Scan Dimensions: Actual Shape: Approx. Length (mm)	C-Scan Dimensions: Actual Shape: Overall Width (mm)	Comments on Tubes 2nd Wall
JSC Shots:																
JSC-A181	10-Apr-87	9s-F-3					2	22.5	0.75	18.1	4.8					
								5	0.25							
JSC-A196	11-May-87	11-T-2														No peeling of tube interior surfaces.
JSC-A201	14-May-87	11-T-4														
JSC-A204	19-May-87	6-T-1														Large circular plume of fine graphite particles impacted second wall interior (with 1.38" cord) but did not penetrate or leave craters.
JSC-A206	20-May-87	6-T-4														Large circular plume of fine graphite particles impacted second wall interior (with 1.38" cord) but did not penetrate or leave craters.
JSC-A208	22-May-87	9s-T-1														Diffuse circular splash of fine S/E particles on second wall with no real damage.
JSC-A209	26-May-87	10-T-1														Diffuse circular plume of fine graphite/epoxy particles impacted second wall with no real damage (no craters, delaminations, or perforations).
JSC-A211	28-May-87	7-T-3														Diffuse, circular plume of particles struck second wall with no apparent damage.
JSC-A212	29-May-87	11s-T-1														Circular plume impacted second wall

Witness Plate Conditions

Shot	Date	Target S/N	Material	Thickness (in)	Dist. from Target (in)	Comments about witness plate	Number of Impact Perfor-ations	Maximum Hole Dia. (mm)	Dia. of Area of Conc. hits/perf (in)	Dispersion half-angle of Conc. Hits (deg)	Dia. of all impacts (in)	Max. Disp. half-angle of any impact (deg)
JSC Shots:												
JSC-A181	10-Apr-87	9s-F-3	Al6061-T6	0.032	2	No perforations, mostly shows sabot impact.	0					
JSC-A196	11-May-87	11-T-2										
JSC-A201	14-May-87	11-T-4										
JSC-A204	19-May-87	6-T-1										
JSC-A206	20-May-87	6-T-4										
JSC-A208	22-May-87	9s-T-1										
JSC-A209	26-May-87	10-T-1										
JSC-A211	28-May-87	7-T-3										
JSC-A212	29-May-87	11s-T-1										

Shot Conditions

Shot	Date	Target S/N	Type	Layup	Nominal Thickness (in)	Fiber Modulus (Mpsi)	Proj. Mat'l	Proj. Dia. (mm)	Proj. Mass (mg)	Proj. Vel. (km/s)	Proj. Dens. (g/cc)	Dist. From C/L hole to C/L tube (mm)	Proj. Obliquity Angle Radially (on curve) (deg) 0=normal	Proj. Obliquity to Longitud. Axis (deg) 0=normal	Comments on Hi-speed Film &/or Shot (clean impact unless stated)
JSC-A242	22-Jun-87	MD-02	Tube	10,30,10	0.066	34	Glass	2.09	11.72		2.45	0.0	0	0	Projectile broke in two. Only one half impacted target.
JSC-A245	30-Jun-87	MT-2	Tube	45,0,0	0.063	75	Al2024-T4	2.37	19.60	7.08	2.796	5.5	13	0	Good film, no secondary impacts.
JSC-A246	01-Jul-87	11-T-2	Tube	10,30,10	0.089	75	Al2024-T4	2.38	19.66	7.38	2.796	5.2	12	0	Good film, no secondary impacts.
JSC-A249	02-Jul-87	6s-T-1	Tube	10,30,10	0.066	34	Al2024-T4	2.38	19.70	7.48	2.796	2.0	5	0	"Cloud" of debris, 1-3 microsec behind projectile, impacting below and to left of projectile, causing craters (w/ interior spall) but no perforations.
JSC-A250	06-Jul-87	6-T-4	Tube w/2 mil Al coating	10,30,10	0.078	34	Al2024-T4	2.37	19.60	7.15	2.796	2.0	5	0	Good film, secondary piece 2 microsec behind projectile, smaller than projectile, impact slightly above projectile. Projectile made a ~7 mm diameter hole while secondary made a ~6 mm diameter hole that overlapped with first hole.

Target Front Side Conditions: (outside of tube's 1st wall)

Shot	Date	Target S/N	Target Mass Before (g)	Target Mass After (g)	1st wall Hole Shape	Hole Dimensions Length (mm)	Hole Dimensions Width (mm)	Equiv. Circular Diameter (mm)	Crater (if evident) Dia. (mm)	Surface Peeling Number	Surface Peeling Length (mm)	Surface Peeling Width (mm)	Total Area (mm^2)	C-Scan Dimensions Area (mm^2)	C-Scan Dimensions Equiv. Circular Diameter (mm)	Actual Shape: Approx. Axial Length (mm)	Actual Shape: Overall (Circumf) Width (mm)	Comments on Target Condition (1st wall condition)
																		direction, C-scan longer in axial direction (along layup direction).
JSC-A242	22-Jun-87	MD-02		72.47	Circ.	4.3		4.3	5.6	3	15 10 3	4 6 2	136					Surface peelings in both +10 and -10 deg. directions on either side of hole due to filament winding.
JSC-A245	30-Jun-87	MT-2	68.15	65.97	Rect.	9.5	8.25	8.9	11.7	0				251.1	17.9	15	16	Hole longer in circumferential direction, same with C-scan.
JSC-A246	01-Jul-87	11-T-2	99.47	86.80	Oval	9.1	10.3	9.7	14.7	0				298.3	19.5	15	20	Hole longer in circumferential direction. C-scan same way.
JSC-A249	02-Jul-87	6s-T-1	66.72	66.27	Rect.	7.1	5.3	6.9	11.3	3	45 45 15	2.5 2.5 6	315	546.9	26.4	25	22	Peeling much shorter on side secondary particles hit, apparently debris "cloud" kept surface plys from peeling back from hole.
JSC-A250	06-Jul-87	6-T-4	80.56	79.73	Circ.	6.9		6.9	9.7	Exposed Area (no aluminum):				641.1	28.6	33	19	Aluminum peeled back along surface ply direction (10 deg. to longitudinal axis). C-scan preferential growth in longitudinal direction. Interior of first wall peeled slightly less than exterior. No perforation of second wall, concentrated impacts on second wall in 1" diameter area, caused peeling of 2nd wall exterior aluminum coat.
									(ring around hole)	4	11 13 13 40	4 5 4 2	248					
										Additional peeled area (Al attached at one end):								
										2	11 13	3 6	111					

Target Second Side Conditions: outside of tube s 2nd wall, or back side of plate)

Shot	Date	Target S/N	Hole Dimensions: 2nd wall Hole Shape	Length (mm)	Width (mm)	Equiv. Circular Diameter (mm)	Surface Peelings: Number	Length (mm)	Width (mm)	Total Area (mm^2)	Equiv. Circular Diameter (mm)	C-Scan Dimensions: Area (mm^2)	Equiv. Circular Diameter (mm)	Actual Shape: Approx. Length (mm)	Overall Width (mm)	Comments on Tubes 2nd Wall
																with no apparent damage (1.75" cord).
JSC-A242	22-Jun-87	MD-02														Craters in second wall, no holes.
JSC-A245	30-Jun-87	MT-2	Rect.	25.5	23	24.2						2085	51.5	47	44	Inside of tube coated with black powder completely around circumference and nearly entire length. No surface peeling on either side of interior surfaces. Only narrow annular ring of "peeling" around hole in backwall (3-5 mm wide). Hole in backwall nearly square, oriented at 45 deg. angle.
JSC-A246	01-Jul-87	11-T-2	Rect.	21.4	19.1	22.8						1889	49.0	48	39	Inside of tube coated with black powder completely around circumference and nearly entire length. No surface peeling on either side of interior surfaces. Peeling in annular ring around hole in 2nd wall, 4-10 mm wide, makes approximately square area 35 mm on side with hole &/or peeling.
JSC-A249	02-Jul-87	6s-T-1	Rect.	16.0	11.0	15.0	4	16	25	1015	35.9	1706	47	60	28	Hole in second wall had 15mmlong x 7mm wide piece of S/E in middle of hole connected by only one end (& thus contributing no mechanical strength). Surface peeling to 2nd wall broken off by holder/mount (peelings would have extended much further).
								16	6							
								16	8							
								17	23							
JSC-A250	06-Jul-87	6-T-4					Exposed Area (no aluminum):					1505	44	50	30	Peeling & delamination of 2nd wall only on exterior, interior shows concentrated cratering in 1" dia. on 2nd wall. Peeling of 2nd wall aluminum stopped by mounting bracket.
							4	25	13	720	30.3					
								10	10							
								8	5							
								28	9							
							Additional peeled area (Al attached at one end):									
							2	30	10	360	21.4					
								15	4							

Witness Plate Conditions

Shot	Date	Target S/N	Material	Thickness (in)	Dist. from Target (in)	Comments about witness plate	Number of Impact Perfor-ations	Maximum Hole Dia. (mm)	Dia. of Area of Conc. hits/perf (in)	Dispersion half-angle of Conc. Hits (deg)	Dia. of all impacts (in)	Max. Disp. half-angle of any impact (deg)
JSC-A242	22-Jun-87	MD-02										
JSC-A245	30-Jun-87	MT-2	Al 3003-0	0.016	2	Many short scratches in surface due to G/E particles, no holes or large craters. Mass before = 22.47 g. mass after = 22.49 g (added mass due to particle impacts).						
JSC-A246	01-Jul-87	11-T-2	Al 3003-0	0.016	2	Many short scratches in surface due to graphite/epoxy particles. One larger dimple from larger impact. No holes. Mass before=22.14g, mass after=22.13g.						
JSC-A249	02-Jul-87	6s-T-1	Al 3003-0	0.016	2	Many short scratches in surface due to small G/E particles. ~4 larger dimples from larger impacts. Mass before & after impact = 22.58 g.						
JSC-A250	06-Jul-87	6-T-4	Al 3003-0	0.016	2	Few G/E scratches, 1 large dimple from aluminum coating fragment (approximately 5mm diameter), no perforations.						

Shot Conditions

Shot	Date	Target S/N	Type	Layup	Nominal Thickness (in)	Fiber Modulus (Mpsi)	Proj. Mat'l	Proj. Dia. (mm)	Proj. Mass (mg)	Proj. Vel. (km/s)	Proj. Dens. (g/cc)	Dist. From C/L hole to C/L tube (mm)	Proj. Obliquity Angle Radially (on curve) (deg) 0=normal	Proj. Obliquity to Longitud. Axis (deg) 0=normal	Comments on Hi-speed Film &/or Shot (clean impact unless stated)
JSC-A261	11-Jul-87	MD-02	Tube	10,30,10	0.066	34	Al2024-T4	2.37	19.53	7.25	2.796	5.6	12	0	Good film, several small secondary particles 1-2 microsec behind proj. and impacting above primary impact. These particles caused only superficial exterior damage (small craters).
JSC-A291	05-Aug-87	11-T-4	Tube	10,30,10	0.077	75	Al2024-T4	1.55	5.47	7.55	2.796	4.6	10	0	Secondary approx. same size as proj 4 microsec behind, hit above primary impact. This caused very slight delam at edge of impact hole.
JSC-A292	05-Aug-87	6-T-2	Tube	10,30,10	0.073	34	Al2024-T4	1.55	5.48	7.78	2.796	4.6	10	0	Secondary impact due to "cloud" of debris (unconsolidated debris), 1 microsec behind projectile, but hitting above impact point. From exterior target damage evidence, this secondary apparently caused little/no additional damage.
JSC-A293	06-Aug-87	9-T-1	Tube	80,30,10	0.070	34	Al2024-T4	1.55	5.41	7.47	2.796	4.3	10	0	Diffuse "comet" like secondary 4 microsec behind projectile. Hit slightly above projectile impact.
JSC-A294	06-Aug-87	10-T-2	Tube	45,10,45	0.077	34	Al2024-T4	1.55	5.45	7.33	2.796	1.5	3	0	Diffuse secondary particle 4 micro seconds behind projectile w/ impact above projectile impact. No obvious surface damage to target from this secondary.
JSC-A302	12-Aug-87	12-T-2	Tube	80,30,10	0.080	34	Al2024-T4	1.55	5.45	7.16	2.796	3.3	7	0	Good film, no secondary debris.
JSC-A305	13-Aug-87	MD-03	Tube	10,30,10	0.066	34	Al2024-T4	1.54	5.38	7.25	2.796	0.0	0	0	No secondary debris.

Target Front Side Conditions: (outside of tube's 1st wall)

Shot	Date	Target S/N	Target Mass Before (g)	Target Mass After (g)	1st wall Hole Shape	Hole Dimensions Length (mm)	Hole Dimensions Width (mm)	Equiv. Circular Diameter (mm)	Crater (if evident) Dia. (mm)	Surface Peeling Number	Surface Peeling Length (mm)	Surface Peeling Width (mm)	Total Area (mm^2)	C-Scan Dimensions Area (mm^2)	C-Scan Dimensions Equiv. Circular Diameter (mm)	C-Scan Dimensions Actual Shape: Approx. Axial Length (mm)	C-Scan Dimensions Actual Shape: Overall (Circumf) Width (mm)	Comments on Target Condition (1st wall condition)
JSC-A261	11-Jul-87	MD-02	72.87	71.90	Square	5.3	5.3	6.0	9.5	4	51 46 43 13	2 5 2 4	444	679.7	29.4	33	23	Plys on exterior of 1st wall peeled in both +/- 10 deg directions while interior peeled only one direction.
JSC-A291	05-Aug-87	11-T-4	87.64	87.32	Oval	8.4	6.9	7.6	9.5	0				312.9	20.0	20	15	Essentially no peeling exterior or interior. Elliptical hole had long axis along circumference of tube, while C-scan is preferentially along longitudinal axis of tube.
JSC-A292	05-Aug-87	6-T-2	72.15	71.93	Rect.	3.8	4.8	4.8	5.7	5	51 36 18 25 18	1 1 0.4 2 0.4	114	372.2	21.8	24	15	Peeling of surface laminae in 10 degree direction, interior peeling on 1st wall in -10 degree direction and appoximately same length as exterior peeling.
JSC-A293	06-Aug-87	9-T-1	68.47	68.27	Rect.	3.8	3.8	4.3	6.1	4	15 14 17 7	3 1.5 2.5 2	123	418.4	23.1	28	15	Peeling of surface laminae in 10 degree direction, interior peeling longer than exterior and in -80 deg direction.
JSC-A294	06-Aug-87	10-T-2	69.70	69.47	Circ	4.3		4.3	5.8	4	15 14 16 18	5.5 5 1 0.5	178	161.3	14.3	12	13	Peeling of surface laminae in +45 deg direction. Inside peeling in -45 deg direction and ~twice as long as external peeling.
JSC-A302	12-Aug-87	12-T-2	86.01	85.71	Circ	7.6		7.6	10.9	0				409.0	22.8	24	17	Essentially no peeling on front or back surfaces of 1st wall.
JSC-A305	13-Aug-87	MD-03	73.40	73.14	Circ.	3.8		3.8	5.6	6	38 44 36 10 25 10	2.5 1 1.3 2 0.9 2.5	261	434.3	23.5	31	14	Surface peeling in both +10 and -10 deg directions on front, and just -10 deg direction on interior of 1st wall.

Target Second Side Conditions: (outside of tube s 2nd wall, or back side of plate)

Shot	Date	Target S/N	2nd wall Hole Shape	Hole Dimensions Length (mm)	Hole Dimensions Width (mm)	Hole Dimensions Equiv. Circular Diameter (mm)	Surface Peelings Number	Surface Peelings Length (mm)	Surface Peelings Width (mm)	C-Scan Dimensions Total Area (mm^2)	C-Scan Dimensions Equiv. Circular Diameter (mm)	C-Scan Dimensions Area (mm^2)	C-Scan Dimensions Equiv. Circular Diameter (mm)	C-Scan Dimensions Actual Shape: Approx. Length (mm)	C-Scan Dimensions Actual Shape: Overall Width (mm)	Comments on Tubes 2nd Wall
JSC-A261	11-Jul-87	MD-02	Rect.	13.0	3.0	7.0	1	52	20	1040	36.4	1650	46	59	28	Hole was not clean through, several loose (typically fractured at one end) graphite/epoxy plys overlay hole. Peelings were stopped by edges of mounting bracket,otherwise longer peelings would have resulted
JSC-A291	05-Aug-87	11-T-4					4	10.2 2.5 5.1 6.4	2.5 1.3 0.5 0.8	36	6.8	653	29	25	26	Impacts on 2nd wall caused several spall delaminations on exterior of 2nd wall. Most craters on interior of 2nd wall occured in area having a 1.1" cord length (circular area).
JSC-A292	05-Aug-87	6-T-2					3	12.7 10.2 7.6	0.5 0.1 0.1	9	3.3	290	19	20	14	Impacts on 2nd wall caused circular pattern of craters (~0.8" diameter for concentrated impacts). Slight spall/peeling from exterior of 2nd wall. Entire interior of tube coated with black powder.
JSC-A293	06-Aug-87	9-T-1					5	22.9 12.7 10.2 5.1 2.5	1.0 0.3 0.3 0.3 0.3	31	6.3	500	25	25	20	Impacts on 2nd wall caused external delaminations/peeling. Concentrated impacts on interior surface of 2nd wall were in a circular area approx 0.7" in diameter.
JSC-A294	06-Aug-87	10-T-2					3	22.9 15.2 5.1	1.5 0.5 0.5	45	7.6	431	23	20	22	Impacts on 2nd wall caused external peeling. Impacts concentrated in circular region ~0.7" in diameter. Entire interior coated with black powder.
JSC-A302	12-Aug-87	12-T-2					5	15 20 2.8 10 8	2.5 1.5 2.0 0.5 0.5	82	10.2	684	30	28	25	2nd wall exterior nearly penetrated Besides peelings, two deep spall areas, ~2mm diameter. Concentrated impacts in 0.8" diameter circular area of interior 2nd wall surface.
JSC-A305	13-Aug-87	MD-03					4	5 10 10 8	0.5 0.5 0.5 0.5	17	4.6	297	19	18	17	Only slight exterior delam of 2nd wall. Concentrated impacts in ~1" circular area of 2nd wall interior. Exterior delam in +10 & -10 deg directions.

Witness Plate Conditions

Shot	Date	Target S/N	Material	Thickness (in)	Dist. from Target (in)	Comments about witness plate	Number of Impact Perfor-ations	Maximum Hole Dia. (mm)	Dia. of Area of Conc. hits/perf (in)	Dispersion half-angle of Conc. Hits (deg)	Dia. of all impacts (in)	Max. Disp. half-angle of any impact (deg)
JSC-A261	11-Jul-87	MD-02	Al 3003-0	0.016	2	Several G/E scratches; no holes or dimples.						
JSC-A291	05-Aug-87	11-T-4										
JSC-A292	05-Aug-87	6-T-2										
JSC-A293	06-Aug-87	9-T-1										
JSC-A294	06-Aug-87	10-T-2										
JSC-A302	12-Aug-87	12-T-2										
JSC-A305	13-Aug-87	MD-03										

Shot Conditions

Shot	Date	Target S/N	Type	Layup	Nominal Thickness (in)	Fiber Modulus (Mpsi)	Proj. Mat'l	Proj. Dia. (mm)	Proj. Mass (mg)	Proj. Vel. (km/s)	Proj. Dens. (g/cc)	Dist. From C/L hole to C/L tube (mm)	Proj. Obliquity Angle Radially (on curve) (deg) 0=normal	Obliquity to Longitud. Axis (deg) 0=normal	Comments on Hi-speed Film &/or Shot (clean impact unless stated)
JSC-A307	14-Aug-87	6-T-6	Tube w/2 mil Al coating	10,30,10	0.086	34	Al2024-T4	1.54	5.39	7.35	2.796	0.0	0	0	Good film. No secondary debris.
JSC-A308	17-Aug-87	6-T-2	Tube	10,30,10	0.073	34	Al2024-T4	3.14	45.20	6.10	2.796	1.3	3	0	No hi-speed pictures.
JSC-A313	19-Aug-87	6-T-3	Tube	10,30,10	0.078	34	Al2024-T4	1.54	5.37	7.08	2.796	2.5	6	45	
JSC-A329	01-Sep-87	6-T-3	Tube	10,30,10	0.078	34	Al2024-T4	1.55	5.43	7.33	2.796	17.0	42	0	Excellent film, some secondary particles, but none hit near primary impact (secondaries actually hit near centerline of tube, well away from primary impact point).
JSC-A333	03-Sep-87	6-F-1	Plate	10,30,10	0.061	34	Al2024-T4	1.55	5.49	7.19	2.796	NA	0	0	No secondary debris.
JSC-A334	08-Sep-87	6s-T-2	Tube	10,30,10	0.064	34	Nylon Slug Length=	4.39 4.40	72.84	6.68	1.1	4.1	9	0	No secondary debris, clean shot.

Target Front Side Conditions: (outside of tube's 1st wall)

Shot	Date	Target S/N	Target Mass Before (g)	Target Mass After (g)	1st wall Hole Shape	Hole Dimensions Length (mm)	Hole Dimensions Width (mm)	Equiv. Circular Diameter (mm)	Crater (if evident) Dia. (mm)	Surface Peeling Number	Surface Peeling Length (mm)	Surface Peeling Width (mm)	Total Area (mm^2)	C-Scan Dimensions Area (mm^2)	C-Scan Dimensions Equiv. Circular Diameter (mm)	Actual Shape: Approx. Axial Length (mm)	Actual Shape: Overall (Circumf) Width (mm)	Comments on Target Condition (1st wall condition)
JSC-A307	14-Aug-87	6-T-6	80.66	80.45	Circ.	4.3		4.3	5.8	Exposed Area (no aluminum):				279.9	18.9	21	13	Surface peeling of aluminum in +10 degree direction. Interior of 1st peeled in -10 degree direction w/ total length ~3 times as long (3") as exterior peeling.
										4	13	1.5	67					
											6	2.3						
											8	4.2						
										Additional peeled area (Al attached at one end):								
										3	10	6.5	106					
											6.5	4						
											6	2.5						
JSC-A308	17-Aug-87	6-T-2	71.96	69.61	Circ.	7.9		7.9	10.4	4	29	4.0	378	656.9	28.9	42	16	Surface peeled in +10 deg direction w/ interior peeling ~same length but in -10 deg. direction.
											30	3.0						
											25	3.5						
											28	3.0						
JSC-A313	19-Aug-87	6-T-3	71.57	71.39	Oval	5.8	4.6	5.2	7.1	5	15	1.3	75	355.1	21.3	25	14	45 deg oblique impact down longitudinal axis of tube. Elliptical hole's longest axis oriented along longitudinal axis of tube. Surface peeled in +10 deg direction and interior peeled approx. same length in -10 degree direction.
											10	1.0						
											21	1.0						
											17	0.8						
											25	0.5						
JSC-A329	01-Sep-87	6-T-3	71.38	71.16	Rect.	4.8	4.3	5.2	6.2 (crater not well defined)	5	20	1.3	103	330.7	20.5	22	15	Surface peeled in +10 deg direction on exterior and -10 deg direction on interior. Interior peelings are as long as exterior peelings.
											23	1.8						
											30	0.5						
											15	1.0						
											16	0.5						
JSC-A333	03-Sep-87	6-F-1	55.95	55.85	Oval	5.1	4.6	4.8	6.1	4	20	1.7	83	537.1	26.1 (Reference plate C-scan length to 0 deg ply dir.)	40	13	Surface peeled in +10 deg direction both front and back sides. Back side peeling approximately same length as front side given.
											8	2.3						
											18	1.5						
											10	0.5						
JSC-A334	08-Sep-87	6s-T-2	66.00	61.60	Oval	10.7	9.7	10.1	12.7	7	13	12.7	348	606.1	27.8	40	15	Longest axis of elliptical hole oriented along circumference of tube. Surface peeled in +10 deg direction on interior and exterior of 1st wall. Interior peeling approximately half as long as exterior peeling.
											9	0.6						
											9	0.6						
											9	0.6						
											13	3.2						
											15	2.5						
											25	3.2						

Target Second Side Conditions: (outside of tube s 2nd wall, or back side of plate)

Shot	Date	Target S/N	2nd wall Hole Shape	Hole Dimensions Length (mm)	Hole Dimensions Width (mm)	Hole Dimensions Equiv. Circular Diameter (mm)	Surface Peelings Number	Surface Peelings Length (mm)	Surface Peelings Width (mm)	Surface Peelings Total Area (mm^2)	Surface Peelings Equiv. Circular Diameter (mm)	C-Scan Dimensions Area (mm^2)	C-Scan Dimensions Equiv. Circular Diameter (mm)	C-Scan Dimensions Actual Shape: Approx. Length (mm)	C-Scan Dimensions Actual Shape: Overall Width (mm)		Comments on Tubes 2nd Wall
							No peeling; Several dimples:										
JSC-A307	14-Aug-87	6-T-6				1 broken:	1	3	2.5	7.5	3.1	134	13	13		10	Several blisters on exterior of 2nd wall, but only one broken, which resulted in aluminum almost detaching from the approx. 3 mm diameter area (attached at one end).
						unbroken:	8	3	3	22	5.2						
								2.5	2								
								2	1								
								1.5	1								
								1	1								
								1	1								
								1	1								
								1	1								
JSC-A308	17-Aug-87	6-T-2	Rect	20.3	22.9	24.8	4	25	20.0	1080	37.1	2278	54	58		40	Peeling only on exterior of 2nd wall, none on interior.
					(cord)			30	7.5								
					23.7			35	5								
					(calc. circumference)			30	6								
JSC-A313	19-Aug-87	6-T-3															No delam or peeling detected on 2nd wall. No impacts detected on interior of 2nd wall along original flight path of projectile, however cloud of dust impacted 2nd wall directly opposite 1st wall impact. Size of circular area was ~1.4" dia but no cratering or delam was detected.
JSC-A329	01-Sep-87	6-T-3					2	25	2.0	55	8.4	142	13	14		10	Several deep craters on interior of 2nd wall across from impact point. Exterior surface peeling on 2nd wall was several plys deep - could detect removed laminates in +10 & -10 degree direction.
								10	0.5								
JSC-A333	03-Sep-87	6-F-1															
JSC-A334	08-Sep-87	6s-T-2	Rect.	33.0	22.9	31.0	2	50	35.0	3350	65.3	3814	70	109		35	Irregular rectangular hole, exterior peeling nearly the entire length of tube (& off end on one side). No interior peeling on 2nd wall.
								40	40								

Witness Plate Conditions

Shot	Date	Target S/N	Material	Thickness (in)	Dist. from Target (in)	Comments about witness plate	Number of Impact Perfor-ations	Maximum Hole Dia. (mm)	Dia. of Area of Conc. hits/perf (in)	Dispersion half-angle of Conc. Hits (deg)	Dia. of all impacts (in)	Max. Disp. half-angle of any impact (deg)
JSC-A307	14-Aug-87	6-T-6										
JSC-A308	17-Aug-87	6-T-2										
JSC-A313	19-Aug-87	6-T-3										
JSC-A329	01-Sep-87	6-T-3										
JSC-A333	03-Sep-87	6-F-1	Al 3003-0	0.016	2	Circular debris pattern.	50	1.2	1	27	3	56
JSC-A334	08-Sep-87	6s-T-2	Al 3003-0	0.008	2	Impact on witness plate crumpled it nearly into ball without putting many holes in it.						

Shot Conditions

Shot	Date	Target S/N	Type	Layup	Nominal Thickness (in)	Fiber Modulus (Mpsi)	Proj. Mat'l	Proj. Dia. (mm)	Proj. Mass (mg)	Proj. Vel. (km/s)	Proj. Dens. (g/cc)	Dist. From C/L hole to C/L tube (mm)	Proj. Obliquity Angle Radially (on curve) (deg) 0=normal	Proj. Obliquity to Longitud. Axis (deg) 0=normal	Comments on Hi-speed Film &/or Shot (clean impact unless stated)
JSC-A346	16-Sep-87	11-F-1	Plate	10,30,10	0.073	75	Al2024-T4	1.55	5.44	6.89	2.796	NA	0	0	
JSC-A352	21-Sep-87	11-F-1	Plate	10,30,10	0.073	75	Al2024-T4	1.55	5.45	6.83	2.796	NA	0	0	
JSC-A409	05-Nov-87	12-F-1	Plate	80,30,10	0.072	75	Al2024-T4	1.56	5.51	7.30	2.796	NA	0	0	Projectile appeared slightly misshapen in high speed film (short spikey tail). Secondary debris approx. 2 micro-sec behind proj. Debris appears very diffuse/wispy on film and from target appearance did not effect test results.
JSC-A410	05-Nov-87	10-F-1	Plate	45,10,45	0.061	34	Al2024-T4	1.55	5.50	7.68	2.796	NA	0	0	Film starts with impact. No data on projectile condition.
JSC-A411	06-Nov-87	9s-F-1	Plate	80,30,10	0.061	34	Al2024-T4	1.56	5.51	6.97	2.796	NA	0	0	Projectile slightly deformed into "pacman" shape, with "mouth" on trailing side of projectile. No debris following projectile.
JSC-A413	09-Nov-87	13-F-1	Plate	45,10,45	0.072	75	Al2024-T4	1.55	5.40	7.29	2.796	NA	0	0	Projectile misshapen, has short "tail".

C-3

Target Front Side Conditions: (outside of tube's 1st wall)

Shot	Date	Target S/N	Target Mass Before (g)	Target Mass After (g)	1st wall Hole Shape	Hole Dimensions: Length (mm)	Hole Dimensions: Width (mm)	Hole Dimensions: Equiv. Circular Diameter (mm)	Crater (if evident) Dia. (mm)	Surface Peeling: Number	Surface Peeling: Length (mm)	Surface Peeling: Width (mm)	Total Area (mm^2)	C-Scan Dimensions: Area (mm^2)	C-Scan Dimensions: Equiv. Circular Diameter (mm)	C-Scan Dimensions: Actual Shape: Approx. Axial Length (mm)	C-Scan Dimensions: Actual Shape: Overall (Circumf.) Width (mm)	Comments on Target Condition (1st wall condition)
JSC-A346	16-Sep-87	11-F-1	66.87	68.67	Circ.	6.7		6.7	9.5	0				656.3 est..	29.1 (Reference plate C-scan length to 0 deg ply dir.)	32	23	C-scan area is rough estimate because it partially overlapped w/ NDE-34 shot effects (hit & secondaries).
JSC-A352	21-Sep-87	11-F-1	62.08	61.86	Circ.	7.1		7.1	9.5	0				725.3	30.4 (Reference plate C-scan length to 0 deg ply dir.)	29	25	
JSC-A409	05-Nov-87	12-F-1	67.71	67.50	Circ.	7.1		7.1	9.5	1	6	3.2	20	368.3	21.7 (Reference plate C-scan length to 0 deg ply dir.)	16	23	Slight peeling around hole - Plys broken off short near hole.
JSC-A410	05-Nov-87	10-F-1	52.78	52.66	Oval	5.2	4.4	4.7	6.3	5	6 33 10 20 29	5 1 2 1.5 1.0	141	913.0 (est.)	32.2 (Reference plate C-scan length to 0 deg ply dir.)	35	23	C-scan estimated due to overlap from secondary impacts in shot NDE-37. Peelings approximately same length on both sides of plate, both in +45 deg. direction, slightly greater area peeled back on front side.
JSC-A411	06-Nov-87	9s-F-1	55.93	55.82	Rect.	5.2	4.8	5.6	6.7	3	15 30 14	2 1.2 3	108	513.3	25.6 (Reference plate C-scan length to 0 deg ply dir.)	25	21	Surface peeled in +80 deg direction front and back. Approximately same length of peelings.
JSC-A413	09-Nov-87	13-F-1	68.95	68.77	Circ.	7.5		7.5	10.3	0				253.5	18.0 (Reference plate C-scan length to 0 deg ply dir.)	14	18	C-scan oriented in 45 deg direction

Target Second Side Conditions: (outside of tube s 2nd wall, on back side of plate)

				Hole Dimensions			Surface Peelings					C-Scan Dimensions				
Shot	Date	Target S/N	2nd wall Hole Shape	Length (mm)	Width (mm)	Equiv. Circular Diameter (mm)	Number	Length (mm)	Width (mm)	Total Area (mm^2)	Equiv. Circular Diameter (mm)	Area (mm^2)	Equiv. Circular Diameter (mm)	Actual Shape: Approx. Length (mm)	Overall Width (mm)	Comments on Tubes 2nd wall
JSC-A346	16-Sep-87	11-F-1														
JSC-A352	21-Sep-87	11-F-1														
JSC-A409	05-Nov-87	12-F-1														
JSC-A410	05-Nov-87	10-F-1														
JSC-A411	06-Nov-87	9s-F-1														
JSC-A413	09-Nov-87	13-F-1														

Witness Plate Conditions

Shot	Date	Target S/N	Material	Thickness (in)	Dist. from Target (in)	Comments about witness plate	Number of Impact Perfor-ations	Maximum Hole Dia. (mm)	Dia. of Area of Conc. hits/perf (in)	Dispersion half-angle of Conc. Hits (deg)	Dia. of all impacts (in)	Max. Disp. half-angle of any impact (deg)
JSC-A346	16-Sep-87	11-F-1	Al 3003-0	0.016	2	Circular debris pattern.	26	0.9	1.2	31	3.25	58
JSC-A352	21-Sep-87	11-F-1	Al 3003-0	0.016	2	Circular debris pattern.	23	0.9	1.5	37	3.5	60
JSC-A409	05-Nov-87	12-F-1	Al 3003-0	0.016	2	Circular debris pattern.	18	1.4	1.4	35	3.0	56
JSC-A410	05-Nov-87	10-F-1	Al 3003-0	0.016	2	Circular debris pattern.	33	2.5	1.1	29	2.8	54
JSC-A411	06-Nov-87	9s-F-1	Al 3003-0	0.016	2	Circular debris pattern.	43	2.0	1.3	32	3.0	56
JSC-A413	09-Nov-87	13-F-1	Al 3003-0	0.016	2	Circular debris pattern.	39	1.2	1.4	35	2.8	54

Shot Conditions

Shot	Date	Target S/N	Type	Layup	Nominal Thickness (in)	Fiber Modulus (Mpsi)	Proj. Mat'l	Proj. Dia. (mm)	Proj. Mass (mg)	Proj. Vel. (km/s)	Proj. Dens. (g/cc)	Dist. From C/L hole to C/L tube (mm)	Proj. Obliquity Angle Radially (on curve) (deg) 0=normal	Obliquity to Longitud. Axis (deg) 0=normal	Comments on Hi-speed Film &/or Shot (clean impact unless stated)
NDE Shots:															
NDE-1	02-Feb-87	6-F-2	Plate	10,30,10	0.062	34	Glass	0.55	0.21	6.40	2.45	NA	0	0	Multiple impacts & large perforations over entire plate.
NDE-2	02-Feb-87	11-F-2	Plate	10,30,10	0.072	75	Glass	0.55	0.21	6.99	2.45	NA	0	0	Some secondary impacts/perforations though widely separated. Five proj. loaded in sabot and fired in this shot. Five impacts at & near edge of plate could be proj. impacts. Other smaller secondary impacts in center of plate.
NDE-3	06-Feb-87	12-F-2	Plate	80,30,10	0.071	75	Glass	0.55	0.21	6.40	2.45	NA	0	0	2 larger impacts presumably from projectile, with many (dozens) of smaller impacts/perforations.
NDE-4	18-Feb-87	10-F-2	Plate	45,10,45	0.063	34	Glass	0.55	0.21	5.91	2.45	NA	0	0	No impacts from projectile, several dozen small none perforating secondary impacts.
NDE-5	18-Feb-87	13-F-2	Plate	45,10,45	0.072	75	Glass	0.55	0.21	6.40	2.45	NA	0	0	2 impacts, each ~0.6mm hole & 1.3mm crater, had magnetic debris embedded in witness plate. Thus, impacts from secondary steel particles produced from sabot stripper/blast plate and not from projectiles. No projectile impacts.
NDE-6	23-Feb-87	9s-F-2	Plate	80,30,10	0.060	34	Glass	0.55	0.21	3.90	2.45	NA	0	0	No impacts from projectile.
NDE-7	15-Apr-87	9s-F-2	Plate	80,30,10	0.060	34	Glass	0.55	0.21	5.49	2.45	NA	0	0	One projectile impact. A few small secondary impacts.
NDE-8	15-May-87	10-F-2	Plate	45,10,45	0.063	34	Glass	0.55	0.21	5.91	2.45	NA	0	0	Two impacts seem too small to be from projectile. Projectile may have broken up. One impact perfor-

Target Front Side Conditions: (outside of tube's 1st wall)

Shot	Date	Target S/N	Target Mass Before (g)	Target Mass After (g)	1st wall Hole Shape	Hole Dimensions Length (mm)	Hole Dimensions Width (mm)	Equiv. Circular Diameter (mm)	Crater (if evident) Dia. (mm)	Surface Peeling Number	Surface Peeling Length (mm)	Surface Peeling Width (mm)	Total Area (mm^2)	C-Scan Dimensions Area (mm^2)	C-Scan Dimensions Equiv. Circular Diameter (mm)	C-Scan Dimensions Actual Shape: Approx. Axial Length (mm)	C-Scan Dimensions Actual Shape: Overall (Circumf) Width (mm)	Comments on Target Condition (1st wall condition)
NDE Shots:																		
NDE-1	02-Feb-87	6-F-2	55.40	54.79	Circ.	1.9		1.9	2.5	3	20 21 12	1 1.5 1	64					C-scan could not be resolved due to multiple impacts. Projectile impact point estimated from hole size; therefore, possiblity exists that hole may not have been made by projectile. Surface peelings in +10 degree direction front side, & +10 deg. direction on back. Back peelings ~1/4 as long as on front.
NDE-2	02-Feb-87	11-F-2	69.09	69.08	Rect.	1.9	1.5	1.9	2.7	0				73.0	10.0 (Reference plate C-scan length to 0 deg ply dir.)	12	6.8	No peeling. 3 other presumed proj. impacts hit on edge of plate making hole. crater and c-scan measurement subject to error. Other impact somewhat smaller with equiv. hole diameter ~1.1 mm.
NDE-3	06-Feb-87	12-F-2	68.57		Circ. Circ.	2.7 2.0		2.7 2.0	3.3 3.1	0 0								C-scans cannot be resolved for individual impacts due to multiple smaller impacts near primary hits.
NDE-4	18-Feb-87	10-F-2	55.21															No data.
NDE-5	18-Feb-87	13-F-2	69.70															
NDE-6	23-Feb-87	9s-F-2	54.78															No data.
NDE-7	15-Apr-87	9s-F-2	54.78		Circ.	1.1		1.1	1.9	2	22 11	1.5 1	44	99.2	11.2 (Reference plate C-scan length to 0 deg ply dir.)	7	13	Peeling in +80 deg. direction on front and +80 deg. on back. Back peelings only ~1/4 length of front peeling.
NDE-8	15-May-87	10-F-2	55.21		Circ. Circ.	0.4 0		0.4	0.8 0.8	2	20 10	1 0.5	25					Peeling in +45 deg. direction on front and +45 deg. on back. Back peelings only ~1/4 length of front

Target Second Side Conditions: (outside of tube's 2nd wall, or back side of plate)

			Hole Dimensions				Surface Peelings					C-Scan Dimensions				
Shot	Date	Target S/N	2nd wall Hole Shape	Length (mm)	Width (mm)	Equiv. Circular Diameter (mm)	Number	Length (mm)	Width (mm)	Total Area (mm^2)	Equiv. Circular Diameter (mm)	Area (mm^2)	Equiv. Circular Diameter (mm)	Actual Shape: Approx. Overall Length (mm)	Width (mm)	Comments on Tubes 2nd Wall
NDE Shots:																
NDE-1	02-Feb-87	6-F-2														
NDE-2	02-Feb-87	11-F-2														
NDE-3	06-Feb-87	12-F-2														
NDE-4	18-Feb-87	10-F-2														
NDE-5	18-Feb-87	13-F-2														
NDE-6	23-Feb-87	9s-F-2														
NDE-7	15-Apr-87	9s-F-2														
NDE-8	15-May-87	10-F-2														

Witness Plate Conditions

Shot NDE Shots:	Date	Target S/N	Material	Thickness (in)	Dist. from Target (in)	Comments about witness plate	Number of Impact Perfor-ations	Maximum Hole Dia. (mm)	Dia. of Area of Conc. hits/perf (in)	Dispersion half-angle of Conc. Hits (deg)	Dia. of all impacts (in)	Max. Disp. half-angle of any impact (deg)
NDE-1	02-Feb-87	6-F-2	Al6061-T6	0.032	0.25	No perforations, multiple impacts.						
NDE-2	02-Feb-87	11-F-2	Al6061-T6	0.032	0.25	Impacts off edge of witness plate. no effect from secondaries.						
NDE-3	06-Feb-87	12-F-2	Al6061-T6	0.032	0.25	Faint dark smudges, no damage to witness plate.						
NDE-4	19-Feb-87	10-F-2	Al6061-T6	0.032	0.25	No damage.						
NDE-5	18-Feb-87	13-F-2	Al6061-T6	0.032	0.25	Dark smudges, ~3.5 mm diameter, magnetic debris in smudges. One magnetic fragment weighed ~ 0.43 mg. It was a flat, triangular piece ~0.75 mm x 0.75mm x 0.92mm x 0.2 mm thick.						
NDE-6	23-Feb-87	9s-F-2	Al6061-T6	0.032	0.25	No damage.						
NDE-7	15-Apr-87	9s-F-2	Al6061-T6	0.032	0.25	Dark smudge, no damage.					0.3	50
NDE-8	15-May-87	10-F-2	Al6061-T6	0.032	0.25	No damage.						

Shot Conditions

Shot	Date	Target S/N	Type	Layup	Nominal Thickness (in)	Fiber Modulus (Mpsi)	Proj. Mat'l	Proj. Dia. (mm)	Proj. Mass (mg)	Proj. Vel. (km/s)	Proj. Dens. (g/cc)	Dist. From C/L hole to C/L tube (mm)	Proj. Obliquity Angle Radially (on curve) (deg) 0=normal	Proj. Obliquity to Longitud. Axis (deg) 0=normal	Comments on Hi-speed Film &/or Shot (clean impact unless stated)
															ated plate while the other left only a deep spall but no through hole.
NDE-9	15-May-87	13-F-2	Plate	45,10,45	0.072	75	Glass	0.55	0.21	5.70	2.45	NA	0	0	2 largest impacts each left small crater, w/ little or no spall, and no hole. Therefore, appears proj. broke up or missed.
NDE-10	11-Jun-87	6-T-3	Tube	10,30,10	0.078	34	Glass	0.77	0.59	4.21	2.45	0.0	0	0	No projectile impacts, just tiny impacts from secondaries.
NDE-11	11-Jun-87	6s-T-2	Tube	10,30,10	0.064	34	Glass	0.77	0.59	4.21	2.45	0.9	2	0	
NDE-12	11-Jun-87	6-T-6	Tube w/2 mil Al coating	10,30,10	0.086	34	Glass	0.77	0.59	3.29	2.45	0.0 (unknown)	0	0	
NDE-13	11-Jun-87	6-T-9	Tube w/6 mil Al coating	10,30,10	0.089	34	Glass	0.77	0.59	4.69	2.45	9.1	21	0	
NDE-14	28-Jul-87 NDE Shot #58	7-T-1	Tube	10,30,10	0.103	34	Glass	0.77	0.59	3.96	2.45	0.0	0	0	4-6 small impacts with no apparent delamination from interior surface. Projectile broke up or missed.
NDE-15	28-Jul-87 NDE Shot #73	11-T-3	Tube	10,30,10	0.082	75	Glass	-0.77	0.59	5.49	2.45	0.0	0	0	Multiple (24+) small impacts with 2 producing delamination from

Target Front Side Conditions: (outside of tube's 1st wall)

Shot	Date	Target S/N	Target Mass Before (g)	Target Mass After (g)	Hole Dimensions: 1st wall Hole Shape	Hole Dimensions: Length (mm)	Hole Dimensions: Width (mm)	Hole Dimensions: Equiv. Circular Diameter (mm)	Crater (if evident) Dia. (mm)	Surface Peeling: Number	Surface Peeling: Length (mm)	Surface Peeling: Width (mm)	Surface Peeling: Total Area (mm^2)	C-Scan Dimensions: Area (mm^2)	C-Scan Dimensions: Equiv. Circular Diameter (mm)	C-Scan Dimensions: Actual Shape: Approx. Axial Length (mm)	C-Scan Dimensions: Actual Shape: Overall (Circumf) Width (mm)	Comments on Target Condition (1st wall condition)
																		peelings.
NDE-9	15-May-87	13-F-2	69.70						1.1									No peeling.
NDE-10	11-Jun-87	6-T-3	71.87	71.87														
NDE-11	11-Jun-87	6s-T-2	66.11	66.11	Rect.	0.3	0.9	0.6	1.6	4	15 6 10 5	0.8 0.5 0.5 0.5	21	66.4	9.2	10	7	Peeling in +10 deg. direction on front and back side of first wall. Peelings on interior of 1st wall are as long as peelings on exterior Little/no effect of plume from 1st wall on 2nd wall.
NDE-12	11-Jun-87	6-T-6		80.68	Rect.	1.6	1	1.4	3.3	Exposed Area (no aluminum): 1	2	1.5	2	91.7	10.8	15	6	C-scan and hole longest axis in direction of the longitudinal axis of tube. Peeling of surface Al slight but noticeable. Peeling on inside of 1st wall ~1" long total, & in the 10 deg. direction. Plume of debris from 1st wall left black diffuse, circular pattern on 2nd wall interior, but did not crater or damage it.
NDE-13	11-Jun-87	6-T-9		88.39	Circ.	1.0		1.0 ring around hole:	1.7	Exposed Area (no aluminum): 1	10	1.0	10	58.7	8.6	8	7	C-scan area slightly longer in direction of the longitudinal axis of the tube. Aluminum coating cut ~1 mm long on either side of hole appearing likely to peel. Inside of 1st wall peeled in 10 deg. dir. for ~1". A diffuse debris plume left a circular pattern on 2nd wall but did not damage it.
NDE-14	28-Jul-87 NDE Shot #58	7-T-1	103.57															
NDE-15	28-Jul-87 NDE Shot #73	11-T-3	89.44															

Target Second Side Conditions: (outside of tube's 2nd wall, or back side of plate)

			Hole Dimensions				Surface Peelings					C-Scan Dimensions				
Shot	Date	Target S/N	2nd wall Hole Shape	Length (mm)	Width (mm)	Equiv. Circular Diameter (mm)	Number	Length (mm)	Width (mm)	Total Area (mm^2)	Equiv. Circular Diameter (mm)	Area (mm^2)	Equiv. Circular Diameter (mm)	Actual Shape: Approx. Length (mm)	Overall Width (mm)	Comments on Tubes 2nd Wall
NDE-9	15-May-87	13-F-2														
NDE-10	11-Jun-87	6-T-3														
NDE-11	11-Jun-87	6s-T-2														
NDE-12	11-Jun-87	6-T-5														
NDE-13	11-Jun-87	6-T-9														
NDE-14	29-Jul-87 NDE Shot #58	7-T-1														
NDE-15	28-Jul-87 NDE Shot #73	11-T-3														

Witness Plate Conditions

Shot	Date	Target S/N	Material	Thickness (in)	Dist. from Target (in)	Comments about witness plate	Number of Impact Perfor-ations	Maximum Hole Dia. (mm)	Dia. of Area of Conc. hits/perf (in)	Dispersion half-angle of Conc. Hits (deg)	Dia. of all impacts (in)	Max. Disp. half-angle of any impact (deg)
NDE-9	15-May-87	13-F-2	Al6061-T6	0.032	0.25	No damage.						
NDE-10	11-Jun-87	6-T-3										
NDE-11	11-Jun-87	6s-T-2										
NDE-12	11-Jun-87	6-T-6										
NDE-13	11-Jun-87	6-T-9										
NDE-14	28-Jul-87	7-T-1										
	NDE Shot #58											
NDE-15	28-Jul-87	11-T-3										
	NDE Shot #73											

Shot Conditions

Shot	Date	Target S/N	Type	Layup	Nominal Thickness (in)	Fiber Modulus (Mpsi)	Proj. Mat'l	Proj. Dia. (mm)	Proj. Mass (mg)	Proj. Vel. (km/s)	Proj. Dens. (g/cc)	Dist. From C/L hole to C/L tube (mm)	Proj. Obliquity Angle Radially (on curve) (deg) 0=normal	Proj. Obliquity to Longitud. Axis (deg) 0=normal	Comments on Hi-speed Film &/or Shot (clean impact unless stated) interior surface, no perforations.
NDE-16	28-Jul-87 NDE Shot #69	9-T-2	Tube	80,30,10	0.071	34	Glass	0.77	0.59	6.71	2.45	2.3	5	0	Impact is too small, projectile appears to have broken up or erroded.
NDE-17	28-Jul-87 NDE Shot #69	9s-T-2	Tube	80,30,10	0.068	34	Glass	0.77	0.59	7.32	2.45	7.9	18	0	Impact is too small, projectile appears to have broken up or erroded. Secondary impact nearly same size as primary.
NDE-18	28-Jul-87 NDE Shot #70	12-T-2	Tube	80,30,10	0.080	75	Glass	0.77	0.59	3.96	2.45	0.0 (unknown altho NDE est. of 23mm seems too large)	0	0	Many secondary impacts, all but 3 are small, those 3 appear to be from large, low speed impacts that produced spall but only shallow surface crater.
NDE-19	30-Jul-87 NDE Shot #83	10-T-2	Tube	45,10,45	0.077	34	Glass	0.77	0.59	6.40	2.45	14.7	35	0	
NDE-20	30-Jul-87 NDE Shot #84	7-T-2	Tube	10,30,10	0.106	34	Al2024-T4	2.38	19.69	4.88	2.796	13.0	31	0	Projectile hit exactly on edge of tube end. Hole, crater, & c-scan information doubtful or useless.
NDE-21	30-Jul-87 NDE Shot #86	8-T-2	Tube	10,30,10	0.133	34	Al2024-T4	2.37	19.58	4.57	2.796	6.4	14	0	
NDE-22	04-Aug-87 NDE Shot #88	6-T-3	Tube	10,30,10	0.078	34	Al2024-T4	1.58	5.72	4.57	2.796	16.8	41	0	Impact very near edge of tube, 0.4" Thus, some edge interference in complete development of surface ply peeling.

Target Front Side Conditions: (outside of tube's 1st wall)

Shot	Date	Target S/N	Target Mass Before (g)	Target Mass After (g)	1st wall Hole Shape	Hole Dimensions Length (mm)	Hole Dimensions Width (mm)	Equiv. Circular Diameter (mm)	Crater (if evident) Dia. (mm)	Surface Peeling Number	Surface Peeling Length (mm)	Surface Peeling Width (mm)	C-Scan Dimensions Total Area (mm^2)	C-Scan Dimensions Area (mm^2)	C-Scan Dimensions Equiv. Circular Diameter (mm)	C-Scan Dimensions Actual Shape: Approx. Axial Length (mm)	C-Scan Dimensions Actual Shape: Overall (Circumf) Width (mm)	Comments on Target Condition (1st wall condition)
NDE-16	28-Jul-87 NDE Shot #69	9-T-2	69.55		Circ.	0.9		0.9	1.7	4	18 19 10 14	0.6 0.4 0.7 0.5	32	39.9	10.7	19	5	Peeling in +10 deg. direction on front side of 1st wall and in -80 deg. direction on interior side of 1st wall. Interior peelings only half as long as exterior.
NDE-17	28-Jul-87 NDE Shot #69	9s-T-2	67.79		Circ.	0.5		0.5	1.0	2	7 5	0.8 0.5	7	50.9	8.0	8	6	Peeling in +80 deg. direction on exterior and interior of 1st wall. C-scan of tube poor indicating much porosity/voids within tube. No interior plume effects on 2nd wall.
NDE-18	28-Jul-87 NDE Shot #70	12-T-2	86.01		Circ.	3.3		3.3	4.5	1	2	1.5	3	119.6	12.3	13	9	Peeling in +10 deg. direction on exterior and slight peeling in -80 degree on interior.
NDE-19	30-Jul-87 NDE Shot #83	10-T-2	69.60		Oval	1.1	0.9	1.0	2.2	4	13 11 8 10	0.8 0.3 0.3 0.3	17	64.1	9.0	8	8	Peeling in +45 deg. direction on exterior and ~same length but in -45 degree direction on interior of 1st wall. Very little plume but most impacted directly opposite centerline of tube, no damage to 2nd wall.
NDE-20	30-Jul-87 NDE Shot #84	7-T-2	103.90		Circ. (from appearance of semi-circle)	3.2		3.2	4.6	2	11 10	2.5 1.0	38					Peeling in +10 deg. direction on exterior and ~3 times longer in -10 deg. direction on interior.
NDE-21	30-Jul-87 NDE Shot #86	8-T-2	135.04		Rect.	3.0	2.5	3.1	5.0	4	18 23 15 20	4.5 2.5 3.0 1.5	214	579.3	27.2	30	19	Peeling in +10 deg. direction on exterior and ~1.5 x length but in -10 degree direction on interior of tube. Many craters on 2nd wall & some slight delamination of 2nd wall exterior.
NDE-22	04-Aug-87 NDE Shot #88	6-T-3	71.71		Circ.	3.3		3.3	4.8	4	18 5 10 9	0.8 1.0 2.0 0.8	45	139.2	13.3	18	8	Peeling in +10 deg. direction on exterior and ~same length but in -10 deg. direction on interior.

Target Second Side Conditions: (outside of tube s 2nd wall, or back side of plate)

Shot	Date	Target S/N	Hole Dimensions: 2nd wall Hole Shape	Hole Dimensions: Length (mm)	Hole Dimensions: Width (mm)	Hole Dimensions: Equiv. Circular Diameter (mm)	Surface Peelings: Number	Surface Peelings: Length (mm)	Surface Peelings: Width (mm)	Surface Peelings: Total Area (mm^2)	Surface Peelings: Equiv. Circular Diameter (mm)	C-Scan Dimensions: Area (mm^2)	C-Scan Dimensions: Equiv. Circular Diameter (mm)	C-Scan Dimensions: Actual Shape: Approx. Overall Length (mm)	C-Scan Dimensions: Actual Shape: Approx. Overall Width (mm)	Comments on Tubes 2nd Wall
NDE-16	28-Jul-87 NDE Shot #69	9-T-2														
NDE-17	28-Jul-87 NDE Shot #69	9s-T-2														
NDE-18	28-Jul-87 NDE Shot #70	12-T-2														
NDE-19	30-Jul-87 NDE Shot #83	10-T-2														
NDE-20	30-Jul-87 NDE Shot #84	7-T-2														
NDE-21	30-Jul-87 NDE Shot #86	8-T-2					2	18 7	0.1 0.1	3	1.8	308.0	19.8	28	11	Concentrated cratering of 2nd wall interior occured in approximately 1" diameter circular area. Slight delamination/peeling of exterior of 2nd wall really was longitudinal splitting without spall break-away. However, near spall break-out ballistic limit for 2nd wall.
NDE-22	04-Aug-87 NDE Shot #88	6-T-3					1	20	0.1	2	1.6	63.3	9.0	12	5	Concentrated cratering of 2nd wall interior occured in approximately a 10 mm diameter area of 2nd wall. Long longitudinal split in surface

Witness Plate Conditions

Shot	Date	Target S/N	Material	Thickness (in)	Dist. from Target (in)	Comments about witness plate	Number of Impact Perfor-ations	Maximum Hole Dia. (mm)	Dia. of Area of Conc. hits/perf (in)	Dispersion half-angle of Conc. Hits (deg)	Dia. of all impacts (in)	Max. Disp. half-angle of any impact (deg)
NDE-16	28-Jul-87	9-T-2										
	NDE Shot #69											
NDE-17	28-Jul-87	9s-T-2										
	NDE Shot #69											
NDE-18	28-Jul-87	12-T-2										
	NDE Shot #70											
NDE-19	30-Jul-87	10-T-2										
	NDE Shot #83											
NDE-20	30-Jul-87	7-T-2										
	NDE Shot #84											
NDE-21	30-Jul-87	8-T-2										
	NDE Shot #86											
NDE-22	04-Aug-87	6-T-3										
	NDE Shot #88											

Shot Conditions

Shot	Date	Target S/N	Type	Layup	Nominal Thickness (in)	Fiber Modulus (Mpsi)	Proj. Mat'l	Proj. Dia. (mm)	Proj. Mass (mg)	Proj. Vel. (km/s)	Proj. Dens. (g/cc)	Dist. From C/L hole to C/L tube (mm)	Proj. Obliquity Angle Radially (on curve) (deg) 0=normal	Proj. Obliquity to Longitud. Axis (deg) 0=normal	Comments on Hi-speed Film &/or Shot (clean impact unless stated)
NDE-23	04-Aug-87 NDE Shot #89	6-T-6	Tube w/ 2 mil Aluminum Coating	10,30,10	0.086	34	Al2024-T4	1.57	5.70	7.01	2.796	11.7	27	0	7-8 secondary impacts produced tiny holes through 2mil aluminum coating These did not effect impact result.
NDE-24	04-Aug-87 NDE Shot #90	6-T-9	Tube w/ 6mil aluminum coating	10,30,10	0.089	34	Al2024-T4	1.59	5.77	6.71	2.796	10.2	24	0	
NDE-25	04-Aug-87 NDE Shot #91	MT-04	Tube	45,0,15,0	0.066	75	Al2024-T4	1.58	5.73	7.32	2.796	11.9	28	0	
NDE-26	04-Aug-87 NDE Shot #92	MD-03	Tube	10,30,10 filament wound	0.066	34	Al2024-T4	1.57	5.70	6.10	2.796	6.6 (est.)	15	0	Centerline not marked on tube, est. obliquity from NDE provided diagram
NDE-27	04-Aug-87 NDE Shot #93	MT-03	Tube	45,0,0,0	0.066	75	Al2024-T4	1.57	5.71	4.88	2.796	10.2	24	0	
NDE-28	25-Aug-87 NDE Shot #94	7-T-2	Tube	10,30,10	0.106	34	Al2024-T4	1.58	5.72	4.27	2.796	5.1	12	0	

Target Front Side Conditions: (outside of tube's 1st wall)

Shot	Date	Target S/N	Target Mass Before (g)	Target Mass After (g)	1st wall Hole Shape	Hole Dimensions Length (mm)	Hole Dimensions Width (mm)	Equiv. Circular Diameter (mm)	Crater (if evident) Dia. (mm)	Surface Peeling Number	Surface Peeling Length (mm)	Surface Peeling Width (mm)	Total Area (mm^2)	C-Scan Dimensions Area (mm^2)	C-Scan Dimensions Equiv. Circular Diameter (mm)	C-Scan Dimensions Actual Shape: Approx. Axial Length (mm)	C-Scan Dimensions Actual Shape: Overall (Circumf) Width (mm)	Comments on Target Condition (1st wall condition)
NDE-23	04-Aug-87 NDE Shot #89	6-T-6			Oval	2.5	3.3	2.9	4.9	Exposed Area (no aluminum): 2 Additional peeled area (Al attached at one end): 2	 2 6 5 1	 5.0 2.5 4.5 5.5	 23 26	134.9	13.1	13	10	Aluminum beginning to peel in +10 deg. direction. Interior peeling short, only ~0.6", and in -10 deg. direction. Only small, shallow cratering visible on 2nd wall interior but no damage evident in c-scan of 2nd wall.
NDE-24	04-Aug-87 NDE Shot #90	6-T-9			Oval	3.6	3.3	3.4	5.5	Exposed Area (no aluminum): 2	 2.5 0.8 1.5	 5.0 4.0 5.5	 24	118.5	12.3	13	9	Aluminum did not peel back except in area directly around impact point, but aluminum stretched with peeling nearly occuring in +10 deg. direction. Long (2") peeling occured on interior of 1st wall. Slight cratering occured on 2nd but no damage detected in c-scan.
NDE-25	04-Aug-87 NDE Shot #91	MT-04			Rect.	4.3	5.3	5.4	7.3	1	29 (delam ring around hole)	2.0	58	257.2	19.1	17	15	No real peeling except around hole.
NDE-26	04-Aug-87 NDE Shot #92	MD-03			Oval (irregular)	2.8	2.3	2.5	3.0 (not well defined)	4	42 33 32 28	1.5 1.0 1.3 1	164	295.1	19.4	33	9	Peeling on exterior in both +10 & -10 degree directions, little peeling on interior of 1st wall (& just in -10 deg. direction).
NDE-27	04-Aug-87 NDE Shot #93	MT-03			Oval (irregular)	5.8	4.3	5.0	8.1	3	8 3 2	0.1 0.1 0.1	1	284.0	19.0	16	18	Cracks around hole on 45 deg angle to longitudinal axis of tube. Two holes produced in 2nd wall.
NDE-28	25-Aug-87 NDE Shot #94	7-T-2			Rect. (irregular)	2.7	2.3	2.8	4.8	3	24 6	1.0 0.5	38	130.6	12.9	12	11	Peeling in +10 deg. direction on exterior and approximately as long

Target Second Side Conditions: (outside of tube's 2nd wall, or back side of plate)

Shot	Date	Target S/N	Hole Dimensions: 2nd wall Hole Shape	Hole Dimensions: Length (mm)	Hole Dimensions: Width (mm)	Hole Dimensions: Equiv. Circular Diameter (mm)	Surface Peelings: Number	Surface Peelings: Length (mm)	Surface Peelings: Width (mm)	Surface Peelings: Total Area (mm^2)	C-Scan Dimensions: Equiv. Circular Diameter (mm)	C-Scan Dimensions: Area (mm^2)	C-Scan Dimensions: Equiv. Circular Diameter (mm)	C-Scan Dimensions: Actual Shape: Approx. Overall Length (mm)	C-Scan Dimensions: Actual Shape: Approx. Overall Width (mm)	Comments on Tubes 2nd Wall
																ply occured. Impacts occured in area between centerline of tube and area opposite impact pt., parallel to projectile flight path.
NDE-23	04-Aug-87 NDE Shot #89	6-T-6														
NDE-24	04-Aug-87 NDE Shot #90	6-T-9														Slight cratering occured on 2nd but no damage detected in c-scan. Plume impacted in 0.9" circular area of 2nd wall, no dimples or other damage occured to aluminum coating of 2nd wall.
NDE-25	04-Aug-87 NDE Shot #91	MT-04	Oval (irregular)	5.3	2.0	3.3	3	8 5 3.5	3 4.5 2.5	55	8.4	807.0	32.1	29	29	Hole in 2nd wall produced 180 deg. around from 1st wall hole (unlike other impacts that produce holes/-damage more on line-of-flight of projectile). Circular spray pattern "centered on 2nd wall hole and approximately 1.2" diameter (somewhat skewed toward line-of-flight of projectile).
NDE-26	04-Aug-87 NDE Shot #92	MD-03										102.7	11.4	17	6	Craters in 2nd wall produced at "intersection of centerline with 2nd wall, therefore, debris seemed to travel between parallel with projectile trajectory from hole and with centerline.
NDE-27	04-Aug-87 NDE Shot #93	MT-03	Rect. Rect.	1.8 2.0	1.3 2.0	1.7 2.3	2	15 10	3 1	55	8.4	601.6	27.7	20	30	Holes in 2nd wall produced on line parallel to line-of-flight of projectile. Much cratering, skewed toward centerline of shot.
NDE-28	25-Aug-87 NDE Shot #94	7-T-2														Slight cratering in circular 0.8" diameter area on 2nd wall did not

Witness Plate Conditions

Shot	Date	Target S/N	Material	Thickness (in)	Dist. from Target (in)	Comments about witness plate	Number of Impact Perfor-ations	Maximum Hole Dia. (mm)	Dia. of Dispersion Area of Conc. hits/perf (in)	half-angle of Conc. Hits (deg)	Dia. of all impacts (in)	Max. Disp. half-angle of any impact (deg)
NDE-23	04-Aug-87	6-T-6										
	NDE Shot #89											
NDE-24	04-Aug-87	6-T-9										
	NDE Shot #90											
NDE-25	04-Aug-87	MT-04										
	NDE Shot #91											
NDE-26	04-Aug-87	MD-03										
	NDE Shot #92											
NDE-27	04-Aug-87	MT-03										
	NDE Shot #93											
NDE-28	25-Aug-87	7-T-2										
	NDE Shot #94											

Shot Conditions

Shot	Date	Target S/N	Type	Layup	Nominal Thickness (in)	Fiber Modulus (Mpsi)	Proj. Mat'l	Proj. Dia. (mm)	Proj. Mass (mg)	Proj. Vel. (km/s)	Proj. Dens. (g/cc)	Dist. From C/L hole to C/L tube (mm)	Proj. Obliquity Angle Radially (on curve) (deg) 0=normal	Obliquity to Longitud. Axis (deg) 0=normal	Comments on Hi-speed Film &/or Shot (clean impact unless stated)
NDE-29	25-Aug-87 NDE Shot #96	8-T-2	Tube	10,30,10	0.133	34	Al2024-T4	1.57	5.66	4.88	2.796	8.6	20	0	
NDE-30	25-Aug-87 NDE Shot #97	9-T-2	Tube	80,30,10	0.071	34	Al2024-T4	1.57	5.68	5.49	2.796	1.8	4	0	Secondary impact away from impact point, does not interfere with data.
NDE-31	25-Aug-87 NDE Shot #98	9s-T-2	Tube	80,30,10	0.068	34	Al2024-T4	1.54	5.37	4.27	2.796	5.6	15	0	
NDE-32	25-Aug-87 NDE Shot #99	6s-T-2	Tube	10,30,10	0.064	34	Al2024-T4	1.54	5.35	7.01	2.796	1.8	4	0	
NDE-33	25-Aug-87 NDE Shot #100	6-F-1	Plate	10,30,10	0.061	34	Al2024-T4	1.55	5.41	6.10	2.796	NA	0	0	Dumbell shaped hole - probable double impact. Following hole info based on estimated projectile hole dimensions.
NDE-34	25-Aug-87 NDE Shot #101	11-F-1	Plate	10,30,10	0.073	75	Al2024-T4	1.54	5.37	5.79	2.796	NA	0	0	Large secondary impact produced irregular hole ~11mm in diameter. Other smaller secondary impacts also occured producing spall damage. Hole damage from projectile can be determined.
NDE-35	20-Oct-87 NDE Shot #102	9s-F-1	Plate	80,30,10	0.061	34	Al2024-T4	1.54	5.39	5.79	2.796	NA	0	0	Impact almost off edge of plate. Large secondary impacts caused shallow surface craters but a large amount of spall damage near proj.

Target Front Side Conditions: (outside of tube's 1st wall)

Shot	Date	Target S/N	Target Mass Before (g)	Target Mass After (g)	1st wall Hole Shape	Hole Dimensions Length (mm)	Hole Dimensions Width (mm)	Equiv. Circular Diameter (mm)	Crater (if evident) Dia. (mm)	Surface Peeling Number	Surface Peeling Length (mm)	Surface Peeling Width (mm)	Total Area (mm^2)	C-Scan Dimensions Area (mm^2)	C-Scan Dimensions Equiv. Circular Diameter (mm)	C-Scan Dimensions Actual Shape: Approx. Axial Length (mm)	C-Scan Dimensions Actual Shape: Overall (Circumf) Width (mm)	Comments on Target Condition (1st wall condition)
											9	1.3						½ in -10 deg. direction on interior surface.
NDE-29	25-Aug-87 NDE Shot #96	8-T-2			Rect.	2.8	2.8	3.2	4.6	4	30 32 47 22	1.0 1.5 0.8 0.8	130	343.2	20.9	24	14	Peeling in +10 deg. direction on front and -10 deg on 2nd surface interior, ~same length.
NDE-30	25-Aug-87 NDE Shot #97	9-T-2			Circ.	4.0		4.0	4.6	4	33 25 38 18	1.8 1.5 1.0 1.8	165	460.9	24.2	28	16	Peeling on exterior in +10 deg. direction while interior at -80 deg direction. Interior ply peeling stopped at interface where ply roll wrap started; this appears to indicate that peeling initiates at hole (while hole is forming) and does not result from transmition of stress waves through the bulk solid.
NDE-31	25-Aug-87 NDE Shot #98	9s-T-2			Rect.	2.5	2.5	2.9	4.3	2	7 15	3.2 1.5	45	138.5	13.3	9	15	Peeling on both front and back of 1st wall in +80 deg. direction and at ~same length.
NDE-32	25-Aug-87 NDE Shot #99	6s-T-2			Rect.	3.0	3.0	3.4	4.9	5	11 34 25 30 7	2.0 1.1 0.8 0.8 3.8	128	306.0	19.7	24	13	Peeling on both front and back of 1st wall in +10 deg. direction. Interior peeling slightly less than exterior.
NDE-33	25-Aug-87 NDE Shot #100	6-F-1			Circ.	4.1		4.1	5.1	4	22 10 11 12	2.5 3.0 1.0 1.5	114	396.7	22.5 (Reference plate C-scan length to 0 deg ply dir.)	30	13	Peeling on both front and back of plate in +10 deg. direction, with back peeling slightly shorter.
NDE-34	25-Aug-87 NDE Shot #101	11-F-1			Circ.	5.8		5.8	6.6	1	1	5.0	5					Can not resolve c-scan damage associated with projectile due to overlap with other secondary impact damage. Only slight peeling around hole.
NDE-35	20-Oct-87 NDE Shot #102	9s-F-1			Circ.	4.6		4.6	5.6	4	11 30 12 11	3.5 1.3 2 1	111					Can not resolve c-scan damage secondary impacts.

Target Second Side Conditions: (outside of tube's 2nd wall, or back side of plate)

Shot	Date	Target S/N	Hole Dimensions: 2nd wall Hole Shape	Hole Dimensions: Length (mm)	Hole Dimensions: Width (mm)	Hole Dimensions: Equiv. Circular Diameter (mm)	Surface Peelings: Number	Surface Peelings: Length (mm)	Surface Peelings: Width (mm)	C-Scan Dimensions: Total Area (mm^2)	C-Scan Dimensions: Equiv. Circular Diameter (mm)	C-Scan Dimensions: Area (mm^2)	C-Scan Dimensions: Equiv. Circular Diameter (mm)	C-Scan Dimensions: Actual Shape: Approx. Overall Length (mm)	C-Scan Dimensions: Actual Shape: Approx. Overall Width (mm)	Comments on Tubes 2nd Wall result in delamination/peeling of 2nd wall exterior.
NDE-29	25-Aug-87 NDE Shot #96	8-T-2														
NDE-30	25-Aug-87 NDE Shot #97	9-T-2					1	30	3	90	10.7	249.9	17.8	24	10	Craters concentrated within 0.9" circular area of 2nd wall interior, slight peeling on interior of 2nd wall in 80 deg. direction. Exterior delamination deepest in center.
NDE-31	25-Aug-87 NDE Shot #98	9s-T-2					2	21.5 15	2 1.25	62	8.9	259.3	18.2	15	17	Concentrated impacts on 2nd wall ~1.7" in diameter. Tube has a lot of porosity/voids as evident from c-scan.
NDE-32	25-Aug-87 NDE Shot #99	6s-T-2					5	46 66 24 21 6	1.5 1 0.8 0.5 0.1	164	14.5	314.8	20.0	26	12	Concentrated impacts on 2nd wall ~0.7" in diameter. Delaminations on exterior surface of 2nd wall in +10 deg. direction.
NDE-33	25-Aug-87 NDE Shot #100	6-F-1														
NDE-34	25-Aug-87 NDE Shot #101	11-F-1														
NDE-35	20-Oct-87 NDE Shot #102	9s-F-1														

Witness Plate Conditions

Shot	Date	Target S/N	Material	Thickness (in)	Dist. from Target (in)	Comments about witness plate	Number of Impact Perfor-ations	Maximum Hole Dia. (mm)	Dia. of Dispersion Area of Conc. hits/perf (in)	half-angle of Conc. Hits (deg)	Dia. of all impacts (in)	Max. Disp. half-angle of any impact (deg)
NDE-29	25-Aug-87 NDE Shot #96	8-T-2										
NDE-30	25-Aug-87 NDE Shot #97	9-T-2										
NDE-31	25-Aug-87 NDE Shot #98	9s-T-2										
NDE-32	25-Aug-87 NDE Shot #99	6s-T-2										
NDE-33	25-Aug-87 NDE Shot #100	6-F-1	Al6061-T6	0.032	0.25	Hole punched through.	1	4.6	0.18	36	0.49	63
NDE-34	25-Aug-87 NDE Shot #101	11-F-1	Al6061-T6	0.032	0.25	Smaller hole, large crater, in aluminum witness plate.	1	2	0.22	41	0.59	67
NDE-35	20-Oct-87 NDE Shot #102	9s-F-1	Al6061-T6	0.032	0.25	Hole punched out. No other dark debris as on other witness plates.	1	5.2	0.20	39	0.20	39

Shot Conditions

Shot	Date	Target S/N	Type	Layup	Nominal Thickness (in)	Fiber Modulus (Mpsi)	Proj. Mat'l	Proj. Dia. (mm)	Proj. Mass (mg)	Proj. Vel. (km/s)	Proj. Dens. (g/cc)	Dist. From C/L hole to C/L tube (mm)	Proj. Obliquity Angle Radially (on curve) (deg) 0=normal	Obliquity to Longitud. Axis (deg) 0=normal	Comments on Hi-speed Film &/or Shot (clean impact unless stated)
NDE-36	20-Oct-87 NDE Shot #103	12-F-1	Plate	80,30,10	0.072	75	Al2024-T4	1.55	5.45	3.96	2.796	NA	0	0	impact (typical of low speed secondary impacts). Peeling on one side of hole stopped by label.
NDE-37	20-Oct-87 NDE Shot #104	10-F-1	Plate	45,10,45	0.061	34	Al2024-T4	1.54	5.36	6.71	2.796	NA	0	0	Several large secondary impacts caused shallow surface craters & delaminations, and large back side spall region.
NDE-38	20-Oct-87 NDE Shot #105	13-F-1	Plate	45,10,45	0.072	75	Al2024-T4	1.54	5.38	5.18	2.796	NA	0	0	Definite double impact - duebell shaped hole. Extrapolated hole outline to derive hole size info.

Target Front Side Conditions: (outside of tube's 1st wall)

Shot	Date	Target S/N	Target Mass Before (g)	Target Mass After (g)	1st wall Hole Shape	Hole Dimensions Length (mm)	Hole Dimensions Width (mm)	Equiv. Circular Diameter (mm)	Crater (if evident) Dia. (mm)	Surface Peeling Number	Surface Peeling Length (mm)	Surface Peeling Width (mm)	Total Area (mm^2)	C-Scan Dimensions Area (mm^2)	C-Scan Dimensions Equiv. Circular Diameter (mm)	C-Scan Dimensions Actual Shape: Approx. Axial Length (mm)	C-Scan Dimensions Actual Shape: Overall (Circumf) Width (mm)	Comments on Target Condition (1st wall condition)
NDE-36	20-Oct-87 NDE Shot #103	12-F-1			Circ.	4.6		4.6	5.8	1	6	1.7	10	194.8	15.7 (Reference plate C-scan length to 0 deg ply dir.)	10	19	Previous void/fault area in plate originally interfered with C-scan measurements somewhat.
NDE-37	20-Oct-87 NDE Shot #104	10-F-1			Circ.	4.3		4.3	5.6	4	20 35 15 15	2.0 1.0 0.5 1	98					No c-scan information possible with large delamination area caused by secondary impacts.
NDE-38	20-Oct-87 NDE Shot #105	13-F-1			Circ.	5.5		5.5	7.5	1	3	7.0	21					Not possible to measure c-scan size with secondary impact damage.

Target Second Side Conditions: (outside of tube s 2nd wall, or back side of plate)

			Hole Dimensions				Surface Peelings					C-Scan Dimensions				
Shot	Date	Target S/N	2nd wall Hole Shape	Length (mm)	Width (mm)	Equiv. Circular Diameter (mm)	Number	Length (mm)	Width (mm)	Total Area (mm^2)	Equiv. Circular Diameter (mm)	Area (mm^2)	Equiv. Circular Diameter (mm)	Actual Shape: Approx. Overall Length (mm)	Width (mm)	Comments on Tubes 2nd Wall
NDE-36	20-Oct-87	12-F-1														
	NDE Shot #103															
NDE-37	20-Oct-87	10-F-1														
	NDE Shot #104															
NDE-38	20-Oct-87	13-F-1														
	NDE Shot #105															

Witness Plate Conditions

Shot	Date	Target S/N	Material	Thickness (in)	Dist. from Target (in)	Comments about witness plate	Number of Impact Perfor-ations	Maximum Hole Dia. (mm)	Dia. of Area of Conc. hits/perf (in)	Dispersion half-angle of Conc. Hits (deg)	Dia. of all impacts (in)	Max. Disp. half-angle of any impact (deg)
NDE-36	20-Oct-87 NDE Shot #103	12-F-1	Al6061-T6	0.032	0.25	Deep crater in aluminum, but no hole.			0.16	32	0.45	61
NDE-37	20-Oct-87 NDE Shot #104	10-F-1	Al6061-T6	0.016	0.25	Hole punched through, no other debris.	1	5.5	0.22	41	0.22	41
NDE-38	20-Oct-87 NDE Shot #105	13-F-1	Al6061-T6	0.032	0.25	No hole, no crater, little dark debris.						

Appendix B - Hercules Failure Criteria Study

SPACE STATION TRUSS TUBE

FAILURE CRITERIA STUDY

JULY 11, 1986

PREPARED FOR

EAGLE ENGINEERING INC.
HOUSTON, TEXAS

PREPARED BY

HERCULES INCORPORATED
AEROSPACE DIVISION
BACCHUS WORKS
MAGNA, UTAH

AUTHOR: R. G. Wendland, Jr.

AUTHOR: R. F. Cilensek

APPROVED BY: A. A. Vicario, Manager
Space Structures Programs

FOREWORD

This study was conducted for Eagle Engineering Incorporated, Houston Texas under A.O. 3215. The purpose of this study was to analytically determine the amount of damage a truss tube element of a given geometry and material design can sustain after hypervelocity impact by orbital debris or meteoroids.

This report summarizes the effort conducted by Hercules. Messrs. R. F. Cilensek and R. G. Wendland, Jr. were the Principal Investigators for Hercules. Messrs. W. Stump and E. Christiansen directed this study for Eagle Engineering. The period of performance was June 1, 1986 to July 11, 1986.

1.0 INTRODUCTION

The objective of this study was to analytically assess the effects of penetrations in Space Station truss tubes subjected to orbital debris and meteoroid impact. The goal was to predict the critical amount of damage which would cause failure of the baseline tube designs which will be tested in the light gas gun at NASA/JSC. Failure is considered as the point at which the tubes can no longer meet the design loads and/or stiffness requirements. In addition to the amount of damage, Hercules was asked to estimate the location along the tube length which is most critically affected by the damage.

The report presents the assumptions and analytical methods used and discusses approaches for the test program to extract meaningful data that can be used to correlate with the analytical predictions.

2.0 APPROACH

2.1 REQUIREMENTS

Requirements for the tubes were provided by Eagle and are summarized in Table I.

Two tube geometries were supplied for analysis. The first was a longeron and batten tube of 16.4 feet in length. The second was a diagonal member of 23.2 feet in length. Both tubes have a 2.0 inch outside diameter and a wall thickness of 0.066 inches. It was agreed in the initial telecon with Eagle Engineering that the 16.4 foot truss member would be the focus of this analysis. The ultimate load of this truss member is 2,134 pounds in tension and compression. For analysis of the tube, the assumed end conditions are critical. It was agreed in the telecon that the analysis would assume both ends of the tube fixed.

2.2 MATERIAL PROPERTIES

The baseline tube design specifies a layup of $(\pm 10°, \pm 30°, \pm 10°)_2$. The baseline material is AS4/3501-6. Tubes of the same layup but using P75 graphite-epoxy will also be tested at NASA/JSC, and we were asked to provide some insight into the effects of using a high modulus material such as P75. Table II presents lamina material properties for AS4/3501-6 and P75/3501-6 and Table III presents the predicted laminate properties for the designed layup. Laminate properties were determined using laminated plate theory. The laminate strength values are based on first ply failure using the maximum strain failure criterion. Table IV presents a comparison of the axial (EA), bending (EI), and torsional (GJ) stiffnesses of the baseline layup for AS4/3501-6 and P75/3501-6.

2.3 ANALYSIS

The failure mode which is critical in the damaged truss tube is a stability failure under compression. Therefore, the analysis was focused on predicting the amount of damage that would cause a stability failure. In selecting an appropriate analytical technique two objectives had to be achieved: 1) the analysis had to correlate to the six inch test specimen, and 2) the analysis had to predict the effect of damage on the full length member. Based on these two requirements, two separate numerical finite element models were used. One model represented the six inch test specimen, the other the full length tube.

The first model was used to discreetly model the applied damage in the six inch test specimen. Two types of damage would occur in the test specimen: 1) through hole penetration, and 2) a large surrounding zone of delamination. In the finite element model, the damage was modeled by completely degrading the mechanical properties of the elements in the damage zone. This assumption was made because it is not obvious how much stiffness is lost in the delamination area. Mechanical testing of the damaged tubes will provide more insight to the actual effect of the delamination zone. For this analysis, completely degrading the properties in the delamination zone is conservative.

TABLE I

TRUSS TUBE REQUIREMENTS

- MATERIAL

  AS4/3501-6

- LAYUP

  $(\pm 10°, \pm 30°, \pm 10°)_2$

- GEOMETRY

  LENGTHS

  LONGERSON & BATTENS = 16.4 FT (TEST PIECES ARE 6 IN. LONG)
  FACE & BATTEN DIAGONALS = 23.2 FT

  THICKNESS = 0.066 IN.

  OUTSIDE DIAMETER = 2.0 IN.

- ULTIMATE LOADS

  AXIAL TENSION AND COMPRESSION

  LONGERONS & BATTENS = 2,134 LB
  FACE DIAGONALS = 1,200 LB

TABLE II

NOMINAL UNIDIRECTIONAL MATERIAL PROPERTIES FOR AS4/3501-6 AND P75/3501-6

PROPERTY	AS4/3501-6	P75/3501-6
LONGITUDINAL MODULUS, E_{11} (msi)	20.7	40.9
TRANSVERSE MODULUS, E_{22} (msi)	1.40	1.63
POISSON'S RATIO, ν_{12}	0.30	0.26
IN-PLANE SHEAR MODULUS, G_{12} (msi)	0.71	1.50
LONGITUDINAL COEFFICIENT OF THERMAL EXPANSION, 10^{-6} IN/IN/°F	-0.035	-0.543
TRANSVERSE COEFFICIENT OF THERMAL EXPANSION, 10^{-6} IN/IN/°F	11.8	16.0
LONGITUDINAL TENSION STRENGTH, S_{11}^{T} (ksi)	253.0	96.5
LONGITUDINAL COMPRESSIVE STRENGTH, S_{11}^{C} (ksi)	174.0	54.4

TABLE III

NOMINAL PROPERTIES FOR $[\pm 10, \pm 30, \pm 10]_2$ LAMINATE OF AS4/3501-6 AND P75/3501-6

PROPERTY	AS4/3501-6	P75/3501-6
AXIAL MODULUS, E_x (msi)	15.3	29.9
TRANSVERSE MODULUS, E_y (msi)	1.68	2.44
POISSON'S RATIO, υ_{xy}	1.03	1.21
IN-PLANE SHEAR MODULUS, G_{xy} (msi)	2.23	4.44
AXIAL COEFFICIENT OF THERMAL EXPANSION, 10^{-6} IN/IN/°F	-0.67	-1.25
TRANSVERSE COEFFICIENT OF THERMAL EXPANSION, 10^{-6} IN/IN/°F	8.77	9.32
AXIAL TENSION STRENGTH, S_x^T (ksi) (1)	90.7	75.6
AXIAL COMPRESSIVE STRENGTH, S_x^C (ksi) (1)	46.2	42.6

[1] First ply failure--maximum strain criterion.

TABLE IV

COMPARISON OF AS4/3501-6 AND P75/3501-6 TRUSS TUBE STIFFNESS

PROPERTY	AS4/3501-6 LAMINATE (1)	P75/3501-6 LAMINATE (1)
AXIAL STIFFNESS, EA (lb)	6.14×10^6	12.0×10^6
BENDING STIFFNESS, EI (lb-in^2)	2.87×10^6	5.61×10^6
TORSIONAL STIFFNESS, GJ (lb-in^2)	0.84×10^6	1.66×10^6

[1] Laminate: $[\pm 10, \pm 30, \pm 10]_2$

The second model used was a finite element beam model. The full length of the tube was used in this model. The beam model was divided into six inch segments. Thus, the damage could be positioned along the length of the tube model to determine the most critical location.

Using the discreet model in conjunction with the beam model, the analytical objectives were achieved. From the detailed test specimen model, the degraded stiffness (EI) due to damage was determined. This information can be compared to actual test results. The degraded stiffness from this analysis was then applied to the full length model to determine at what compression load collapse occurred.

The detailed model of the six inch test segment was developed with 3-D solid elements. The ADINA finite element program was used for analysis. The model was fixed at one end and loaded at the other end. Figure 1 shows a schematic of the loading and boundary conditions. The loading subjects the model to combined cantilever bending and shear. The deflection of the model is then used to determine the effective stiffness of the segment. In order to verify the model, the results for the undamaged case was compared to the closed form solution for a cantilevered beam which is:

$$\delta = \frac{PL^3}{3EI} + \frac{6PL}{5AG} \qquad (1)$$

Where:
- δ = deflection
- P = load
- L = length
- E = effective axial modulus
- G = effective shear modulus
- I = area moment of inertia
- A = tube cross-sectional area

6PL/5AG is included for shear deflection. The comparison between the closed form solution and the finite element solution was within 1%. The details of this comparison are presented in Appendix A. Using this technique, the effective stiffness (EI) can be solved from Equation (1) as:

$$EI = \frac{PL^3}{3\left[\delta - \frac{6PL}{5AG}\right]}$$

Thus, if the shear deflection is assumed to be constant in the presence of damage, the stiffness (EI) can be calculated from the model. This technique was used to determine stiffness for different levels of damage.

The beam finite element model was used to predict the critical load at which the full length truss tube member fails. The model consists of six inch beam segments. The model has fixed end conditions with an axial load on the end. Figure 2 is a schematic of the end conditions and loading. The analysis code used was the ADINA finite element program. In this model, the load is applied incrementally; the analysis code solves for equilibrium at each load step. When a load step is reached where equilibrium convergence is not reached, the solution method assumes that the critical load has been reached, and the structure is unstable. To verify this model, an undamaged column solution was compared to the closed form Euler column buckling solution.

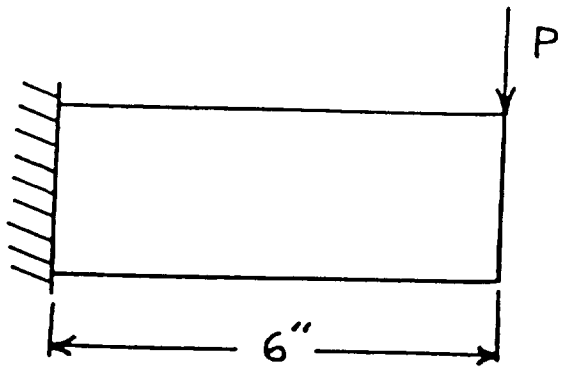

Figure 1. Test Segment Model Schematic

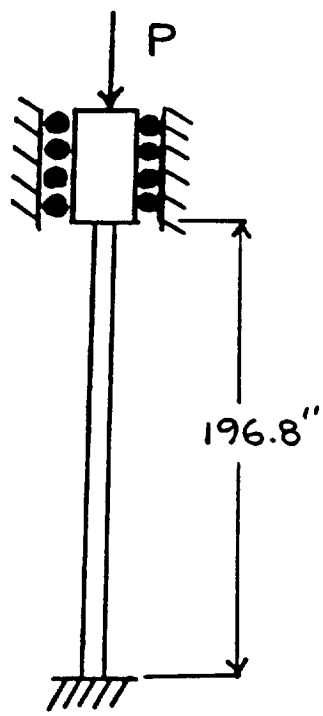

Figure 2. Beam Model Schematic

The finite element solution predicted the same critical load as the Euler's equation. The details of this comparison are shown in Appendix A. To include damage in the model, the stiffness (EI) is degraded in one of the elements. The stiffness for a damaged state is predicted using the 6 inch long tube finite element model. From these analysis methods, it is therefore possible to predict failure loads at different levels of damage in the tube. This model does not, however, account for the local moment generated at the point of damage. This moment is due to the eccentricity caused by a shift in the neutral axis of the tube due to the damage. The induced moment will contribute to a stability failure. Because this eccentric loading is not analyzed herein, the collapse results are unconservative.

3.0 RESULTS

The analysis approach described in Section 2.0 was used to determine the critical amount of damage in the truss tubes. Several failure modes were considered prior to performing the analysis. These failure modes included removal of part of the first wall of the tube, a hole through the first wall with damage to the second wall, and holes through both walls. After evaluation, it was concluded that a hole through the first wall was the most critical case since it produced an unsymmetrical condition in the tube which would more severely affect the tube stability under compressive loads.

Figure 3 shows an example of the damage modeled in the test specimen model. The unshaded elements have had their properties eliminated. Damage was modeled on one side of the tube and the damage zone was located at mid column. Figure 4 is a plot of the damage area versus the bending stiffness (EI). Using these degraded stiffnesses, the corresponding critical loads were predicted using the column stability model. The results are presented in Figure 5. Using this plot, the approximate amount of damage to cause failure at the ultimate load was determined. By this analysis approach, the amount of damage to cause failure is approximately 5.4 in^2 for the ultimate load. This area is the total amount of damage including the delamination zone. The two assumptions in the analysis that most strongly effect the results are: 1) the tube had fixed end conditions, and 2) the delamination zone is considered to have no residual stiffness.

Using the beam finite element model, the position of the damage along the length was also varied. Three locations along the length were investigated: 1) the end, 2) one quarter, and 3) halfway. The analysis showed that damage was equally critical at the center and the ends. The plots in Figures 4 and 5 are for the center position. Damage at one quarter of the length was found to be less critical. This can be explained by the fact that the quarter point is an inflection point in a fixed-fixed column, and the moment is subsequently zero.

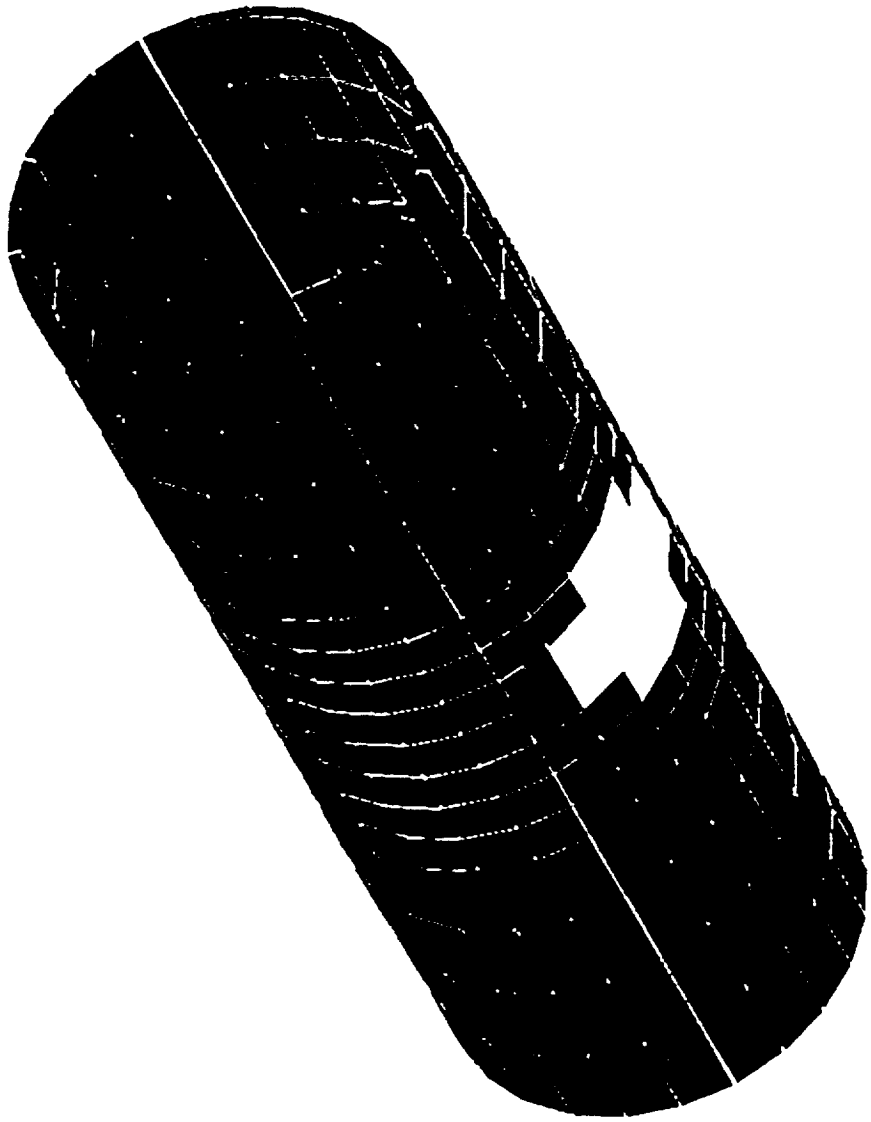

Figure 3. Damage Example

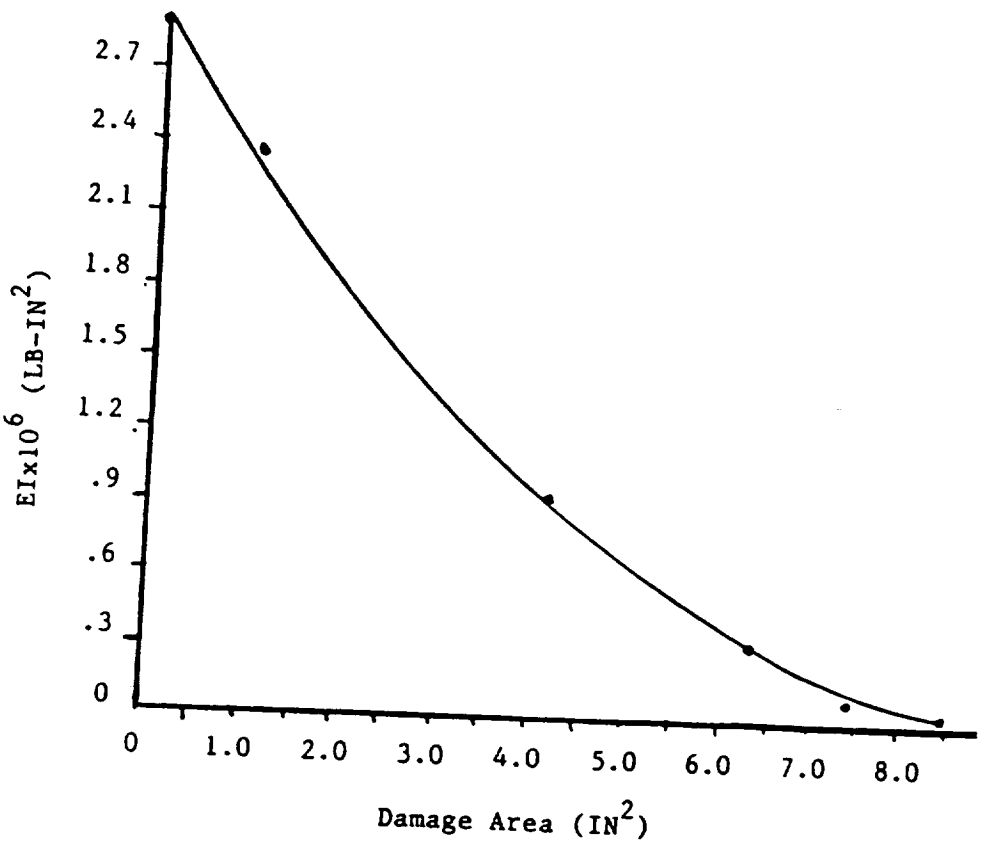

Figure 4. Damage Area Versus Stiffness

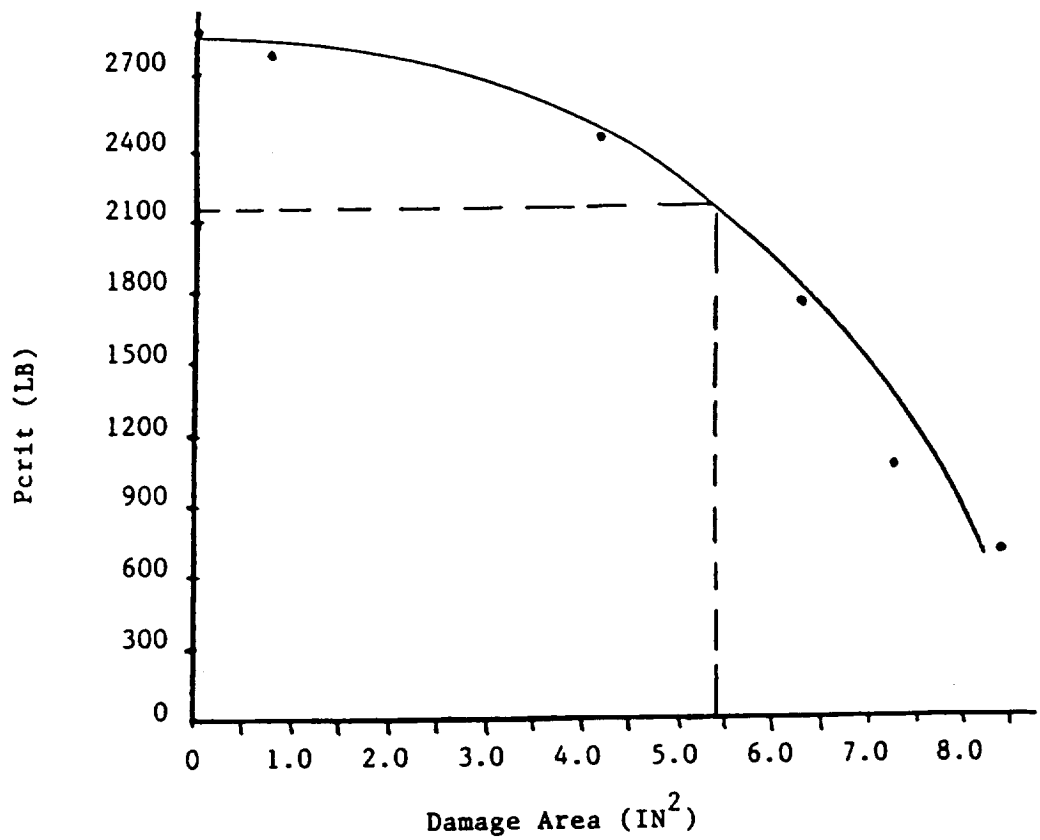

Figure 5. Damage Area Versus Critical Load

4.0 CONCLUSION

In conclusion, the critical amount of damage to cause failure under the ultimate load was determined. This area was 5.4 in^2 and was located at the center or ends of the truss member.

The analytical technique developed in this analysis can be used in future truss tube damage studies. This technique can be applied to different end conditions, geometries, layup, and materials.

The analysis conducted in this study were for tubes made from AS4/3501-6. Tubes made using the very high modulus P75/epoxy material will also be tested in the NASA/JSC test program. Because P75/epoxy composites have much higher stiffness and lower strength/strain, they would be expected to be more sensitive to impact damage than lower modulus, high strength materials. Increased damage zones could result in lower tube stability even though the basic material modulus is high.

The boundary conditions used in this analysis identified the critical location for damage along the tube length to be at the mid-length and end points. Other boundary conditions would produce different critical locations along the tube length. In order to quantify an effective length for damage, it would be necessary to perform a more detailed study of the effect of boundary conditions on tube damage.

5.0 RECOMMENDATIONS

In the analysis of the six inch specimen, the model was subjected to bending to determine stiffness (EI). During the pre and post characterization of tubes to be inspected at NASA/JSC, it is recommended that bending tests be conducted. By bending the test specimen and measuring deflection, the actual tube stiffness can be determined. This will provide a correlation between analysis and testing. It is recommended that bending tests be performed before and after the tube is damaged. Performing a C-scan of the damage will provide the information for more accurate modeling of damage in the analysis models. In addition, by testing tubes in bending, the effects of the delamination zone on stiffness can be assessed, and this information could be included in analysis models for more accurate predictions.

Additional analysis of different damage states is an obvious extension of this work. The damage modeled in this analysis was a penetration and damage zone on one side of the tube. It is likely that damage will occur on both sides of the tube from a hypervelocity impact. Using the detailed damage model of the test specimen, this damage state could be modeled. The same approach to predict the critical load versus damage area could also be used.

As stated previously, the beam finite element model does not account for the eccentric loading at the damage zone. To address this problem, some additional analysis work would be required. One approach to account for eccentricity is to extend the detailed damage model to the full length of the truss member. This model could then be incrementally loaded to determine the critical load.

APPENDIX A

COMPARISON BETWEEN FINITE ELEMENT & CLOSED FORM SOLUTIONS

Appendix A

Deflection Comparison for test Segment model.

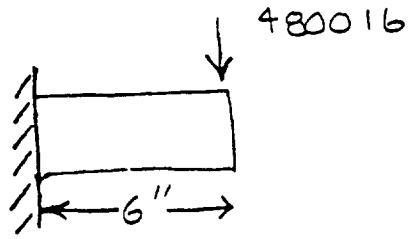

• Undamaged Segment

From finite element analysis the deflection is:

$$\delta = 0.18 \text{ IN} \checkmark$$

Closed form

$$\delta = \frac{PL^3}{3EI} + \frac{6PL}{5AG}$$

$$G \simeq \frac{G12 + G13}{2} = \frac{2.23 \text{ MSI} + 0.65 \text{ MSI}}{2}$$

$$= 1.44 \text{ MSI}$$

$$\delta = \frac{(4800 \text{ LB})(6 \text{ IN})^3}{(3)(2.87 \times 10^6 \text{ LB-IN}^2)} + \frac{(6)(4800 \text{ LB})(6 \text{ IN})}{(5)(.401 \text{ IN}^2)(1.44 \times 10^6 \text{ psi})}$$

$$= 0.12 + 0.06 = 0.18 \text{ IN} \checkmark$$

ENGR.	Wendland	6/21	REVISED	DATE	HERCULES ENGINEERING DEPARTMENT	SKETCH NO. 1 OF 2
CHECK						PROJECT NO.
APR					TITLE Space Station Truss Tube Damage Analysis	
					232	PLANT

Buckling load comparison for the full length beam model.

• Fixed-fixed column

From the finite element results the critical load is:

$$P_{crit} = \underline{2916\ LB}$$ ✓

Closed form

Fixed-fixed

$$L_e = \frac{L}{2}$$

$$P_{crit} = \frac{\pi^2 E I}{L_e^2}$$

$$= \frac{4\pi^2 E I}{L^2}$$

$$= \frac{4\pi^2 (2.87 \times 10^6\ LB\text{-}IN^2)}{(196.8\ IN)^2}$$

$$= \underline{2925\ LB}$$ ✓

ENGR.	Wendland	6/21	REVISED	DATE	HERCULES ENGINEERING DEPARTMENT	SKETCH NO. 2 OF 2
CHECK						
APR					TITLE Space Station Truss	PROJECT NO.
					233 Tube Damage Analysis	PLANT

For AS4/3501-6 Tube Laminates

Property	Unit	$(\pm 10, \pm 30, \pm 10)_n$*	$(\pm 80, \pm 30, \pm 10)_2$	$(\pm 45, \pm 10, \pm 45)_2$
E_{11}	MSI	15.3	10.7	8.04
E_{22}	MSI	1.68	7.64	3.55
E_{33}	MSI	1.45	1.54	1.53
G_{12}	MSI	2.23	2.23	3.98
G_{13}	MSI	.681	.606	.622
G_{23}	MSI	.518	.572	.558
ν_{12}	—	1.03	.244	.769
ν_{13}	—	.036	.291	.103
ν_{23}	—	.309	.306	.237
CTE_{11}	10^{-6} IN/IN/F°	-.665	.615	-.126
CTE_{22}	10^{-6} IN/IN/F°	8.77	1.29	2.67

* n = 2, 3, 4

SKETCH NO. 1 OF 1
PROJECT NO.
PLANT Bacchus

HERCULES ENGINEERING DEPARTMENT

TITLE Truss Tube Laminates

ENGR.	Wendland	7/8	
CHECK			
APR			

REVISED | DATE

BW-6000/1102 (6-85)

HER 1951-2
PRINTED IN U.S.A.

HERCULES INCORPORATED
ENGINEERING DEPARTMENT

SKETCH NO. 1/4

PLANT _____ PROJECT NO. _____ DATE 7-1-86 AUTHOR Cilensek

BLDG. _____ TITLE SUMMARY OF DAMAGE ANALYSIS

- Figure 1 - Bending deflection of short damaged tube

- Figure 2 - Bending stiffness (EI) of damaged tube

$$\delta = \frac{PL^3}{3EI} + \frac{6PL}{5AG}$$

- Figure 3 - Critical compressive load on 16.4' truss tube. Determined by modeling a local decrease in "EI" in a full length tube.

  Note: Solution agrees with Euler equation for undamaged case.

- Assumptions

  1) Damage area = 100% Delamination area

  2) Fixed-Fixed end condition

- Any Questions Call,

  Rob Cilensek (801) 251-6076

  or Ron Wendland (801) 251-6078

HER 1951
PRINTED IN U.S.A.

HERCULES INCORPORATED
ENGINEERING DEPARTMENT

SKETCH NO. 2/4

PLANT _____ PROJECT NO. _____ DATE 7-1-86 AUTHOR _____

BLDG. _____ TITLE TUBE DAMAGE

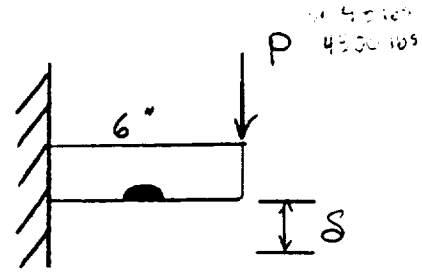

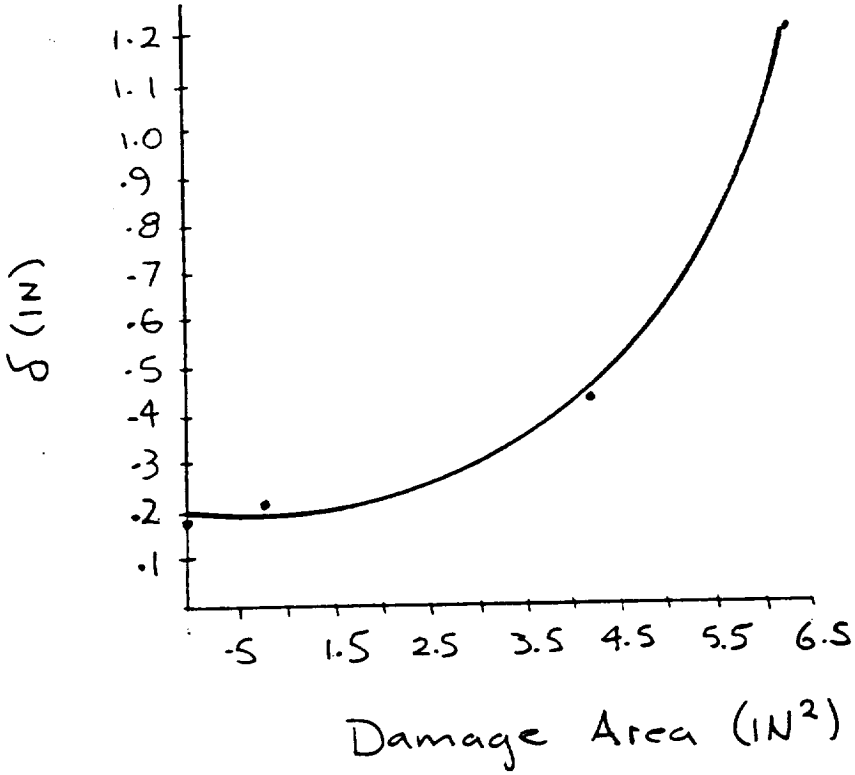

Figure 1.

HER 1951
PRINTED IN U.S.A.

HERCULES INCORPORATED
ENGINEERING DEPARTMENT

SKETCH NO. 3/4

PLANT _____ PROJECT NO. _____ DATE 7-1-86 AUTHOR _____

BLDG. _____ TITLE TUBE DAMAGE

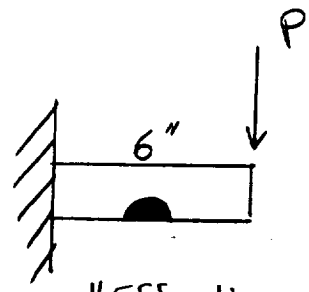

"Effective Bending Stiffness, EI"

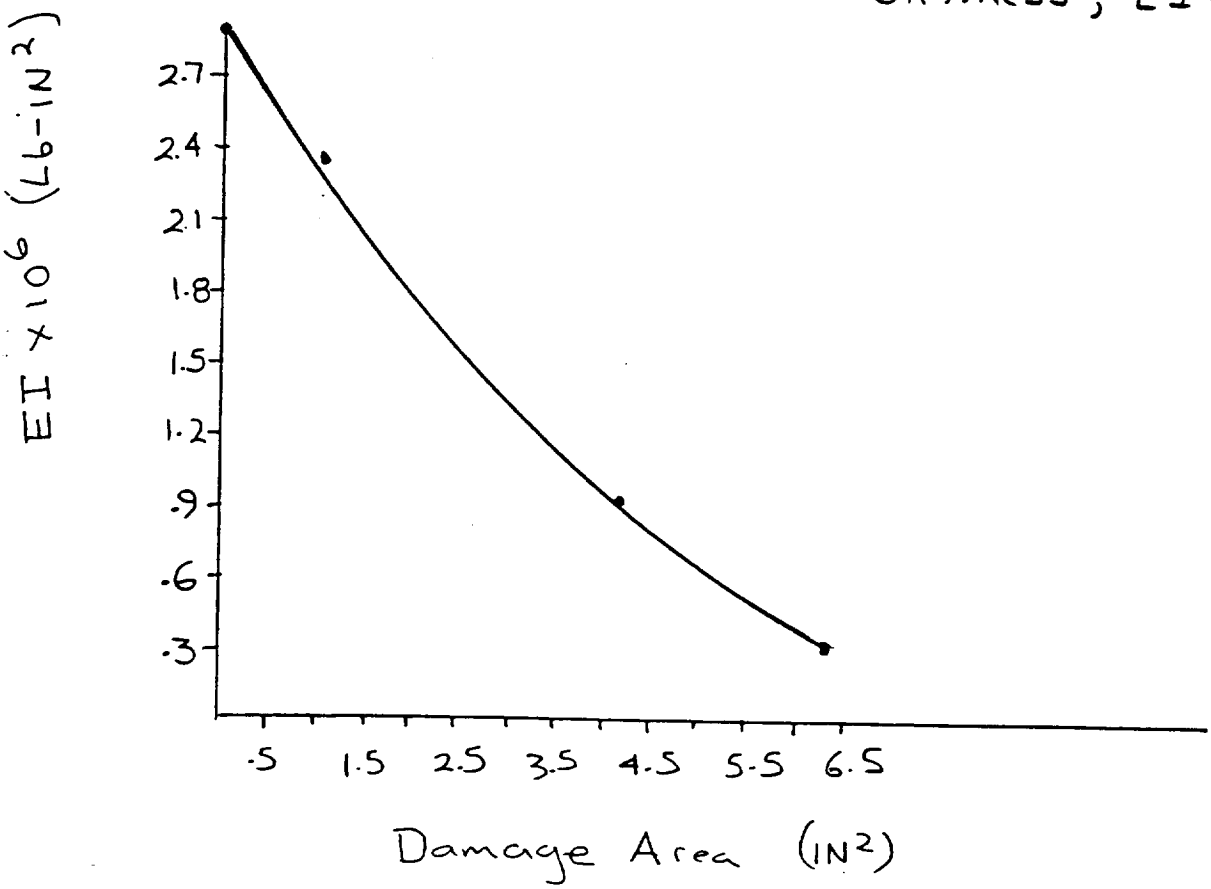

Figure 2.

HER 1951
PRINTED IN U.S.A.

HERCULES INCORPORATED
ENGINEERING DEPARTMENT

SKETCH NO. 4/4

PLANT _____ PROJECT NO. _____ DATE 7-1-86 AUTHOR _____

BLDG. _____ TITLE TUBE DAMAGE

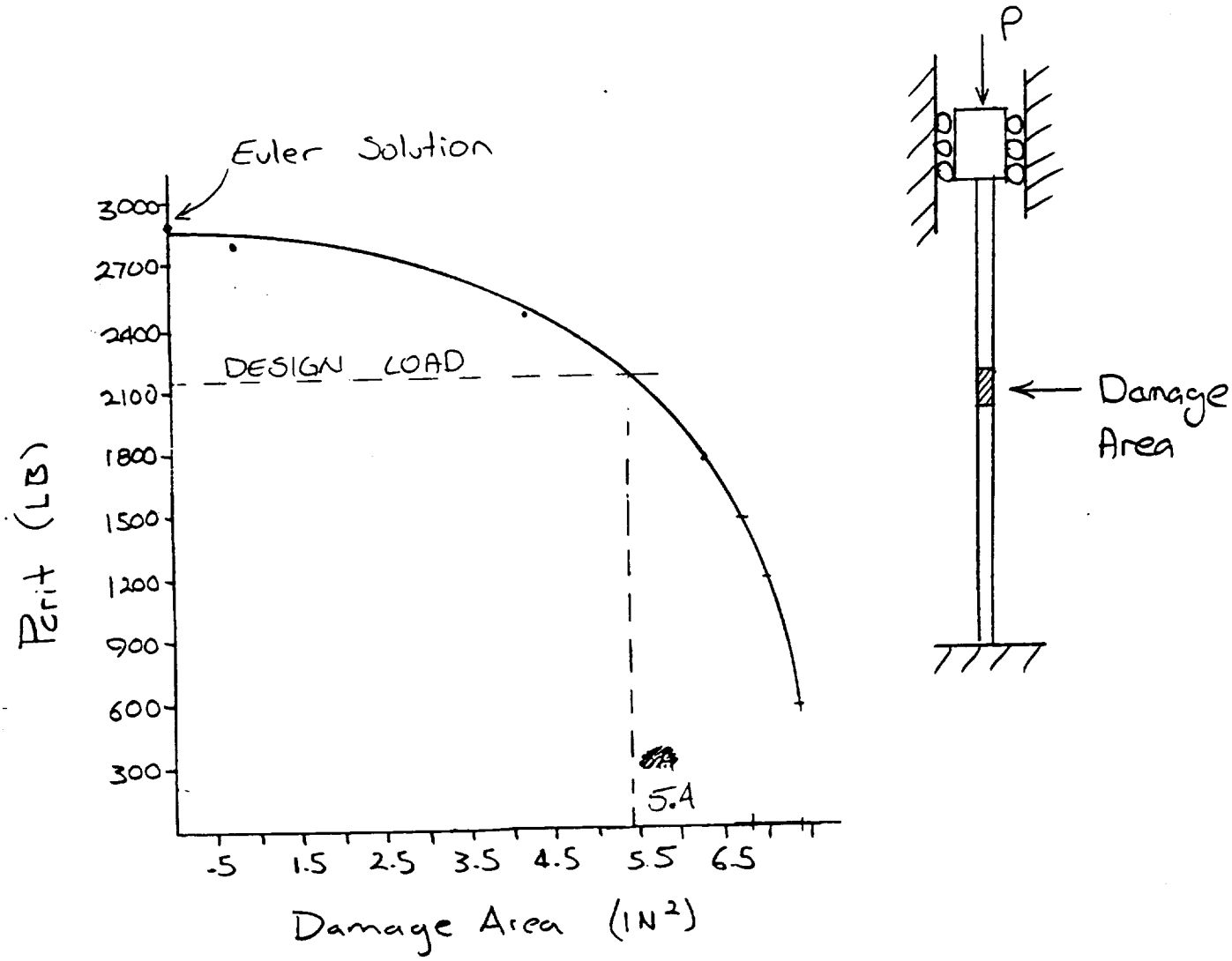

Figure 3.

Appendix C - C-Scan Records

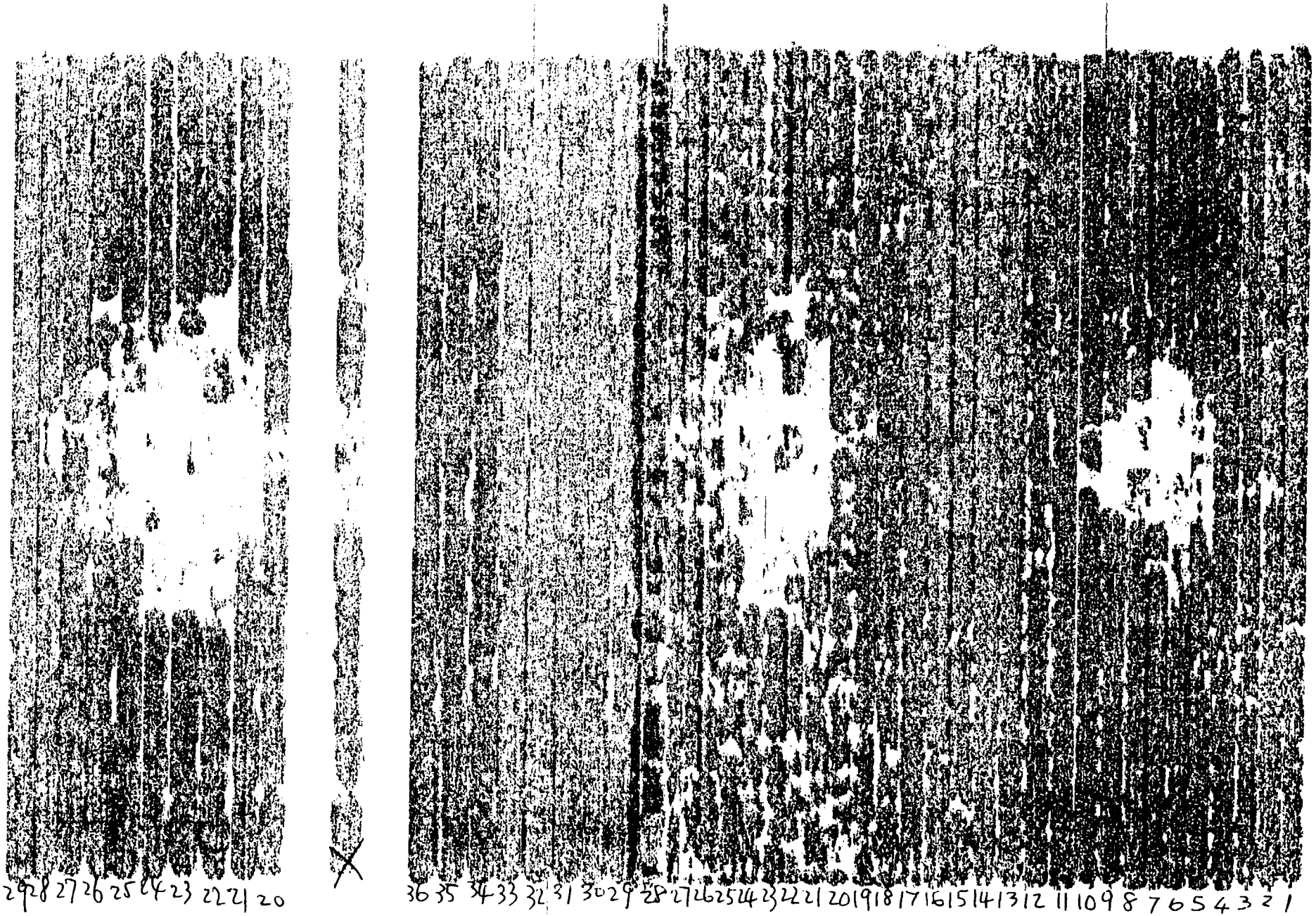
36 35 34 33 32 31 30 29 28 27 26 25 24 23 22 21 20 19 18 17 16 15 14 13 12 11 10 9 8 7 6 5 4 3 2 1
29 28 27 26 25 24 23 22 21 20

6-S-T-1

6-S-T-1

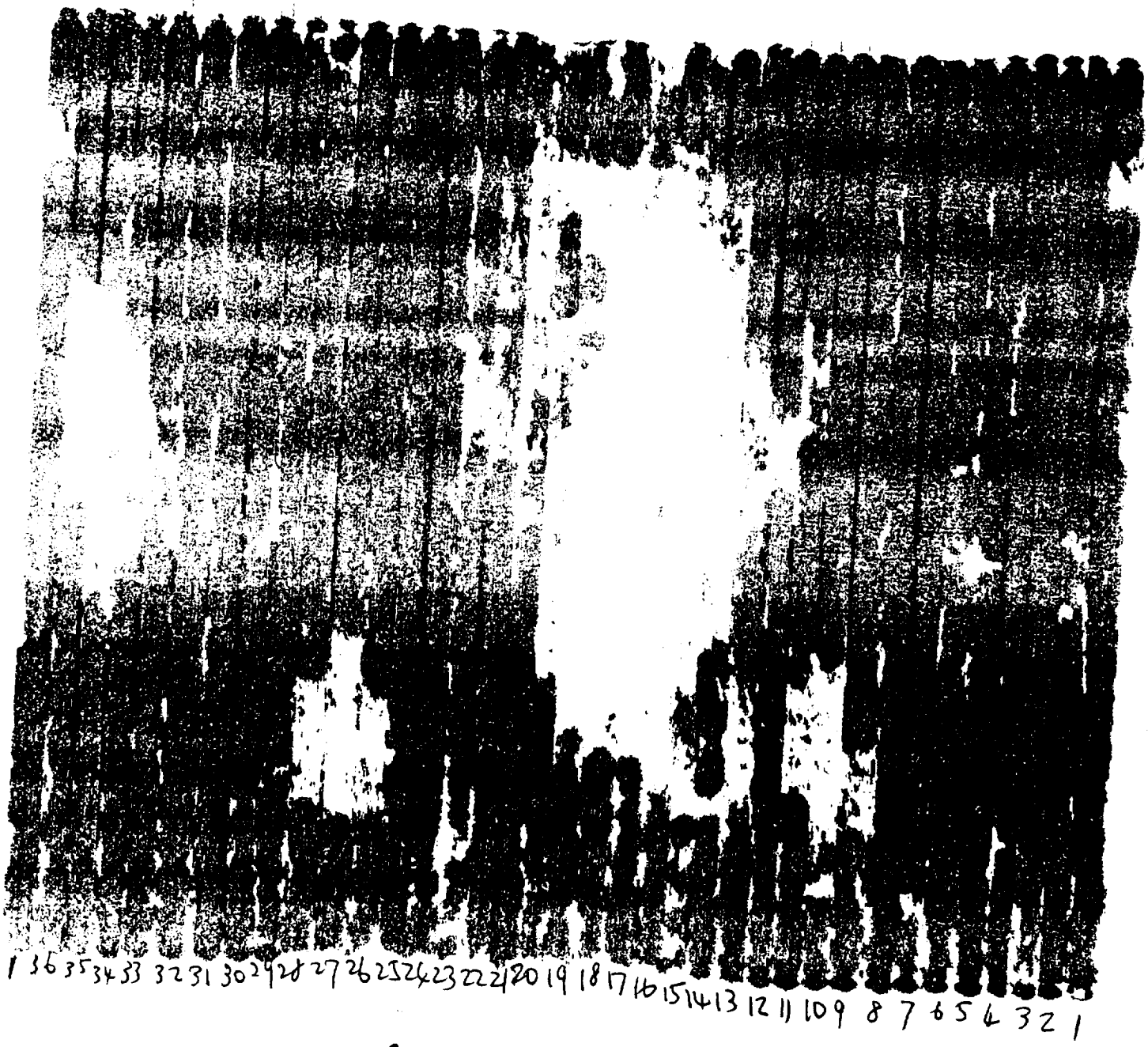
1 36 35 34 33 32 31 30 29 28 27 26 25 24 23 22 21 20 19 18 17 16 15 14 13 12 11 10 9 8 7 6 5 4 3 2 1

6s-T-2

6-T-1

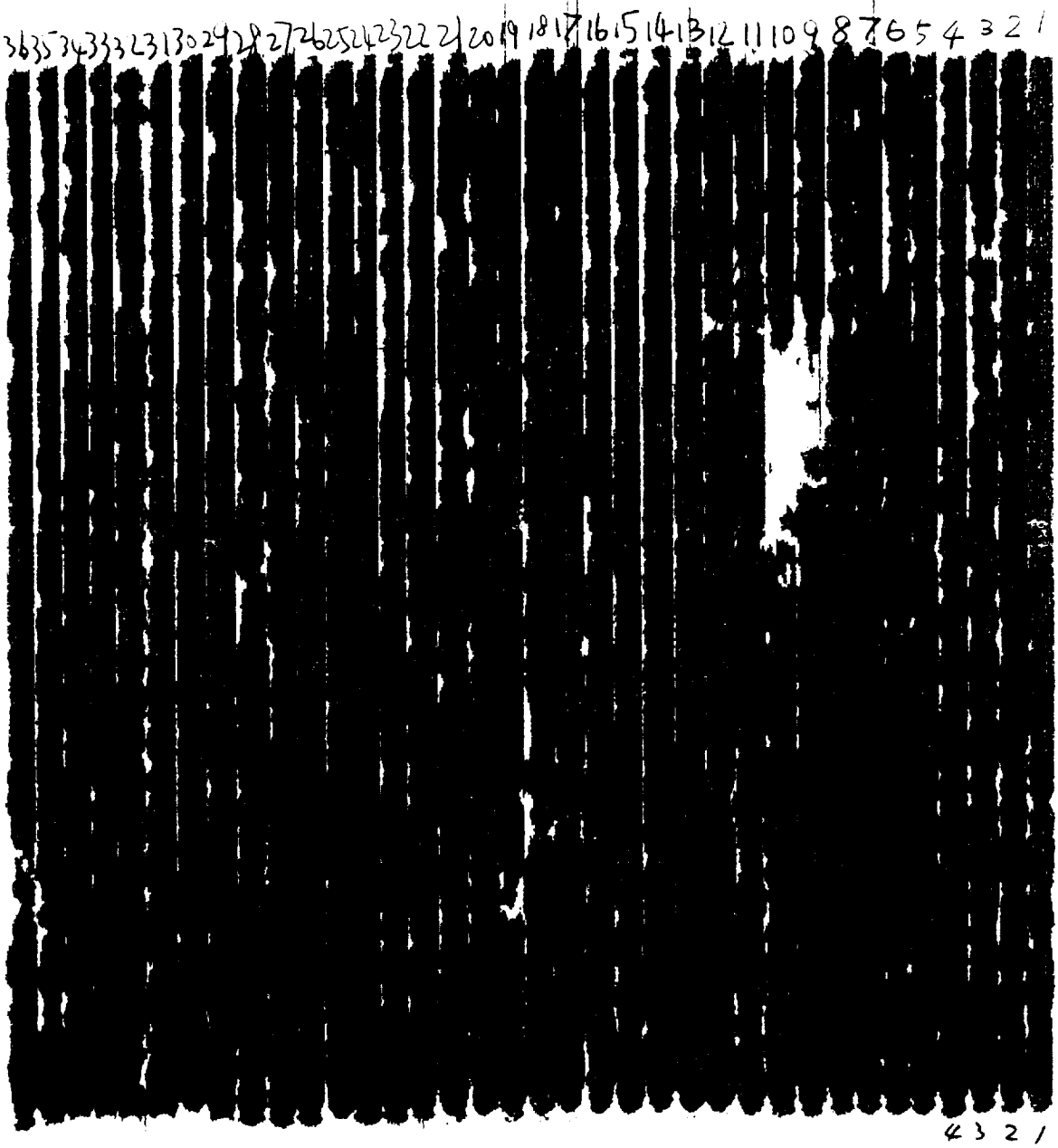

6-T-1

15-25 40 RT DL
H 28 4
H 10
1

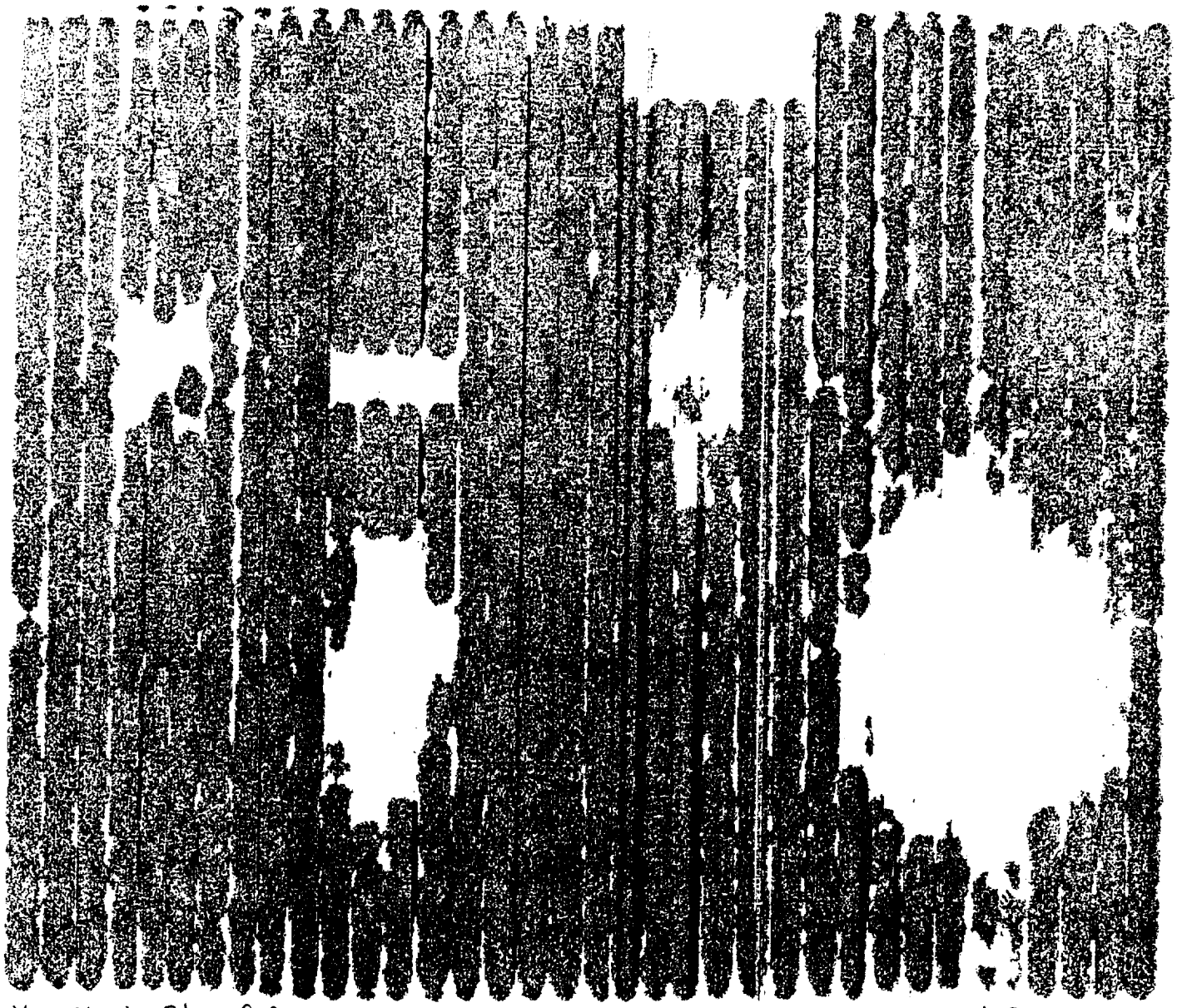

36 35 34 33 32 31 30 29 28 27 26 25 24 23 22 21 20 19 18 17 16 15 14 13 12 11 10 9 8 7 6 5 4 3 2 1

6-T-2

6-T-3

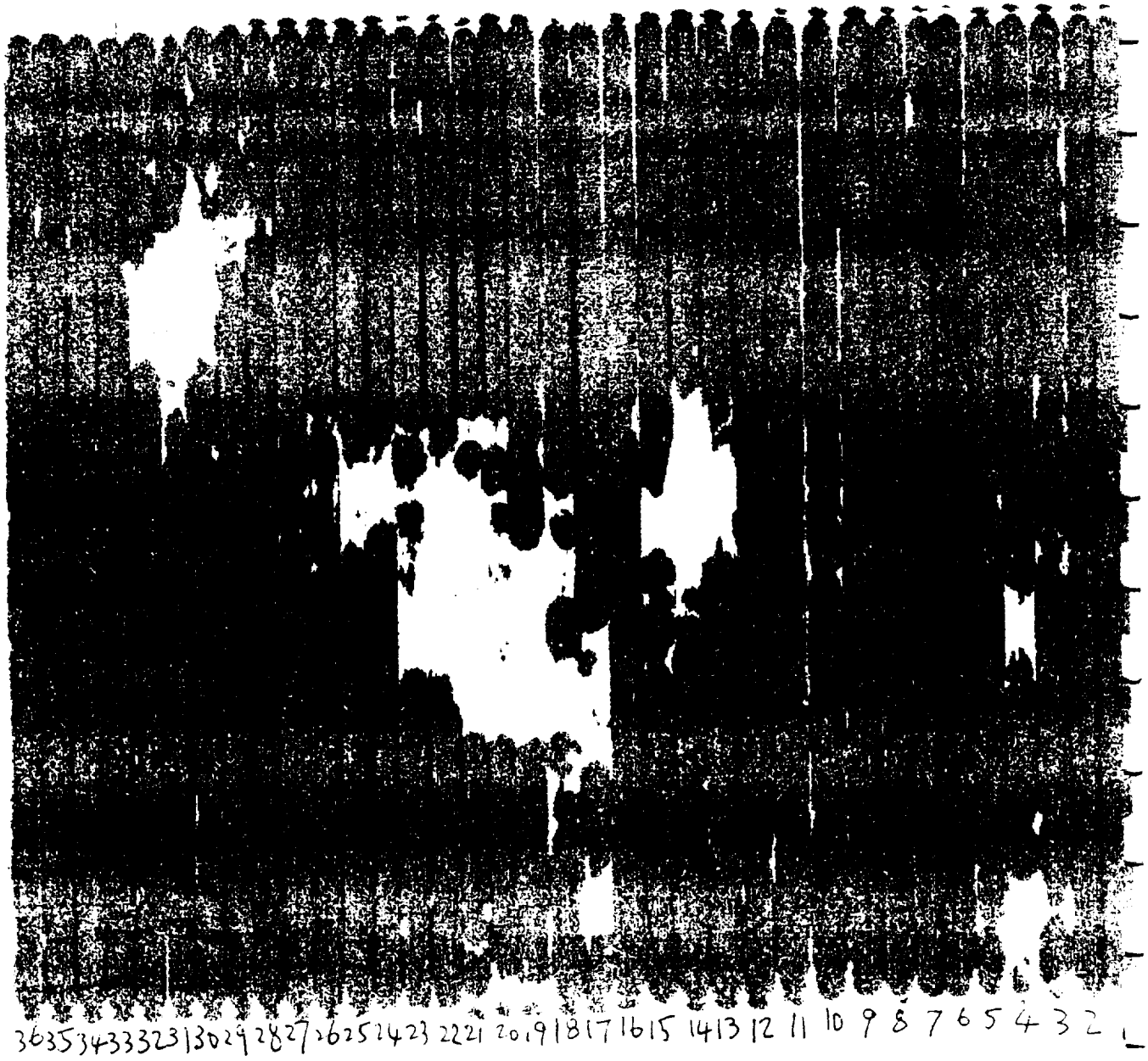
36 35 34 33 32 31 30 29 28 27 26 25 24 23 22 21 20 19 18 17 16 15 14 13 12 11 10 9 8 7 6 5 4 3 2

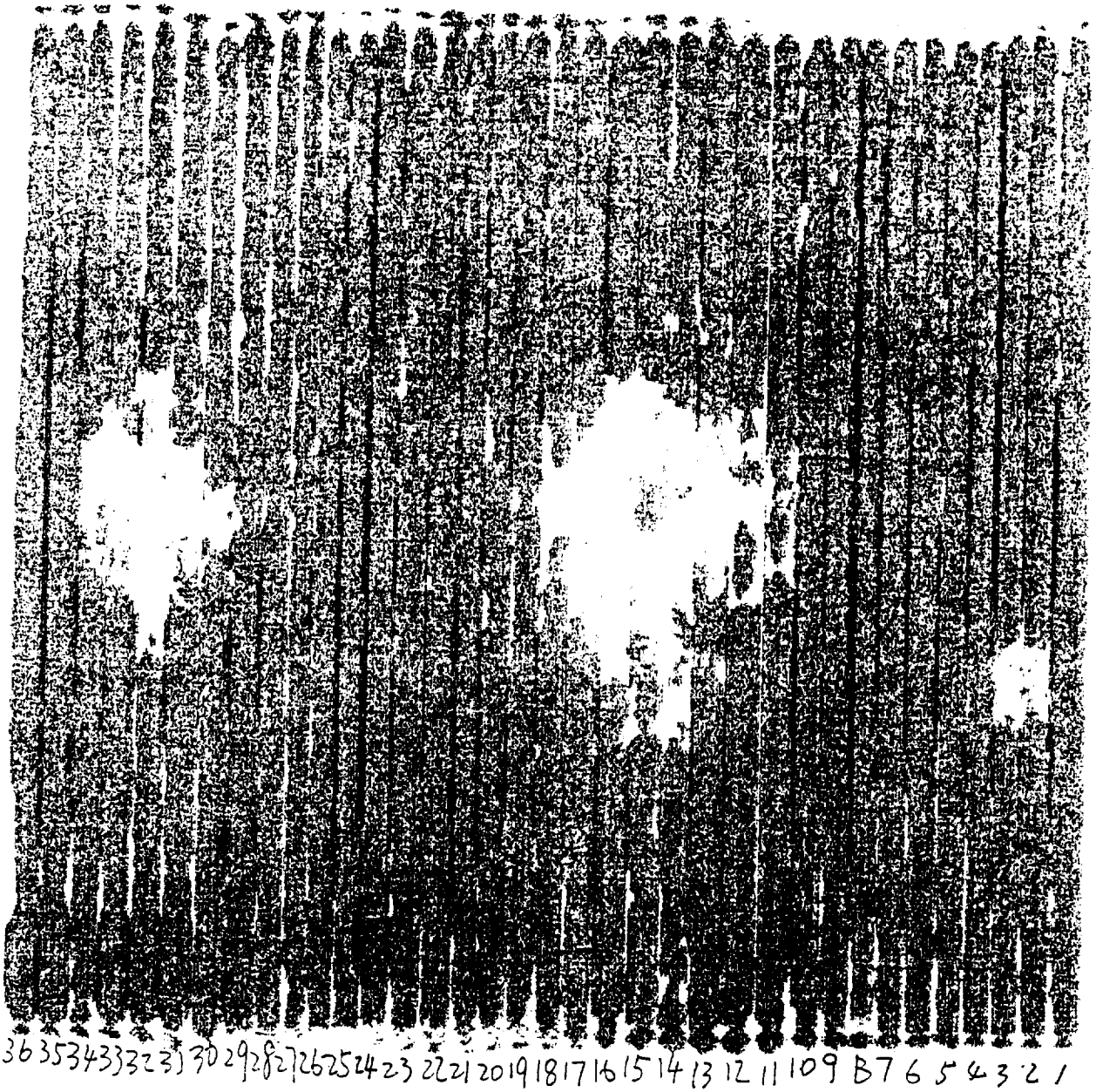
36 35 34 33 32 31 30 29 28 27 26 25 24 23 22 21 20 19 18 17 16 15 14 13 12 11 10 9 8 7 6 5 4 3 2 1

6-T-4

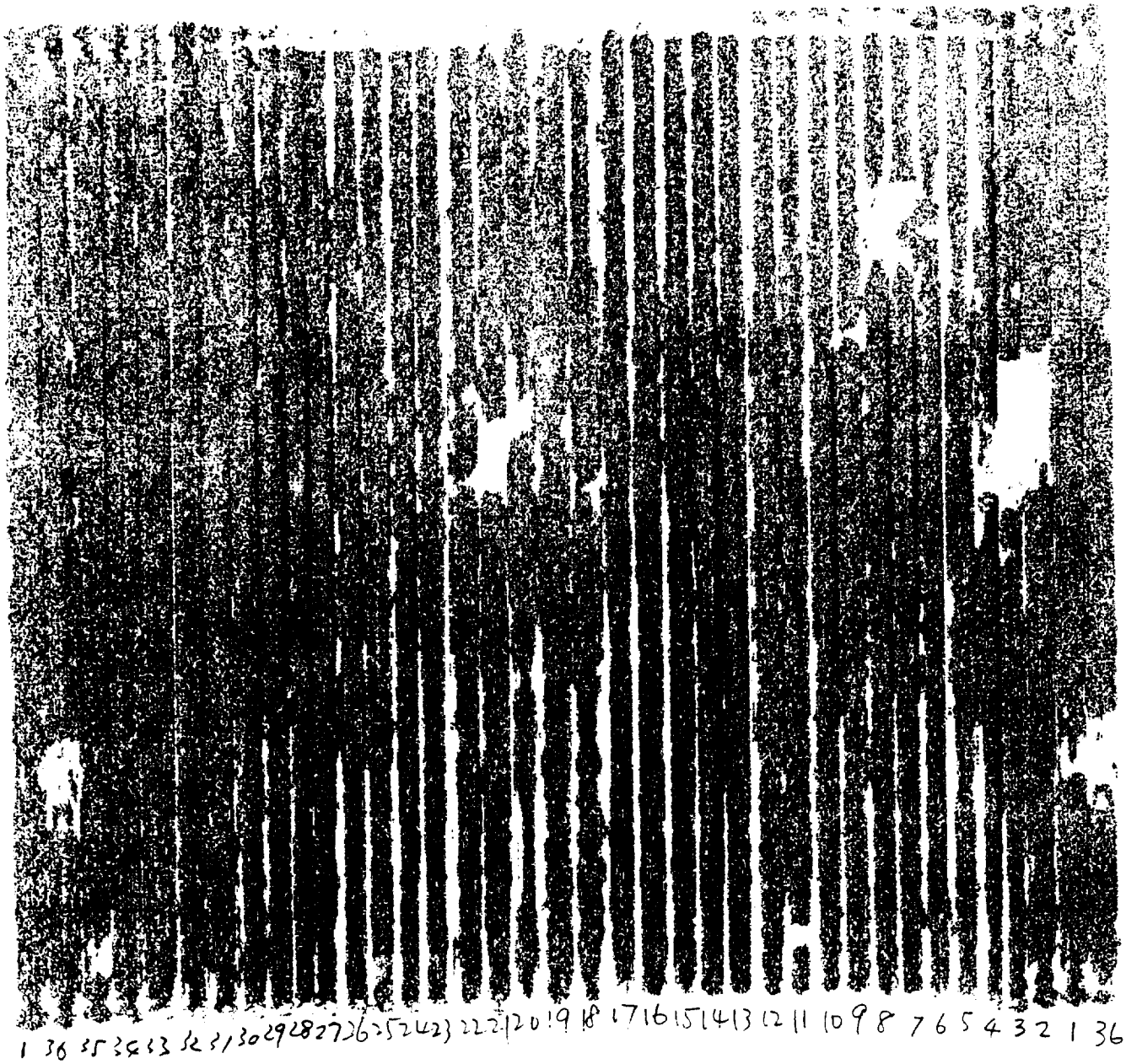

6-T-6

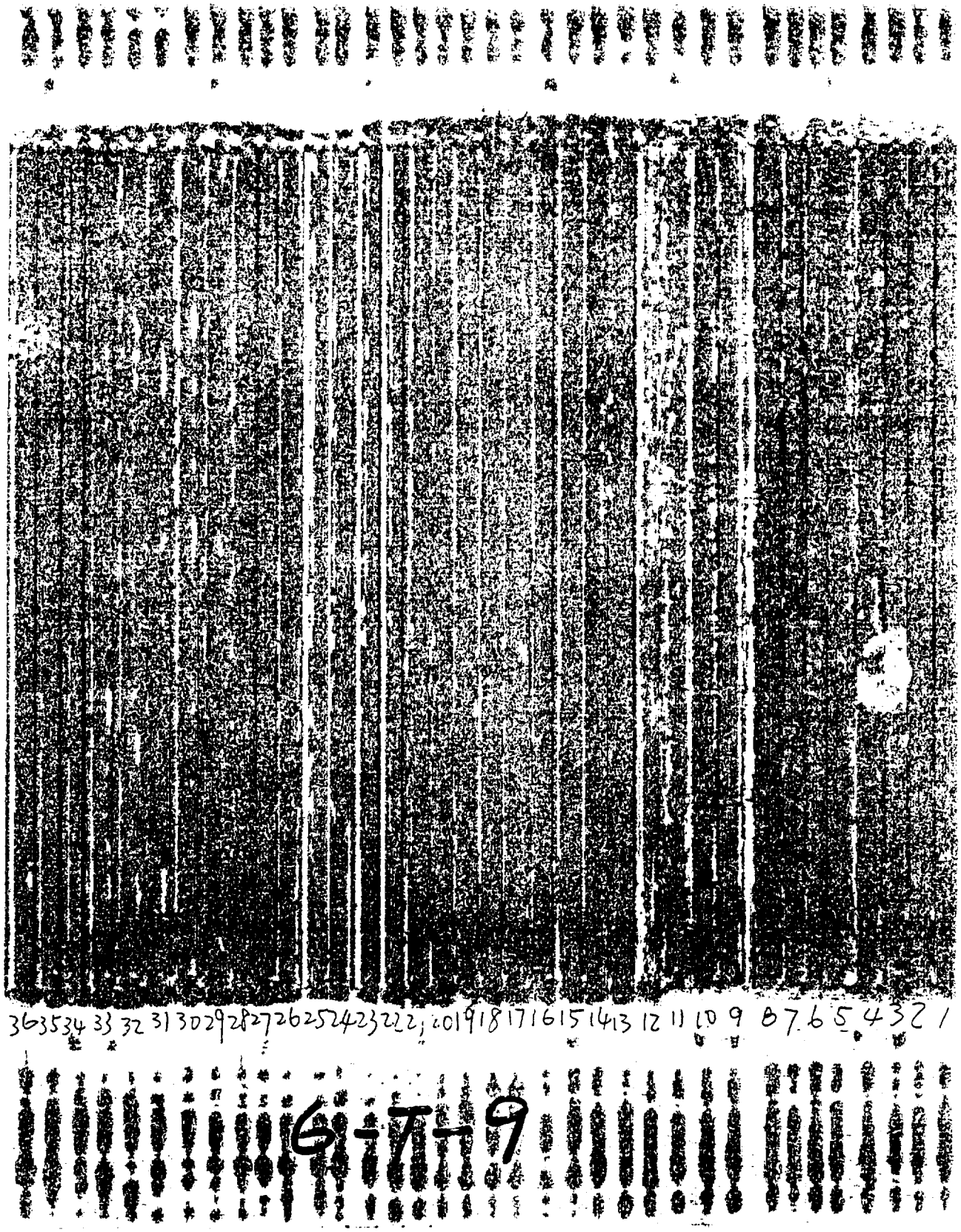

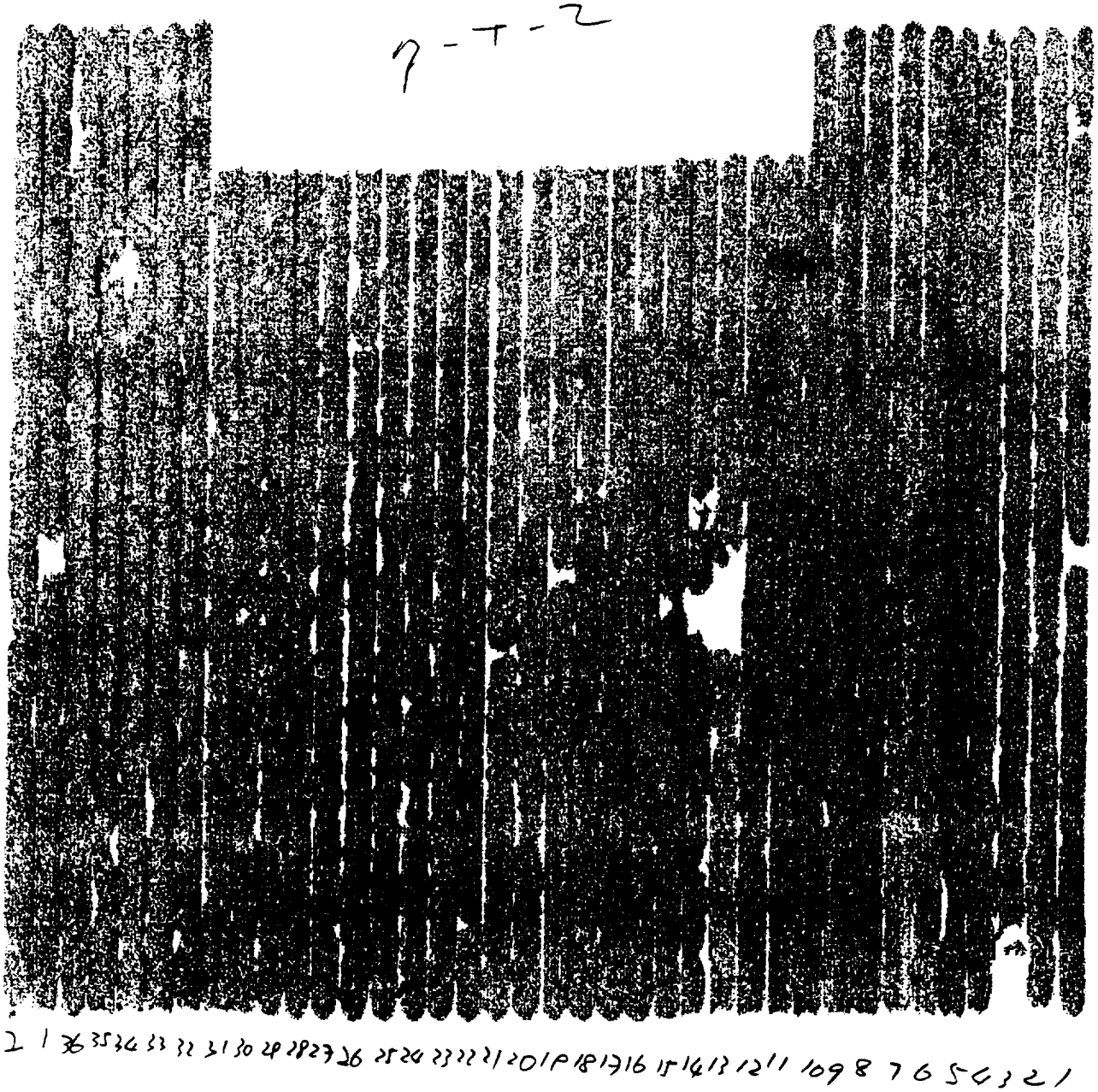

7-T-2

7-T-3

15-25 MHz 40 REJECT
H 26 5
H.Q. 1
10

Min Pulse
width 4.5

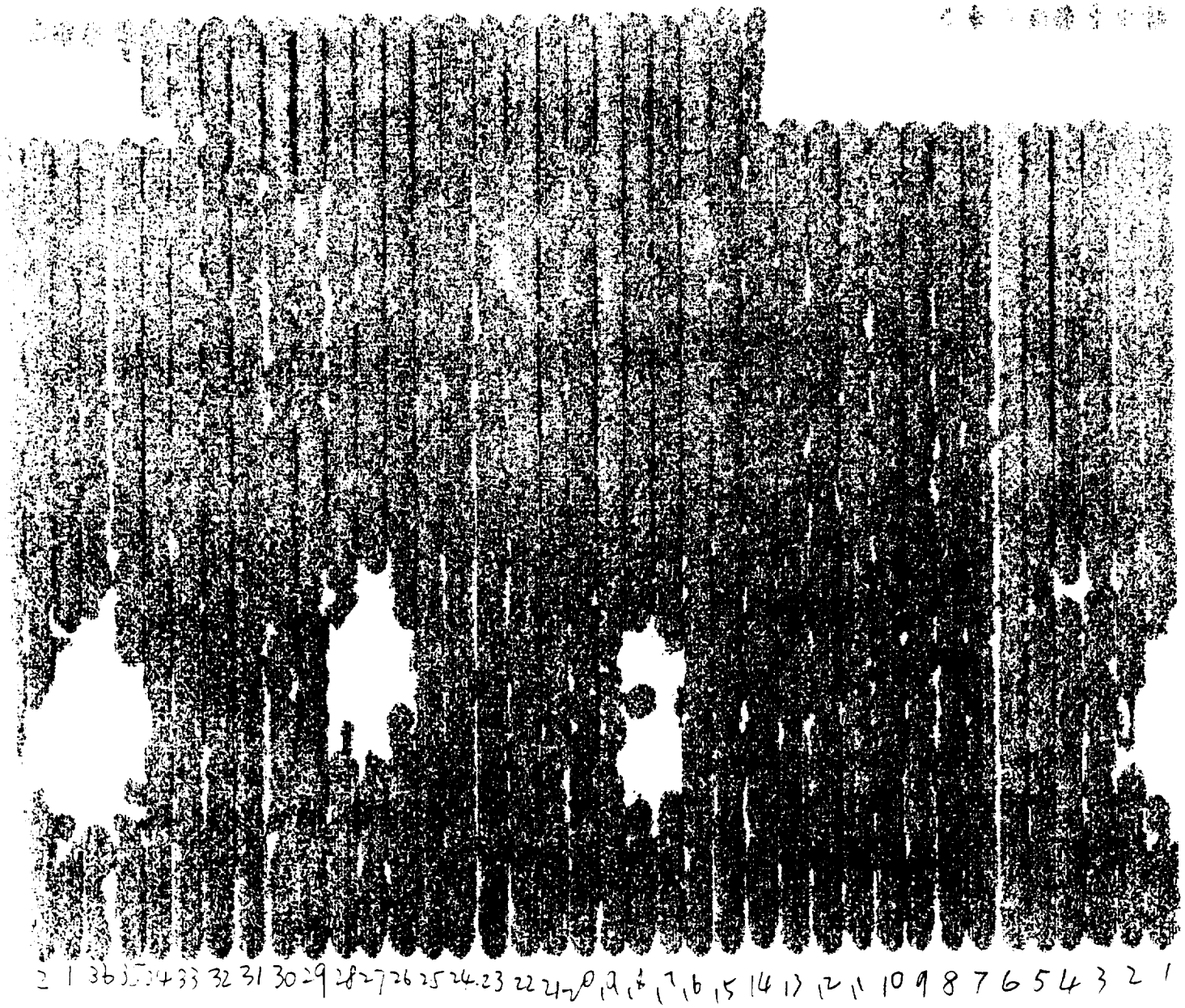

8-T-2

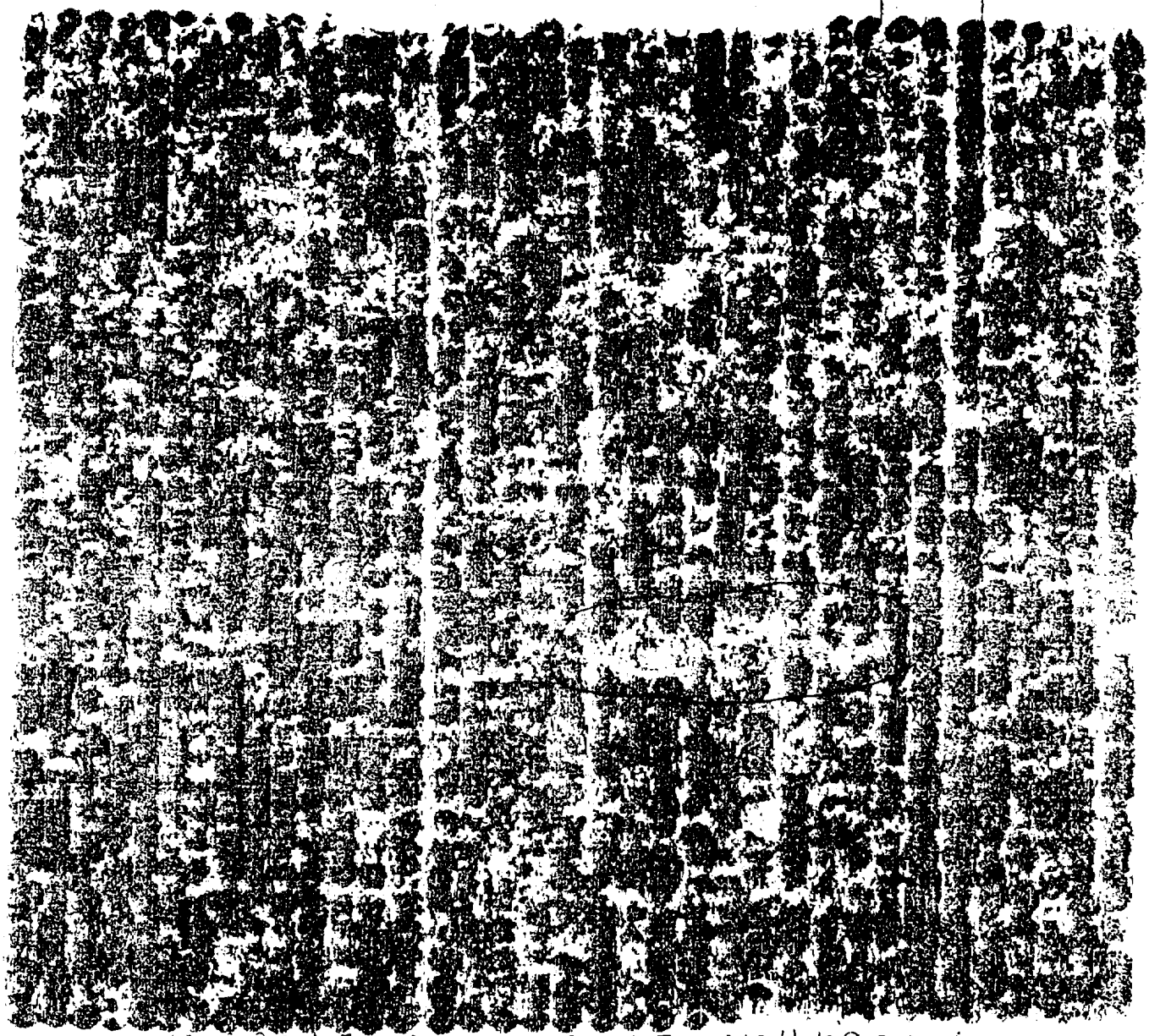

9S-T-1

95-T-2

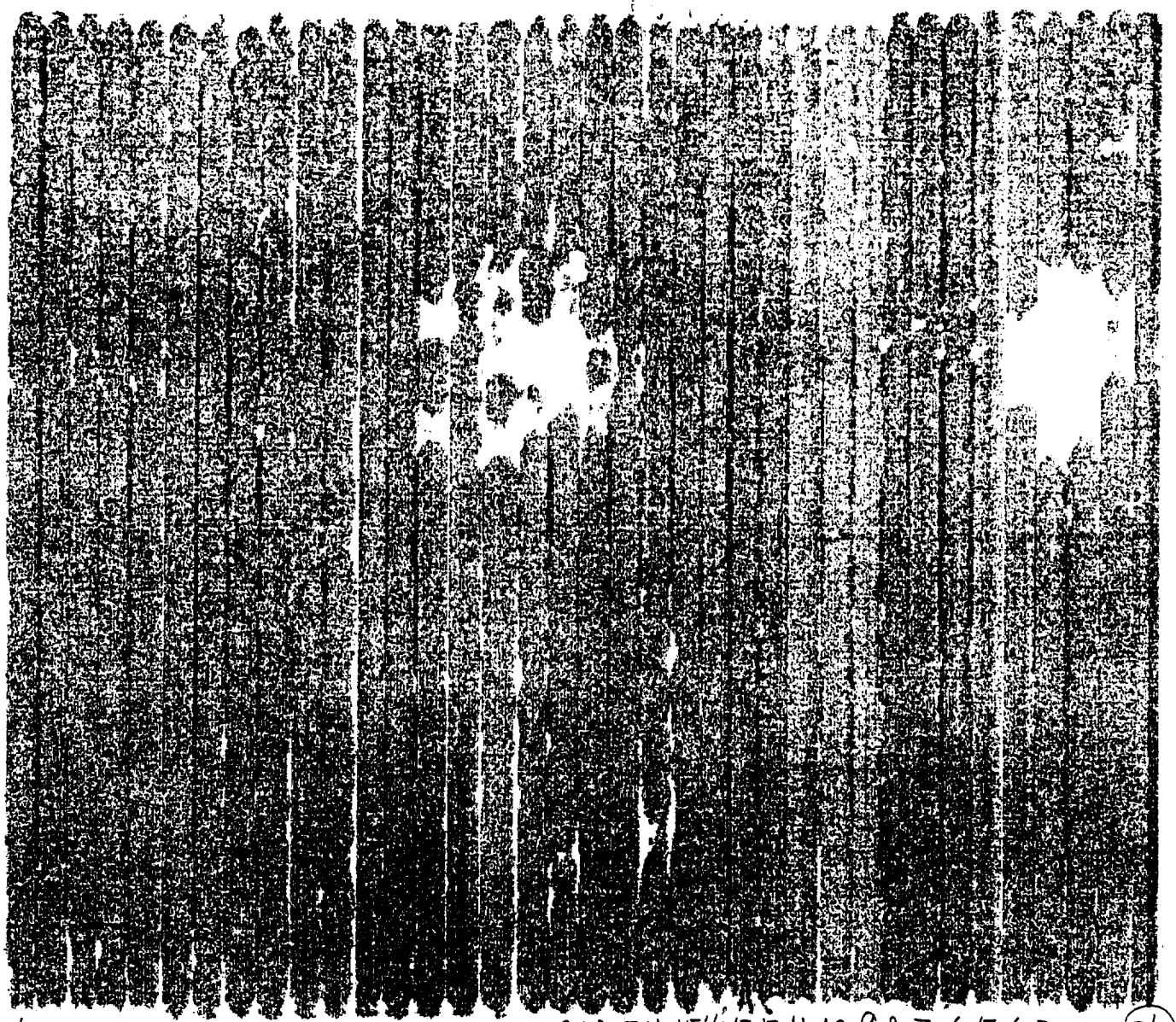

36 35 34 33 32 31 30 29. 28 27 26 25 24 23 22 21 20 19 18 17 16 15 14 13 12 11 10 9 8 7 6 5 4 3 2 1 (36)

9-T-1

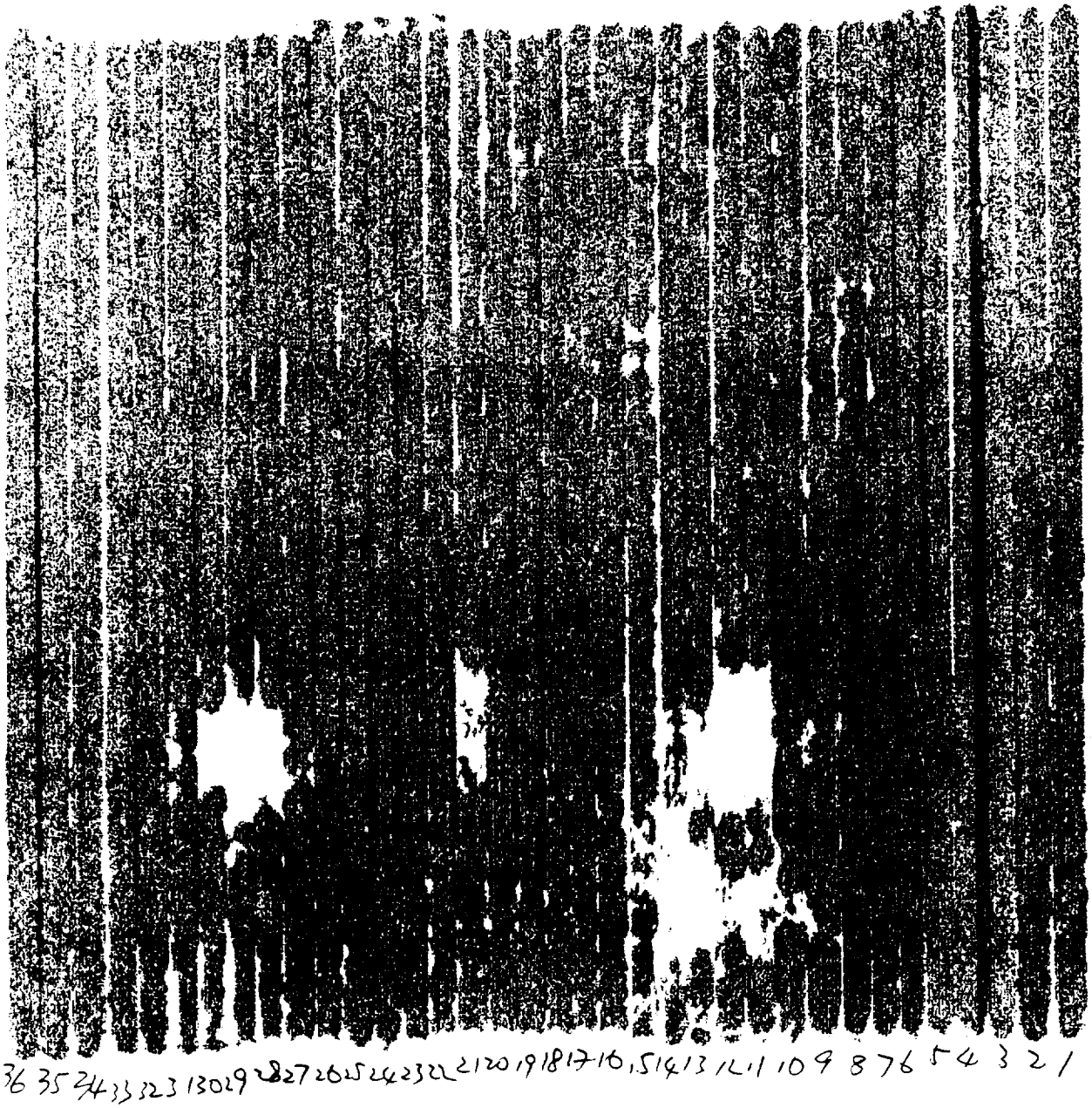

9-T-2

10-T-1

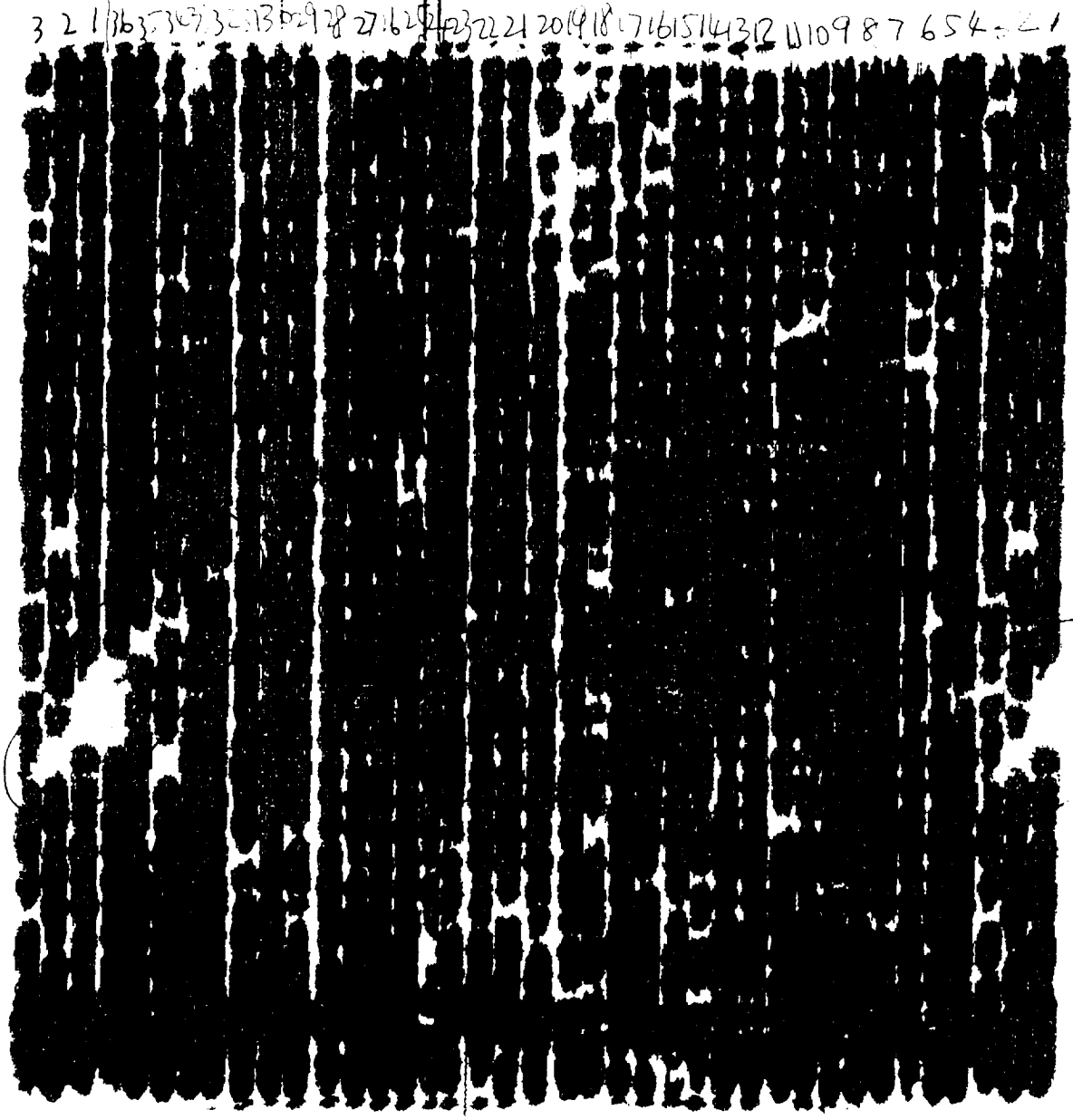

15-25 MHz 40 RJ PL Gate 4.5
HZ-V 26 5 min
HZ-Q 1.0
1

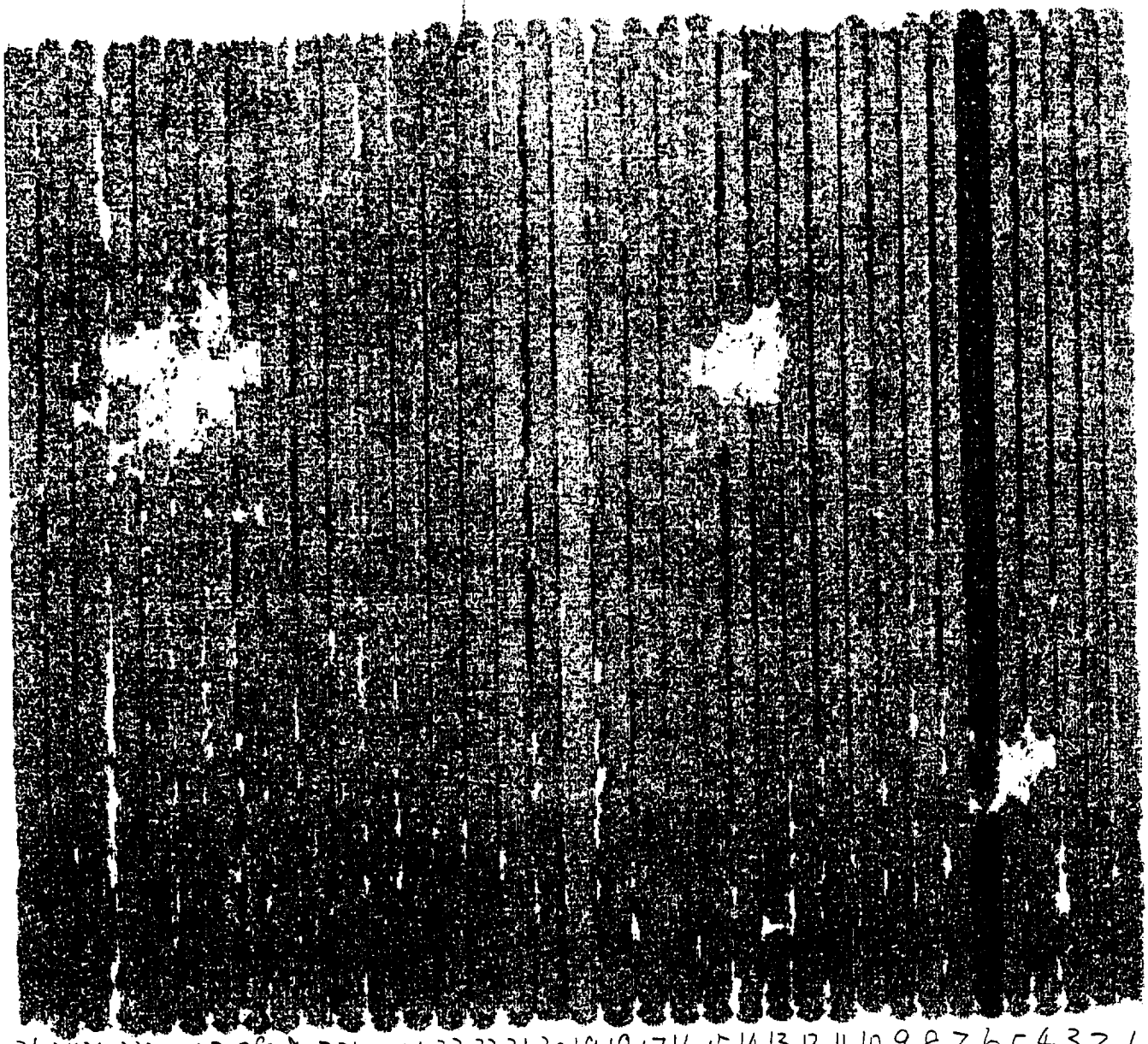

36 35 34 33 32 31 30 29 28 27 26 25 24 23 22 21 20 19 18 17 16 15 14 13 12 11 10 9 8 7 6 5 4 3 2 1

10-T-2

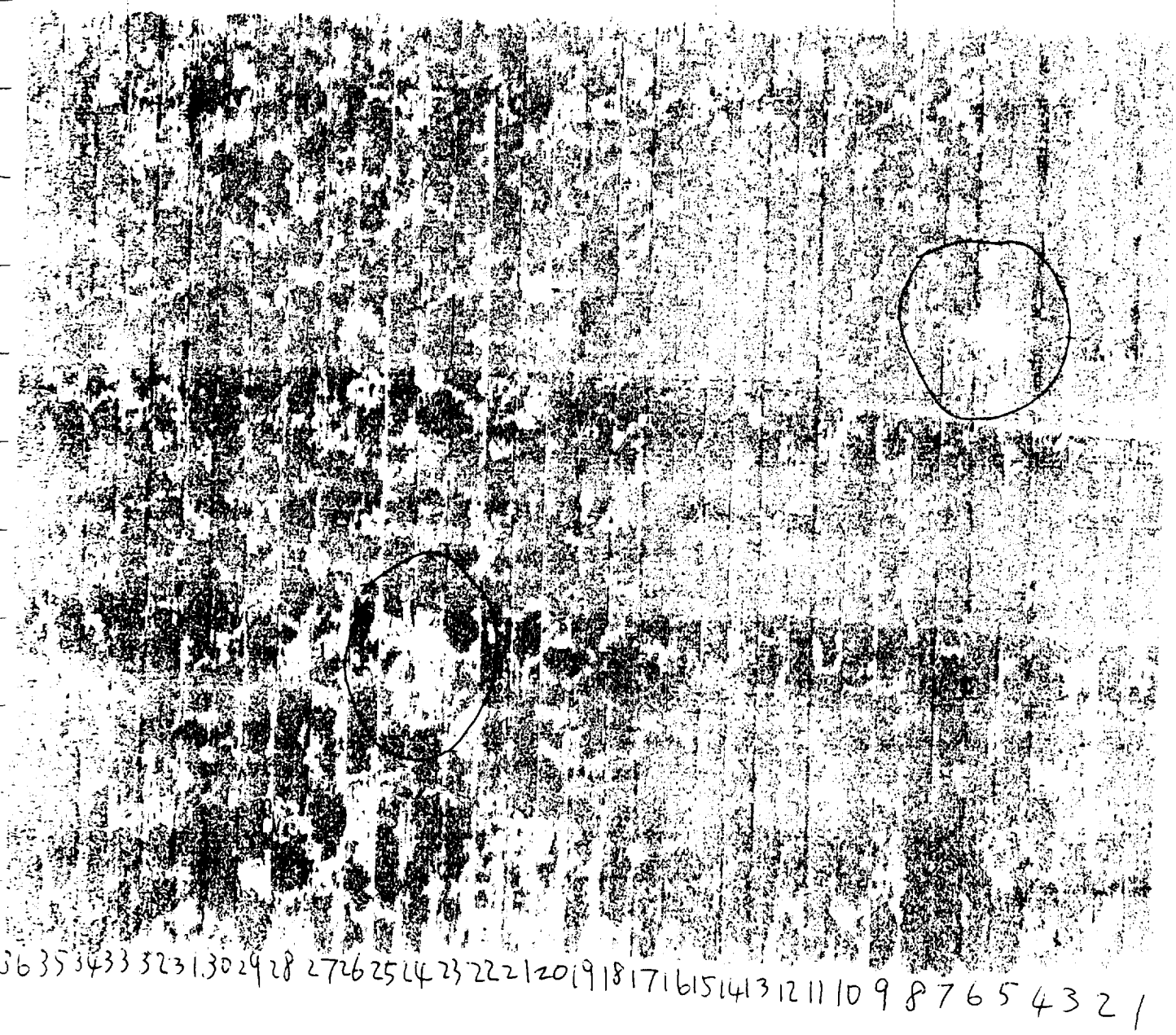
36 35 34 33 32 31 30 29 28 27 26 25 24 23 22 21 20 19 18 17 16 15 14 13 12 11 10 9 8 7 6 5 4 3 2 1

11 5 T-1

11-T-2

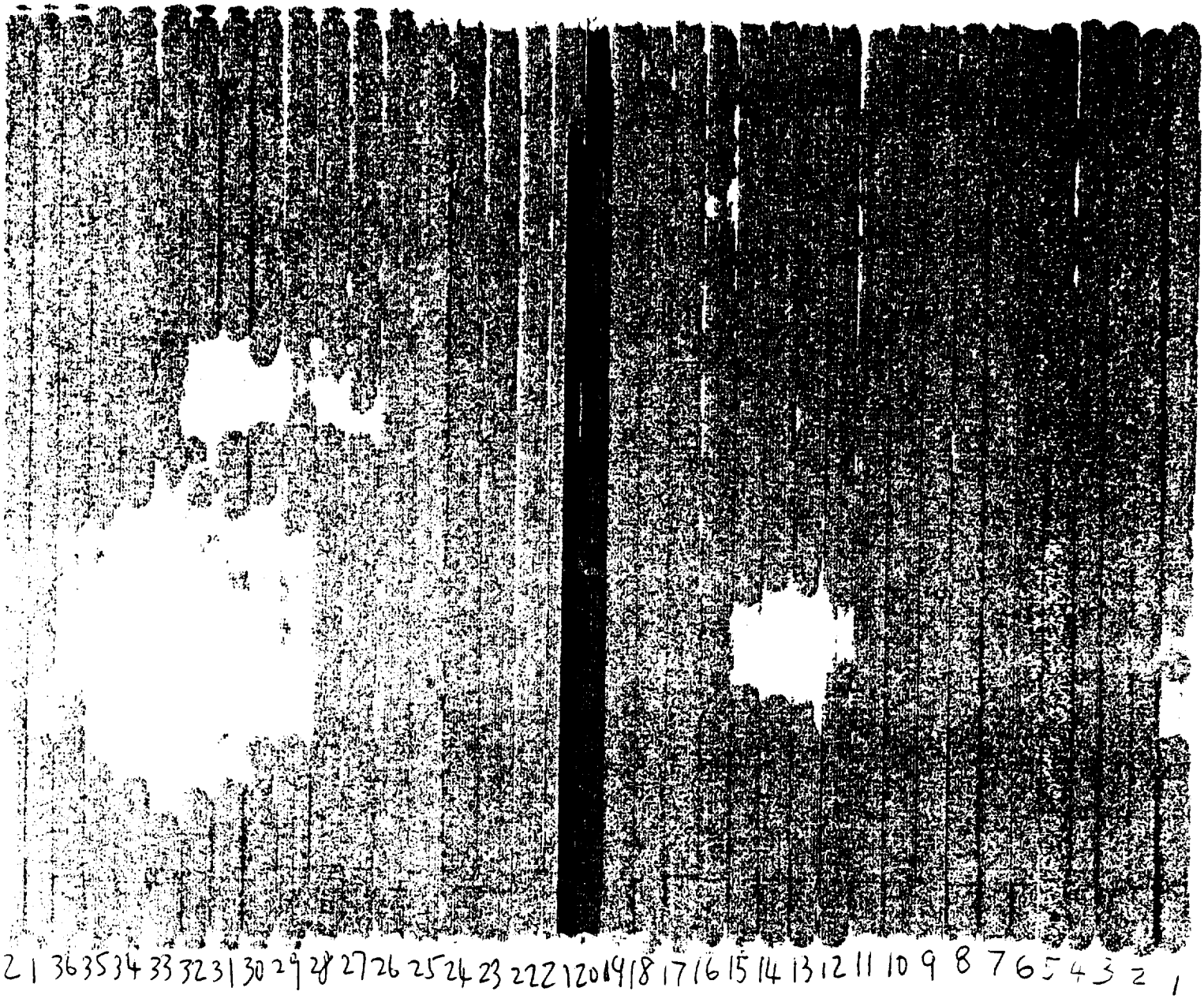
21 36 35 34 33 32 31 30 29 28 27 26 25 24 23 22 21 20 19 18 17 16 15 14 13 12 11 10 9 8 7 6 5 4 3 2 1

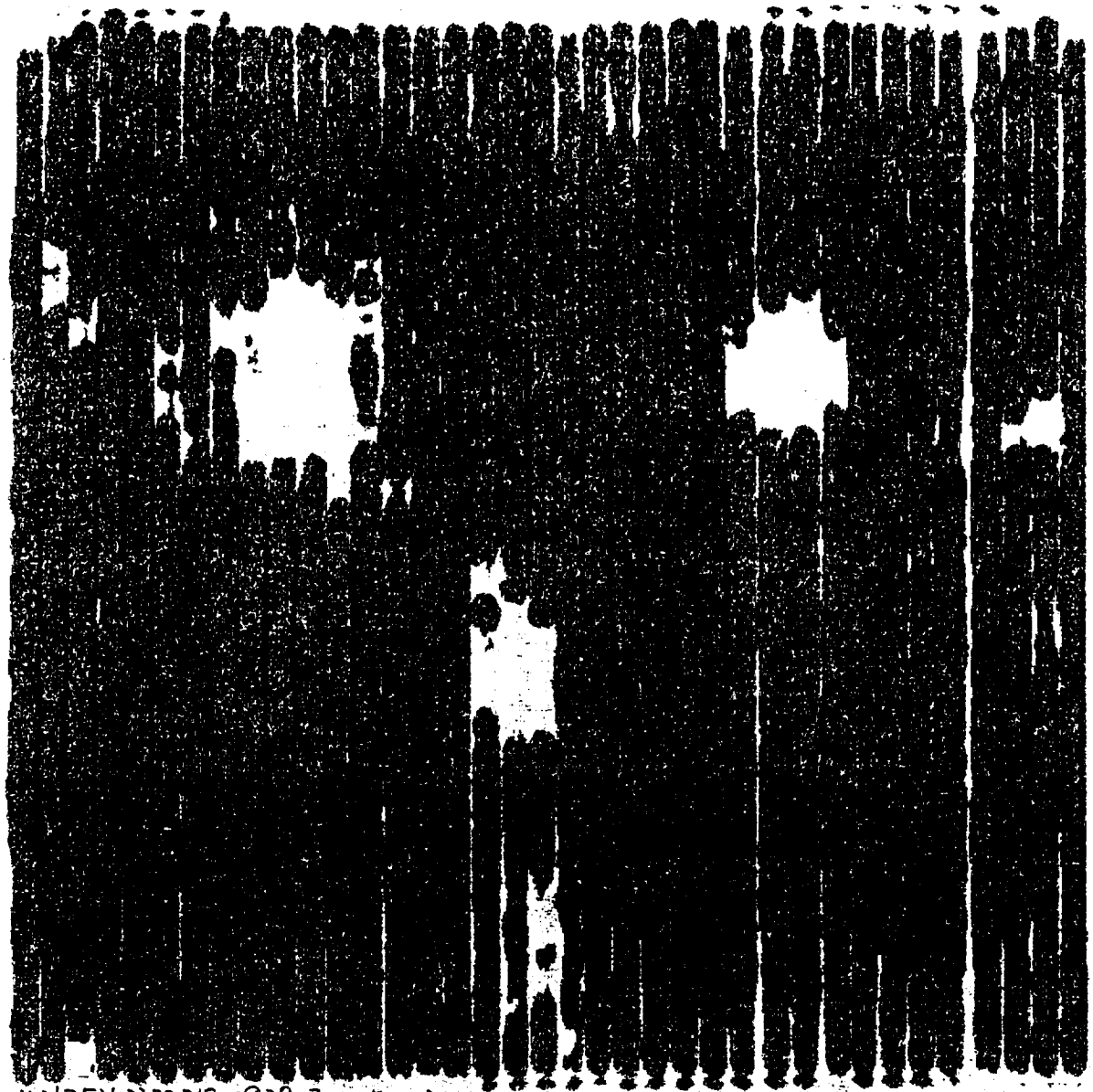

1 36 35 34 33 32 31 30 29 28 27 26 25 24 23 22 21 20 19 18 17 16 15 14 13 12 11 10 9 8 7 6 5 4 3 2 1

11-T-4

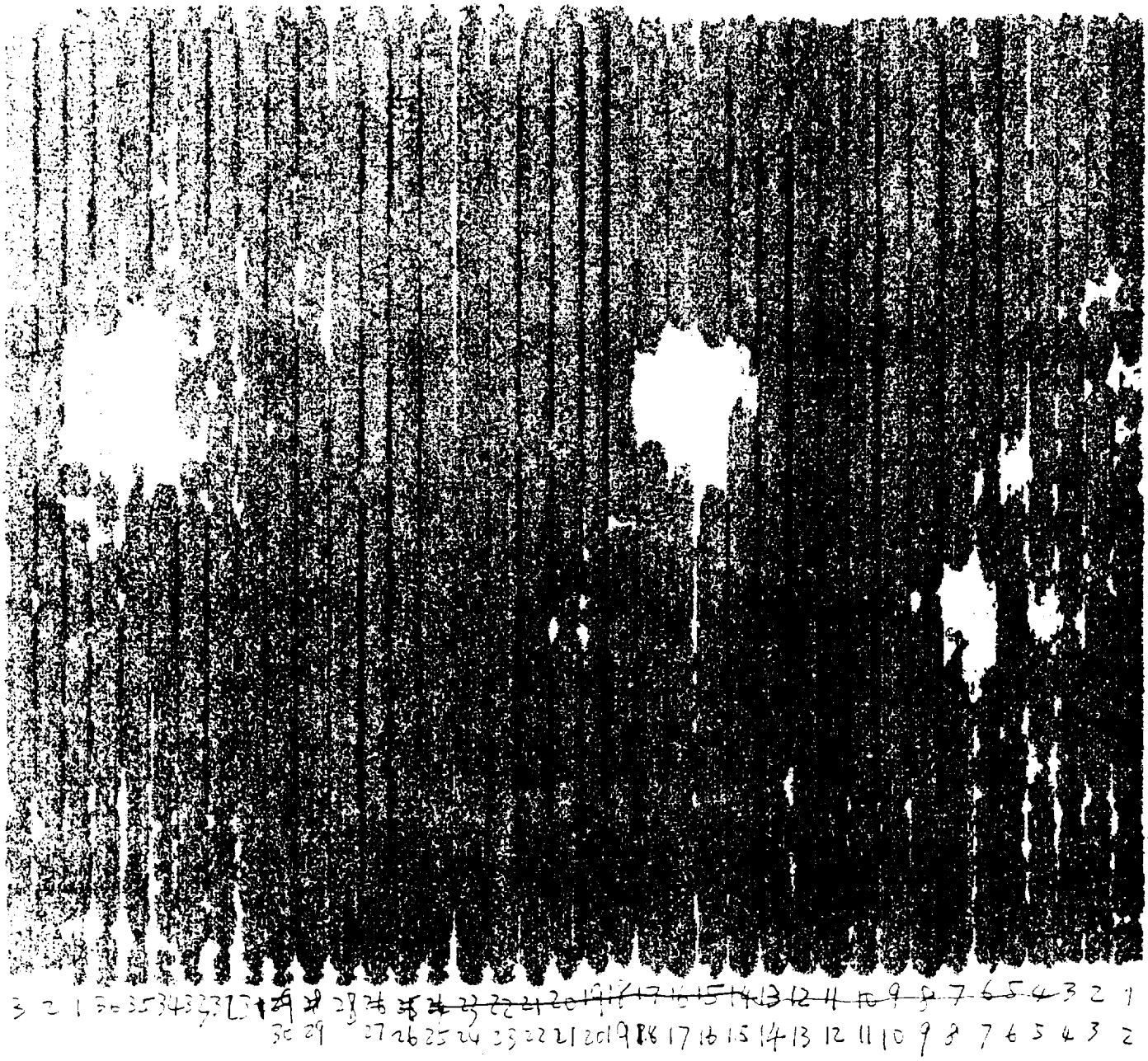

12-T-2

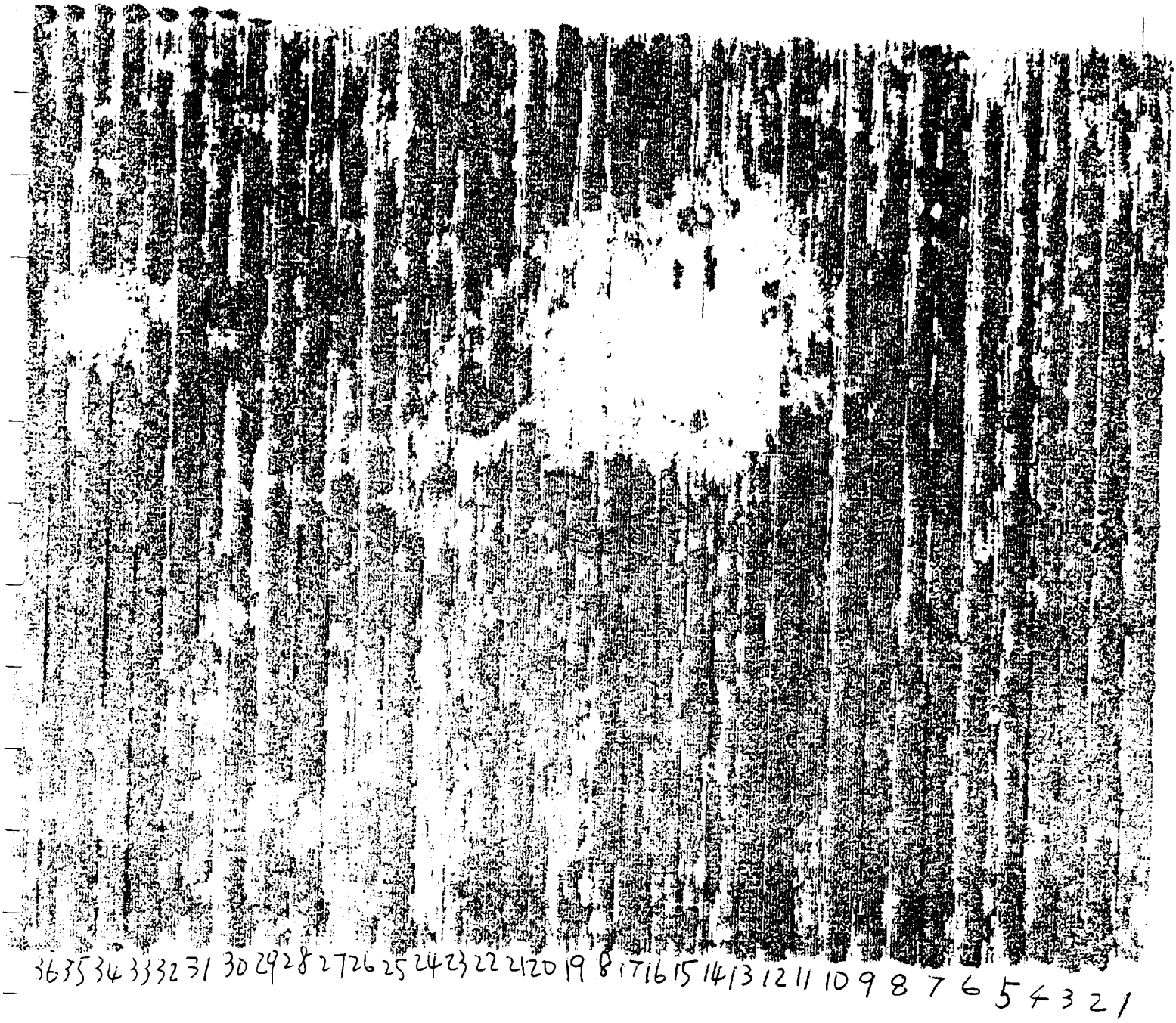
36 35 34 33 32 31 30 29 28 27 26 25 24 23 22 21 20 19 18 17 16 15 14 13 12 11 10 9 8 7 6 5 4 3 2 1

JSC-002

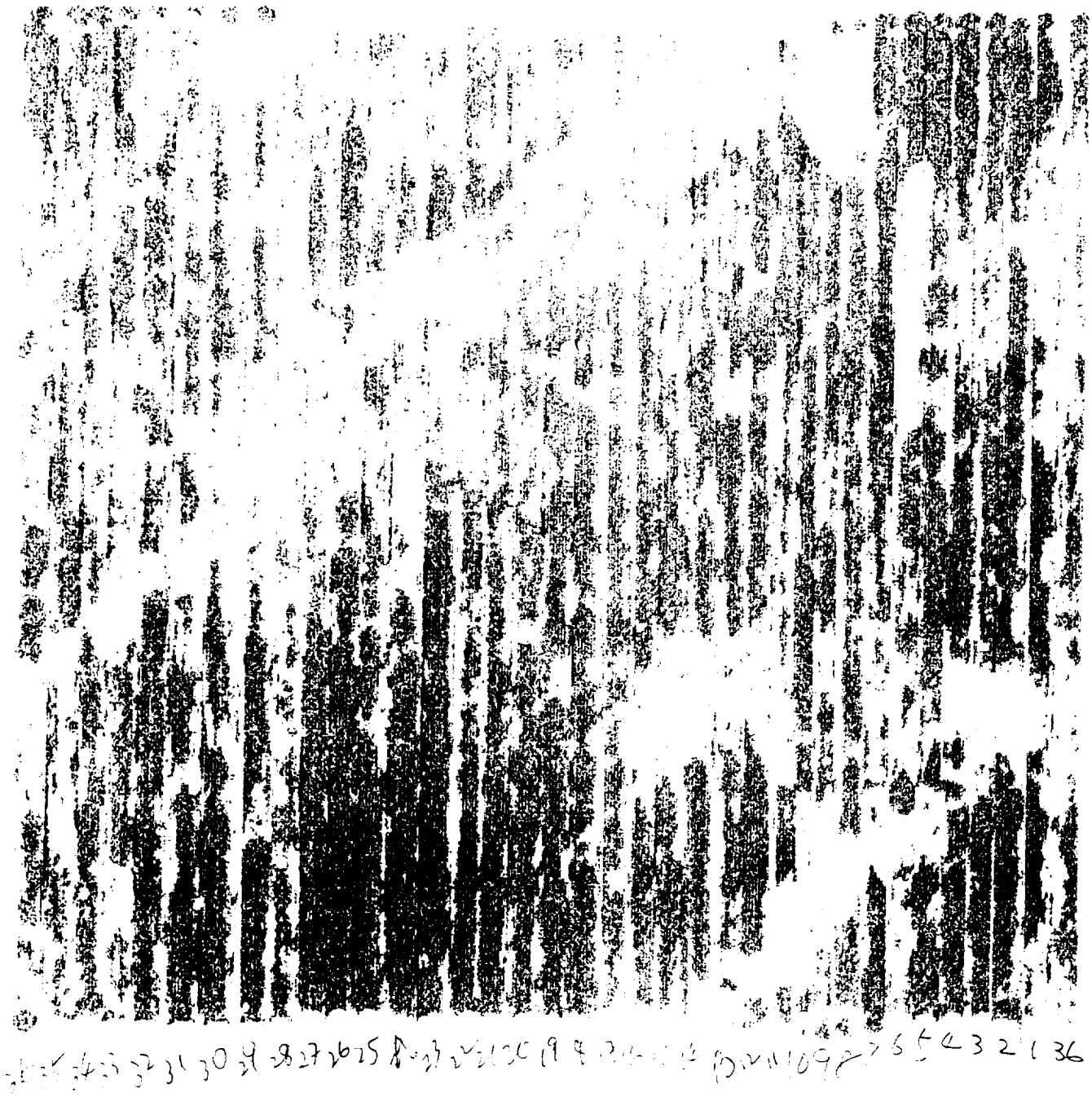

JSC-003

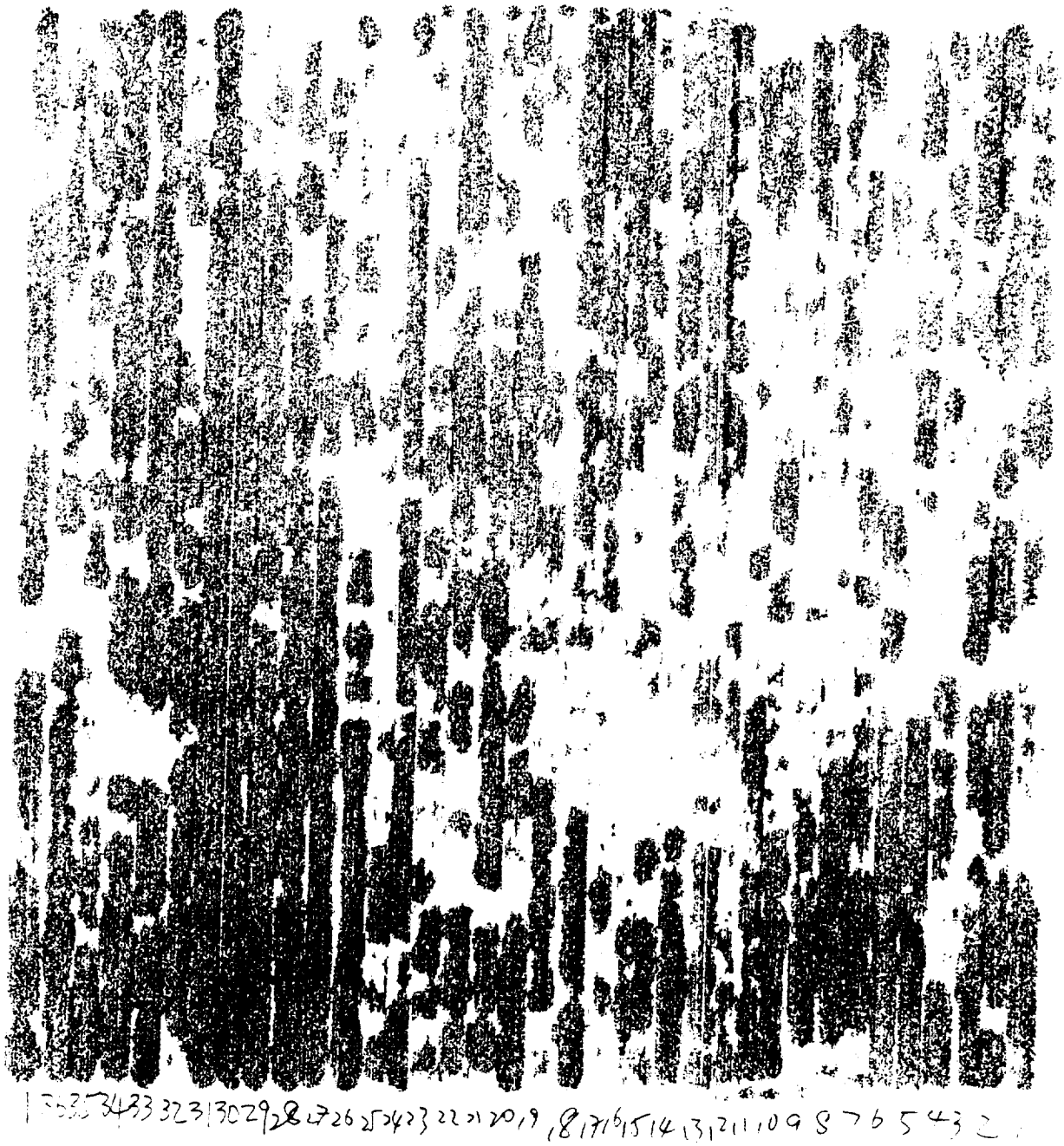

JSC-004

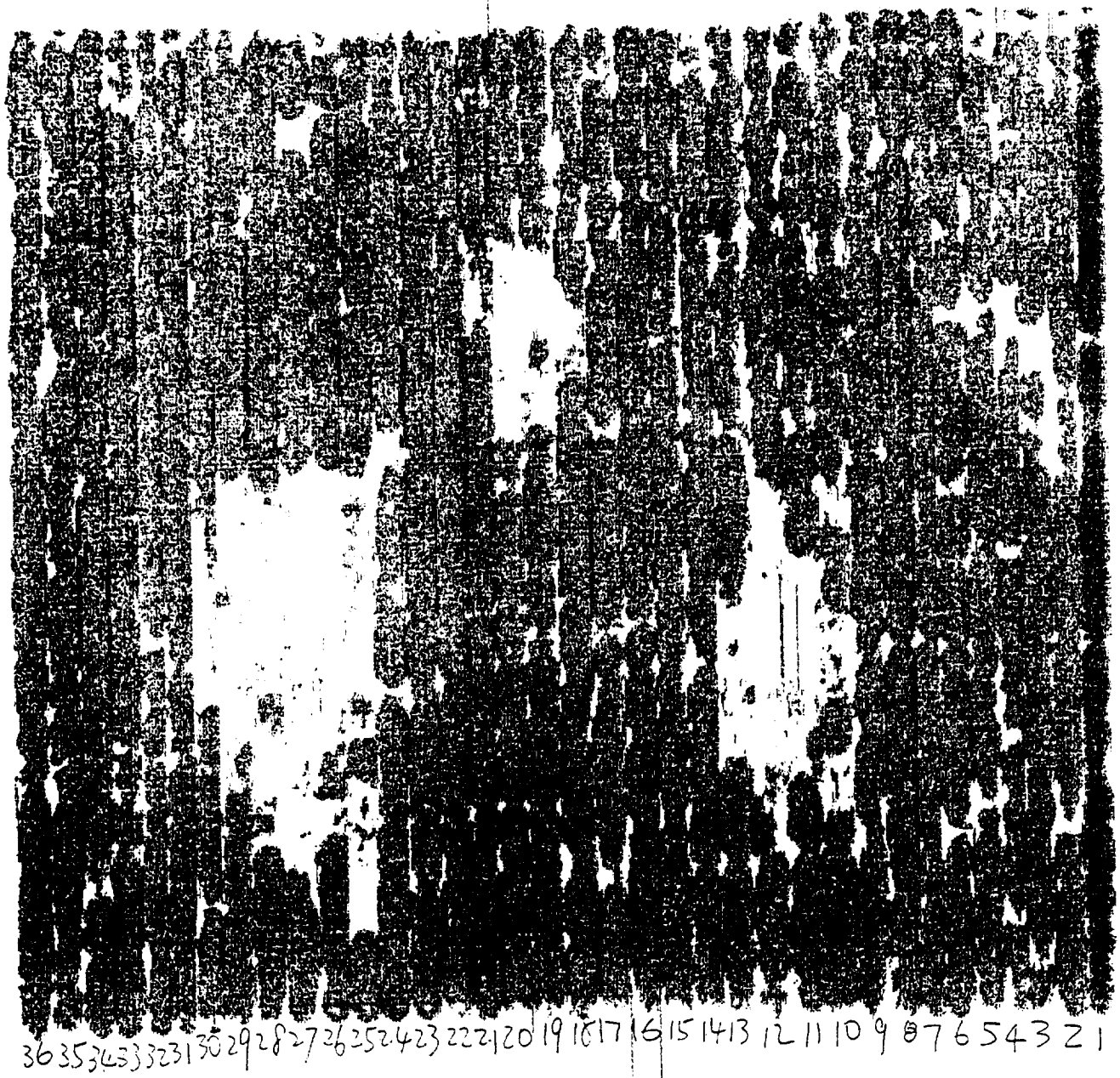
36 35 34 33 32 31 30 29 28 27 26 25 24 23 22 21 20 19 18 17 16 15 14 13 12 11 10 9 8 7 6 5 4 3 2 1

MD-02

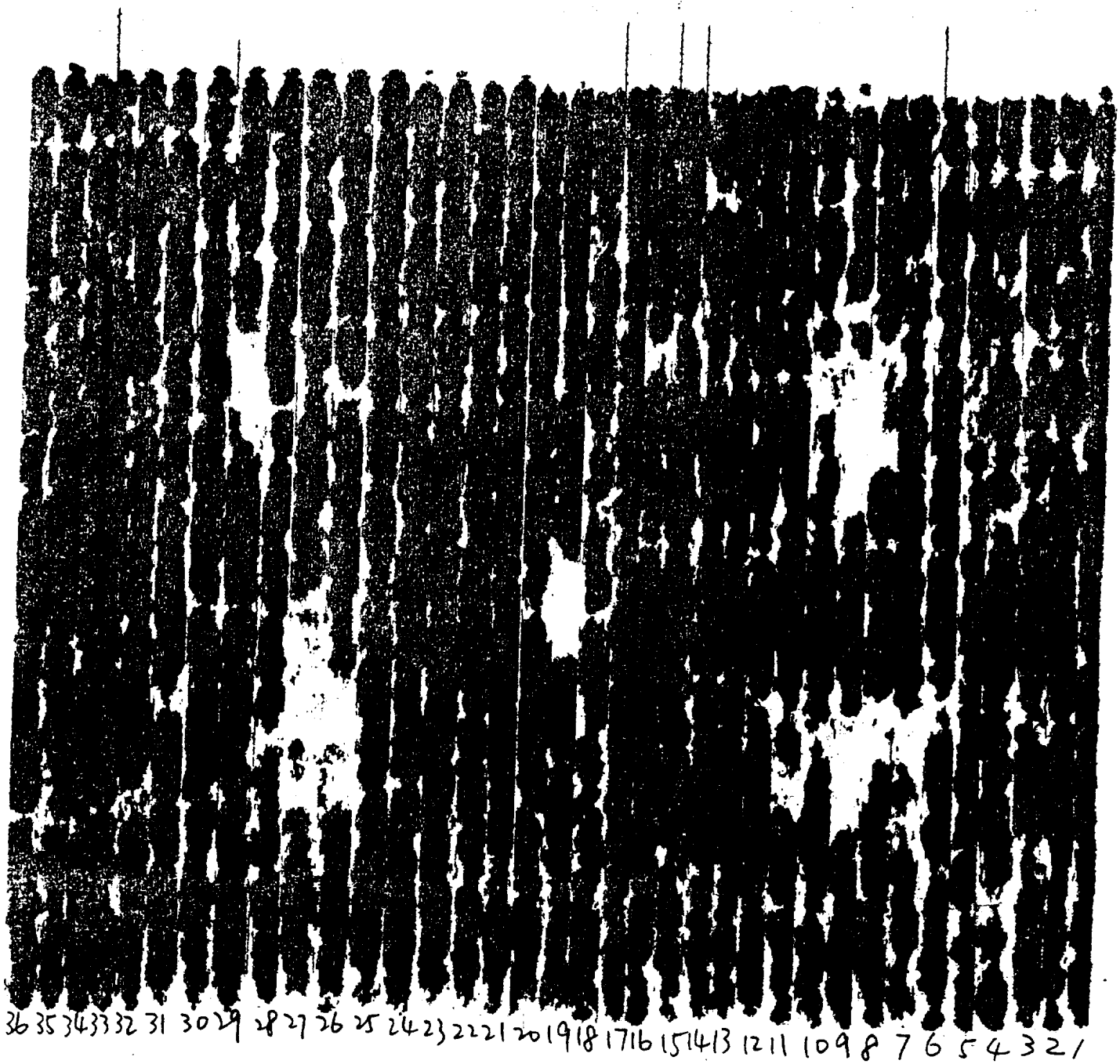
36 35 34 33 32 31 30 29 28 27 26 25 24 23 22 21 20 19 18 17 16 15 14 13 12 11 10 9 8 7 6 5 4 3 2 1

MD-03

6-F-1

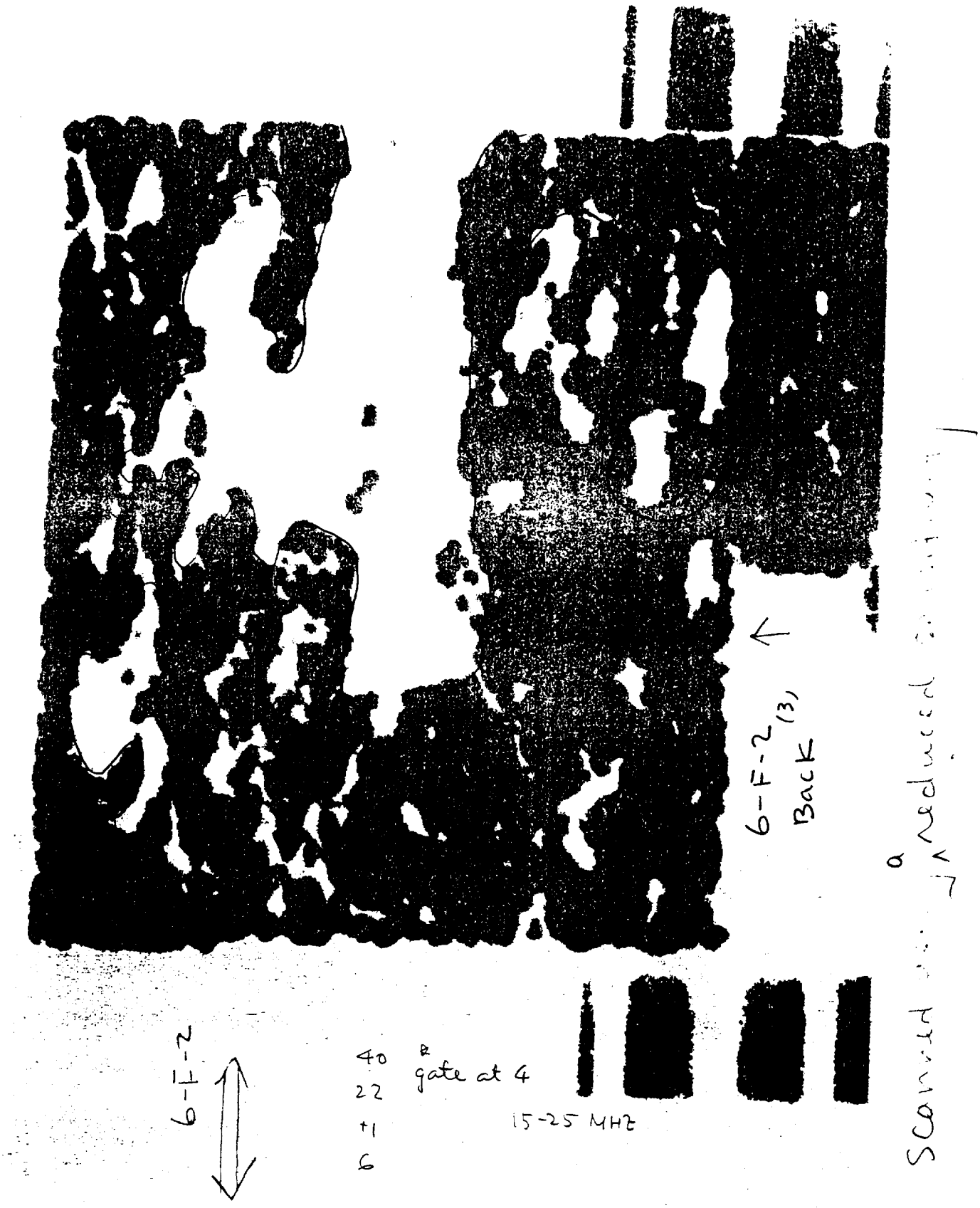
6-F-2 (3)
Back
Scanned
a
reduced
6-I-2
40
22
+1
6
gate at 4
15-25 MHz

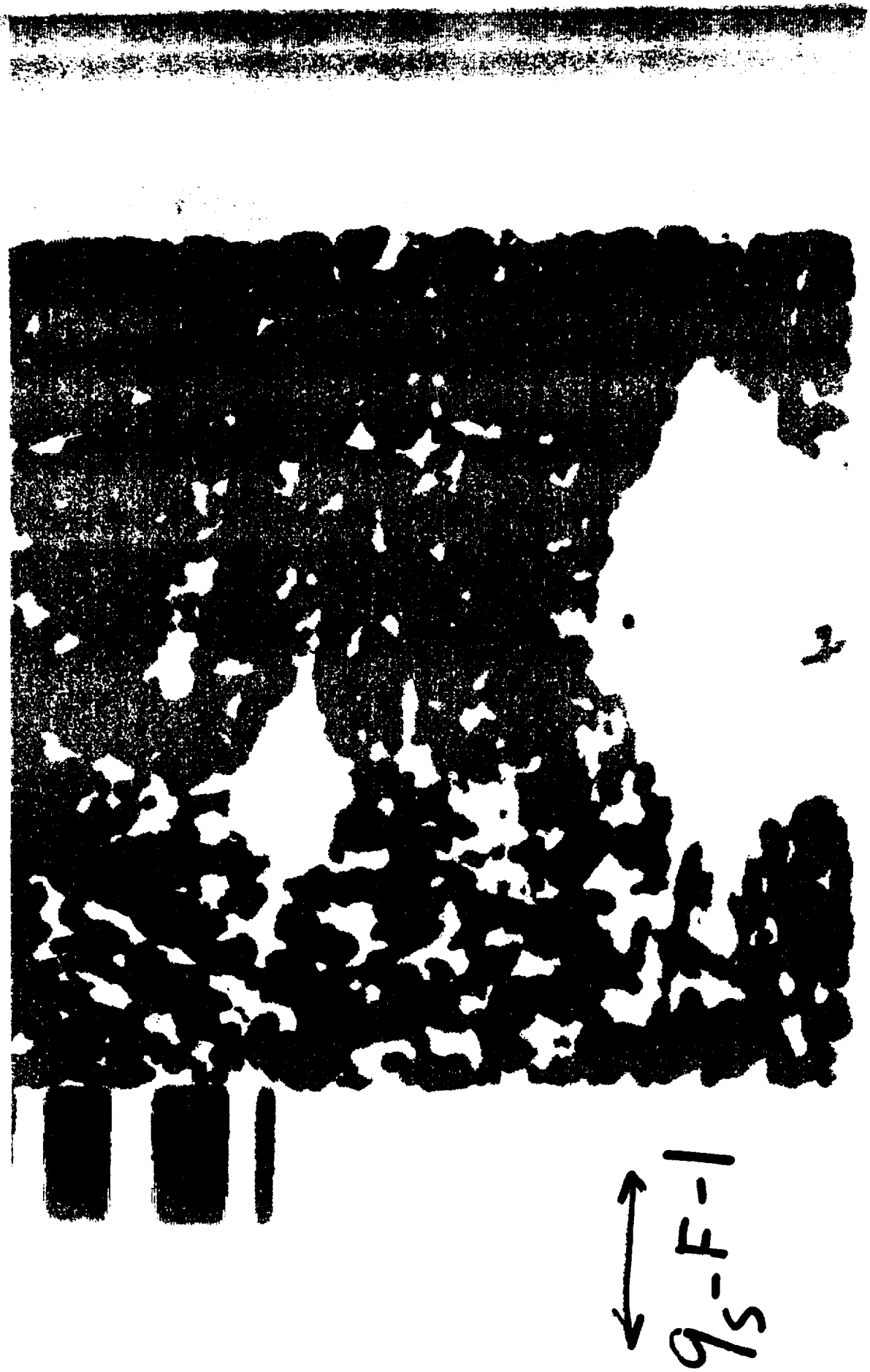
9S-F-1

damage from
2nd Impact

damage
from 1st
Impact

Gate at 4 (reduced sensitivity).

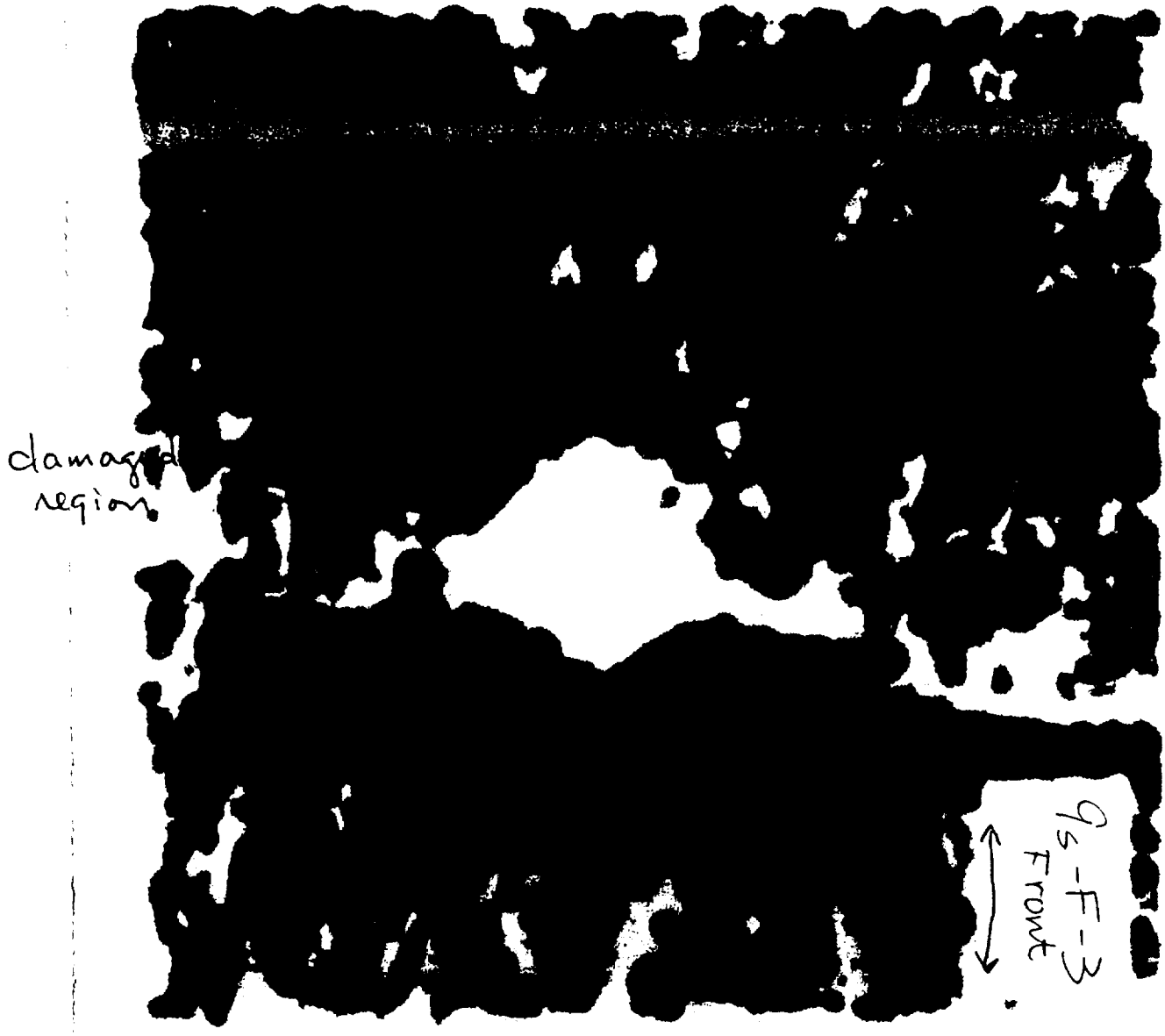

Gate at 4 (reduced sensitivity)

10-F-1
scan-2

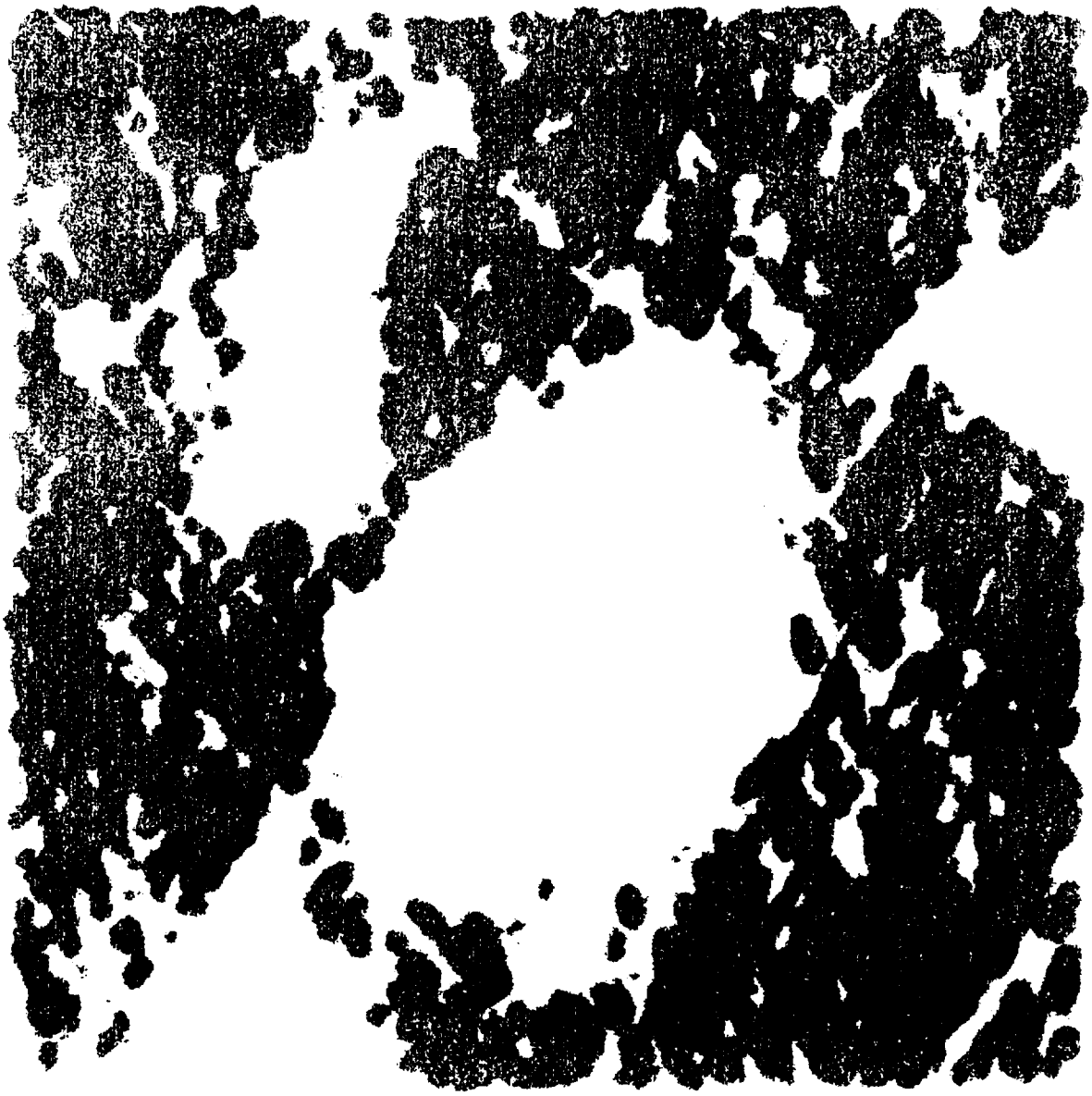

SCAN 2
Gate at 4
40, 26 + 10

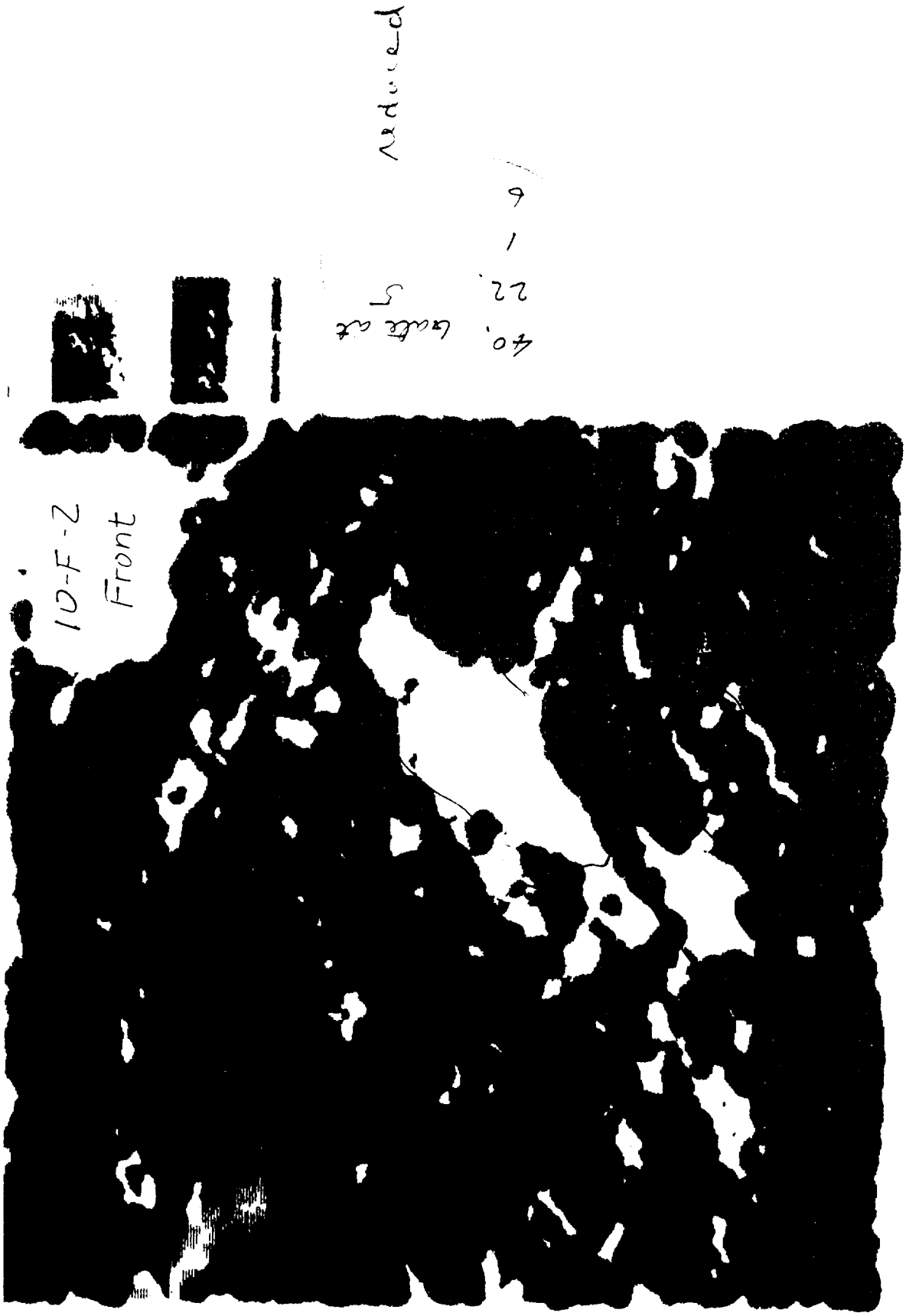
10-F-2
Front
40, back of
22, 5
1
6
Reduced

11-F-1

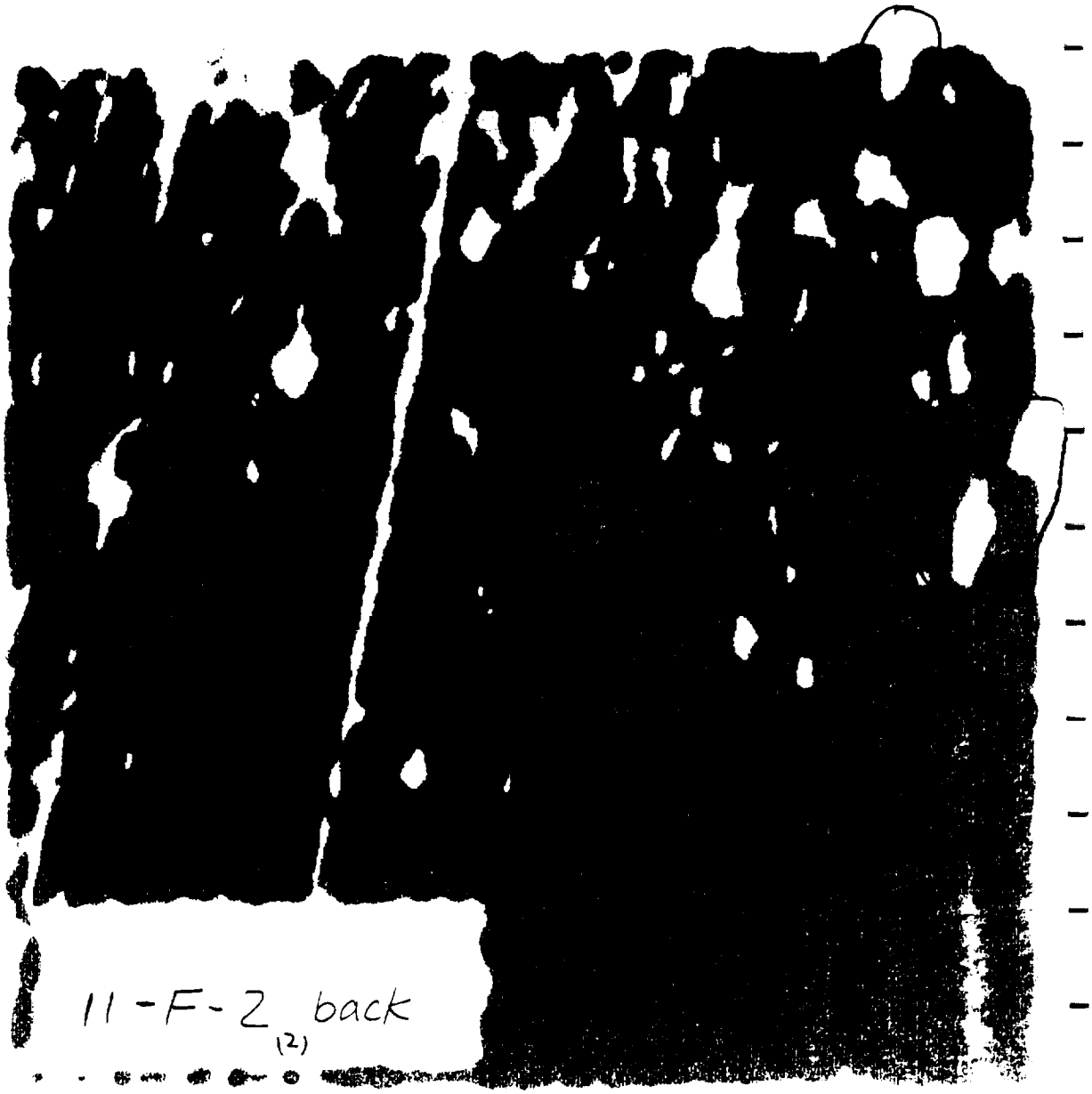

Scanned using a
reduced sensitivity
(new head).

12-F-1
12-F-1

Scanned using a
reduced sensitivity
(new sensor head).

12-F-2 (1)

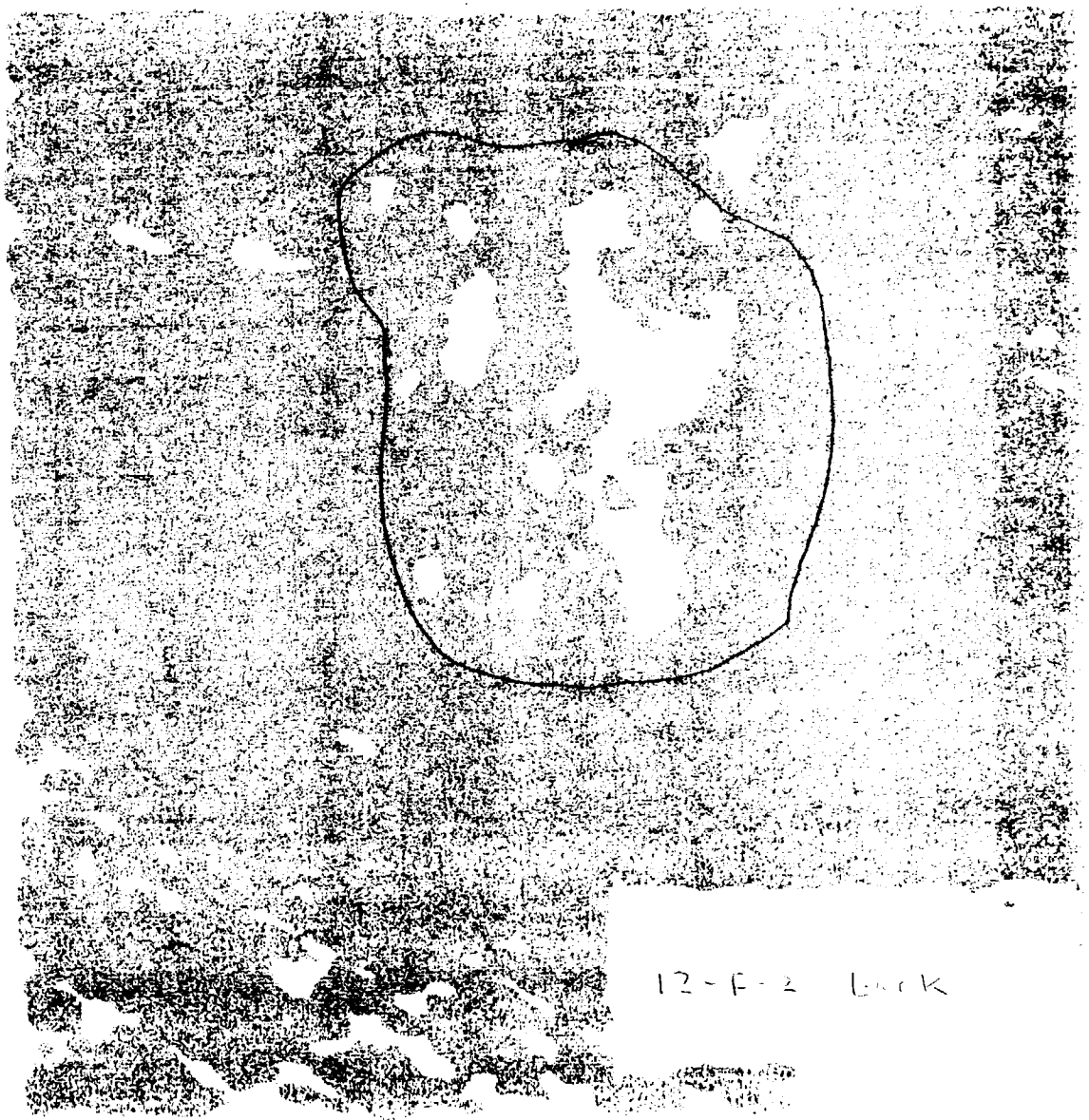

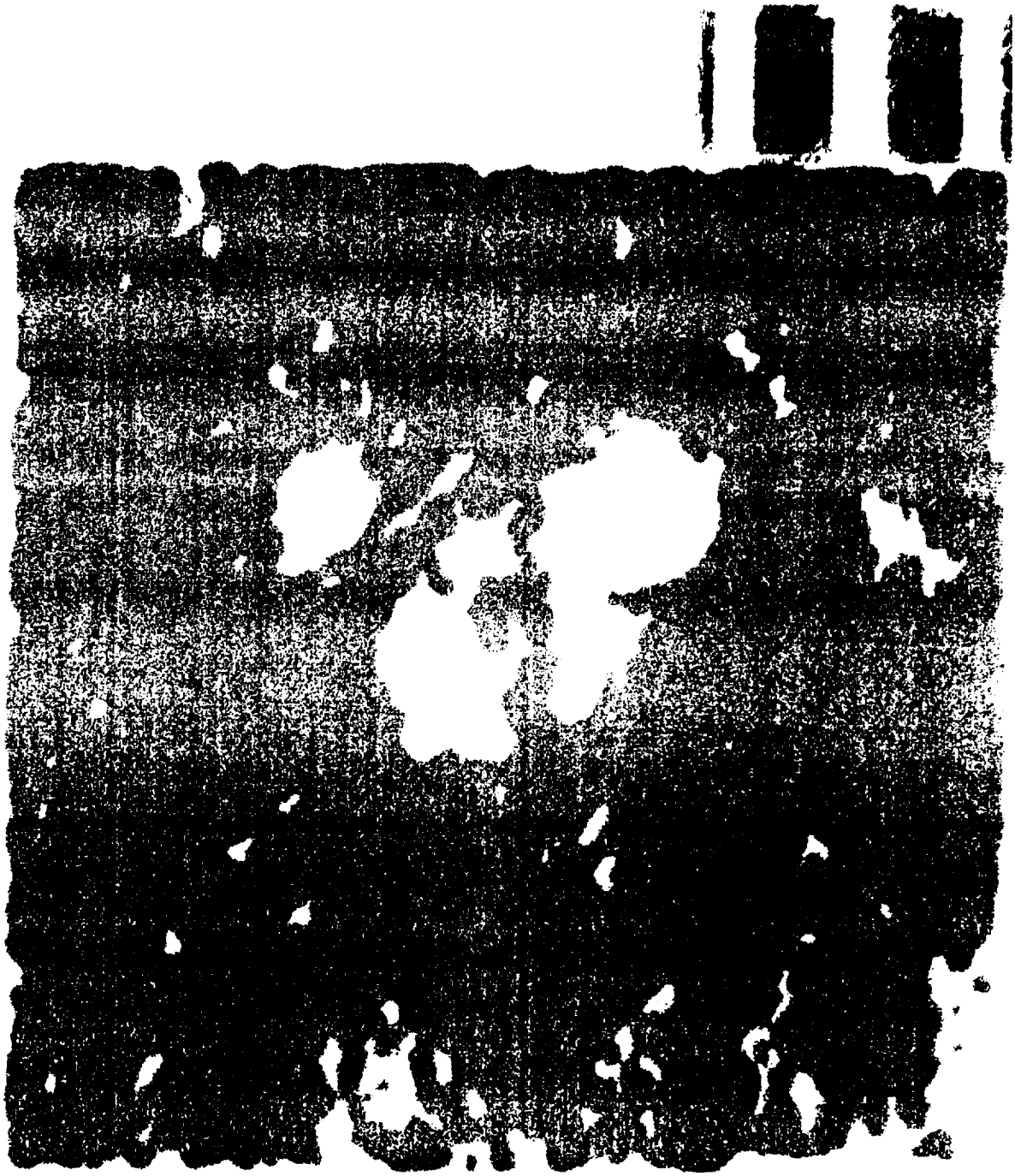

13-F-1

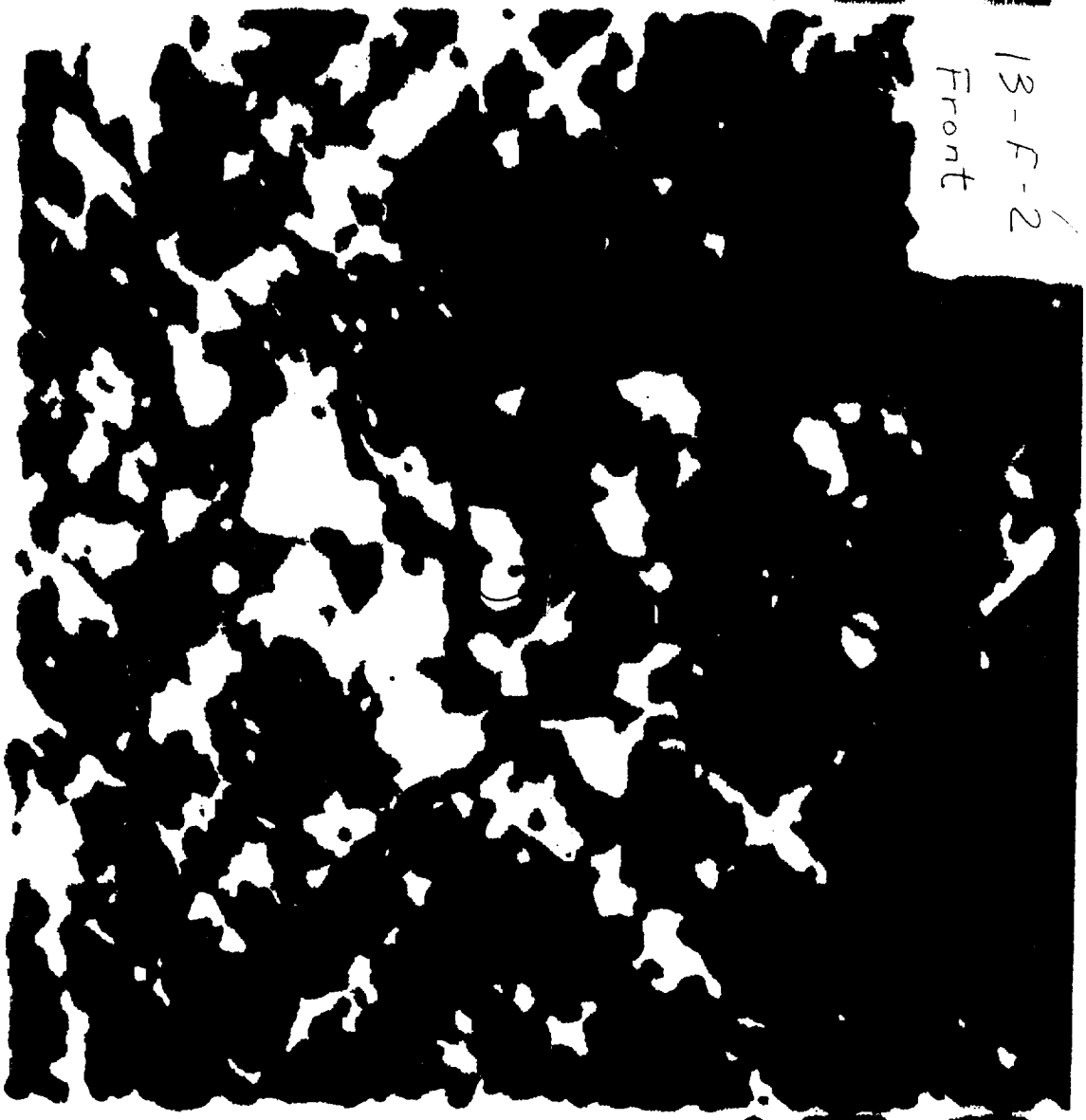

Label corresponds to that shown in the sketch of the plate used in the experiment.

40
30
1
6

Gate at 5

C-SCAN SETTING

DATE : 12 / 31 / 87

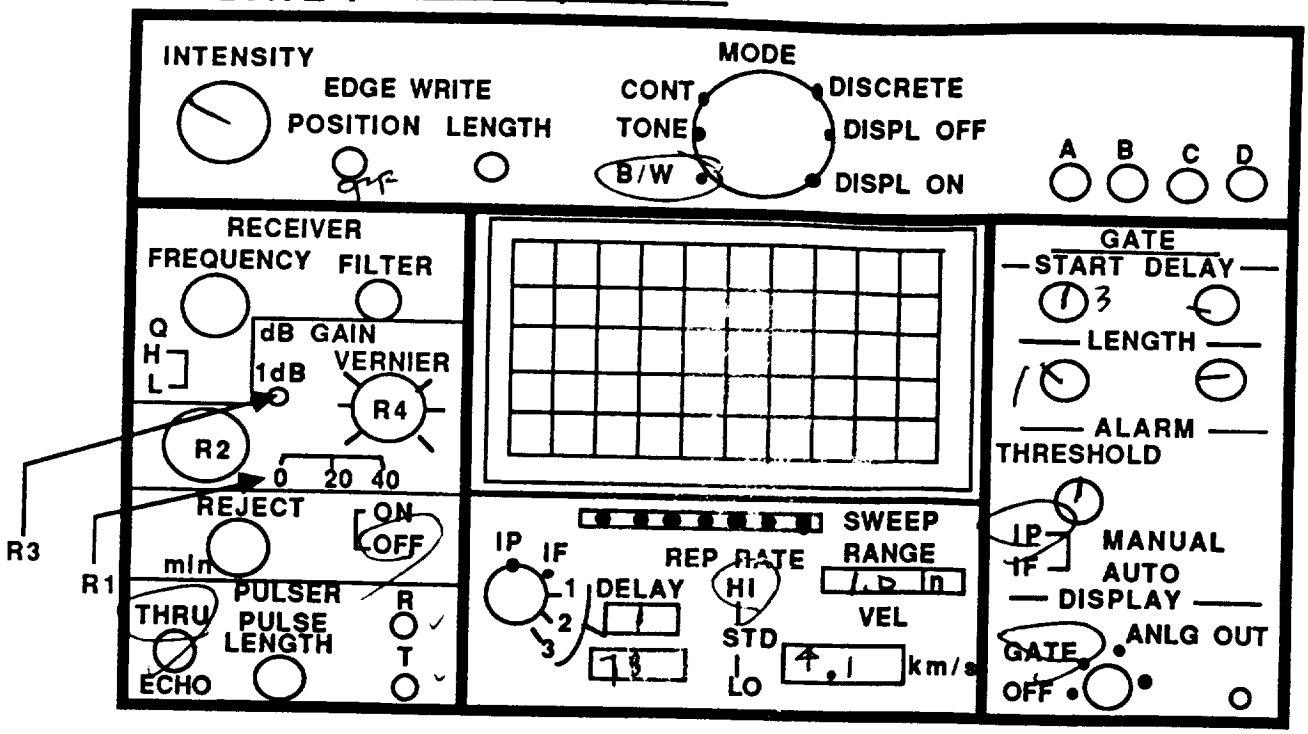

SAMPLE NO.	RECEIVER			dB GAIN				REJECT		PULSE LENGTH	GATE LEVEL	COMMENT
	OPER. FREQ.	Q HI/LO	FILTER	R1	R2	R3	R4	ON OFF	LEVEL			
6-F-1	15-25	Lo	Hi	40	22	1	6	OFF	0	0	5	
9s-F-1	15-25	Lo	Hi	40	24	1	6	"	0	0	5	THRU MODE
10-F-1	15-25	Hi	Hi	40	18	+1	10	"	0	0	4	SCAN-2 ([redacted]) R2=26
11-F-1	15-25	Lo	Hi	40	26	+1	6	"	0	0	4	
12-F-1	15-25	Lo	Hi	40	30	+1	6	"	0	0	5	
13-F-1	15-25	Lo	Hi	40	30	+1	6	"	0	0	5	
6s-T-2	15-25	Hi	Hi	40	16	+1	23	ON	4	mini	5	
6-T-3	15-25	Lo	Hi	40	26	+1	10	ON	6	mini	5	

C-SCAN SETTING

DATE : 9 / 6 / 87

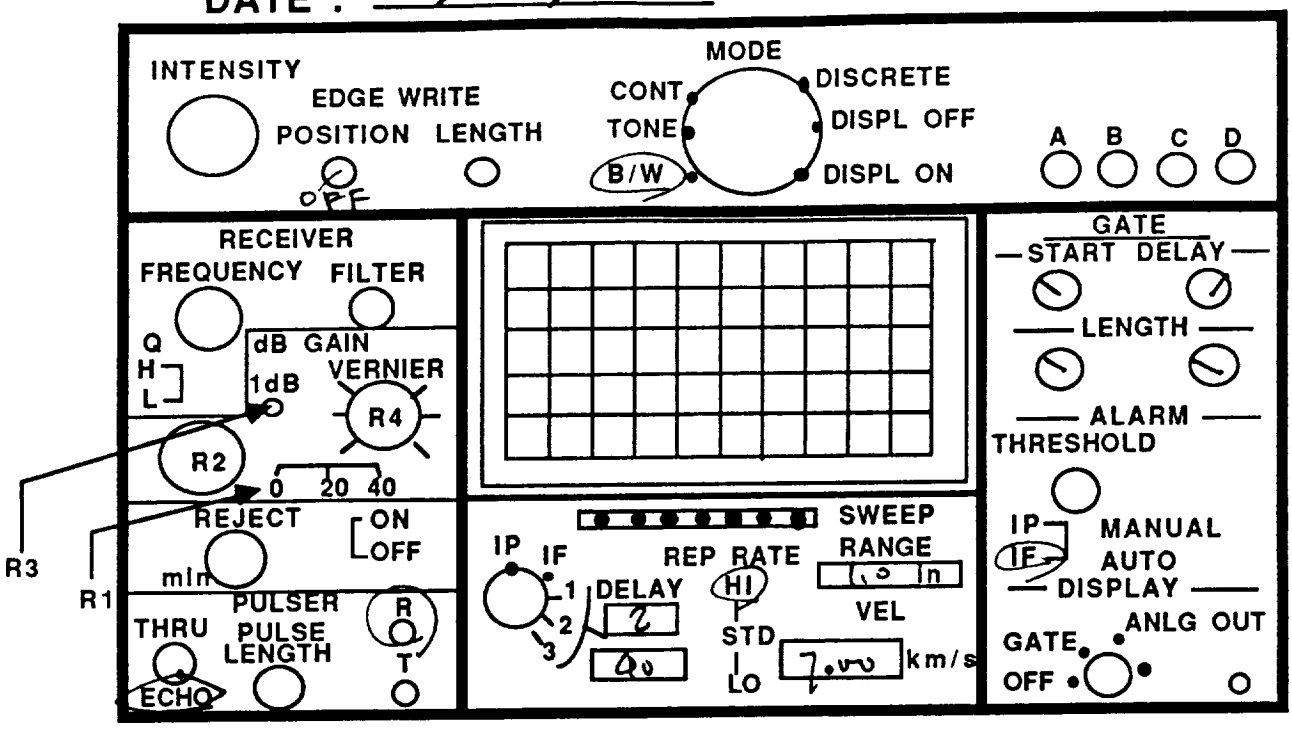

SAMPLE NO.	RECEIVER			dB GAIN				REJECT		PULSE LENGTH	GATE LEVEL	COMMENT
	OPER. FREQ.	Q HI/LO	FILTER	R1	R2	R3	R4	ON OFF	LEVEL			
95-T-2	10	HI	H	40	14	+1	10	ON	4	min	5.0	
6-T-2	15-25	LO	H	40	24	+1	10	ON	6	min	5.0	
12-T-2	10	LO	H	40	16	+1	8	ON	6	min	5.0	
6-T-6	15-25	LO	H	40	20	+1	10	ON	3	min	5.0	
8-T-2	15-25	LO	H	40	30	+1	10	ON	6	min	5.0	
7-T-2	15-25	LO	H	40	22	+1	10	ON	5	min.	5.0	
9-T-2	15-25	HI	H	40	30	+1	10	ON	6	min.	5.0	
MD-03	15-25	HI	H	40	30	+1	10	ON	6	mini	4.0	
JSC-003	15-25	HI	H	40	28	+1	10	ON	2	mini	4	
JSC-004	15-25	HI	H	40	26	+1	10	ON	3	min.	4	
11-F-1	15-25	LO	H	40	26	+1	6	OFF	0	min	4	* Thru mode

C-SCAN SETTING

DATE : 8 / 29 / 87 Chungtyue Wang

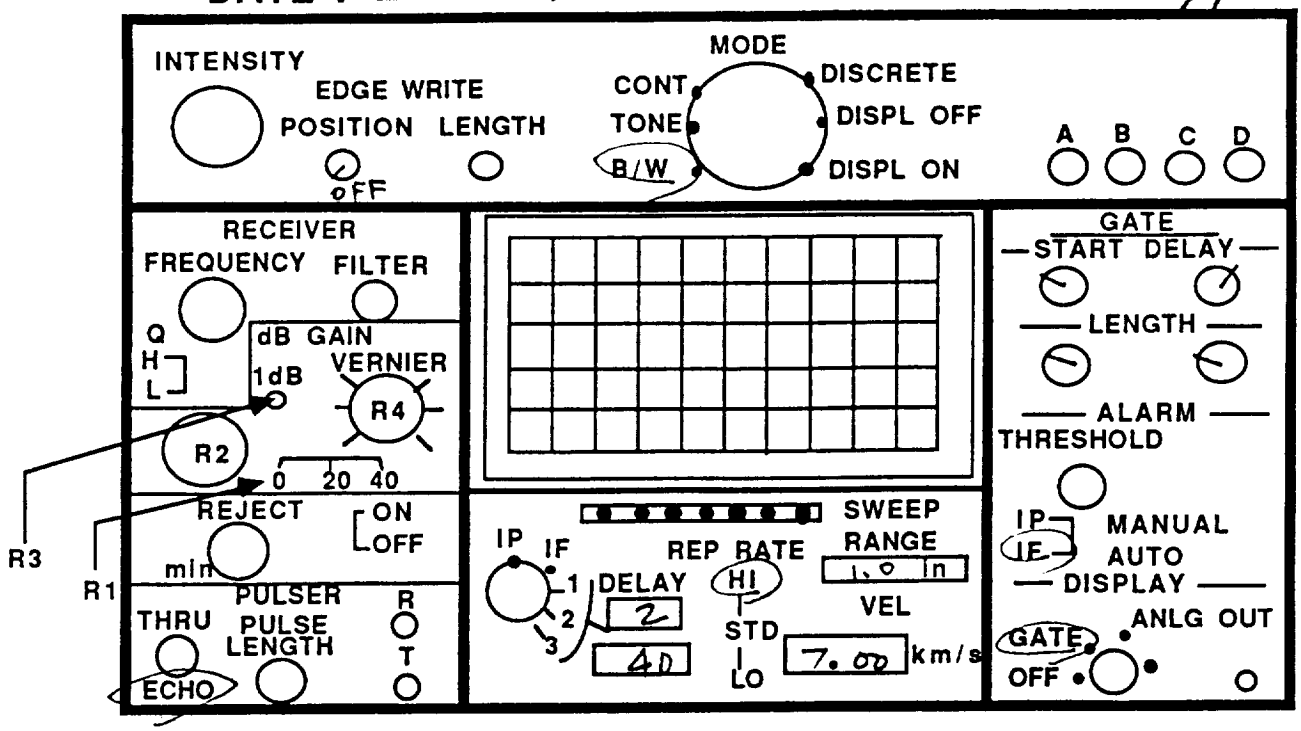

SAMPLE NO.	RECEIVER			dB GAIN				REJECT		PULSE LENGTH	GATE LEVEL	COMMENT
	OPER. FREQ.	Q HI/LO	FILTER	R1	R2	R3	R4	ON OFF	LEVEL			
6-S-T-2	10	HIGH	Hi	40	16	1	2.3	ON	4	mini	5	
6-T-4	15-25	HI	Hi	40	28	1	10	ON	4	3 ~~mini~~	4	with .002" AL. foil
11-T-4	15-25	HI	Hi	40	18 (24)	1	10 (10)	ON	6 (4)	mini	5 (4)	*
6-T-9	15-25	Low	Hi	40	28	1	10	ON	1.9	mini	4	with .006" AL. foil
9-T-1	15-25	HI	Hi	40	30	1	10	ON	6	mini	5	
10-T-2	15-25	LO	Hi	40	26	1	10	ON	6	mini	5	
MD-02	15-25	HI	Hi	40	28	1	10	ON	6	mini	4	* Never scaned Before

Note: The setting of tube 11-T-4 has been adjusted to obtain wider strip plot compared with the original one.

C-SCAN SETTING

DATE : 7/16/87

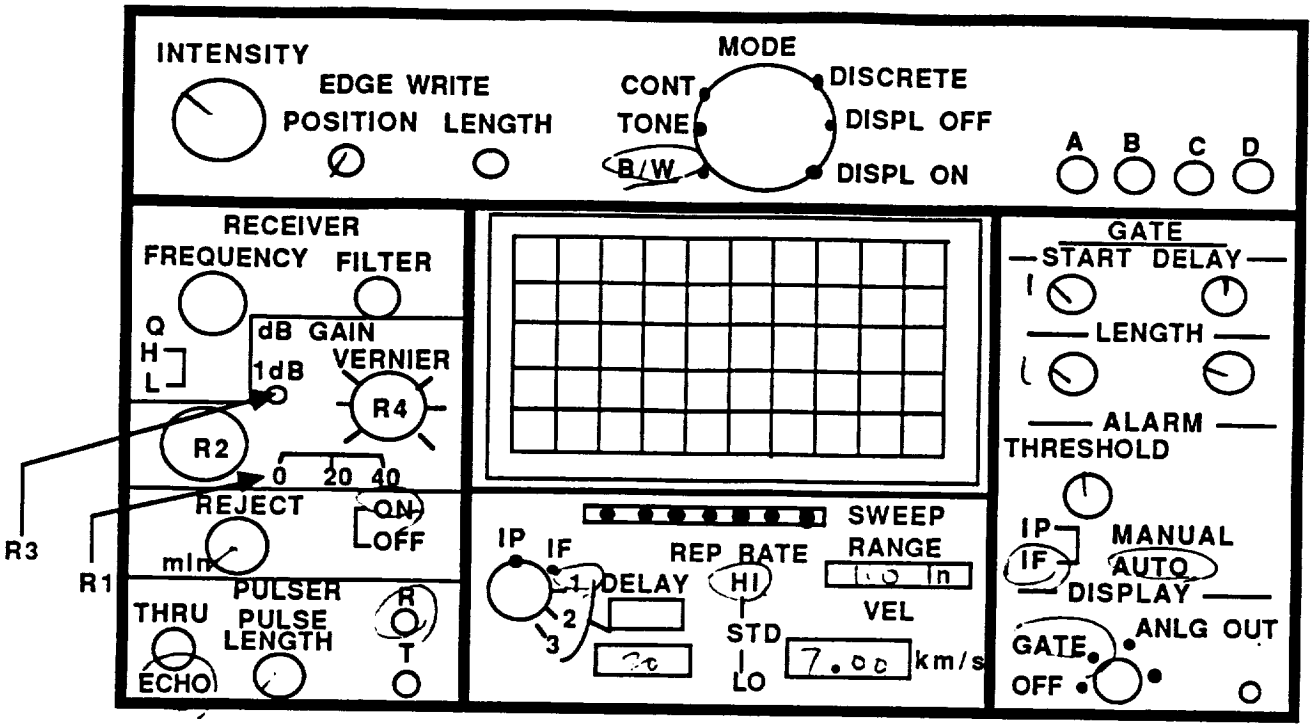

SAMPLE NO.	RECEIVER			dB GAIN				REJECT		PULSE LENGTH	GATE LEVEL	COMMENT
	OPER. FREQ.	Q HI/LO	FILTER	R1	R2	R3	R4	ON OFF	LEVEL			
6-S-T-1	10	HI	H	40	16	1	2.3	ON	4	mini	5	
11-T-2	15-25	Lo	H	40	22	1	10	ON	6	mini	5	
TSC-002	15-25	Lo	H	40	28	1	10	ON	6.	mini	5	

C-SCAN SETTING

DATE : 7 / 1 / 87

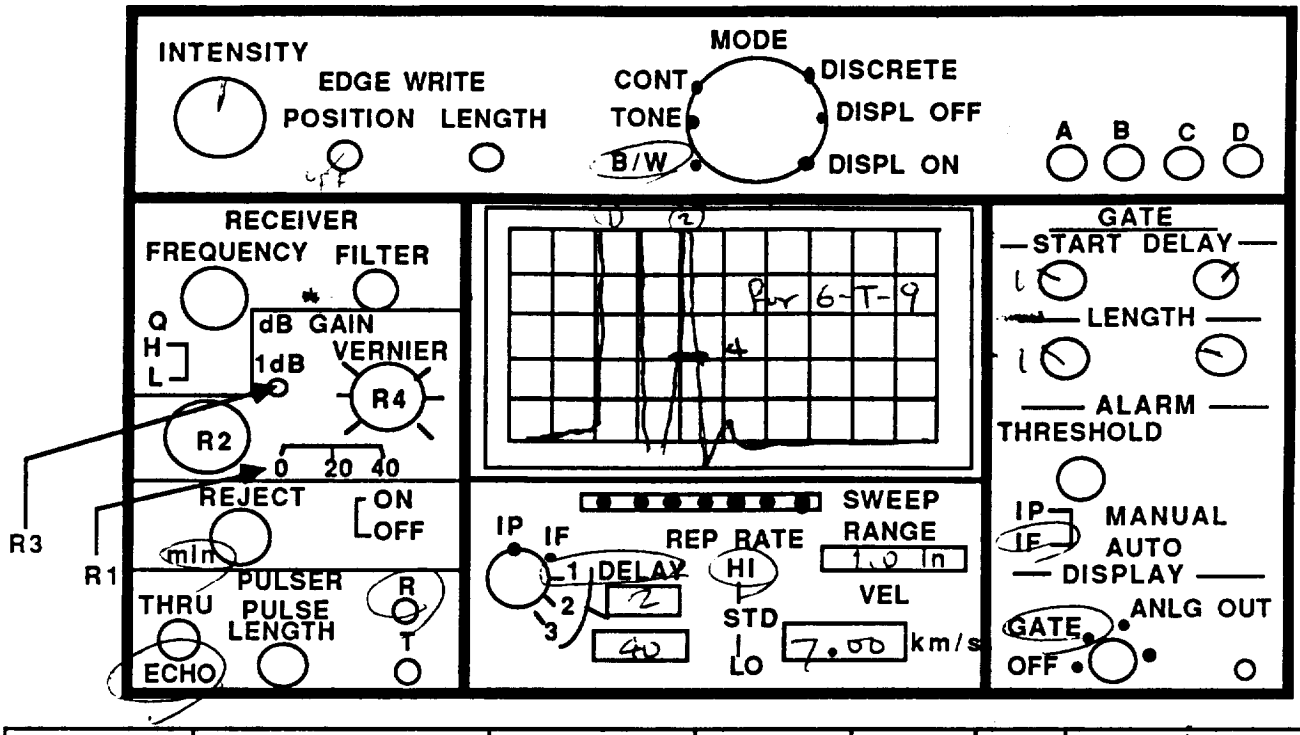

SAMPLE NO.	RECEIVER			dB GAIN				REJECT		PULSE LENGTH	GATE LEVEL	COMMENT
	OPER. FREQ.	Q HI/LO	FILTER	R1	R2	R3	R4	ON OFF	LEVEL			
6-T-9	15-25	Low	Hi	40	28	1	10	ON	1.9	min	4	*
6-T-6	15-25	Low	Hi	40	24	1	10	ON	3	min	5	*
6-S-T-2	10	HIGH	Hi	40	16	1	2.3	ON	4	min	5	
6-T-3	15-25	Low	Hi	40	26	1	10	ON	6	min	5	
11-S-T-1	10	HIGH	Hi	40	20	1	2.2	ON	6	min	5	
9S-T-1	10	HI	H	40	14	1	4	ON	4	min	5	

Note : * The original setting for 6-T-6, 6-T-9 are the arrangement for the tubes without Aluminum foils.
The above settings for the tubes 6-T-6, 6-T-9 are adjusted for the reflected signal having the db gain at the level of 10.

ORIGINAL PAGE IS
OF POOR QUALITY

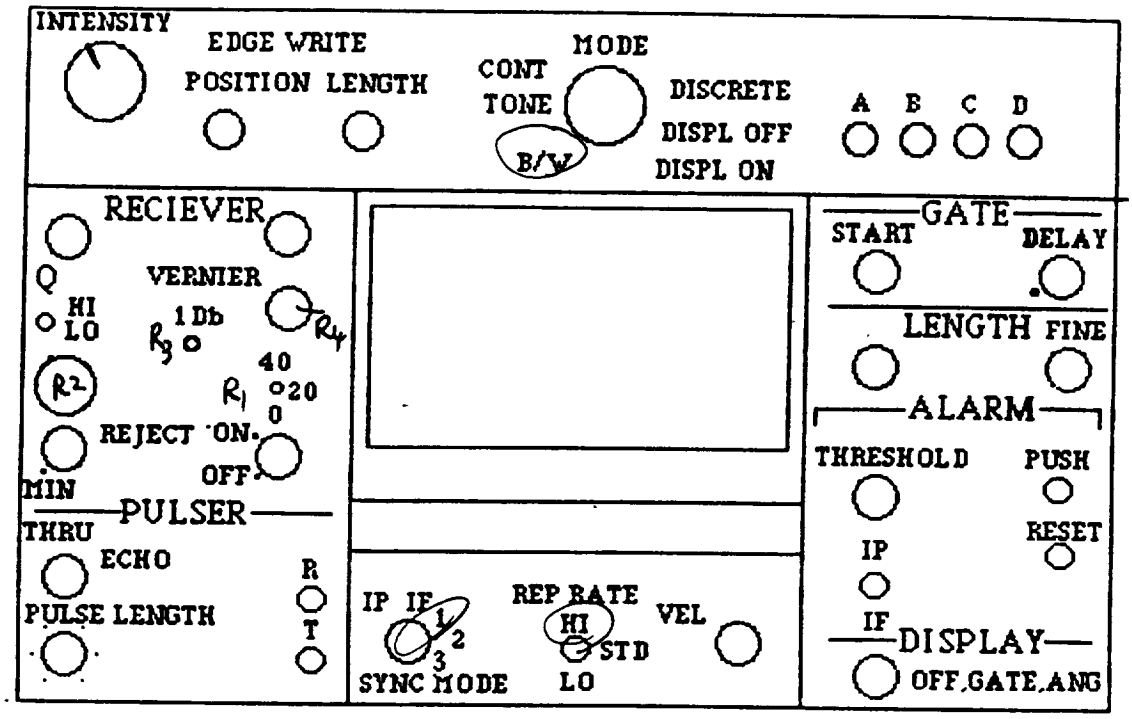

SAMPLE NUMBER_____

DATE 6/7/87

COMMENTS:

SPECIMEN NO.	OPERATING FREQUENCY	REJECT LEVEL	HI/LO	R1	R2	R3	R4	Gate	PULSE LENGTH	NOTE
13-F-2	15-25	0	HI	40	30	1	6	3 4.5 5	min	IP, THROUGH method
10-F-2	15-25	0	HI	40	22	1	6	5	min	IP, Through method
11-T-2	15-25	6	HI	40	22	1	10	5	min.	IF mode, Echo Method
11-T-4	15-25	6	HI	40	18	1	10	5	min	Change the operating Frequency to 15-25
6-T-1	15-25	4	HI	40	28	1	10	5	min	no original [illegible]
6-T-4	15-25	4	HI	40	30	1	10	4	3	First time to scan; no original no[illegible]
10-T-1	15-25	5	HI	40	26	1	10	4.5	min	
7-T-3	15-25	5	HI	40	26	1	10	4.5	min.	
11-S-T-1	10	4	HI	40	14	1	4	5	min	
9s-T-1	10	6	HI	40	20	1	22	5	min	

Originals

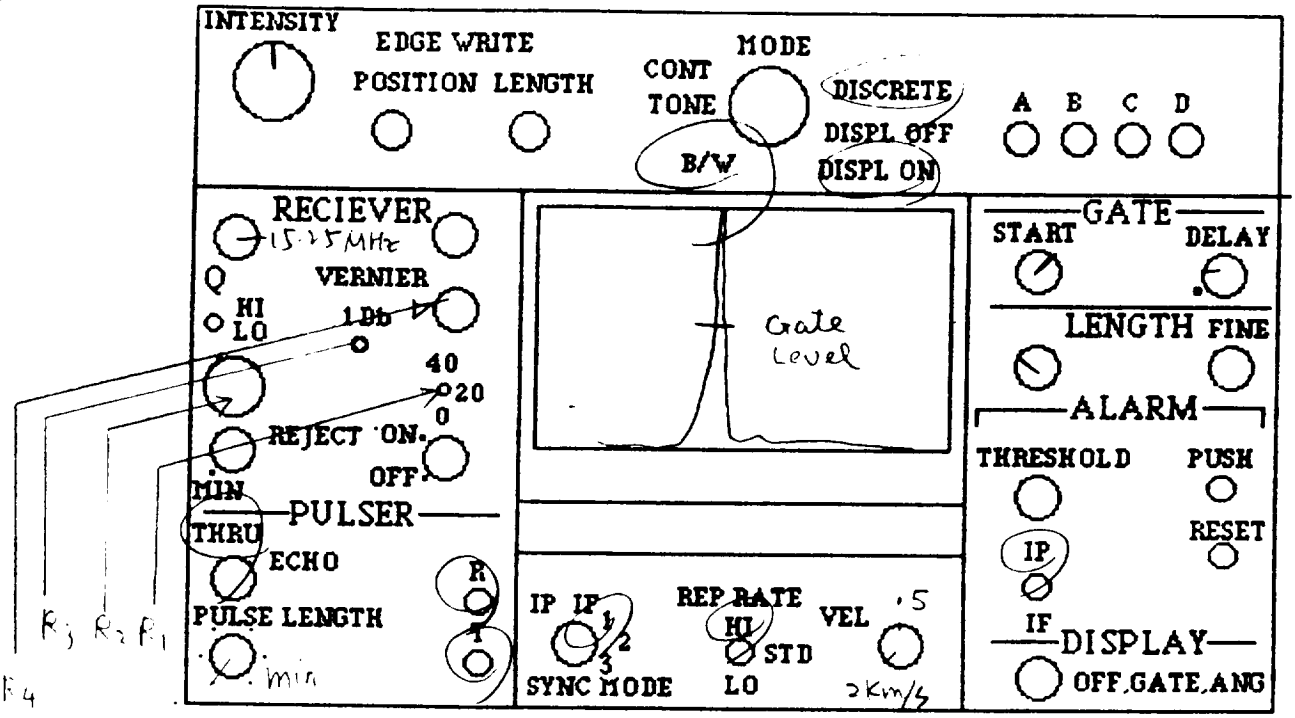

SAMPLE NUMBER 9s-F-2 9s-F-3

DATE 4/20/87

COMMENTS:

	Specimen No.	Operation Frequency	Reject Level	Hi/Lo	R1	R2	R3	R4	Gate level
1	9s-F-2	15-25	OFF	Hi	40	24	+1	6	5
2	9s-F-2	15-25	OFF	Hi	40	24	+1	6	4
3	9s-F-3	15-25	OFF	Hi	40	24	+1	6	5
4	9s-F-3	15-25	OFF	Hi	40	24	+1	6	4

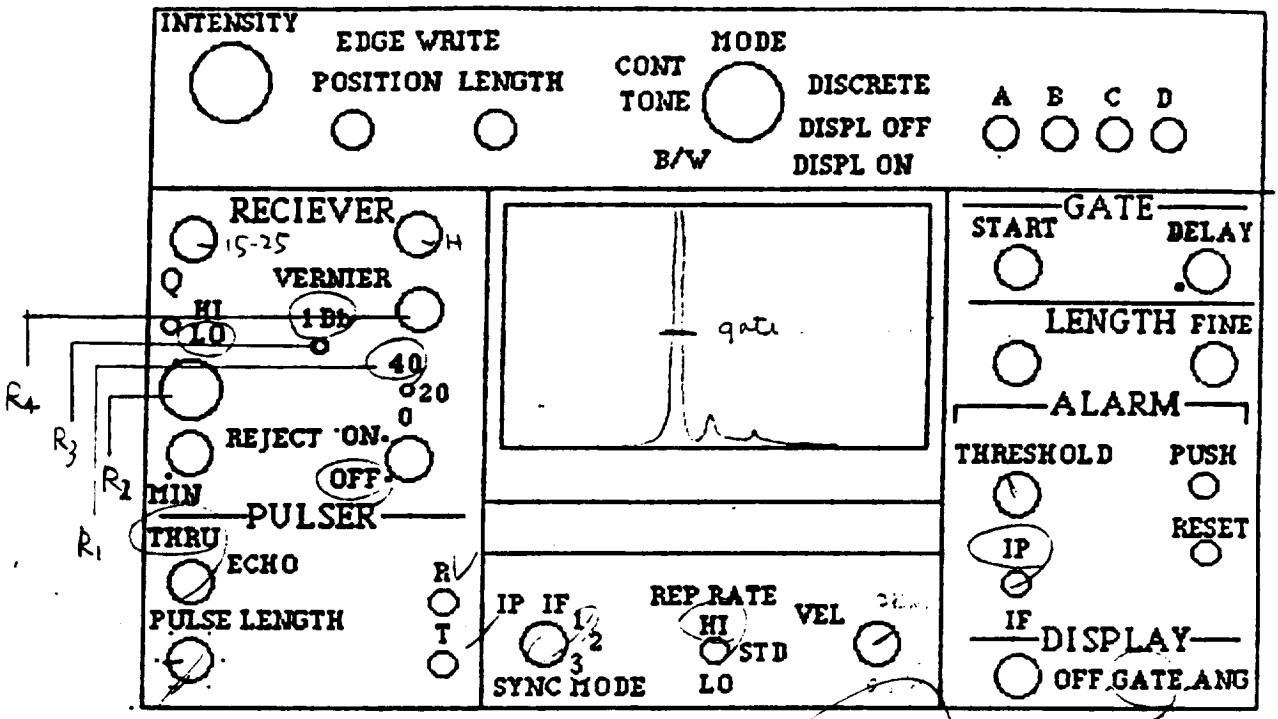

SAMPLE NUMBER 6-F-2, 12-F-2, 11-F-2

DATE

COMMENTS:

SPECIMEN	OPERATING FREQUENCY	REJECT	HI/LO	R1	R2	R3	R4	Gate level
11-F-2 (1)	15-25 MHz	OFF	LO	40	26	+1	6	5
(2)	15-25 MHz	OFF	LO	40	26	+1	6	4
12-F-2 (1)	15-25 MHz	OFF	LO	40	30	+1	6	5
(2)	"	OFF	LO	40	30	+1	6	4
6-F-2 (1)	15-25 MHz	OFF	LO	40	22	+1	6	5
(2)	"	"	"	"	"	"	"	5
(3)	"	"	"	"	"	"	"	4
11-F-2 (3)	15-25 MHz	OFF	"	40	26	+1	6	6
12-F-2 (3)	"	"		40	30	+1	6	6

pulse length at 2

Appendix D - Compression Test Records

SPEC. NO. 6-T1 AVG. O.D. 2.124 IN., AVG. WALL THK 0.068 IN., 6.019 IN. LONG
DATE = 8/25/86 AVERAGE INTERVAL 1.0 SEC TIME = 10: 3:42.1 TO 11: 8:42.0
PROCESSING DATE 8/25/86

DEFL. CHANNEL NO. 2

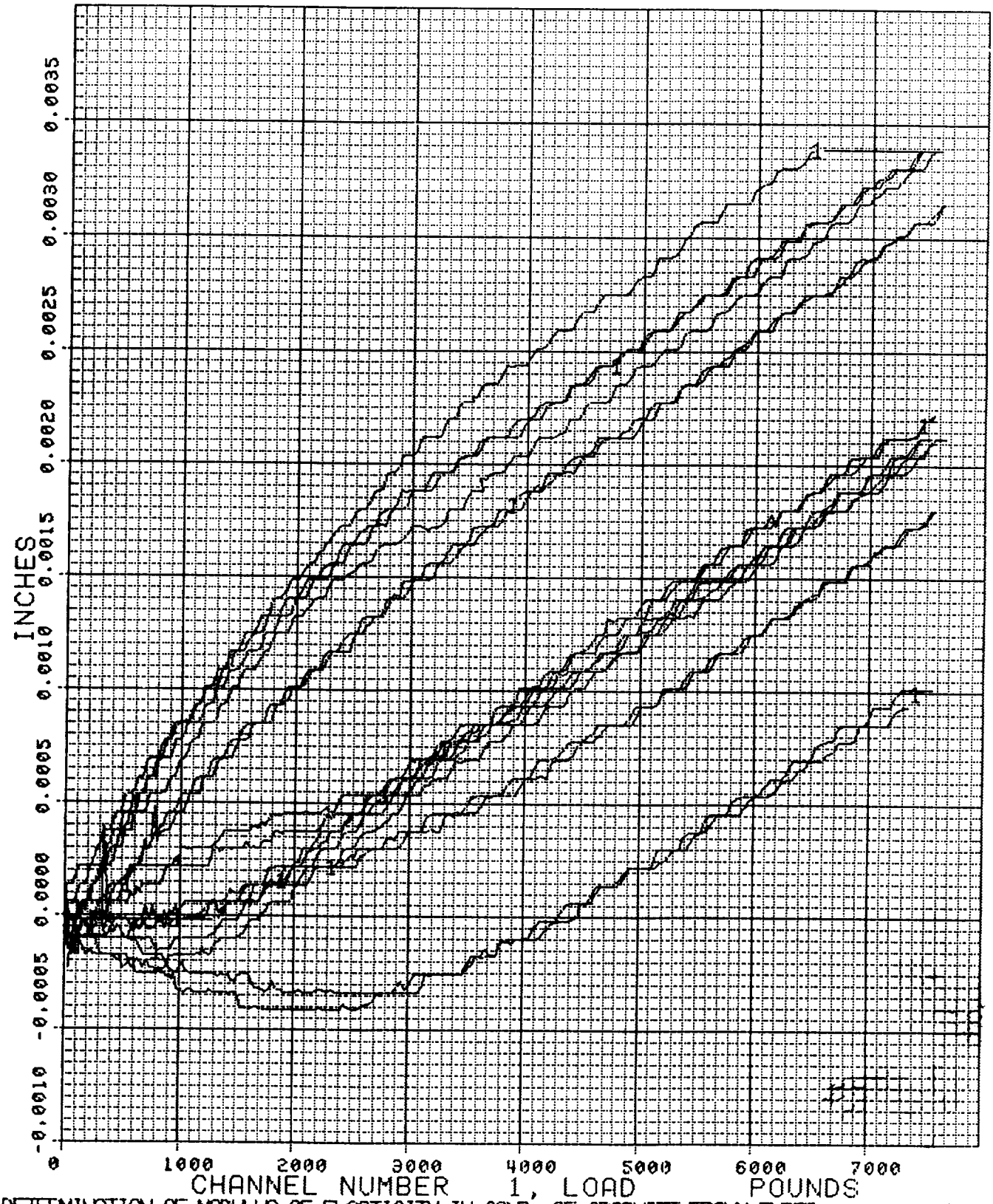

DETERMINATION OF MODULUS OF ELASTICITY IN COMP. OF GRAPHITE/EPOXY TUBES 1

SPEC. NO. 6-T1 AVG. O.D. 2.124 IN., AVG. WALL THK. .068 IN., 6.019 IN. LONG
DATE = 8/26/86 AVERAGE INTERVAL 1.0 SEC TIME = 13:13:49.0 TO 14:11:12.0
PROCESSING DATE 8/27/86

DEFL. CHANNEL NO. 2

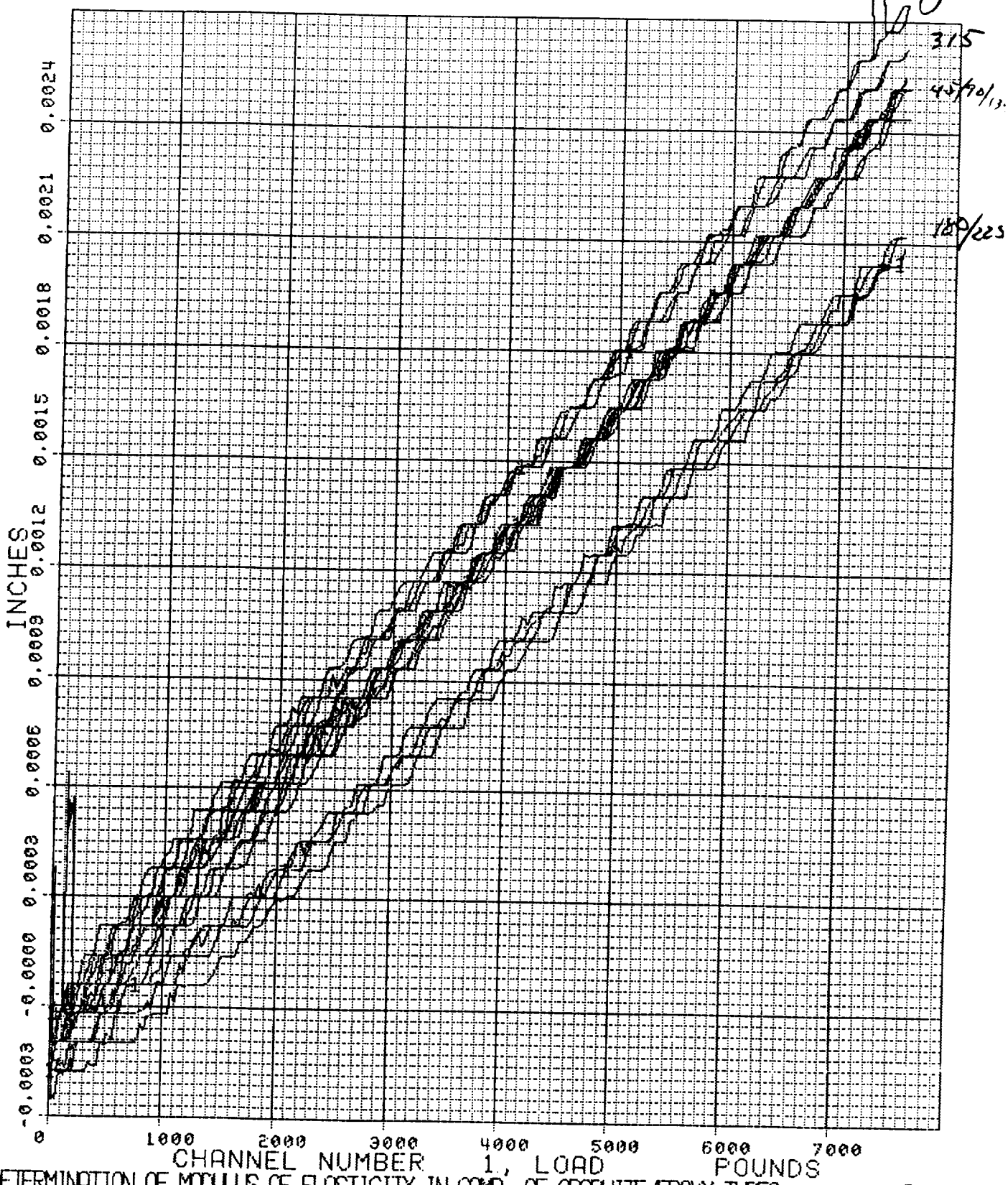

DETERMINATION OF MODULUS OF ELASTICITY IN COMP. OF GRAPHITE/EPOXY TUBES 2

SPEC. NO. 6-T-3 AVG. 2.130 IN., AVG. WALL THK. 0.068 IN., 5.975 IN. LONG
DATE = 8/25/86 AVERAGE INTERVAL 1.0 SEC TIME = 13:58:28.5 TO 14:23:29.0
PROCESSING DATE 8/26/86

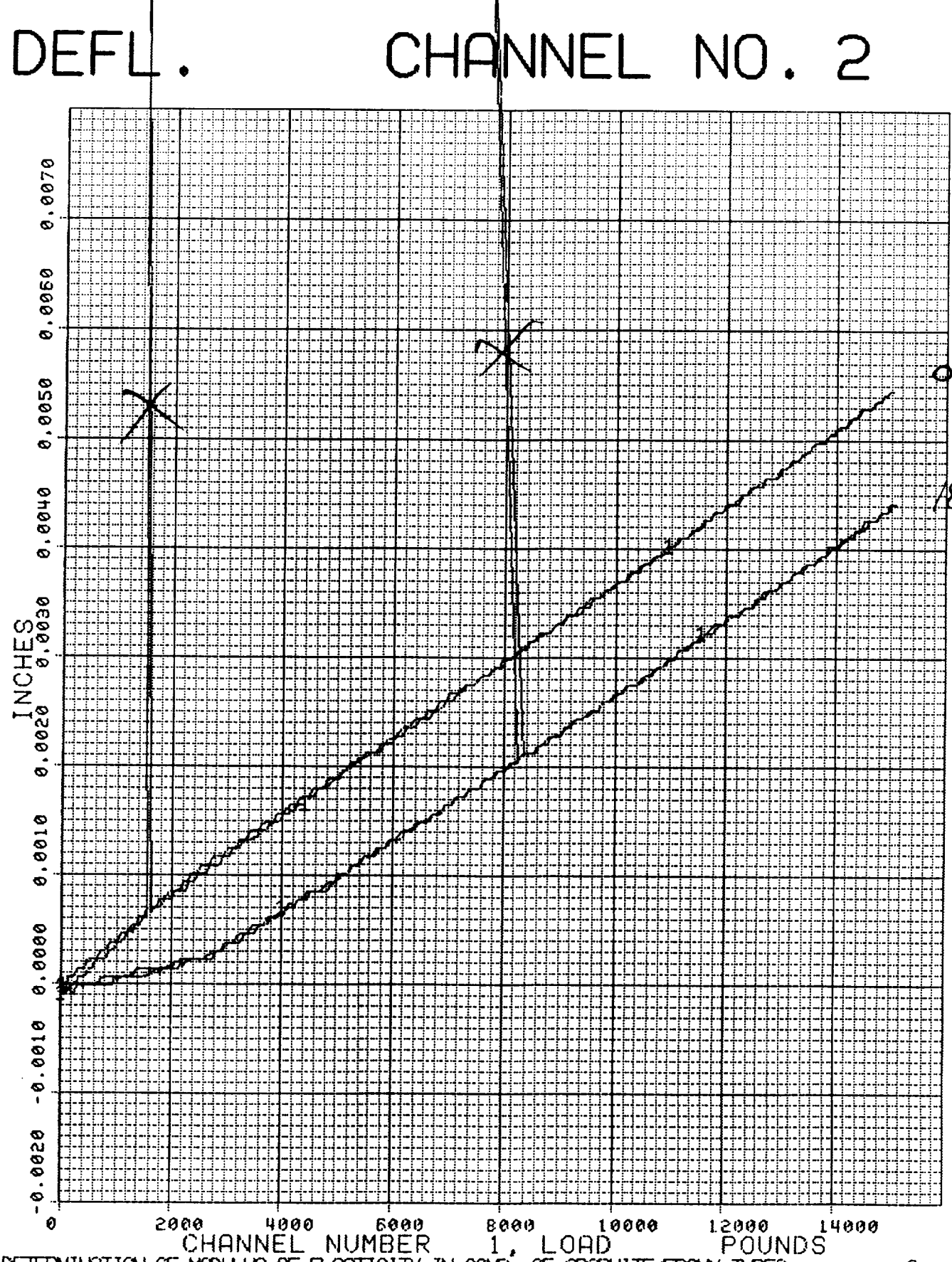

DETERMINATION OF MODULUS OF ELASTICITY IN COMP. OF GRAPHITE/EPOXY TUBES 3

SPEC. #9-T1 AVG. O.D. 2.136 IN., AVG. WALL THK. 0.064 IN., 5.983 IN. LONG
DATE = 8/27/86 AVERAGE INTERVAL 1.0 SEC TIME = 10:43: 1.1 TO 11:12:13.2
PROCESSING DATE 8/27/86

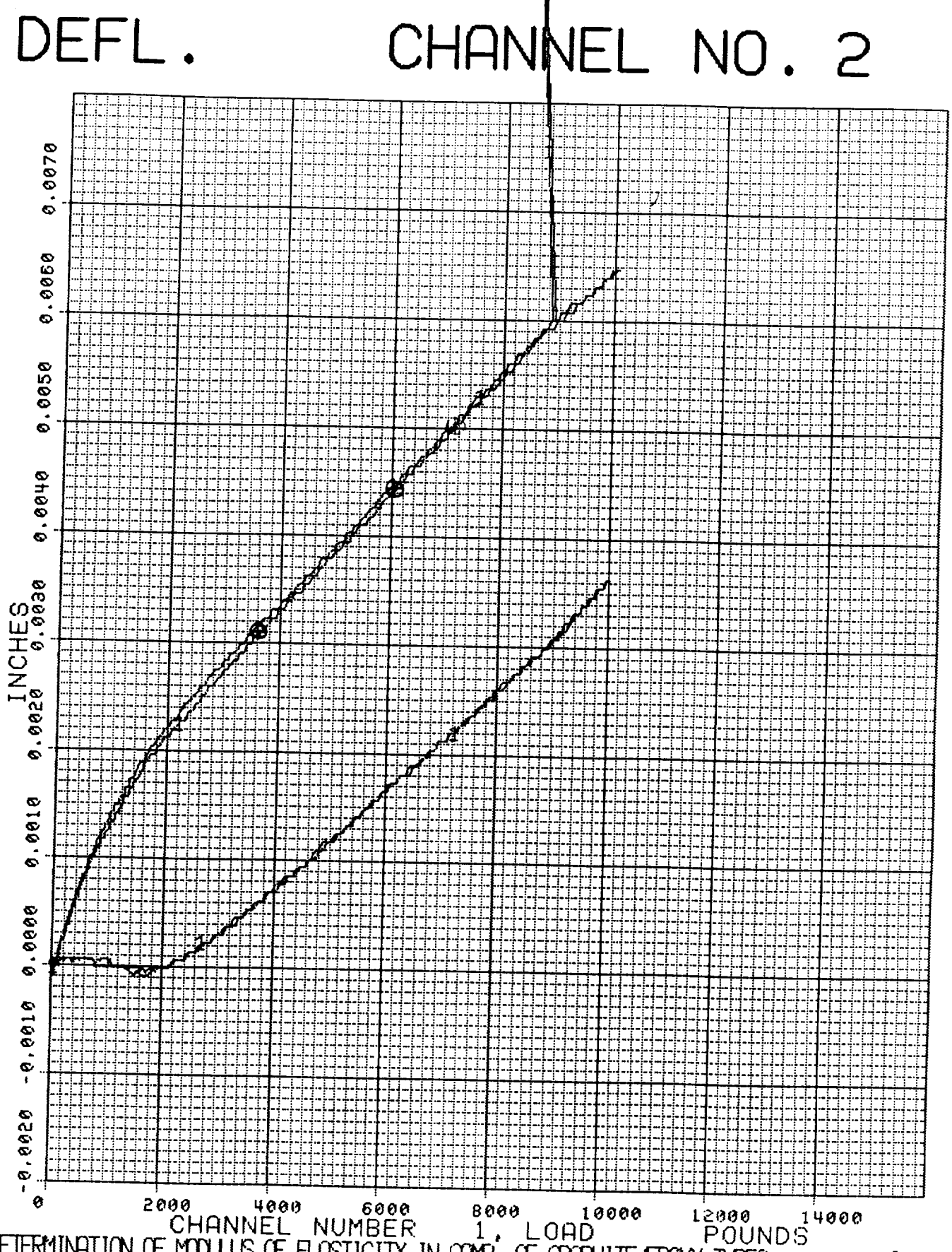

DETERMINATION OF MODULUS OF ELASTICITY IN COMP. OF GRAPHITE/EPOXY TUBES

3

SPEC. #9-T2 AVG. O.D. 2.140 IN., AVG. WALL THK. 0.065 IN., 5.981 IN. LONG
DATE = 8/27/86 AVERAGE INTERVAL 1.0 SEC TIME = 13:[illegible]4.5 TO 13:53:36.5
PROCESSING DATE 8/27/86

DEFL. CHANNEL NO. 2

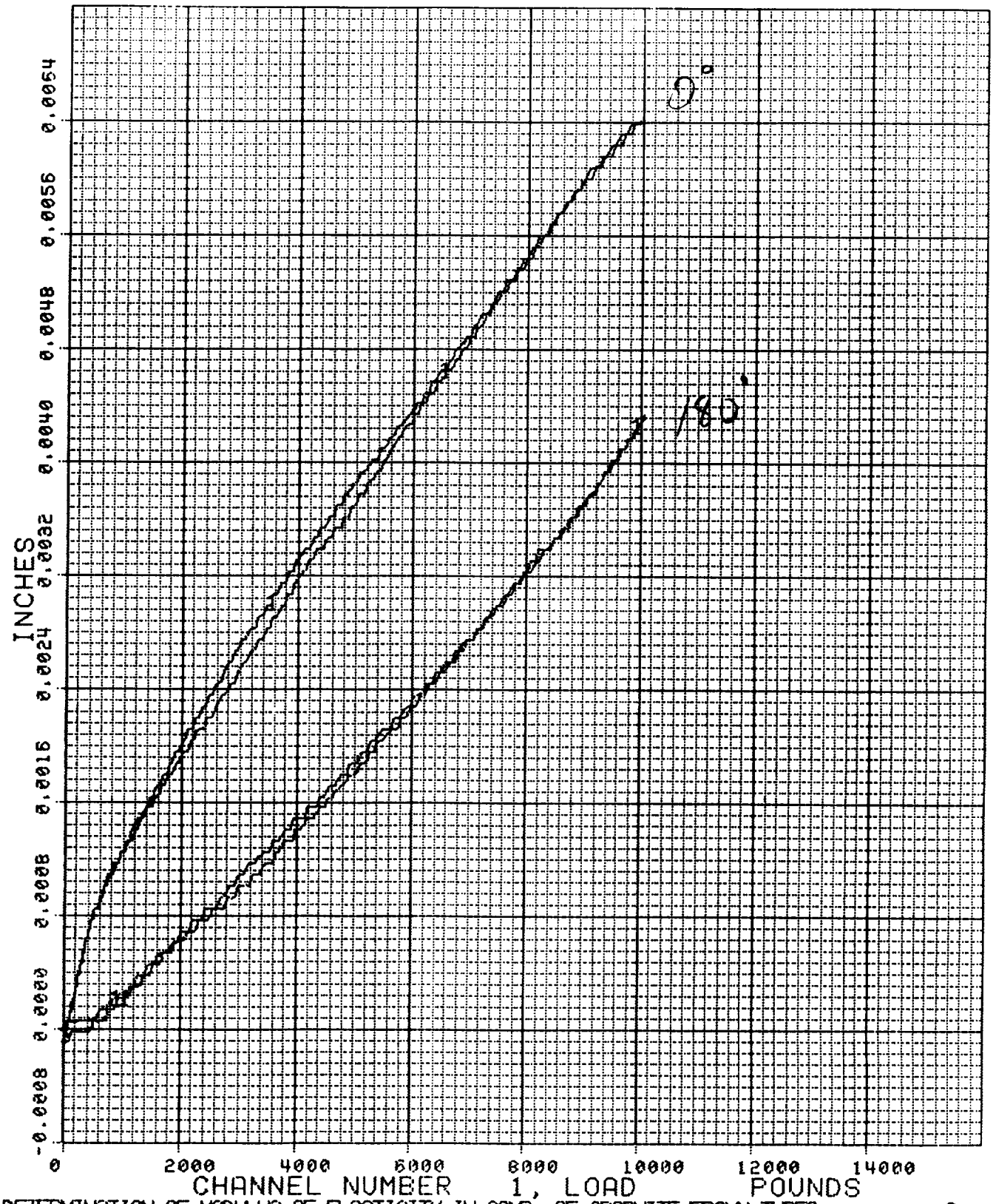

DETERMINATION OF MODULUS OF ELASTICITY IN COMP. OF GRAPHITE/EPOXY TUBES 3

SPEC. [illegible] 1 AVG. O.D. 2.142 IN., AVG. WALL THK. 0.0[illegible] IN., 5.981 IN. LONG
DATE = [illegible] AVERAGE INTERVAL 1.0 SEC TIME = 14:[illegible]51.2 TO 14:3[illegible]41.1
PROCESSING DATE 8/28/86

DEFL. CHANNEL NO. 2

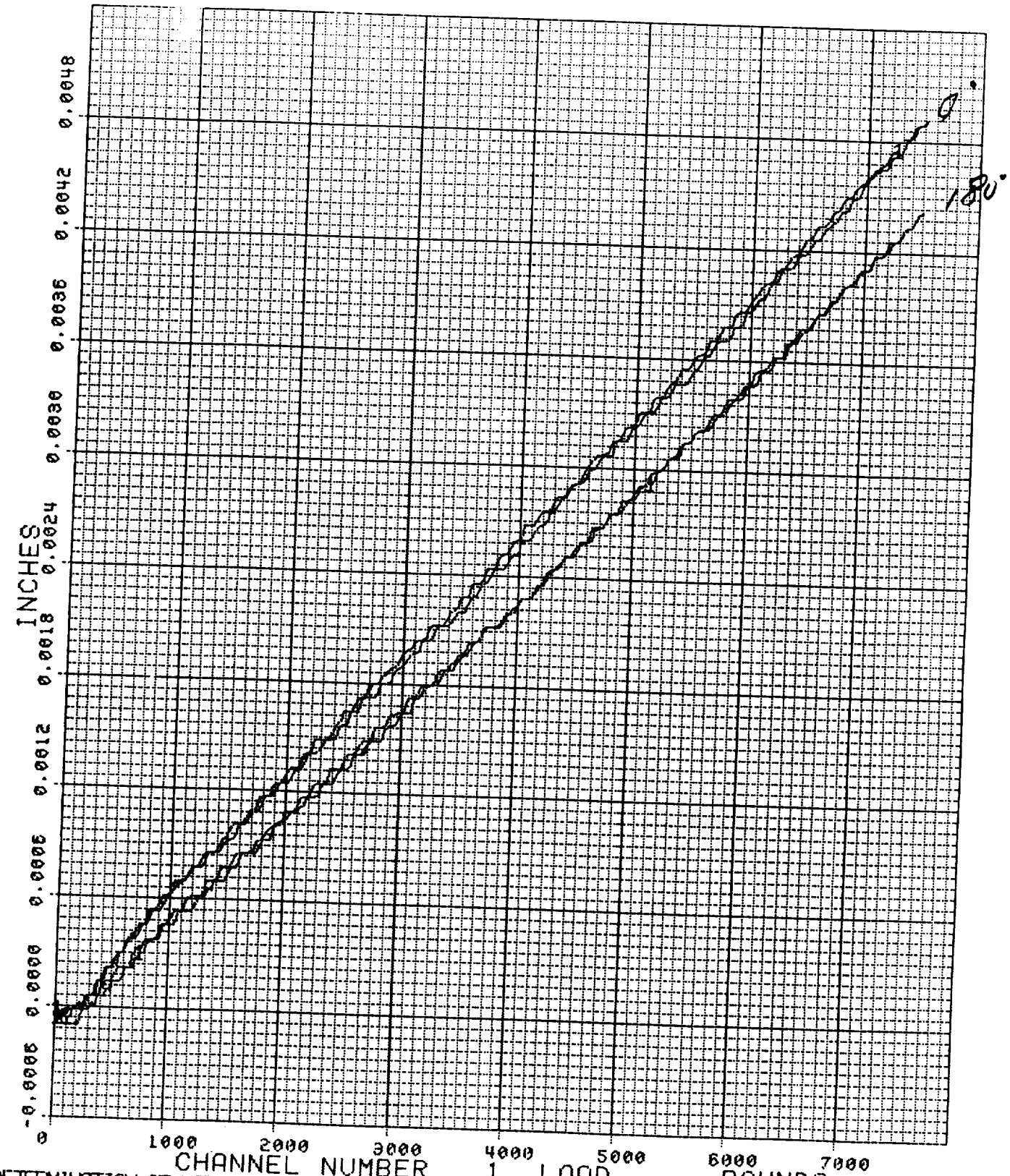

DETERMINATION OF MODULUS OF ELASTICITY IN COMP. OF GRAPHITE/EPOXY TUBES

3

SPEC. NO. [illegible] 2.040 I[illegible] [illegible] .003 [illegible], 5.988 IN. LONG
DATE = 8/[illegible]/90 AVERAGE INTERVA[illegible] 1.6[illegible] TIME = 14:4[illegible]:52.9 TO 15: 7:2[illegible].4
PROCESSING DATE 9/28/88

10-T-2

DEFL. CHANNEL NO. 2

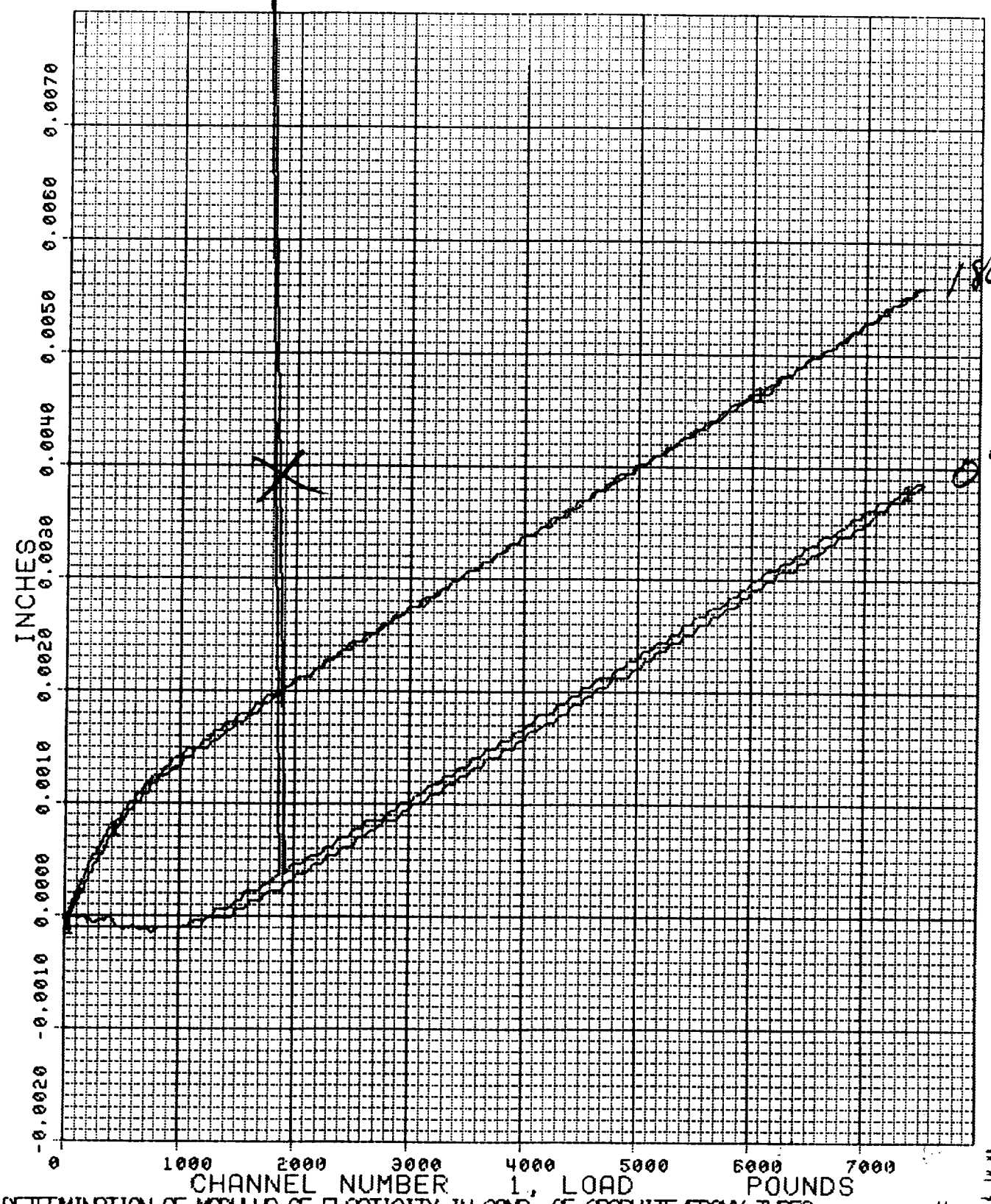

DETERMINATION OF MODULUS OF ELASTICITY IN COMP. OF GRAPHITE/EPOXY TUBES 4

SPEC. NO. 11-T-1 AVG. O.D. 2.154, AVG. WALL THK. 0.079 IN., 6.001 IN. LONG
DATE = 8/25/86 AVERAGE INTERVAL 1.0 SEC TIME = 15: 3:29.2 TO 15:10: 1.7
PROCESSING DATE 8/26/86

DEFL. CHANNEL NO. 2

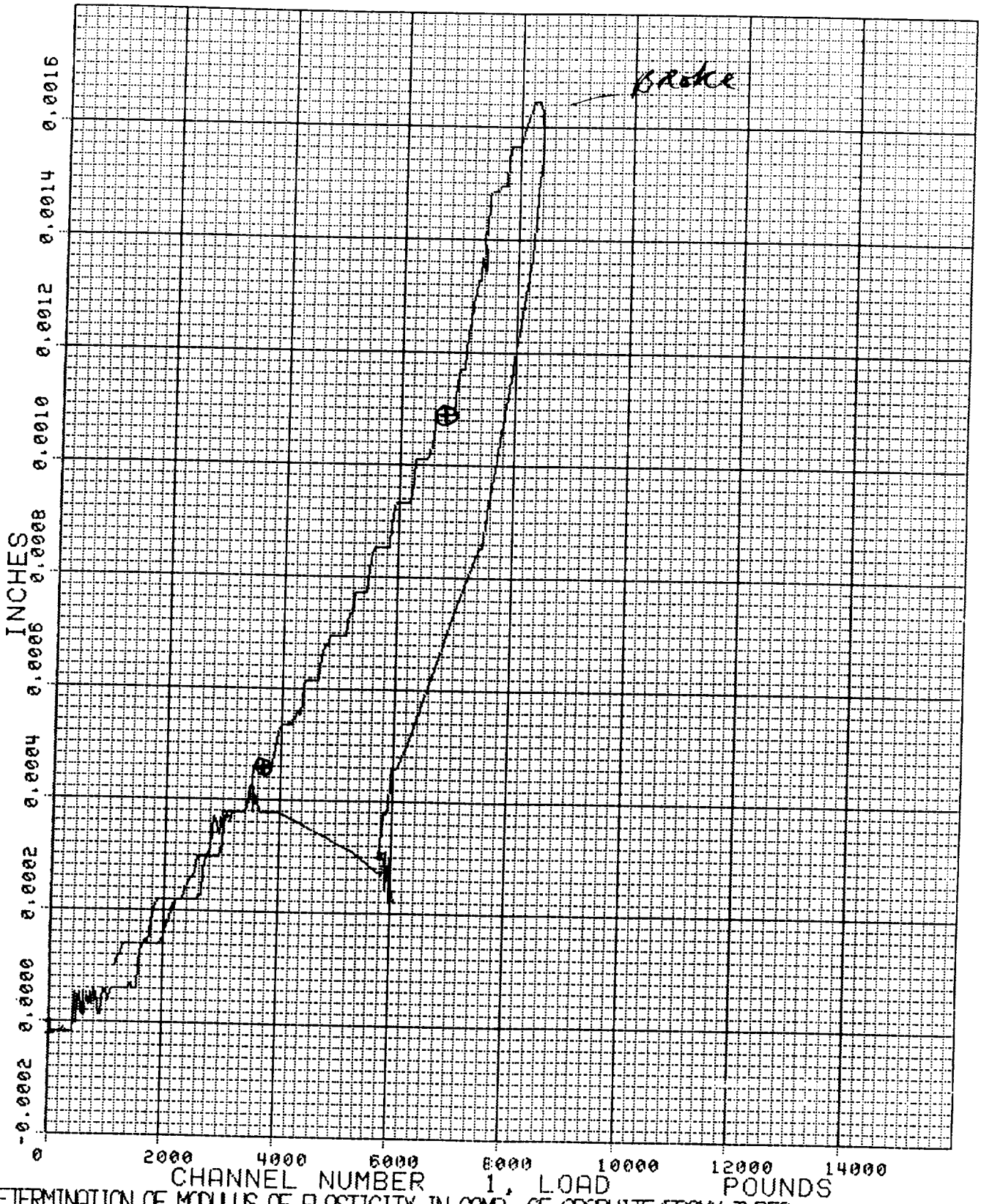

DETERMINATION OF MODULUS OF ELASTICITY IN COMP. OF GRAPHITE/EPOXY TUBES

8

SPEC. 11-T-3 AVG. O.D. 2.156 IN., AVG. WALL THK. 0.079 IN. 6.001 IN. LONG
DATE = 8/28/86 AVERAGE INTERVAL 1.0 SEC TIME = 9:42:43.0 TO 9:59: 3.3
PROCESSING DATE 8/29/86

DEFL. CHANNEL NO. 2

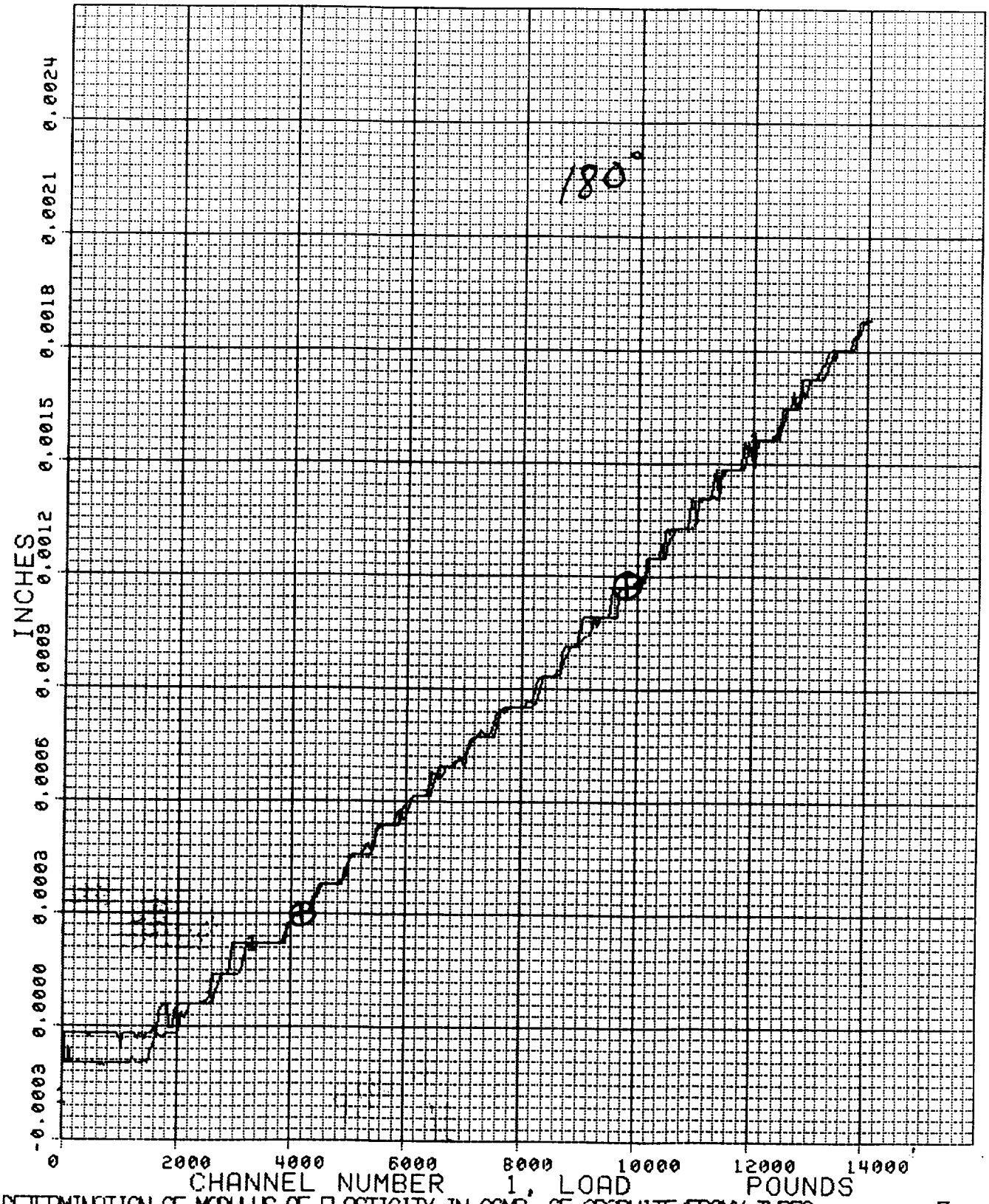

DETERMINATION OF MODULUS OF ELASTICITY IN COMP. OF GRAPHITE/EPOXY TUBES 7

SPEC. #12-T-1, AVG. O.D. 2.158 IN., AVG. WALL THK. .080 IN., 6.005 IN. LONG
DATE = 8/28/86 AVERAGE INTERVAL 1.0 SEC TIME = 8:57:19.5 TO 9:14:57.4
PROCESSING DATE 8/29/86

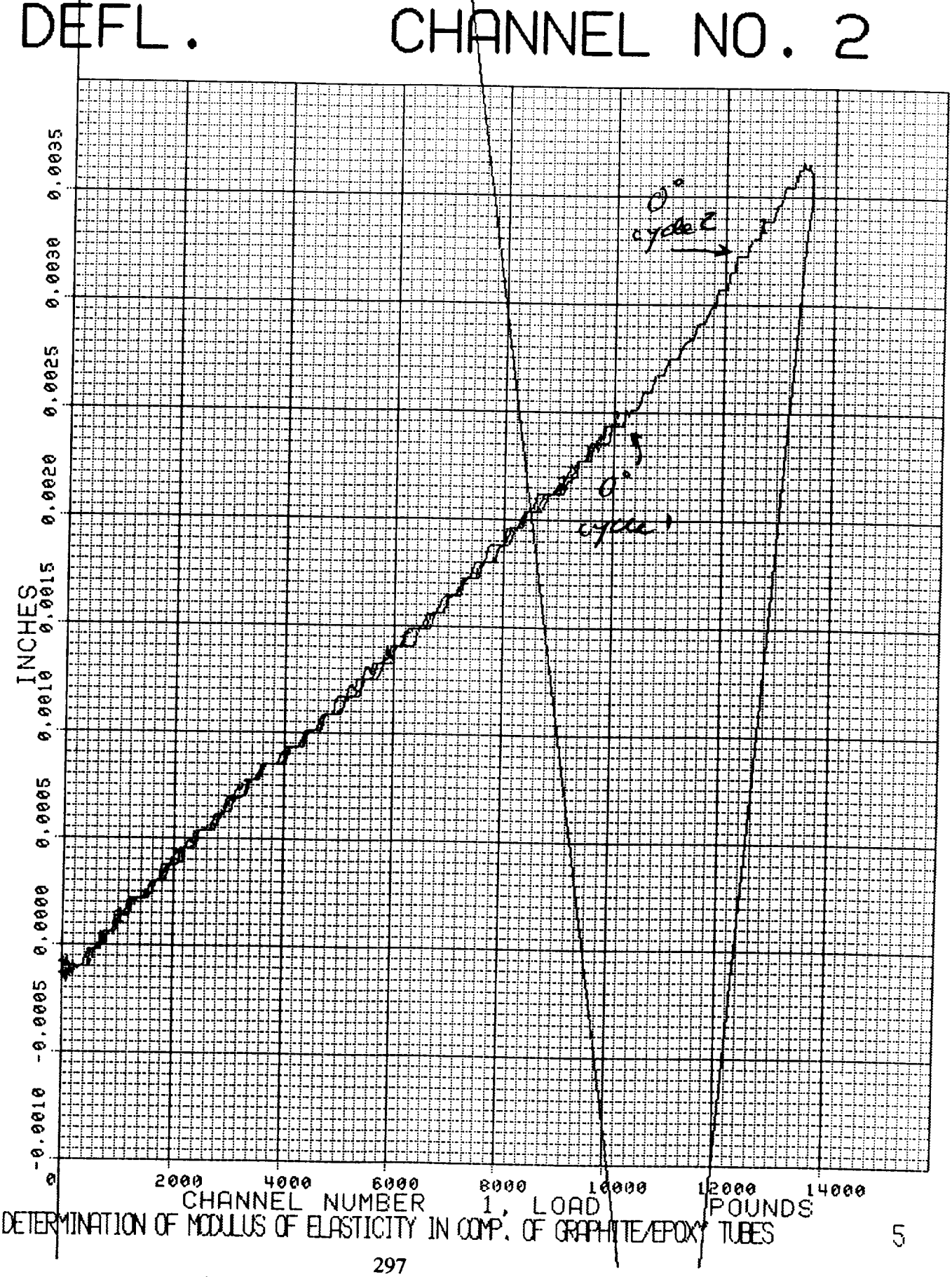

DETERMINATION OF MODULUS OF ELASTICITY IN COMP. OF GRAPHITE/EPOXY TUBES

5

SPEC. #12-T2 AVG. O.D. 2.155, IN., AVG. WALL THK. 0.079 IN., 6.001 IN. LONG
DATE = 8/27/86 AVERAGE INTERVAL 1.0 SEC TIME = 10:11:57.7 TO 10:31:41.2
PROCESSING DATE 8/27/86

DEFL. CHANNEL NO. 2

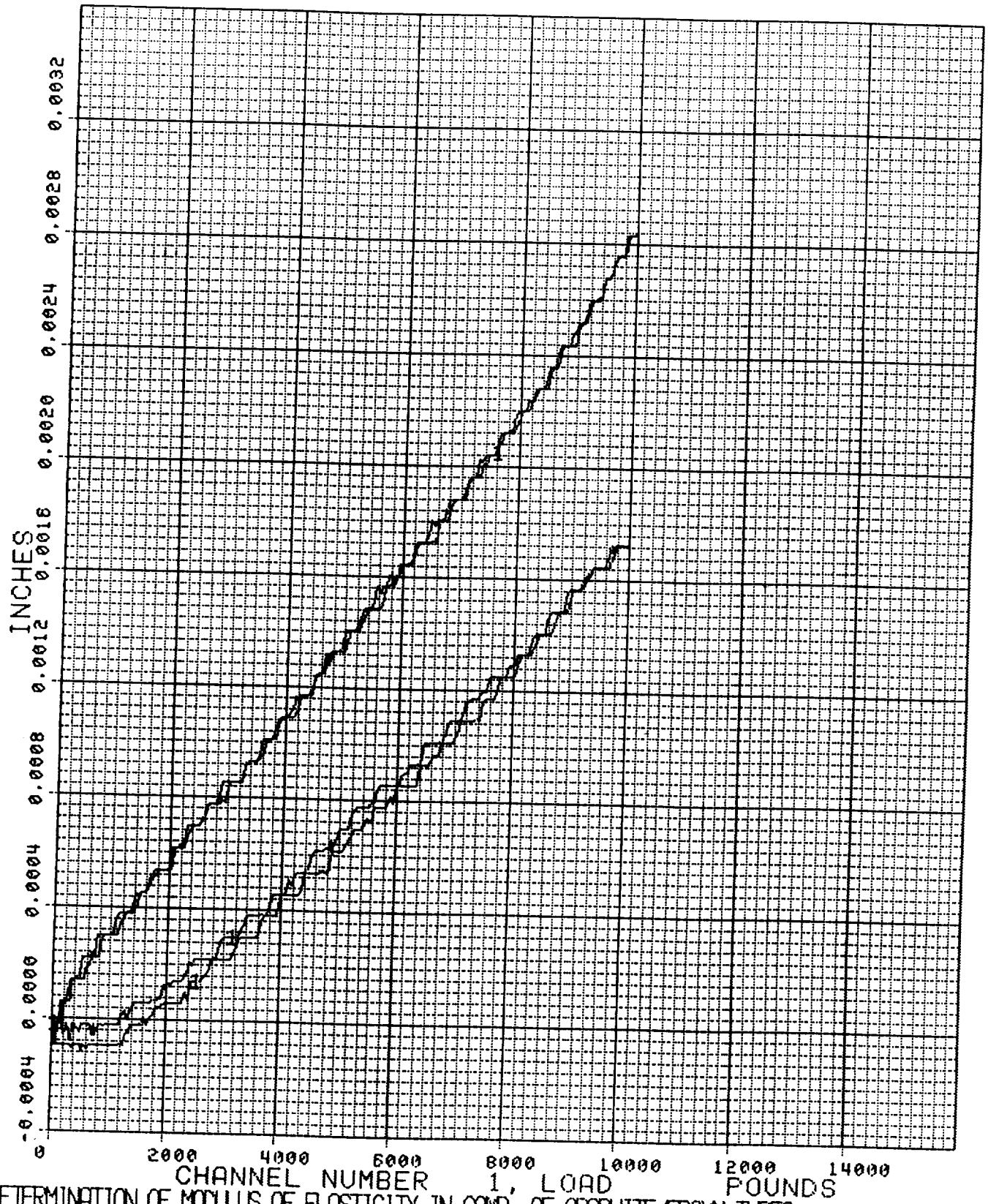

DETERMINATION OF MODULUS OF ELASTICITY IN COMP. OF GRAPHITE/EPOXY TUBES

3